Modular Concepts for the Synthesis of Functional Chromophores

Zur Erlangung des akademischen Grades einer

DOKTORIN DER NATURWISSENSCHAFTEN

(Dr. rer. nat.)

von der KIT-Fakultät für Chemie und Biowissenschaften

des Karlsruher Instituts für Technologie (KIT)

genehmigte

DISSERTATION

von

M.Sc. Mareen Stahlberger

aus Rastatt

Dekan: Prof. Dr. Hans-Achim Wagenknecht

1. Referent: Prof. Dr. Stefan Bräse

2. Referent: Prof. Dr. Frank Breitling

Tag der mündlichen Prüfung: 29.04.2022

"Despite the overwhelming odds, tomorrow came."

*— **Rise against, Tragedy + Time***

Honesty Declaration

This work was carried out from December 01st 2017 through March 16th, 2022, at the Institute of Organic Chemistry, Faculty of Chemistry and Biosciences at the Karlsruhe Institute of Technology (KIT) under the supervision of Prof. Dr. Stefan Bräse.

Die vorliegende Arbeit wurde im Zeitraum vom 01. Dezember 2017 bis 16. März 2022 am Institut für Organische Chemie (IOC) der Fakultät für Chemie und Biowissenschaften am Karlsruher Institut für Technologie (KIT) unter der Leitung von Prof. Dr. Stefan Bräse angefertigt.

Hiermit versichere ich, MAREEN STAHLBERGER, die vorliegende Arbeit selbstständig verfasst und keine anderen als die angegebenen Hilfsmittel verwendet, sowie Zitate kenntlich gemacht zu haben. Die Dissertation wurde bisher an keiner anderen Hochschule oder Universität eingereicht.

Hereby I, MAREEN STAHLBERGER, declare that I completed the work independently, without any improper help and that all material published by others is cited properly. This thesis has not been submitted to any other university before.

German Title of this Thesis

Modulare Konzepte zur Synthese funktioneller Chromophore

Preface

Some of the presented results were published or submitted during the preparation of this thesis (*vide infra*). The relevant content is reprinted with the permission of WILEY-VCH publishing and the Royal Society of Chemistry.

If applicable, each chapter includes a list of authors with the individual contributions described briefly. Additionally, if some of the presented results have already been partly discussed in other theses, it is stated at the beginning of the respective chapters.

M. Stahlberger, N. Schwarz, C. Zippel, J. Hohmann, M. Nieger, Z. Hassan, S. Bräse,

Chem. Eur. J. **2022**, 28, e202103511.

Diversity-oriented Synthesis of [2.2]Paracyclophane-derived Fused Imidazo[1,2-*a*]heterocycles by Groebke–Blackburn–Bienaymé Reaction: Accessing Cyclophanyl Imidazole Ligands Library

M. Stahlberger, O. Steinlein, C. R. Adam, M. Rotter, J. Hohmann, M. Nieger, B. Köberle and S. Bräse,

Org. Biomol. Chem. **2022**, 20, 3598.

Fluorescent Annulated Imidazo[4,5-c]isoquinolines *via* a GBB-3CR/Imidoylation Sequence – DNA-Interactions in pUC-19 Gel Electrophoresis Mobility Shift Assay

M. Stahlberger, S. Bräse, N. Bugdahn, *patent pending*.

Method for producing 2,4,6-substituted triazines.

Table of Contents

Kurzzusammenfassung

Funktionelle Chromophore spielen aufgrund ihrer vielfältigen, stetig wachsenden Anwendungen eine zentrale Rolle in vielen Aspekten von Naturwissenschaft und Technologie. Im Sinne des steigenden Bewusstseins für Nachhaltigkeit sind die Minimierung der Umweltbelastung durch chemische Synthese sowohl im Labor- als auch im industriellen Maßstab, sowie die Anpassung an die Prinzipien grüner Chemie außerordentlich wichtig.

Die Groebke-Blackburn-Bienaymé Dreikomponentenreaktion (GBB-3CR), eine isonitril-basierte Multikomponentenreaktion, zog in der Vergangenheit viel Aufmerksamkeit auf sich, da aus ihr Imidazo[1,2-*a*]heterocyclen hervorgehen. Während die biologischen Eigenschaften dieser privilegierte Gerüststruktur gut untersucht sind, bleiben Berichte über ihre Anwendung in den Materialwissenschaften rar. Im Zuge dieser Arbeit wurden Imidazo[1,2-*a*]heterocyclen für die Synthese funktioneller Fluorophore untersucht.

Einerseits wurde die GBB-3CR für die Derivatisierung von bereits existierenden Gerüststrukturen genutzt. Basierend auf [2.2]Paracyclophan, einer überbrückten aromatischen Kohlenwasserstoffverbindung wurden strukturell vielfältige imidazo[1,2-*a*]heterocyclische Fluorophore synthetisiert. Ihre Fluoreszenzeigenschaften sowie ihre Eignung als Liganden für katalytisch aktive *N,C*-Palladacyclen mittels einer regioselektiven *ortho*-Palladierung wurden erforscht. Außerdem wurde eine Bibliothek an fluoreszenten Derivaten des marinen Steroids Gorgosterol synthetisiert um Imidazo[1,2-*a*]heterocyclen als fluoreszente Lable für Biomoleküle in Bioimaging Experimenten zu etablieren. Die gelabelten Steroide wurden in einem Zytotoxizitätsassay und in Co-Lokalisationsstudien an HeLa Zellen untersucht.

Andererseits wurden sequenzielle Syntheserouten für die Postmodifizierung von GBB-Produkten erforscht. Dabei wurde aus Imidazo[1,2-*a*]pyridinbausteinen eine Serie an Donor Akzeptor-Chromorophore hergestellt und photophysikalisch charakterisiert. Mittels einer zweistufigen Synthesesequenz bestehend aus einer GBB-3CR gefolgt von einer intramolekularen imidoylativen Hartwig-Buchwald Aminierung wurden GBB-Produkte zu polyheterocyclischen Strukturen cyclisiert. Die Interaktionen dieser Substanzen mit doppelsträngiger DNA wurden in einem neu dafür etablierten pUC19 Gel Elektrophorese Mobilitätsshiftassay untersucht.

Ein weiterer Aspekt dieser Arbeit war der Transfer modularer Synthesen auf das von der Breitling Gruppe entwickelte nano3D Druck System, um dessen Potential für die miniaturisierte Synthese dichter Molekül Arrays zu zeigen. Um außerdem die Möglichkeit der CO_2-Umwandulung demonstrieren zu können wurde eine fluoreszente Sonde entwickelt.

Darüber hinaus wurde in Zusammenarbeit mit der Symrise AG ein verbesserter Syntheseansatz für den kommerziellen UV-Absorber und Sonnencreme Inhaltsstoff Bemotrizinol, einem unsymmetrischen 1,3,5-Triazin, erarbeitet. Synthetische Schritte wurden unternommen, um abfallreiche Reaktionen zu ersetzen. Eine neuartige Methode für de nukleophile Aromatensubstitution an Chloro-1,3,5-triazinen mit Enolaten als Kohlenstoffnukleophile wurde entwickelte. Ein intermediärer Bemotrizinol-Vorläufer, genannt Tetrahydro-Bemotrizinol wurde genau charakterisiert. Abschließend wurde Tetrahydro-Bemotrizinol in einem neuartigen Elektro chemischen oxidativen Aromatisierungsprotokoll zum Zielprodukt Bemotrizinol umgesetzt.

Abstract

Due to their vast, ever-growing application perspectives, functional chromophores play a pivotal role in many aspects of both life sciences and technology. Accounting for the increasing awareness for sustainability, the minimization of the overall environmental impact of chemical synthesis on both a laboratory and an industrial scale, as well as conforming to the principles of green chemistry are imperative. Diversity-oriented and modular synthesis methods, and the implementation of greener, less waste-intense procedures are important tools to improve chemical syntheses.

The Groebke-Blackburn-Bienaymé three-component reaction (GBB-3CR), an isonitrile-based three component reaction, has drawn a lot of attention since it furnishes imidazo[1,2-*a*]heterocycles. The biological properties of this privileged heterocyclic scaffold are well investigated, while reports of their application in material science remain scarce. In this dissertation, imidazo[1,2-*a*]heterocycles were explored in the synthesis of functional fluorophores.

On one side, GBB-3CR was employed for the derivatization of existing scaffolds. Based on [2.2]paracyclophane, a π-stacked hydrocarbon scaffold, skeletally diverse imidazo[1,2-*a*]heterocyclic fluorophores were synthesized. Their fluorescent properties and pH dependency were investigated and their suitability as ligands for catalytically active *N,C*-palladacycles was demonstrated through regioselective *ortho*-palladation.

Moreover, a library of fluorescent derivatives of the marine steroid Gorgosterol was synthesized to establish the imidazo[1,2-*a*]pyridine as a fluorescent tag for the labeling of biomolecules in imaging studies. The tagged steroid derivatives were investigated in an MTT-assay and colocalization studies in HeLa cells.

Sequential synthesis routes for the post modification of GBB-scaffolds were explored. Therefore, imidazo[1,2-*a*]pyridine building blocks were used to synthesize a series of donor-acceptor chromophores that were photophysically characterized.

Through a two-step reaction sequence comprising a GBB-3CR, followed by an intramolecular imidoylative amination, the GBB-scaffold was cyclized to furnish polyheterocycles. Their interactions with double-stranded DNA were evaluated in a newly established pUC-19 gel electrophoresis mobility shift assay.

Another aspect was the transfer of modular syntheses to a nano3D printing system developed by the Breitling group, demonstrating the system's potential in the parallel miniaturized synthesis of highly dense molecular arrays. To also showcase the possibility of CO_2 conversion, a fluorescent probe was developed.

Furthermore, in cooperation with Symrise AG, an improved synthetic approach to the commercial UV-absorber and sunscreen ingredient Bemotrizinol, an unsymmetric triaryl-1,3,5-triazine, was developed. Synthetic efforts were made to replace waste-intensive reaction steps. A novel method for the nucleophilic aromatic substitution of chloro-1,3,5-triazines with enolates as carbon nucleophiles was developed. An intermediate Bemotrizinol surrogate, termed tetrahydro Bemotrizinol, was characterized thoroughly. Finally, tetrahydro-Bemotrizinol was converted to the target Bemotrizinol through an unprecedented electrochemical oxidative aromatization protocol.

1   Introduction

The conception of color is one of the essential factors in how we perceive our environment. Scientifically, this effect stems from the absorption, emission, and reflection of electromagnetic radiation in a specific range of wavelength by objects (visible spectrum) that can be perceived by our visual receptors. On a chemical level, molecules capable of interacting with light are called chromophores. Structural features of chromophores are commonly small molecular structures with conjugated π-electron systems, like polyenes or (hetero-)aromatic scaffolds, or transition metal complexes.[1]

As color is such an integral element of our lives and culture, it is not without reason that there has been a steady commercial interest for developing novel chromophores ever since the synthesis of the first artificial dye mauveine by PERKIN in 1860.[2] Over the course of the last century, dyes evolved beyond having a solely aesthetic purpose, but instead are now specifically tailored for a defined function or application. Chromophores can be classified by their functions, such as light absorption, light emission, photochemical or photoelectric activity, or polarization (see **Figure 1**).[3] These functional dyes are molecular systems capable of absorbing light accompanied by the excitation of electrons and exerting a specific function upon irradiation.[4] One of the best examples is certainly the natural chromophore chlorophyll, serving the purpose of a sensitizer for photosynthesis.
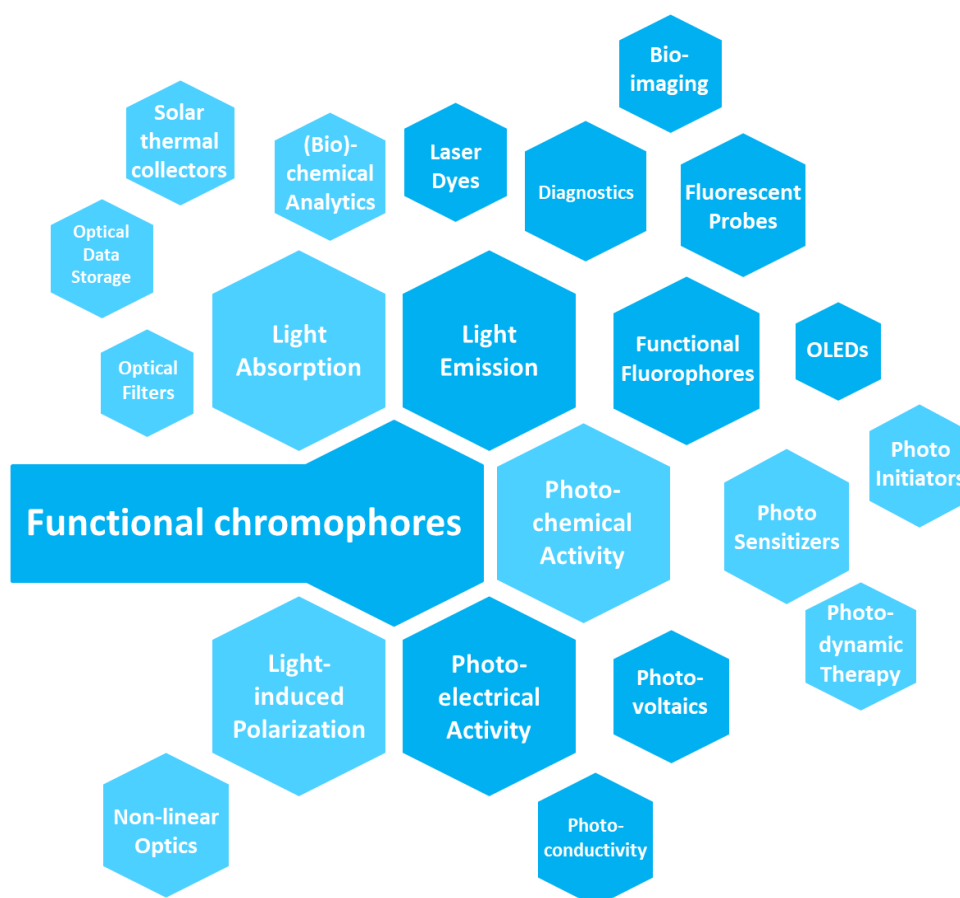
Figure 1. Classification of functional chromophores according to their properties and applications.

1.1.1   Luminescence

From glowing plants and insects to the pigments in the displays of digital devices, the occurrence and applications of luminescence are manifold, as are the mechanisms leading to luminescence phenomena. In general, luminescence describes the spontaneous emission of light upon the external excitation of certain materials. While there is a wide variety of types of luminescence depending on the external stimuli causing the emission of radiation, the most common type is certainly photoluminescence in which the excitation energy is provided in the form of photons. Photoluminescence itself can be subdivided into fluorescence and phosphorescence. These processes are displayed in the JABLONSKI diagram (**Figure 2**).[5]
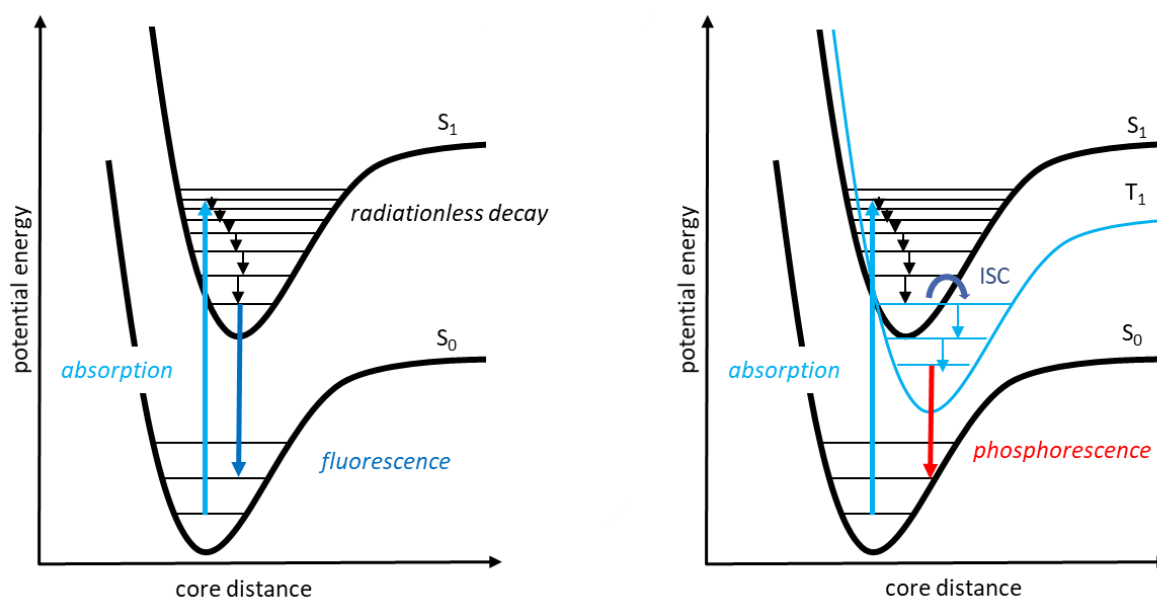
Figure 2. JABLONSKI diagram of fluorescence (left) and phosphorescence (right).

Excitation of a molecule from its electronic ground state (S_0) into an excited state (S_1) occurs vertically according to the FRANCK-CONDON principle. Since the electron density distribution is different in the S_1-state but the positions of the cores remain steady during the transition, the molecule excited into a higher vibrational level of the S_1-state. This additional energy is dissipated through vibrational relaxation, and the cores relocate to reach the vibrational ground state of the S_1-state. After a lifetime of 10^{-9} to 10^{-7} seconds, the excited molecule relaxates back to the electronic ground state by the emission of radiation observed as fluorescence. Due to the decreased energy gap between S_1 and S_0 in the altered geometry, the wavelength of the emitted radiation is commonly larger than the excitation resulting in the emission of red-shifted light, also referred to as STOKES shift.

In contrast, phosphorescence involves another excited state aside from the S_1-singlet state. Ordinarily, transitions from singlet states to the T_1-triplet state are spin-forbidden. However, by implementing heavier atoms or specific geometries, these strict rules do not apply anymore, resulting in an intersystem crossing (ISC) from S_1 to T_1. Relaxation from T_1 to S_0 will result in the emission of radiation. As this transition is technically also spin-forbidden, this process is slower. Phosphorescence's lifetimes can last from several milliseconds up to a few seconds.

The fluorescence at a specific wavelength (v) is characterized by three parameters: intensity (I_F), lifetime (τ) and quantum efficiency or yield (Q_E, Φ).[6] These variables are connected as follows.

$$(1) \quad Q_E = \frac{n \text{ (emitted Photons)}}{n \text{(absorbed Photons)}} = \frac{k_F}{k_F + \Sigma k_{nr}}$$

$$(2) \quad k_F = \frac{1}{\tau} = A_{21}$$

$$(3) \quad A_{21} = \frac{8\pi h v^3}{c^3} B_{12} \quad \text{with } B_{12} = \frac{e^2}{6\varepsilon_0 h^3} |R_{12}|^2$$

$$(4) \quad A_{21} \propto \varepsilon(v)$$

$$(5) \quad E_v = log \frac{I}{I_0} = \int \varepsilon(v) \, l \, c \, dv$$

$$(6) \quad \varepsilon(v) \propto f \text{ or } |R_{12}|^2$$

Q_E – quantum efficiency; n – number; k_F – rate constant of fluorescence; k_{nr} – rate constant of non-radiative pathways; τ – fluorescence lifetime; A_{21} – Einstein coefficient of spontaneous emission; B_{12} – Einstein coefficient of induced absorption; e – elementary charge; h – Planck constant; c – speed of light; ε – vacuum permittivity; $|R_{12}|$ – transition dipole moment; $\varepsilon(v)$ – extinction coefficient; v – wavelength; E_v – absorbance/extinction; I – intensity of transmitted light; I_0 – irradiation intensity; l – path length; c – concentration; f – oscillator strength.

Q_E is proportional to the fluorescence rate k_F (**Eqn. 1**) which is reciprocal to the lifetime (**Eqn. 2**).[6] The rate k_F is derived from the transition probability for spontaneous emission. Einstein postulated the connection of the transition probabilities for induced absorption B_{12} and spontaneous emission A_{21} (**Eqn. 3**).[7] According to the STRICKLER and BERG or BIRKS and DYSON relationship derived from the EINSTEIN coefficient, the excited state or fluorescence lifetime is proportional to the absorption intensity (**Eqn. 4**),[8] defined by LAMBERT-BEER's law (**Eqn. 5**).[5] In the equation for absorption intensity, the wavelength-dependent extinction coefficient ε is related to the oscillator strength f, a dimensionless constant corresponding to the transition dipole moment (**Eqn. 6**).[7] To put it simply, the transition dipole moment describes a molecule's ability to absorb and emit electromagnetic radiation. It depends on the orbital overlap of the involved states and, in turn, on the transferred charge over distance. Thus, oscillator strength is a critical parameter to assess fluorophore efficiency. From a structural point, maintaining good transition dipole moment and oscillator strength values, *e.g.*, *via* extensive π-systems with a substantial frontier molecular orbital overlap and charge distribution, therefore is a key design element for fluorophores.

The absorption and emission wavelength can be shifted by altering the gap between the ground and the respective excited state. Typically, larger π-systems correspond to longer wavelengths.

1.1.2 Advanced Fluorescence Mechanisms

In reality, the general mechanisms of fluorescence and phosphorescence rarely apply. Instead, more complex processes occur when molecules are irradiated, depending on their molecular structure and electronic properties. Additionally, as the molecules cannot be observed individually, environmental influences such as solvent effects, intermolecular and bulk interactions or external quenching pathways must be considered.[9] Commonly observed effects include solvatochromism, in which the stabilization of the excited species by the solvent leads to shifting of the emission wavelength depending on solvent polarity.[10] Aside from this, several special mechanisms apply depending on the molecular structure itself, of which some will be discussed in detail.

ESIPT. Certain molecules can undergo photoreactions when irradiated, such as excited state intramolecular proton transfer (ESIPT).[11] This four-level process (**Figure 3-left**) is an example of phototautomerizations which occurs when different tautomers are stabilized in the ground and excited state. Most ESIPT-fluorophores rely on photo-induced keto-enol tautomerism.[12] Selected, commonly used ESIPT scaffolds are depicted in **Figure 3-right**. In the ground state, the enol is usually more stable. Upon excitation, the charge distribution throughout the molecule is altered, stabilizing the keto form. From there, the molecule relaxates to the keto ground state. The decreased energy gap between S_1 and S_0-state thus results in a significantly increased STOKES shift for the keto emission. In the ground state, tautomerization to the more stable enol form occurs *via* a reverse proton transfer.
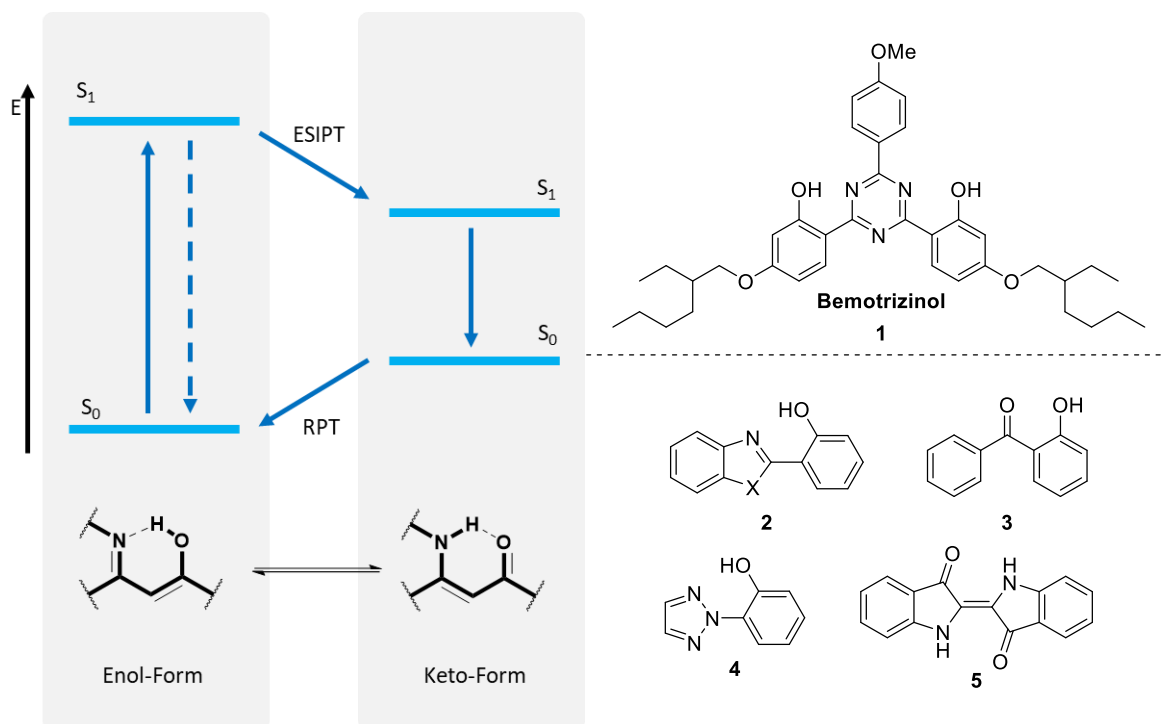
Figure 3. Simplified JABLONSKI diagram illustrating the ESIPT process (left) and examples for ESIPT fluorophores (right).

This effect can be used to design molecular switches and sensors.[13] By implementing a capping mechanic or a protecting group to suppress the ESIPT-process, the sensor is switched off. The sensor is switched on by removing

this group, leading to a significant shift in fluorescence color, thus indicating the presence of the deprotecting species.

This design principle has also been exploited for the development of optical filters. In this case, the transition to the tautomeric ground state is not accompanied by light emission. Instead, deactivation occurs *via* radiation emission outside of the visible range (*e.g.*, infrared) and the energy is dissipated thermally.[14] One of the most prominent examples is certainly the UV-absorber Bemotrizinol (**1**).

TADF. Another mechanism that has been discussed in terms of OLEDs is thermally activated delayed fluorescence (TADF).[15] **Figure 4** depicts the differences between the TADF effect and the other luminescence phenomena. In real systems, the excited states are not entirely decoupled. Hence, when molecules are excited, singlet and triplet states are populated according to spin-statistics, resulting in a distribution of 1:3.However, fluorescence, only occurs from the singlet state which means only one-fourth of the excitons can be harvested. The internal quantum efficiency (IQE) is thus capped at 25%. In phosphorescent emitters, the emission occurs from the triplet state, which is constantly repopulated from singlet excitons *via* intersystem crossing. Therefore, the IQE is not limited by spin statistics. Despite this, phosphorescent emitters pose several disadvantages, as they are commonly made up of transition metal complexes with either expensive, rare or toxic heavy metal atoms like iridium or platinum.
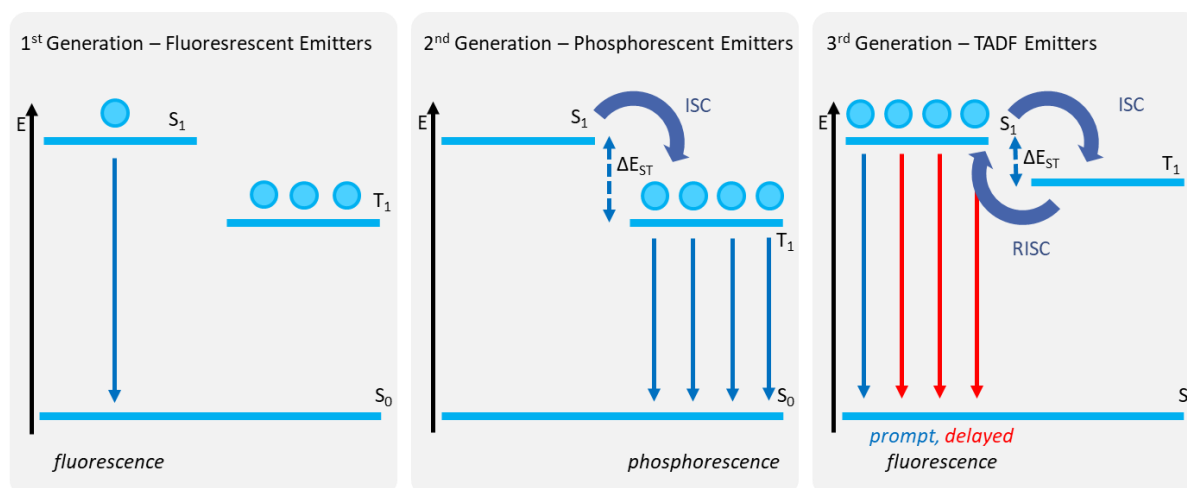
Figure 4. Simplified Jablonski diagrams for the three generations of OLED emitter design.

In contrast, TADF fluorophores are organic compounds designed to have a small energy gap between the S_1 and T_1 state enabling excitons to transit this gap by reverse intersystem crossing to populate the S_1 state. The width of ΔE_{ST} needs to be lower than 0.2 eV for thermal energy to enable the RISC. The repopulated S_1 state can be harvested to achieve efficient emission. The RISC process occurs over a timespan of milliseconds, resulting in an extended fluorescence lifetime, the delayed fluorescence. In transient photoluminescence (PL) decay measurements, TADF emitters show both a prompt decay in the order of nanoseconds which can be attributed

to the S_1 to S_0 transition, and a delayed decay in the microsecond range corresponding to the TADF effect. At lower temperatures, the lifetime is not prolonged, which serves as proof of the TADF effect.

Historically, the TADF behavior was first observed for Eosin in an ethanolic solution at elevated temperatures.[16] Acetophenone, thioketones and fullerene also exhibit this effect.[17] The first compounds of a novel generation of emitters based on the TADF principle were developed by ADACHI *et al.*,[18] and since then, several emitter designs have been established, including dinuclear copper complexes, borine-based compounds or purely organic molecules. A selection of relevant TADF emitters is shown in **Figure 5**.
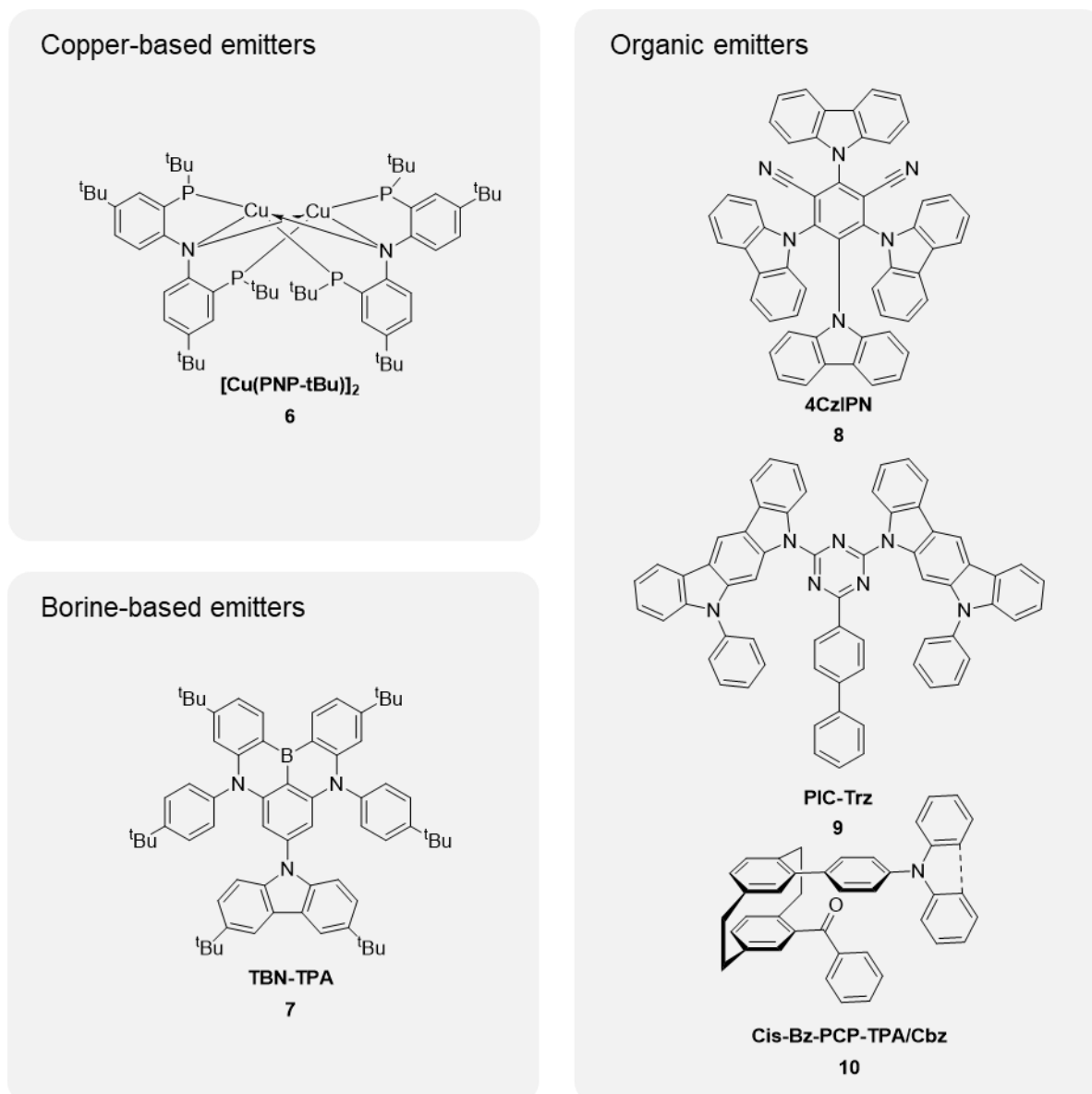
Figure 5. Selected examples for copper-, borine-based and organic emitters.

The underlaying design principles originate from theoretical considerations (see **Eqn. 7 – 9**).[19] The rate of RISC (k_{RISC}) is proportional to ΔE_{ST} which is, in turn, proportional to the exchange integral of HOMO and LUMO, J_{12}. Consequently, a small spatial overlap (*i.e.*, exchange integral approaching zero) of the frontier orbitals leads to a small ΔE_{ST} (< 0.1 eV), enabling the TADF effect.

$$(7)\ k_{RISC} \propto\ e^{-\frac{\Delta E_{ST}}{k_B T}}$$

$$(8)\ \Delta E_{ST} = E_s - E_T = 2J_{12}$$

$$(9)\ J_{12} = \iint \phi_{HOMO}(r_1)\ \phi_{LUMO}(r_2) \frac{1}{|r_2 - r_1|} \phi_{LUMO}(r_1) \phi_{HOMO}(r_2) dr_1 dr_2$$

k_{RISC} –RISC rate constant; k_B – Boltzmann constant; T – temperature; ΔE_{ST} – singlet-triplet energy gap; E_S / E_T – singlet/triplet energy level; J_{12} – exchange integral; ϕ – wave function, r – position vector.

This spatial separation can be accomplished by installing a bridge between donor and acceptor moiety that induces a twist to minimize the overlap. Alternatively, spiro junctions and through-space bridges have been demonstrated to introduce a minimal overlap between the frontier orbitals. An overview of common TADF-building blocks is given in **Figure 6**.[20]
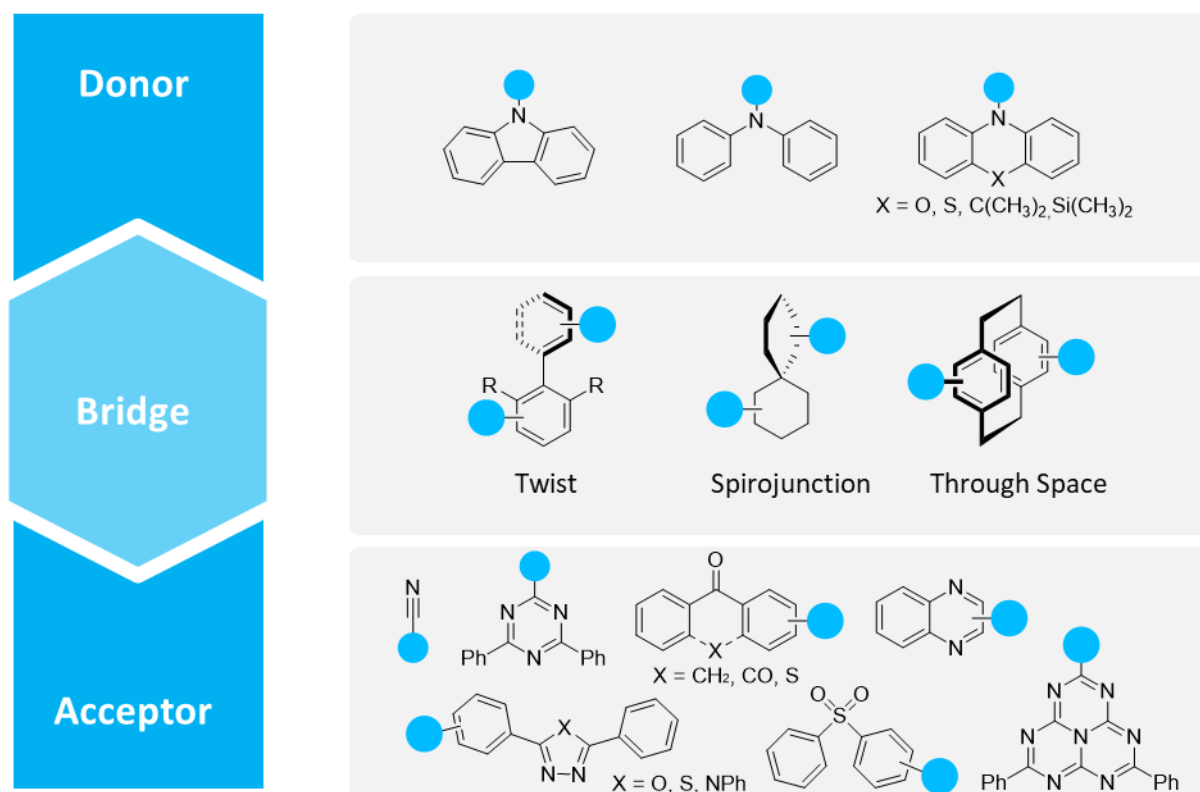
Figure 6. Design principle and exemplary donor, acceptor, and bridge building blocks for organic TADF emitters.

However, minimizing spatial separation also decreases S_1-S_0 overlap and therefore the transition dipole moment, oscillator strength and radiative decay rate, thus rendering the emitters less efficient. An alternative method to increase oscillator strength is large delocalization of the frontier orbitals. Balancing orbital overlap to obtain low ΔE_{ST} values while retaining a reasonably high oscillator strength is crucial for the design of efficient TADF emitters.

FRET. The FÖRSTER resonance energy transfer describes a common bimolecular fluorescence mechanism. In this process, one molecule is excited by absorbing light, and instead of deactivation *via* emission, the energy is transferred through nonradiative dipole-dipole coupling from this donor molecule to an acceptor, which, in turn, is excited and then able to emit radiation itself (**Figure 7**).[21]
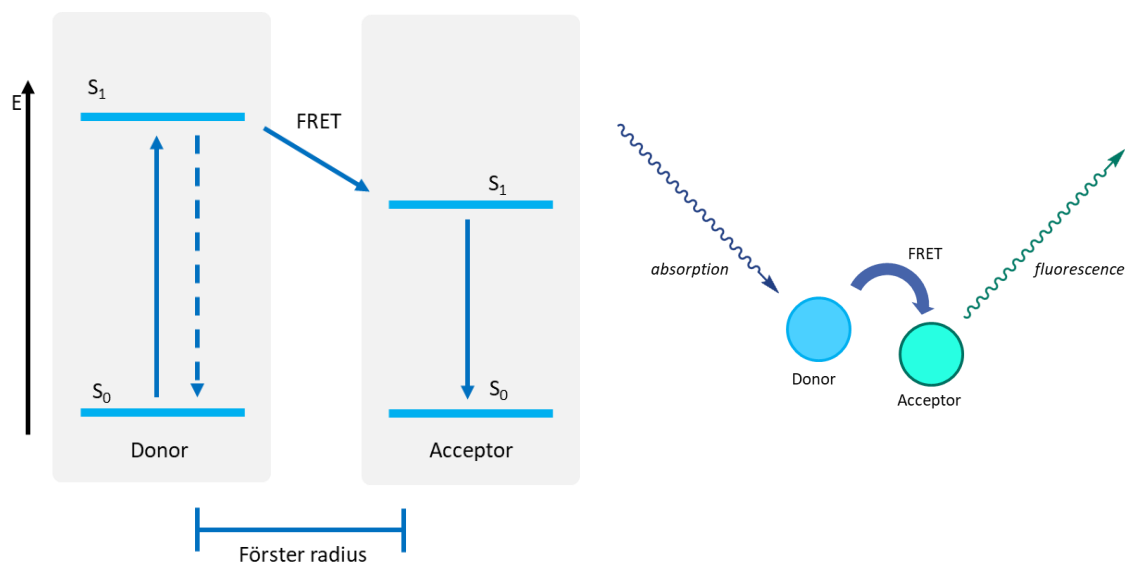
Figure 7. Simplified JABLONSKI diagram (left) and schematic illustration of the FRET process (right).

This effect is proximity-dependent and requires donor and acceptor to be located within the so-called FÖRSTER radius. Consequently, this mechanism is often used for designing fluorescent probes to investigate spatial interactions.[22] For instance, FRET pairs can be attached to different sites within a molecule to monitor conformational changes. Attaching donors and acceptors to different substrates allows us to study the interactions of these substrates.

1.1.3   Applications of Functional Chromophores

Since the introduction of microscopic analysis methods, the request for special purpose fluorophores has increased steadily.[23] Moreover, outside of biochemistry, there is a high demand for functional fluorophores and chromophores in, for instance, material science applications as part of OLEDs,[24] lasers,[25] solar cells,[26] or data storage,[27] and in cosmetics[28] and art[29] as optical brighteners, UV-absorbers, highlighters, or reactive dyes.[30] Therefore, sophisticated fluorophores are needed, which are custom designed to fit increasingly complex prerequisites. Modular design strategies enable facile tuning of the properties by variation of the individual building blocks. In general, one of the main goals is designing more efficient fluorophores by increasing quantum yield, minimizing non-radiative deactivation pathways, and preventing photobleaching. Aside from this, other tunable properties depend on the application, of which some are discussed hereinafter.

Bioimaging. The development of fluorescence microscopy constitutes a big milestone for the high-resolution elucidation of small cellular structures, even beyond the limits of conventional microscopy. Some biomolecules exhibit intrinsic fluorescence, *e.g.,* aromatic amino acids like tryptophane. To investigate structures without intrinsic fluorescence (lipids, steroids, nucleic acids, *etc.*), extrinsic fluorophores have to be introduced to stain the respective compartments.[31]

The specific purpose, however, demands a careful fluorophore selection. For instance, the compatibility of the fluorophore and the investigated environment must be considered.[32] Solubility in the respective (mainly aqueous medium) and cellular uptake are crucial parameters that can be managed by introducing polar residues, molecular carriers, or encapsulation. For *in vivo* experiments, low toxicity is preferable.[33] Moreover, the absorption and emission profile of the fluorophore are an important factor as irradiation of cell or tissue samples with UV-light promotes UV-induced DNA-damage and thus apoptosis. Therefore, shifting the fluorophore's absorption to the visible range is beneficial as irradiation with visible light is less harmful, reduces the autofluorescence of surrounding compartments, and is able to transverse deeper into the tissue.[34]

For the target-oriented staining of specific compartments, it is important to manage the fluorophore's affinity to the structure of interest. Fluorophores can either be designed to exhibit properties that enhance their affinity to the target biomolecules, *e.g.*, flat, polar molecules for nucleic acids or lipophilic structures for lipid membranes or attached to a carrier that is known to locate at or bind to the respective target.[35] In turn, fluorophores can also be employed as fluorescent tags which are covalently bound to a carrier molecule or bigger structures to visualize them in experimental setups and investigate their behavior (*e.g.*, localization) within cells.[36] For this, the fluorophore's properties are required not to influence the behavior of the analyte molecule. Therefore, comparably small fluorophores are needed in localization studies of small molecule analytes.[37]

Aside from *in vivo* analysis, fluorescent or chromophoric tags are also employed as stains in *in vitro* assays, such as nucleic acid or protein stains in gel electrophoresis, or tagged antibodies and enzymes in ligand binding or immunological assays.[38] Alternatively, detection is also possible through external fluorescent probes which are switched on in the presence of certain enzymes.

Fluorescent Probes. Aside from visualizing the presence of proteins, enzymes, antibodies, or other biomolecules, fluorescent probes can also be used as chemosensors to detect other species like certain ions, molecules, or functional groups. They rely on a switching mechanism resulting in an optical signal only triggered by the analyte. Commonly used design strategies are the coordination of metal ions to the probe or certain functionalities that induce intramolecular reactions or cleave off protecting groups or quenchers, thus enabling fluorescence. Aside from conventional fluorophores, ESIPT and FRET probes are often chosen due to their inherent switching method.[13b, 22]

OLEDs. In contrast to the applications discussed above, OLED chromophores rely on electroluminescence instead of photoluminescence.[39] In an OLED device, the emissive dye layer is embedded between two electrode layers separated by injection and conductive layers (**Figure 8**).[24b, 40]
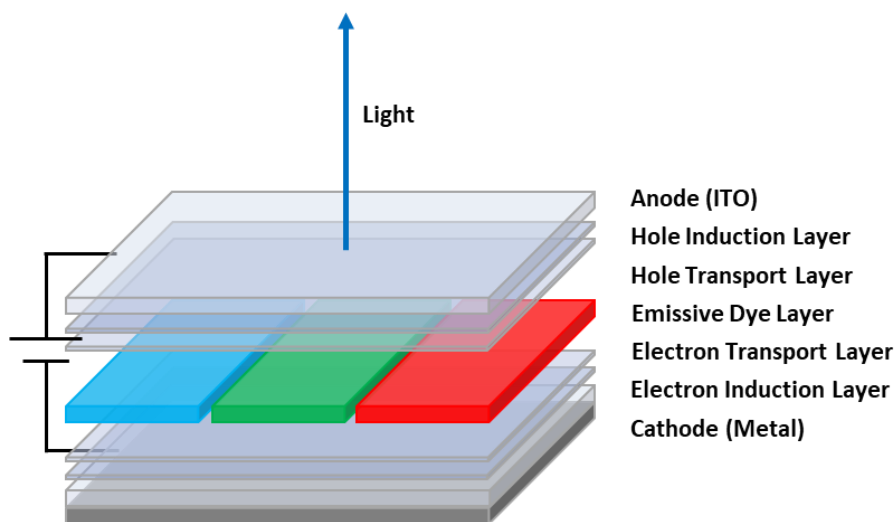
Figure 8. Schematic representation of a multilayer OLED.

Through applying an external voltage, electrons are injected into the LUMO of the dye molecules while holes are injected into the HOMO by the anode. These charge carriers migrate through the dye layer towards the opposite electrode until they recombine under the formation of excitons. These excited dye molecules relaxate under the emission of radiation. The anode is commonly made of transparent material like indium tin oxide (ITO) to allow the light to leave the device. Metallic cathodes and the conductive layers are made of large, conjugated molecules to enable good electron mobility, such as electron-rich conjugated nitrogen-heterocyclic systems for hole transport or electron-deficient borine-based substrates for electron transport. The injection layers consist of materials that mediate and facilitate the electron induction or abstraction processes, *e.g.*, polymers for holes, and metals or alkali metal fluorides for electrons. The core of the OLED, the emissive layer consists of the dye which can also be surrounded by host material. The dyes have evolved throughout the history of OLEDs to be more efficient and environmentally benign as discussed in **Chapter 1.2 – TADF**. However, there is still room for optimization as currently, especially blue OLEDs are still lacking in terms of efficiency.[41]

In 2021, ADACHI and co-workers exploited the FRET-mechanism to develop hyperfluorescent, deep-blue OLEDs.[42] By employing a TADF molecule as FRET-donor, an efficient energy transfer of all singlet and triplet excitons to the acceptor can be achieved. The acceptor then emits light of a specific wavelength. By exchanging the FRET acceptor, different emission wavelengths are accessible. The major advantage of this hyperfluorescence approach is the decoupling of the TADF effect and emission wavelength, enabling the fabrication of unprecedented efficient OLEDs of previously inaccessible colors.

Optical and UV-Filters. Depending on their excitation profile, organic chromophores can selectively filter light of a certain wavelength by absorbing and then dissipating the energy while other light is unaffected. Due to their well-defined and easily adjustable absorption bands, absorptive organic compounds either in solution or embedded in a solid matrix can be applied as optical filters which are used in, for instance, colorimeters. Aside from absorptive materials, other optical filters rely on light reflection, polarization, or interference.[14]

A special class of optical filters are UV-filters. The exposure of human skin to UV radiation causes tremendous damage, leading to various kinds of diseases including skin cancer. Similarly, outdoor surfaces often suffer from photodegradation upon extended irradiation with sunlight. As shown in **Figure 9**, UV-radiation is divided into three categories with increasing energy: UV-A (400 – 315 nm), UV-B (315 – 280 nm) and UV-V (280 – 100 nm).
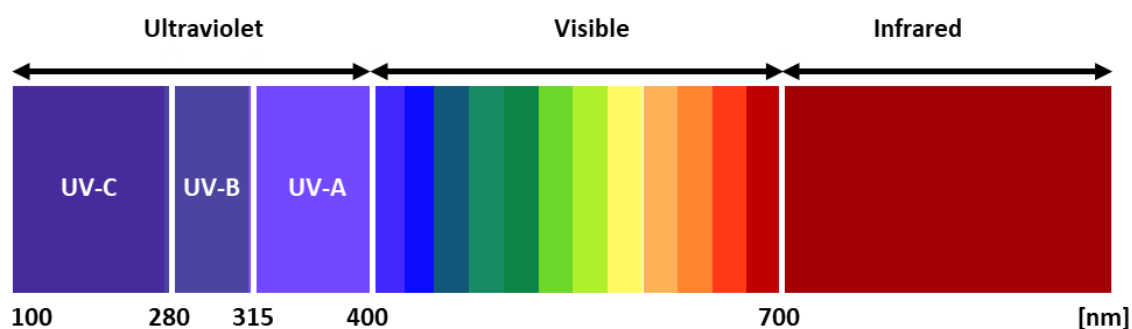
Figure 9. Cut-out of the electromagnetic spectrum.

The main part of UV-rays is already blocked by the earth's atmosphere, so the UV-portion of terrestrial sunlight is reduced to about 3%.[43] To protect human skin as well as outdoor surfaces and coatings against this remaining UV-radiation, several types of UV-filtering substances have been developed. UV-filters and their formulations are characterized depending on their absorption profile as UV-A, UV-B, or broad band filters, and by their sun protection factor (SPF).[44] The SPF describes the extension of exposure time to UV-B-radiation in which no damage is inflicted on the skin or surface. It is calculated according to **Eqn. 10** as a function of the spectrum of sunlight $E(v)$, the erythemal action spectrum $A(v)$ and the monochromatic protection factor $MPF(v)$ which depends on the transmission. Additionally, the UV-A-protection factor describes the efficiency against UV-A rays.

$$(10) \ SPF = \frac{\int A(v)E(v)dv}{\int A(v)E(v)MPF(v)dv}$$

SPF – sun protection factor; *A* – erythemal action spectrum; *v* – wavelength; *E* – spectrum of sunlight; *MPF* – monochromatic protection factor.

Inorganic compounds like titanium dioxide, certain iron oxides or zinc oxide nanoparticles either absorb UV-radiation due to their band gap or scatter the light as a result of their particle size.[45] Organic UV-filters, on the other hand, operate by absorbing the UV-light and re-emitting the energy in the form of lower energy radiation.[46] For this, large STOKES shifts are necessary to efficiently dissipate the energy. ESIPT-type absorbers are therefore ideal as they possess inherently large STOKES shifts. Common ESIPT-scaffolds are hydroxyphenyl triazines (Bemotrizinol, **1**), hydroxyphenyl triazoles (Bisoctriazole, **11**), hydroxy benzophenones

(Sulisbenzone, **12** or Uvinul A+, **13**), salicylates (Homosalate, **15**) or 1,3-diketones (Avobenzone, **14**). Other UV-filter types include alkenes like camphor derivatives (Enzacamene, **17**) or cinnamates (Octinoxate, **16**), and extensive π-scaffolds (Isoctrizinol, **18**). Some of the most prominent commercial organic UV-absorbers are depicted in **Figure 10**.[21a, 47]
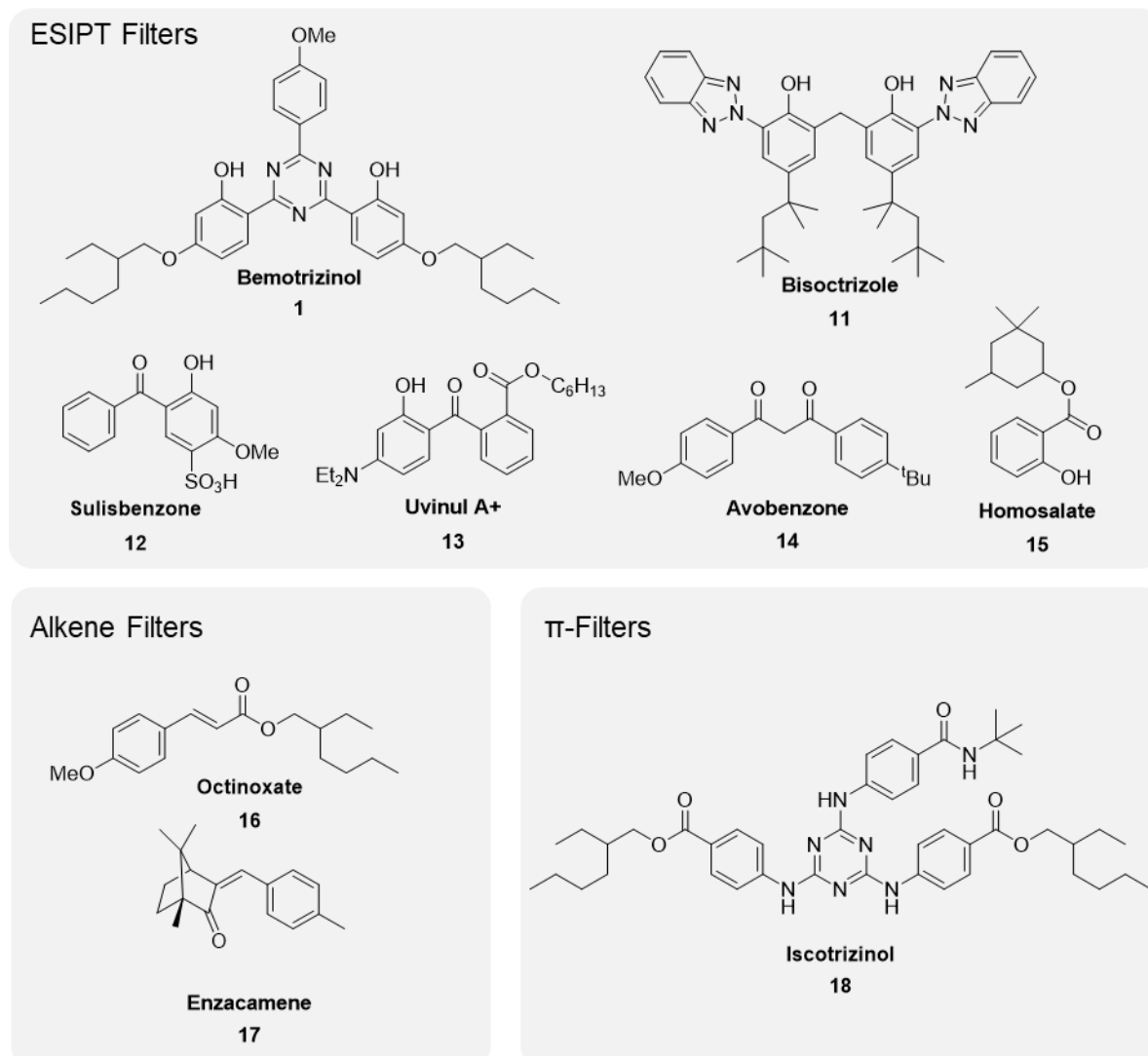
Figure 10. Structures of selected commercially available UV-absorbers.

In sunscreens, mixtures of these absorbers are employed to further improve their performance due to synergistic effects. However, some small molecule organic UV-absorbers have severe drawbacks, exhibiting unwanted bioactivities. Some substances, especially of the benzophenone type, show estrogenic effects, hinting towards genotoxicity. Accumulation in the environment has been observed, posing a threat to aquatic ecosystems. Additionally, some are lacking in terms of photostability, showing degradation upon extended irradiation times. Hence, novel, non-toxic and environmentally benign UV-absorbers are sought after. Over the last decade, progress in the development and commercialization of UV-absorbers has been delayed as the US market was inaccessible which was caused by restrictions in the FDA approval of new compounds. In 2014, the Sunscreen Innovation Act was passed to improve revision of UV-absorbers already approved in *e.g.*, Europe and Australia.[48]

1.2 Multicomponent Reactions

Among the vast variety of chemical transformations, the reaction class of multicomponent reactions (MCRs) stands out thanks to their unmet variability and diversity.[49] In contrast to conventional multistep synthesis approaches, MCRs describe the transformation of three or more starting materials to a complex product molecule in which the majority of the starting materials' atoms are incorporated. Consequently, the number of by-products is quite low, and the overall atom economy is excellent. Thus, MCRs offer convenient shortcuts for the assembly of sophisticated structures, also cutting down on the overall number of reaction and purification steps needed to achieve a certain degree of complexity.[50] Since most MCRs rely on condensation chemistry, they are operationally simple one-pot procedures and usually do not demand harsh or inert reaction conditions while having a high functional group tolerance. Hence, MCR methodologies are often regarded as sustainable tools meeting the criteria of green chemistry.[51] Due to these advantages, MCRs nowadays find widespread application across many different disciplines of organic,[52] medicinal,[53] and polymer chemistry.[54] A schematic comparison of multistep synthesis and MCR methodology is shown in **Scheme 1**.
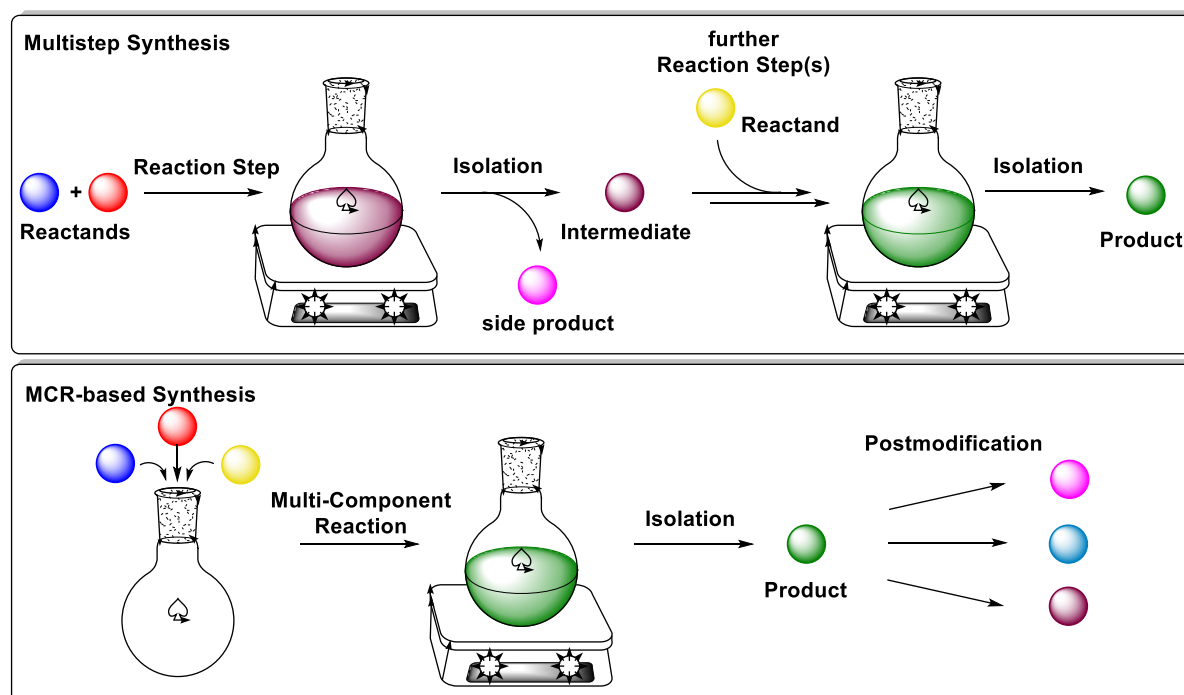
Scheme 1. Comparison of multistep synthesis and MCR methodology.[55]

Some noteworthy examples are shown in **Scheme 2**. Historically, the first MCR was the STRECKER reaction, a racemic method for the synthesis of α-amino acids (**22**) from aldehydes (**19**), a cyanide (**20**) and ammonia (**21**).[56] Another prominent example is the MANNICH aminomethylation of ketones (**23**) using formaldehyde (**25**) and amines (**24**).[57] In contrast to this, the HANTZSCH dihydropyridine synthesis[58] and the BIGINELLI dihydropyrimidone synthesis[59] afford heterocyclic structures, giving access to more drug-like scaffolds. Similarly, in the GEWALD reaction 2-amino thiophenes (**33**) are synthesized from ketones (**23**), nitriles (**31**), and elemental sulfur (**32**).[60]

In the PETASIS reaction, an aldehyde (**19**), a boronic acid (**34**) and an amine (**24**) are coupled to diversely substituted tertiary amines (**35**).[61]
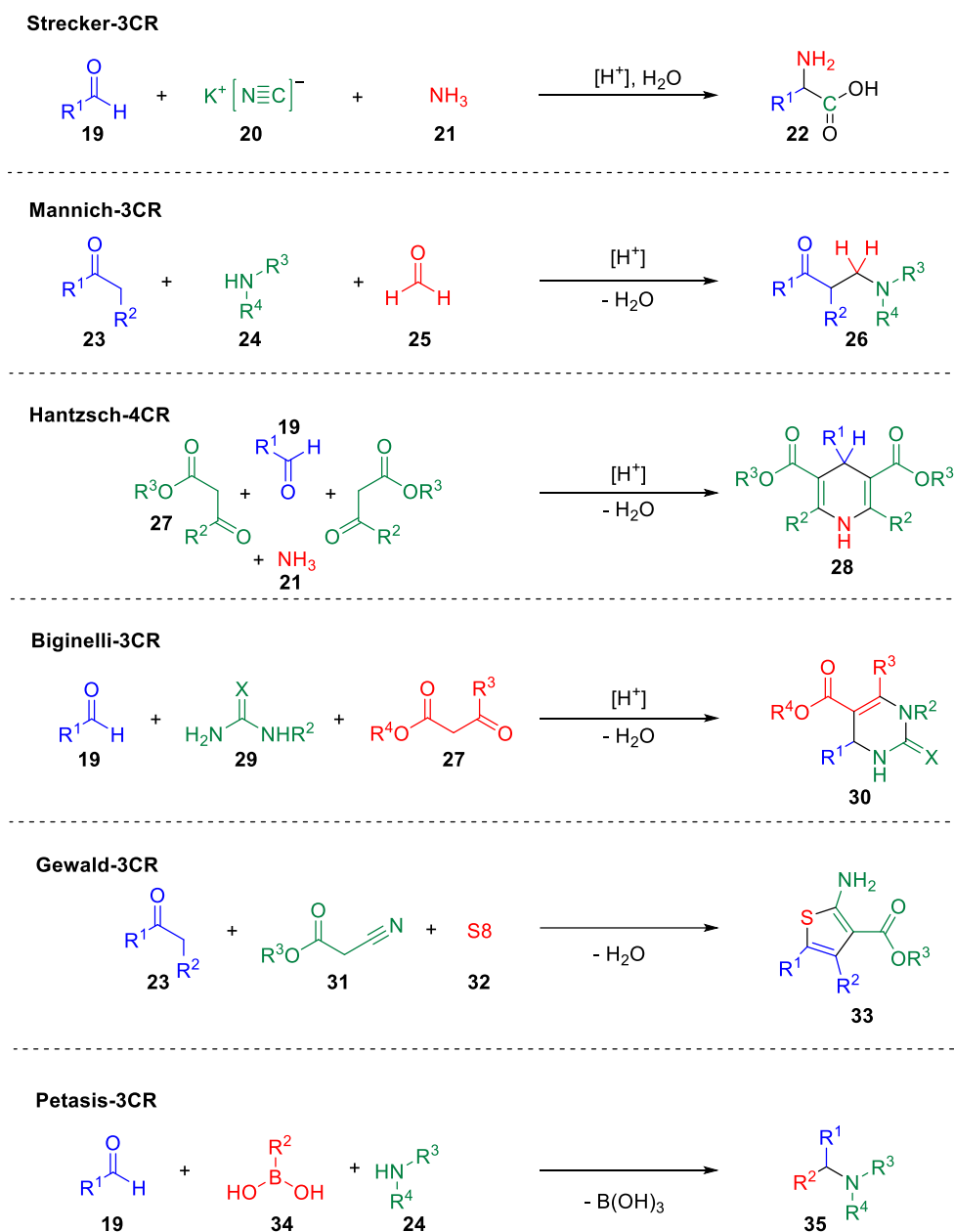
Scheme 2. Overview of historically relevant MCRs.

Granting facile access to a vast chemical space, MCRs are the prime examples of modular, yet straightforward diversity-oriented synthesis methods. Thus, they are ideally suited for the rapid generation of extensive compound libraries meeting the demand of high throughput screening platforms in medicinal and pharmaceutical chemistry.[62] Estimates show that at least 5% of the small molecular drugs sold in 2019 could be accessed through MCR-based synthesis routes.[63] Selected examples for marketed drugs accessible *via* MCR-methodologies are presented in **Figure 11**, including the calcium channel blocker Nifedipine (**36**), the antipsychotic Olanzapine (**37**), the local anesthetic Lidocaine (**38**), the antiviral HIV-medication Indinavir (**39**) and the statin Atorvastatin (**40**).
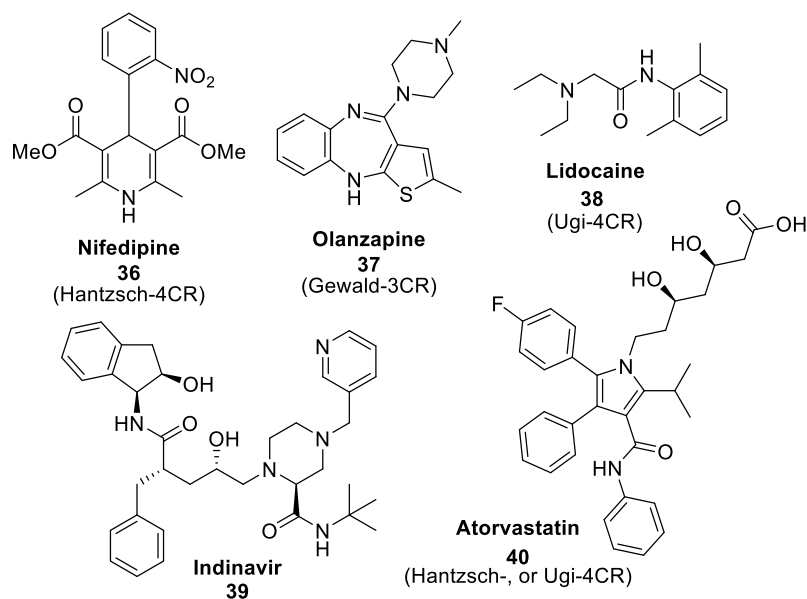
Figure 11. Examples for marketed drugs accessible *via* MCR methodologies. The MCR involved in the synthetic route is indicated in parentheses.

1.2.1 Isonitriles and IMCRs

In the context of multicomponent reactions, the substance class isonitriles, frequently also referred to as isocyanides, is of particular importance. That is not without reason, as isonitrile-based multicomponent reactions constitute their own category within the field of MCR transformations.[64] Isonitriles have attracted attention in view of their peculiar, multi-facetted reactivity, but at the same time, they are notorious for their repugnant, yet unique smell.[65] However, aside from a few exceptions, they do not exhibit any notable toxicity to mammals as investigated by the BAYER AG in the 1960s.[66] There are even plenty of naturally occurring isonitriles, some examples are depicted in **Figure 12, top**. Natural products like the antibiotic xanthocillin or the antifungal agent welwitindolinone A have been discovered in (cyano-)bacteria, fungi, or marine sponges, exhibiting a variety of bioactive properties.[67] Recently, isonitriles thus gained attention as potential pharmacophores despite having been disregarded due to their potentially limited metabolic stability for a long time.[68] A few artificial isonitrile-based substances have also been investigated as potential drugs (**Figure 12, bottom**), *e.g.* 1-adamantyl isonitrile as an antiviral agent,[69] or are already marketed like the nuclear imaging agent Tc-MIBI (Cardiolite).
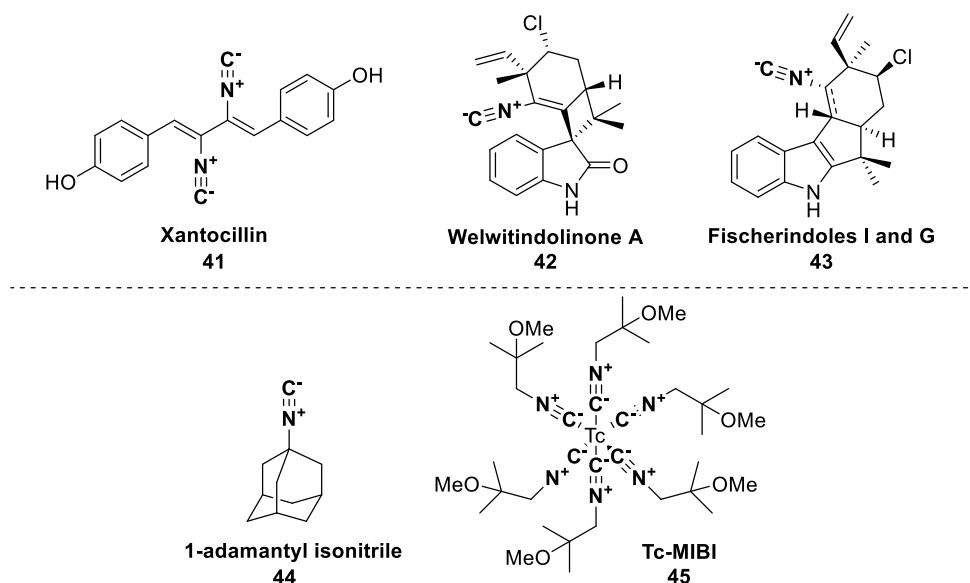
Figure 12. Natural products containing an isonitrile moiety (top) and isonitrile drugs (bottom).

The isonitrile group can be described by the resonance structures depicted in **Figure 13**. The carbenoid structure **46'** is more stable, thus dominating the electronic properties. On the other hand, the zwitterionic resonance formula **46** is more appropriate to explain their linearity. This extraordinary electronic structure results in the broad variety of reactivity of isonitriles.[70]
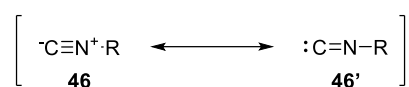
Figure 13. The zwitterionic (left) and the carbenoid (right) resonance structure of the isocyano group.

Along with *N*-heterocyclic carbenes and carbon monoxide, isonitriles are amongst the few stable organic substance classes with a formally divalent carbon atom. Consequently, they are quite reactive since isonitrile transformations are driven by the exothermic and practically irreversible oxidation of C^{II} to C^{IV}. Hence, short reaction times and high yields can be achieved even at ambient temperatures. Moreover, considering their ambiphilic carbon atom, isonitriles possess the unique ability to perform α-addition reactions. In this process, a reaction with a nucleophile and an electrophile takes place on the same atom simultaneously rather than on different reaction sites. which is commonly exploited in IMCRs enabling cascade reactions. Owing to these properties, isonitriles offer great synthetic possibilities and play a key role in the field of MCRs. Aside from this, isonitriles also possess a quite pronounced α-acidity due to the strong electron-withdrawing nature of the isocyano group.[71] As they are isoelectronic to carbon monoxide, isonitriles can also serve as ligands for transition metals in a similar way.[72] Their ability to coordinate to palladium also allows them to insert into newly formed C-C-or C-X-bonds in cross coupling reactions. In analogy to carbonylation reactions through CO insertion affording ketones, these transformations are referred to as imidoylation reactions (**Scheme 3**).[73]
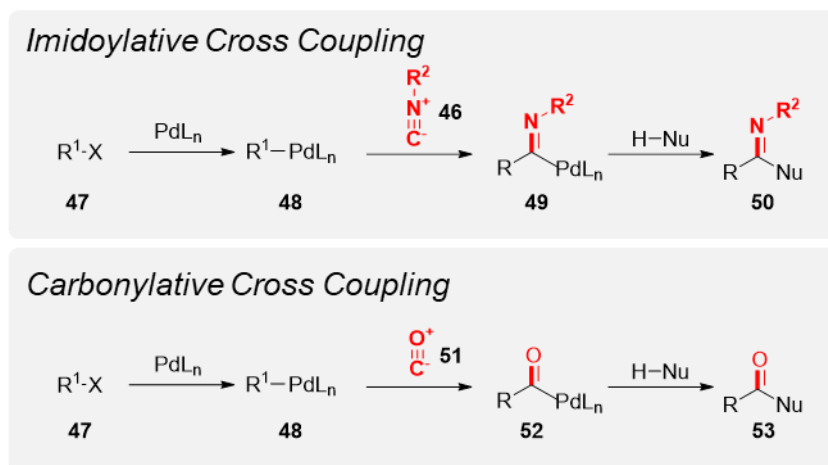
Scheme 3. Comparison of Pd-catalyzed imidoylative and carbonylative cross coupling reactions.

Synthetically, isonitriles are accessible *via* a variety of different routes as shown in **Scheme 4**.[8]
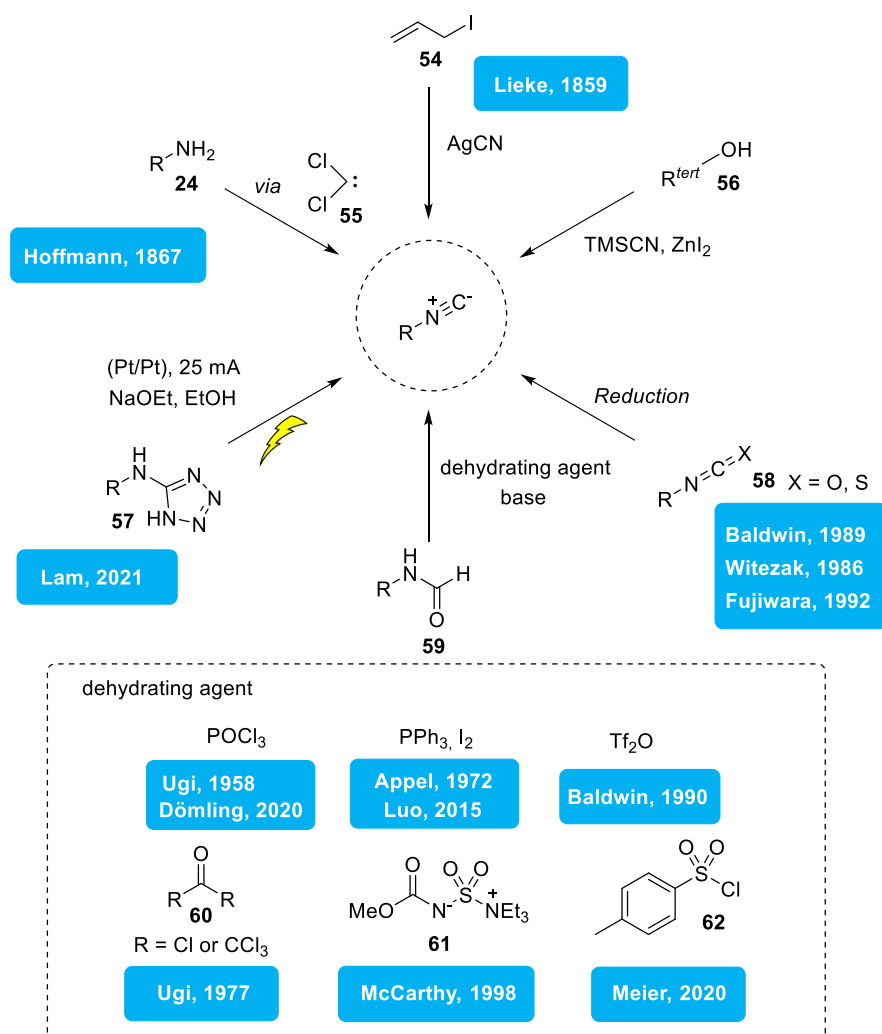
Scheme 4. Synthetic routes towards isonitriles.

In 1859, the first ever route towards isonitriles was reported by LIEKE.[74] Mistakenly published as a synthesis of allyl cyanide, allyl iodide (**54**) was reacted with silver cyanide in an S$_N$2 reaction. The silver cation acts as a protecting group, masking the cyanide's carbon atom and enabling the nucleophilic attack of the nitrogen atom. While historically relevant, nowadays this reaction is rather a synthetic curiosity due to its limited scope and applicability. A more practical approach was first published by HOFFMANN in 1867, in which primary amines (**24**) are reacted with dichlorocarbene (**55**) generated from chloroform and potassium hydroxide.[75] A similar method was reported in 2020 by SI *et al.* employing difluorocarbene.[76] The most popular route towards isonitriles, however, is the dehydration of formamides (**59**). The first method by UGI and MEYER from 1958 employs phosphoryl chloride as dehydrating agent and pyridine as the base.[77] Since then, several similar reactions of dehydrating agents and bases have been developed, especially focusing on improving the sustainability of isonitrile synthesis.[78] Aside from these, other approaches include the conversion of tertiary alcohols (**56**) or epoxides,[79] as well as the reduction of isocyanates or isothiocyanates (**58**).[80] Recently, LAM *et al.* reported an entirely novel route towards isonitriles in which tetrazoles (**57**) are electrochemically converted under the evolution of nitrogen.[81]

One of the main applications of isonitriles are isonitrile based multicomponent reactions (IMCRs). The PASSERINI-3CR published in 1921 constituted the first example for the subclass of IMCRs.[82] However, IMCRs did not receive much attention until the discovery of the UGI-4CR in 1959 by IVAR UGI.[83] In the classical PASSERINI-3CR and UGI-4CR, carboxylic acids (**63**), aldehydes (**19**) and isonitriles (**46**) (and an amine **24** in the UGI-4CR) are transformed into α-acyloxy amides (**64**) or bis-amides (**65**), respectively. The general reactions are depicted in **Scheme 5**.
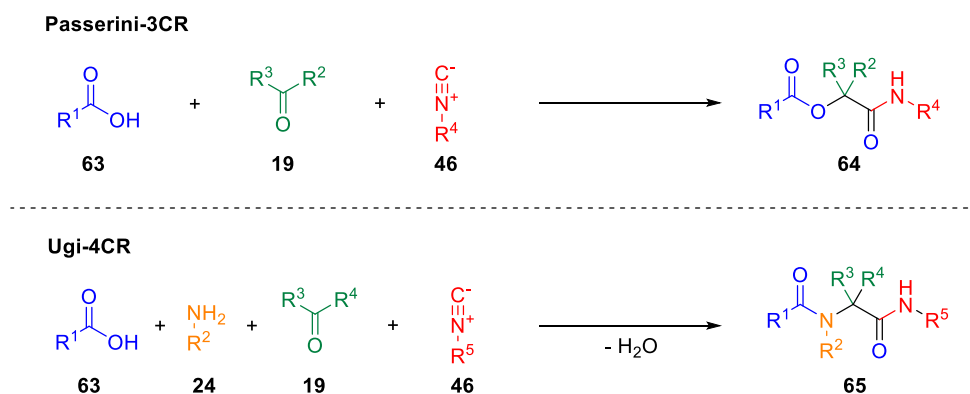
Scheme 5. The PASSERINI and UGI reactions.

Over the years, the acid component has been substituted by a variety of other reagents to develop different variations of the original reactions, *e.g.*, PASSERINI- or UGI-SMILES reactions with phenols.[84] Furthermore, variations using multifunctional components also increase the accessible substrate scope and enable possibilities for the post-modification of these linear scaffolds.

In terms of variety, the isonitrile component is often quite limiting due to the scarce availability of commercial isonitriles. Thus, more complex, custom isonitriles have to be synthesized in a separate procedure. However, as their limited stability, as well as the obnoxious smell, pose quite a big challenge for synthesis and purification,

avoiding the isolation of the isonitrile is preferable. For instance, in a procedure developed by DÖMLING *et al.* the isonitrile is formed *in situ* from the respective formamide by dehydration using triphosgene and consecutively mixed with the other MCR components.[85] This allows for a facile introduction of novel isonitrile-derived residues into MCR-scaffolds and enlarging the overall scope of isonitrile components while circumventing the inconvenient separate dehydration and isolation of the possibly sensitive isonitrile itself.

1.2.2   MCR-based Strategies in chromophore Synthesis and Bioconjugation

Due to their broad, yet unique reactivity, MCRs have been applied for the conjugation or labeling of biological compounds.[86] For instance, MCRs have already been employed for the bioconjugation or immobilization of lipids, carbohydrates, oligosaccharides, steroids, peptides, enzymes, and antibodies. Aside from MCRs, isonitriles are also employed in coordination ligation for transition metal complexes.

Regarding the combinatorial synthesis of functional chromophores, both for the design of tailored pigments, emitters, and sensors, as well as the introduction of chromophore tags to biomolecules, two concepts have emerged: scaffold approach and chromophore approach (**Figure 14**).[87]
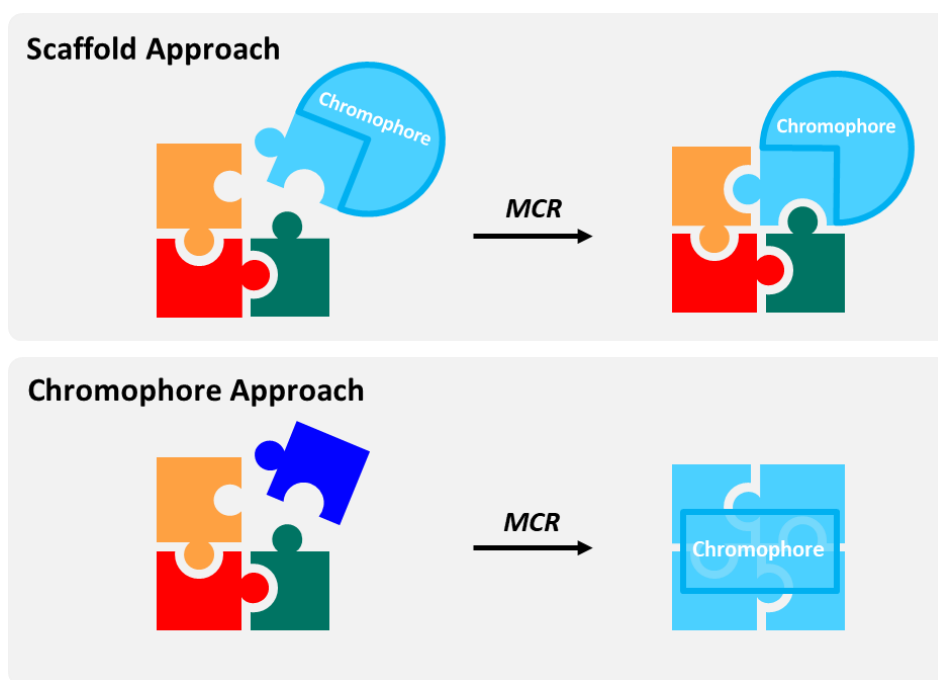
Figure 14. Comparison of the scaffold and chromophore approach for the combinatorial synthesis of chromophores.

In the first one, an existing chromophore bearing one of the components is functionalized in an MCR. Isonitriles, in particular, are well suited as biorthogonal handles because of their distinct reactivity. In the latter, a chromophore is generated in an MCR from non-luminescent components. Among these, classical MCRs are less prominent as they mainly afford partially saturated rather than conjugated structure. Instead, transition metal catalyzed tandem cyclization which form (hetero-)aromatic or polyene core structures are more representative for this concept.

1.2.3   The GBB-3CR and its Imidazo[1,2-*a*]pyridines

In 1998, three independent research groups published a method for the synthesis of fused imidazo heterocycles using aromatic amidines, aldehydes and isonitriles under LEWIS acid catalysis.[88] Formally, the GROEBKE-BLACKBURN-BIENAYMÉ three component reaction (GBB-3CR) is a variant of the UGI reaction, in which the carboxylic acid and the amine component are combined in the amidine. However, instead of linear structures, the GBB-3CR furnishes heterocyclic scaffolds. Due to the biological relevance of these, the GBB-3CR has emerged as a valuable tool in the discovery of novel bioactive compounds. The general reaction, as well as the widely accepted mechanism originally proposed by BIENAYMÉ and BOUZID, are depicted in **Scheme 6**.[88a]

Scheme 6. The GBB-3CR (top) and the generally accepted mechanistic rationale proposed by BIENAYMÉ and BOUZID.[88a]

At first, the iminium ion is formed through the acid catalyzed condensation of the aldehyde and the amino group of the amidine. The following step is the concerted [4+1]-cycloaddition of the isonitrile furnishing the intermediate imine. Subsequently, this imine is converted into the final aromatic 3-aminoimidazole via a 1,3-H-shift. The reaction is commonly performed in polar, protic solvent like methanol or water with catalytic amounts of acid (e.g., protic acids like glacial acetic acid, perchloric acid, or LEWIS acids like Sc(OTf)$_3$). This mechanism is generally agreed upon; however, similar to the UGI reaction, it is questionable whether the α-addition of the isonitrile is, in fact, concerted. Furthermore, other mechanistic pathways might also be relevant, since small amounts of other regioisomers can be formed.[89] The scope of the individual components is quite diverse and has recently been reviewed by BOLTJES and DÖMLING.[63a]

To this date, the GBB-3CR sparks most interest due to the widespread biological activities of its products as imidazo[1,2-*a*]pyridines belong to the class of privileged scaffolds.[90] The term privileged structure was coined

by EVANS in 1988, who defined them as simple structural subunits shared by different pharmaceutically relevant molecules with distinctive therapeutic applications being recognized as a ligand by several types of receptors.[91]

In medicinal chemistry, privileged scaffolds can serve as templates for derivatization in order to find novel bioactive compounds, receptor-affine ligands and ultimately new drugs. Regarding this, facile derivatization of basic frameworks through combinatorial approaches is highly advantageous. Among these, the majority are *N*-heterocyclic scaffolds of which the class of imidazo[1,2-*a*]pyridines and related structures is highlighted here in anticipation of the substances synthesized within the context of this dissertation.

Figure 15 and **Figure 16** show the most important marketed imidazo[1,2-*a*]pyridine-derived drugs.[92] Among those, Zolpidem (**70**) is probably the most prominent example. As a member of the so-called Z-drugs, a group of non-benzodiazepines GABA$_A$ receptor agonists exhibiting sedative and anxiolytic effects used to treat insomnia.[93] Other commercial GABA$_A$ modulators are the psychopharmaceuticals Alpidem (**71**), Divaplon (**72**), Necopidem (**73**), Saripidem (**74**) and DS-1 (**75**). Aside from their psychoactive properties, several imidazo[1,2-*a*]pyridine-related drugs have also been marketed, for instance, the gastroprotective agent Zolimidine (**77**), the anti-inflammatory Miroprofen (**76**), anti-rheumatic Upadacitinib (**80**) or Minodronic acid (**78**)against osteoporosis. A saturated imidazo[1,2-*a*]pyrazine-derived substrate is Ganaplacide (**81**), an experimental malaria drug.[94] The development of novel drugs based on the imidazo[1,2-*a*]pyridine scaffold is still ongoing. The autotaxin inhibitor Ziritaxestat (**79**) was in late-stage clinical trials for the treatment of idiopathic pulmonary fibrosis and systemic sclerosis but was discontinued in 2021.[95]
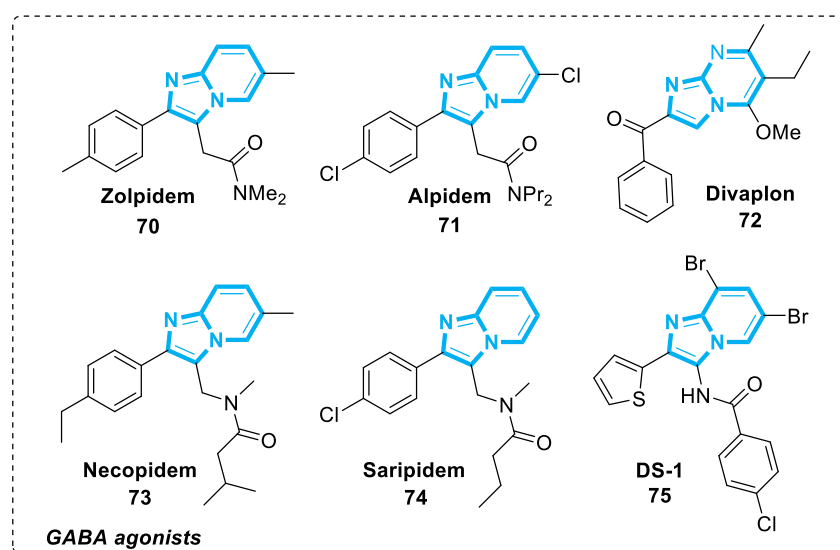
Figure 15. Selected examples for marketed drugs based on imidazo[1,2-*a*]pyridines, -pyrimidines, and -pyrazines.
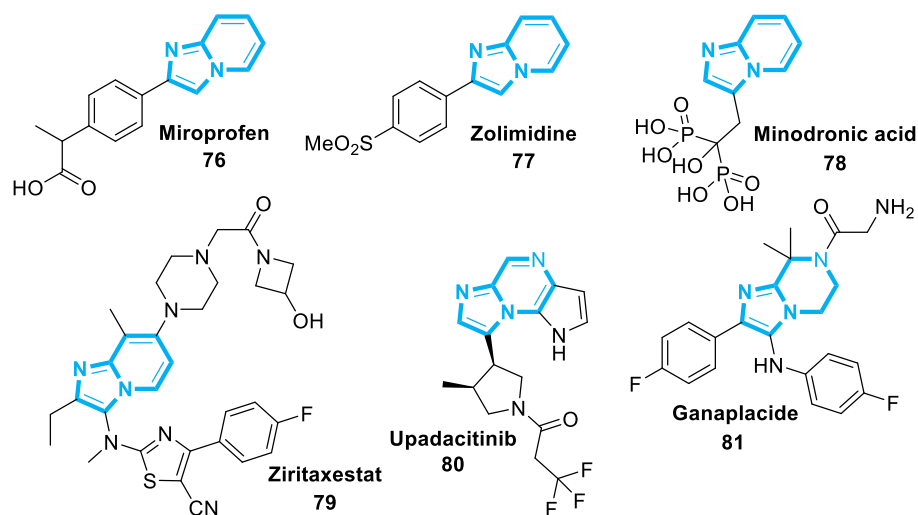
Figure 16. Selected examples for marketed drugs based on imidazo[1,2-*a*]pyridines, -pyrimidines, and -pyrazines.

Arguably, the obvious structural difference between most of the aforementioned drugs and the GBB-scaffolds is the secondary amine originating from the isonitrile component. As this amine can also interact with proteins and receptors, it might alter the biological profile of the scaffold. However, a variety of different strategies have been reported to remove or convert the 3-amino residue. Nevertheless, the biological activity of 3-aminoimidazopyridines is also interesting and can serve as a platform for the discovery of novel drugs, possibly also addressing different targets. The effects of various substances directly accessible *via* the GBB-3CR have been studied in a variety of different assays revealing a broad spectrum of biological activities including anti-bacterial,[96] anti-viral,[97] and anti-cancer properties.[98] Currently, the first promising drug candidates that involved a GBB-3CR-step at some point within their development have entered clinical trials. Hence, the GBB-3CR has emerged as a valuable tool in medicinal chemistry and pharmaceutical science over the last 20 years since its discovery.[99]

Despite being well-established in this field, however, other possible applications of the and its products have not been explored thoroughly. One of the few examples for the synthesis of chromophore based on the GBB-3CR was reported by BURCHAK *et al.* in 2011 (**Scheme 7-top**).[100] In a surface tension microarray format, a set of imidazo[1,2-*a*]heterocycles were synthesized in a combinatorial manner from twelve amidine components, 40 aldehydes and eight isonitriles. The fluorescence spectra of thirty-five selected substrates were recorded and the potential as autofluorescence zolpidem analogs in bioimaging experiments was investigated. Aside from this, SHAHRISA *et al.* reported a library of donor-acceptor fluorophores consist of imidazo[1,2-*a*]pyridines as donors in combination with tetrazole, dihydropyridine or dihydropyrimidones acceptor *via* sequential GBB-3CR-UGI-Azide-4CR/HANTZSCH-4CR/BIGINELLI-3CR syntheses (**Scheme 7-middle**).[101] BALIJAPALLI and IYER also designed imidazo[1,2-*a*]pyridine fluorophore exhibiting ESIPT properties, however, in a copper-catalyzed three component reaction rather than a GBB-3CR (**Scheme 7-bottom**).[102]
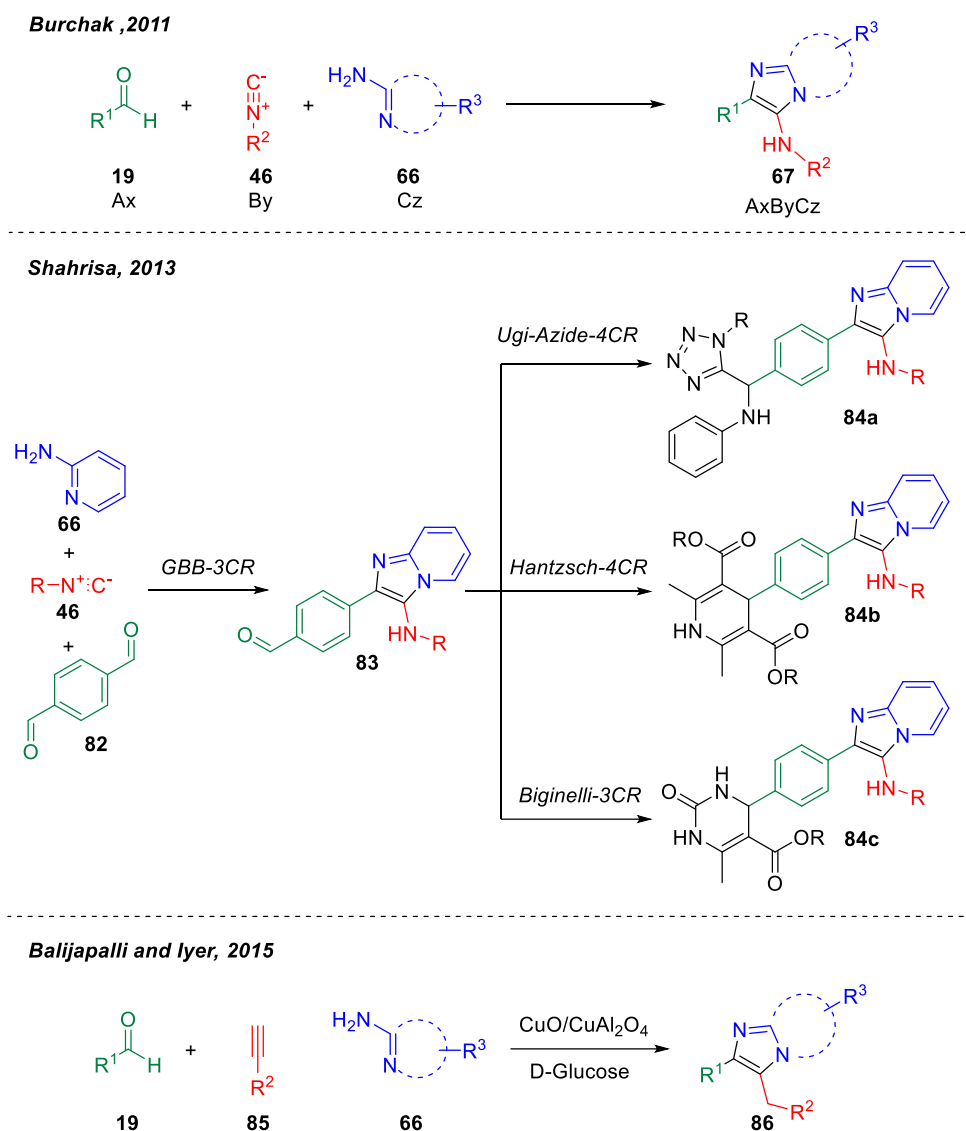
Scheme 7. Synthetic approaches towards imidazo[1,2-*a*]pyridine-based chromophores.

In terms of functional materials or polymers, the GBB-3CR is underrepresented compared to other IMCRs like PASSERINI and UGI reactions, which have been extensively explored, *e.g.*, for the synthesis of sequence-defined macromolecules.[103] The only application example for the GBB-3CR-is the synthesis of covalent organic frameworks by employing multifunctional building blocks reported by LIU *et al*. in 2020 (**Scheme 8**).[104]
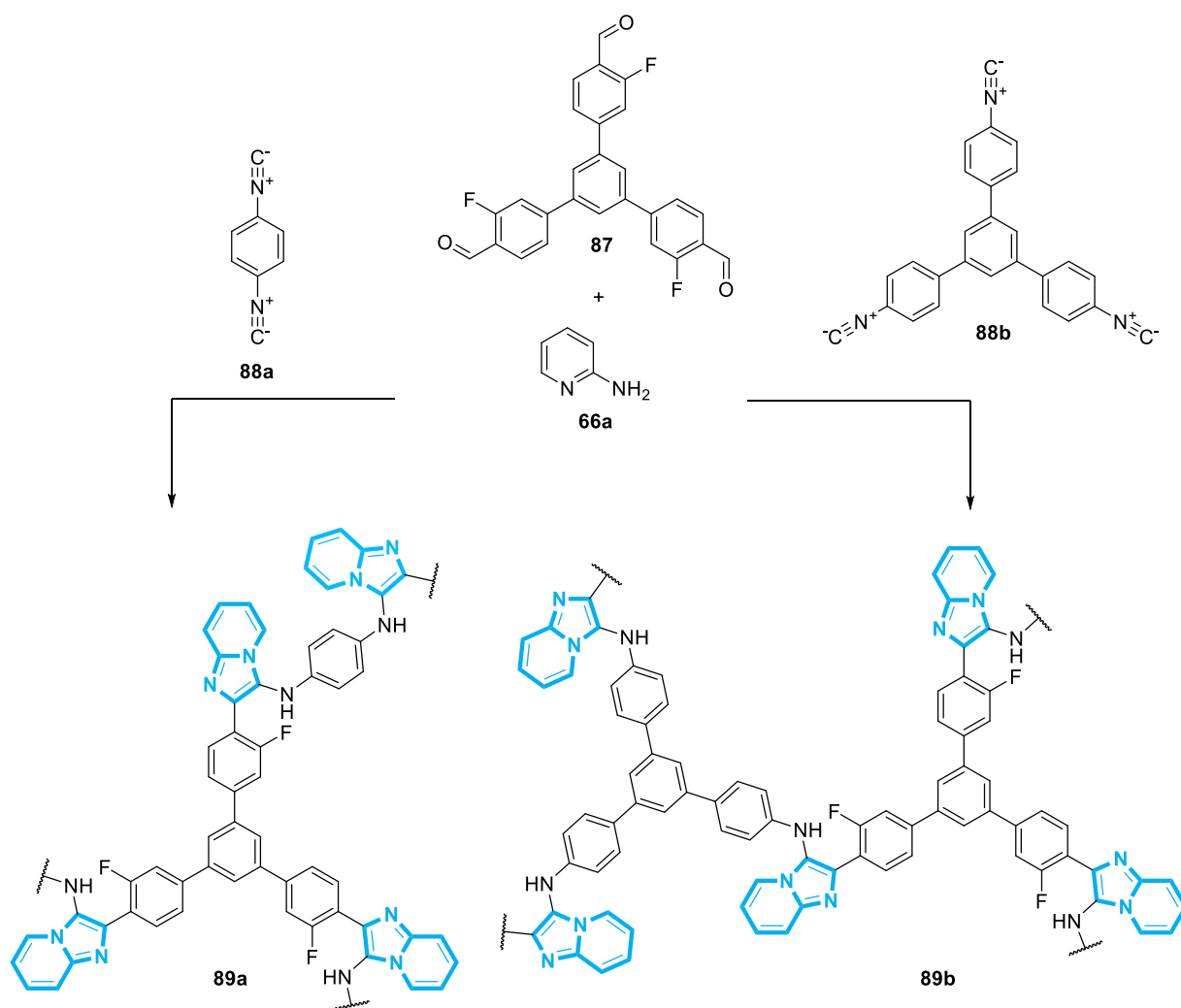
Scheme 8. Synthesis of imidazo[1,2-*a*]pyridine-based COFs *via* GBB-3 CR.

In particular, the intrinsic fluorescence of imidazopyridines and related fused systems is quite intriguing and could be very promising for the development of novel fluorophores.[15] The modular nature of multicomponent reactions would also allow for an easy assembly, customization and fine-tuning of the fluorophores' properties. In their recent review, BOLTJES and DÖMLING also described the current lack of research efforts towards GBB-3CR-based materials.

"Currently still underdeveloped are materials science application of the GBB-3CRs, such as functional polymers or organic conductors or light to energy transformers. Clearly the GBB scaffold has the potential that many interesting electronic and optical applications will be described in the future." —*ALEXANDER DÖMLING* [63a]

2   Objective

Due to the ever-growing demand for functional chromophores, which are specifically tailored for a certain purpose, the development of methods to synthesize novel chromogenic structures are constantly sought after. In respect of the increasing awareness of environmental concerns, research should also focus on improving the overall sustainability of synthetic methods for functional materials. Hence, the research of this thesis focuses on the investigation of novel scaffolds in chromophore design and the improvement of their synthetic routes in terms of sustainability. Inspired by the unexplored, yet vast potential of the GBB-3CR in material science, this thesis aimed to develop novel synthesis strategies around this reaction and its product scaffolds, the imidazo[1,2-*a*]pyridines, and investigate application perspectives as luminescent compounds (**Figure 17**).
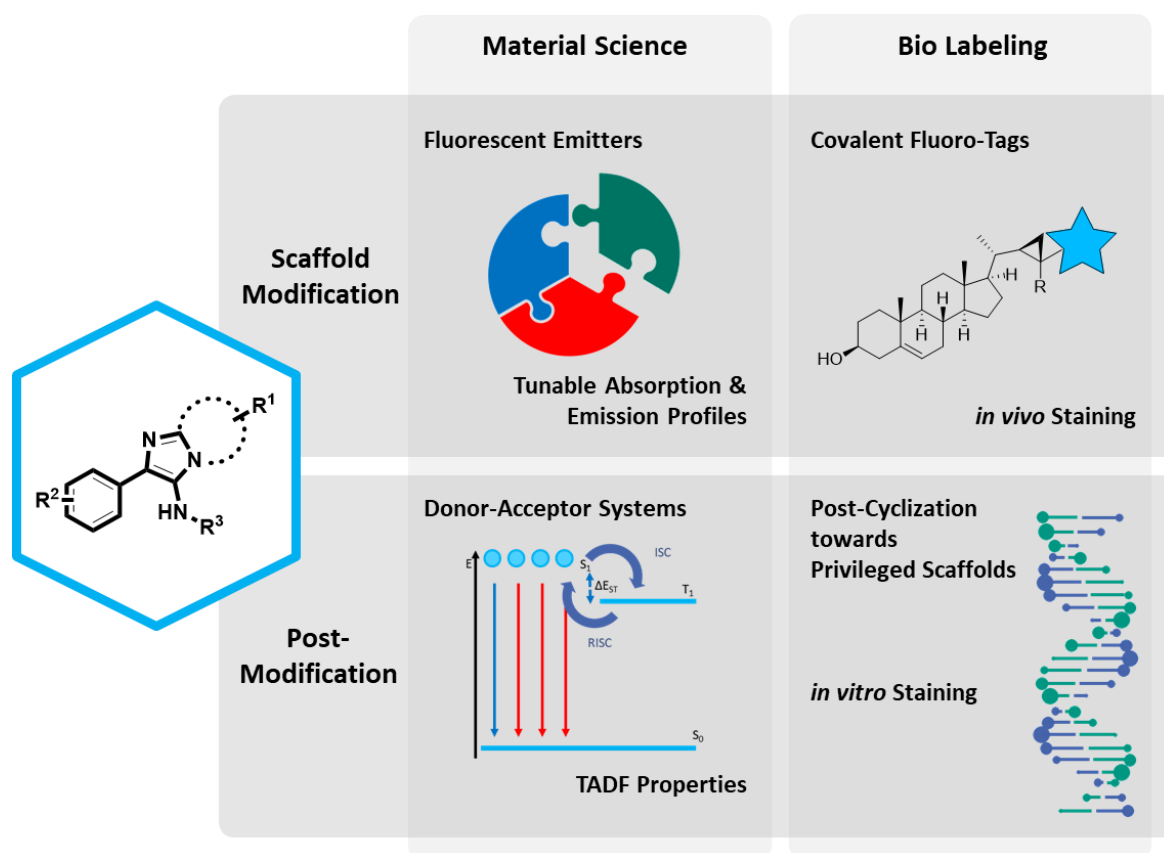
Figure 17. Projects of this thesis for the development of novel imidazo[1,2-*a*]heterocyclic functional fluorophores.

In the first part of this thesis, functional fluorophores for material science applications were designed by the modification of the [2.2]paracyclophane scaffold, and by the post-modification of GBB-based building blocks to donors. The fluorophore properties of these compounds were investigated thoroughly.

The second part of this thesis aimed to develop novel fluorophores for the *in vitro* and *in vivo* staining of biomolecules. On the one side, the GBB-3CR was employed to modify a bioactive steroid by adding an imidazo[1,2-*a*]pyridine fluorescent tag. These fluorophore-steroid conjugates were examined in cytotoxicity and cell localization studies. Moreover, GBB-scaffolds were post-civilized *via* an intramolecular HARTWIG-BUCHWALD

amination to afford highly fluorescent polyheterocycles. The interaction potential of these substrates with double-stranded DNA was assessed in a newly established pUC19 DNA gel electrophoresis mobility shift assay.

The miniaturization of chemical reactions constitutes a promising technique for the parallelization and high-throughput screening of compounds and is simultaneously environmentally benign due to the inherently reduced demand for material and solvents. One particular method the synthesis of highly dense molecular arrays *via* nano-3D printing (**Figure 18**). In cooperation with the BREITLING group, the scope of reactions which can be implemented into the nano-3D printing system should be increased and investigated by the means of fluorescent spectroscopy. Moreover, to prove the applicability of this method for the parallel screening of CO_2 converting reagents, a model reaction for the incorporation of CO_2 into fluorescent scaffolds should be designed.
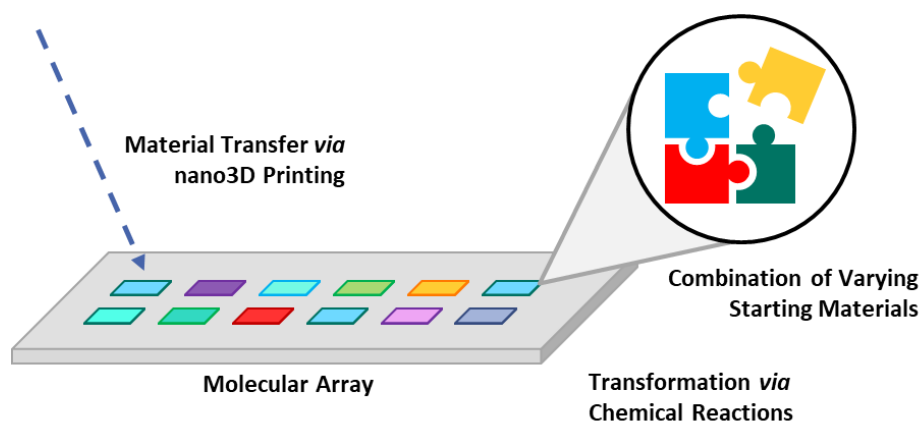
Figure 18. Schematic representation of the synthesis of molecular microarrays *via* nano3D printing.

In cooperation with the SYMRISE AG, the goal was to develop a novel, environmentally benign route towards the commercially available UV-absorber Bemotrizinol, meeting the ecological and safety prerequisites for large-scale industrial synthesis (**Figure 19**). Specifically, the reaction steps which produce large amounts of waste should be replaced by the implementation of more sustainable synthesis methodologies.
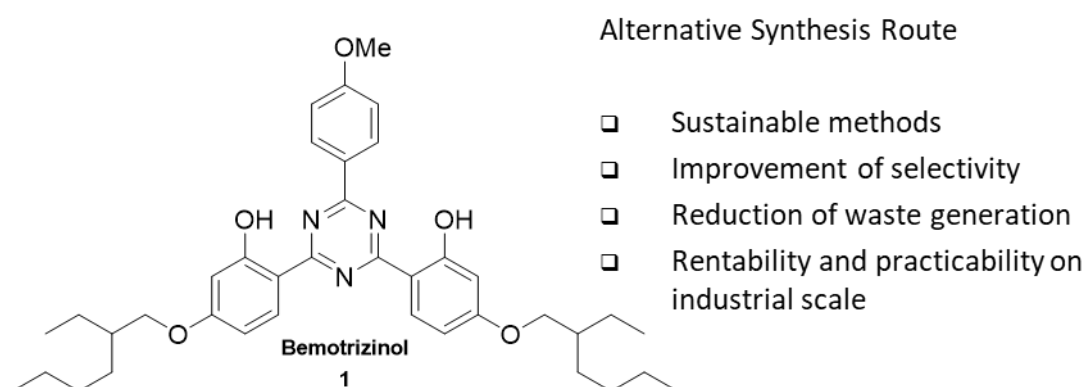
Figure 19. Structure of Bemotrizinol and aspects of the synthesis to improve.

3   Main Section

3.1   PCP-based Imidazo[1,2-*a*]heterocycles as Fluorophores and Ligands

Preface. Parts of the following chapter were published in Chemistry – A European Journal (Wiley-VCH).

M. Stahlberger, N. Schwarz, C. Zippel, J. Hohmann, M. Nieger, Z. Hassan, S. Bräse, Diversity-Oriented Synthesis of [2.2]Paracyclophane-derived Fused Imidazo[1,2-*a*]heterocycles by Groebke-Blackburn-Bienaymé Reaction: Accessing Cyclophanyl Imidazole Ligands Library, *Chem. Eur. J.,* **2022**, 28, e202103511.

Introduction. [2.2]Paracyclophane is an aromatic hydrocarbon with unique structural features. The short ethylene bridges connecting the benzene rings in the *para*-positions results in both a highly rigid as well as strained and deformed geometry (**Figure 20**).
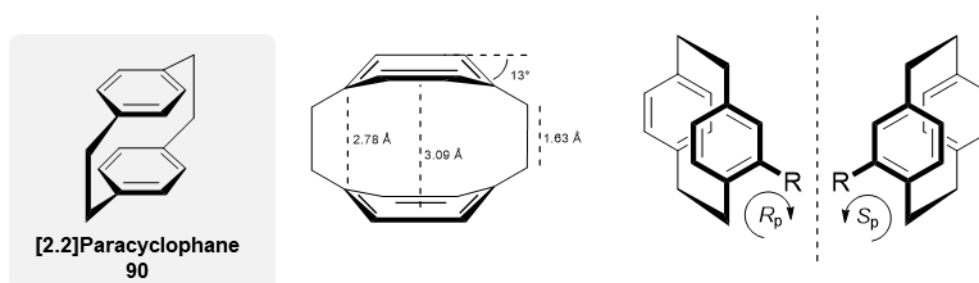
Figure 20. Structure and geometry of [2.2]paracyclophane (left) and planar chirality of mono-substituted PCP-derivatives.[105]

The close proximity of the benzene rings enables transannular communication between the non-conjugated π-systems.[106] Introducing substituents on the benzene decks leads to an inherent planar chirality making it an interesting synthetic platform. Derivatization of this scaffold allows application in catalysis and asymmetric synthesis,[107] material science and polymer chemistry. Thus, continuous efforts to further enlarge the accessible chemical space around the PCP-core were made.[108] For instance, through-space TADF-emitters were designed exploiting the transannular interactions.[109] To explore the effects of the transannular communication on cooperative catalysis, chimeric photoredox catalysts consisting of a PCP-core bearing both a Ru(bpy)₃ moiety as well as a gold complex were synthesized and employed for AuRu-catalyzed MEYER-SCHUSTER rearrangement.[110] Literature-known synthesis strategies, however, cannot be easily transferred to the PCP-scaffold due to the extraordinary reactivity originating from its unique structure. The attachment of aromatic or heteroaromatic residues, in particular, pose a bigger challenge.[111] Hence, novel methods to functionalize the PCP-core are constantly sought after. One methodology that has not yet been explored in this regard, is MCR-chemistry. The development of MCR-based protocols would give access to a broad spectrum of unprecedented residues for PCP in a combinatorial manner. Applying PCP-components in the GBB-3CR would furnish imidazo[1,2-*a*]pyridyl-substituted PCPs. As the PCP-building blocks are planar chiral elements, these imidazopyridines could serve as chiral fluorophores. These are particularly interesting for non-linear optical properties and chiroptical applications.[112] Thus, combining the GBB-approach and the PCP scaffold allows facile introduction of both a

sophisticated residue to the PCP-core as well as a chiral element into the non-chiral imidazo[1,2-*a*]pyridine-based fluorophores.

Synthesis. Evaluation of the optimal reaction conditions for the GBB-3CR of 4-formyl-PCP (**91**), 2-aminopyridine (**66a**), and *tert*-butyl isonitrile (**46a**) revealed a similar performance of the two commonly used catalysts, glacial acetic acid and perchloric acid for our model system. Due to the low solubility of **91** in methanol, a mixture of methanol and dichloromethane was used. Through the GBB-3CR of 4-formyl-PCP with 2-aminopyridine, 2-aminopyrazine and various isonitriles (**46**), a library of nine PCP-derived 3-amino-imidazo[1,2-*a*]pyridines (**92a-f**) or -pyrazines (**93a-c**) was synthesized in 42-87% yields (**Scheme 9**).
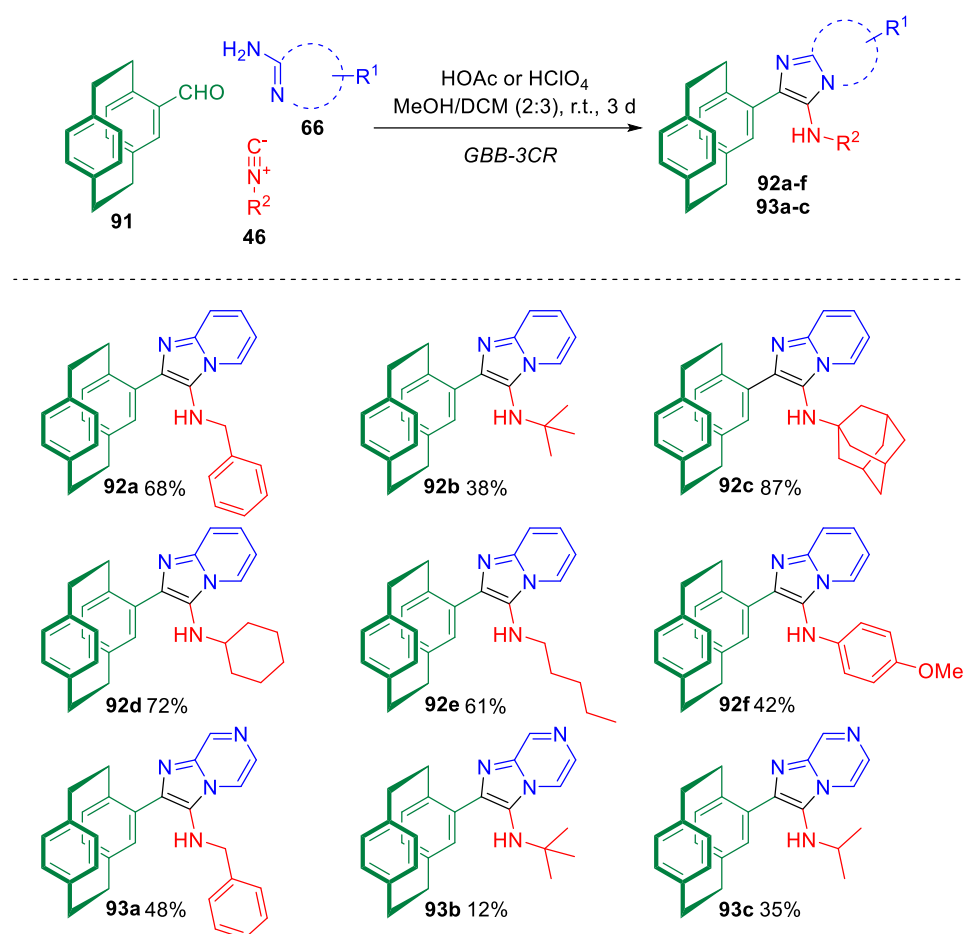
Scheme 9. Synthesis of PCP-derived imidazo[1,2-*a*]pyridines 4a–f and imidazo[1,2-*a*]pyrazines 5a–c *via* GBB-3CR through varying isocyanide and amidine components.

Aromatic and aliphatic isonitrile variants were compatible, corresponding to the expected reactivity. As noted in **Chapter 1.2.3**, the yields of the imidazo[1,2-a]pyrazines (**93a-c**) are lower (12-48%) since 2-aminopyrazine is less nucleophilic. The structure of imidazo[1,2-a]pyridine **92d** was verified unambiguously by single crystal X-ray analysis. From **93a**, a single crystal X-ray structure was obtained. However, this structure corresponds to the imine compound **93a'**, probably due to an oxidation process (**Figure 21**).
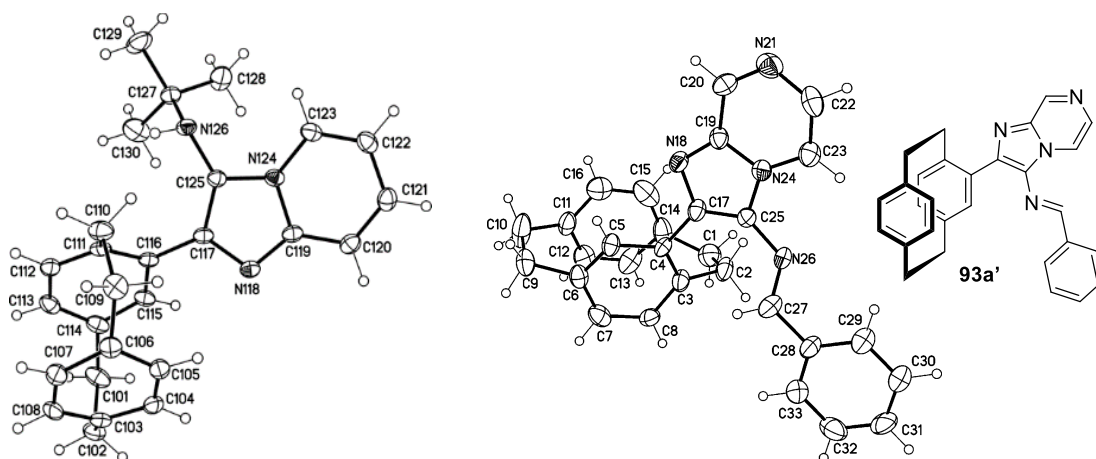
Figure 21. Single-crystal X-Ray structure of **92d** (left) and **93'** (right) (one of the crystallographic independent molecules is shown, displacement parameters are drawn at 50% probability level).

Apart from the 4-formyl[2.2]paracyclophane, difunctionalized-PCP aldehyde **95** bearing additional formyl moiety was also investigated to prepare pseudo *para*-cyclophanyl bis-imidazo[1,2-*a*]heterocycles. As two reaction centers are present in **95**, the reaction time was extended to six days. Afterwards, **96** was obtained in a yield of 43% (**Scheme 10**). The structure of **96** was confirmed through single crystal X-ray analysis (see **Page 189**). For 2-aminopyrazine, the bis-imidazo[1,2-*a*]pyridine could not be obtained due ti the decreased reactivity of 2-aminopyrazine. Instead, the mono-imidazo[1,2-*a*]pyrazine **97** was isolated.
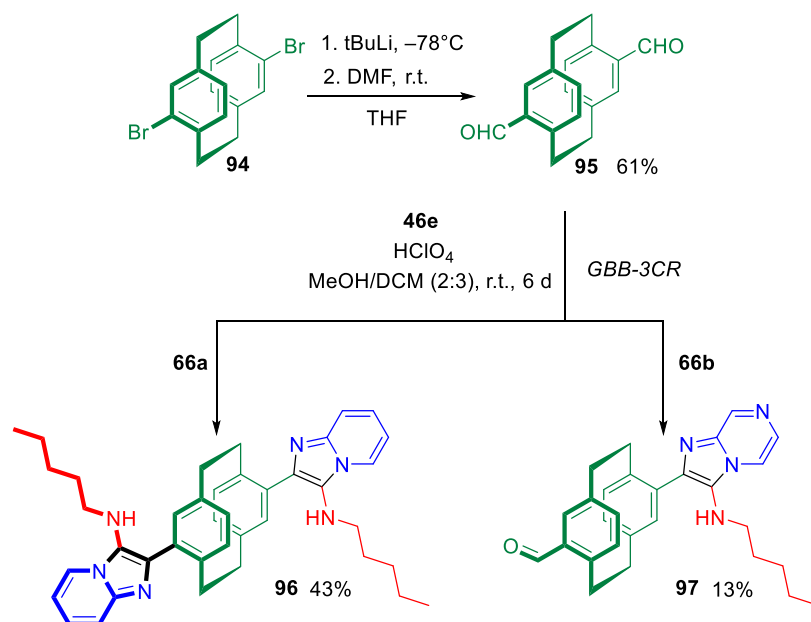
Scheme 10. Synthesis of PCP-derived mono- and bis-imidazo[1,2-*a*]heterocycles *via* GBB-3CR.

To further expand the structural diversity of motives around the PCP core, PCP-isonitrile from the corresponding 4-formamido[2.2]paracyclophane was synthesized and according to a modified procedure by CLÉMENT *et al.*and utilized in a GBB-3CR.[113] PCP-formamide **100** was synthesized starting from PCP. First, PCP was converted to 4-nitro-PCP (**98**). The reduction of **98** usually is reported using iron as a reducing agent. However, as this method

is rather impractical, Pd-catalyzed hydrogenation using a pressure reactor was employed. The obtained 4-amino-PCP was then converted into the formamide in a modified procedure originally reported by LYGIN and DE MEIJRE.[114] Despite being already reported in literature, PCP isonitrile has not been applied in any IMCR, yet. Instead, reports only focus on its application as a ligand for transition metal complexes.[113, 115] To avoid isolating the sensitive isonitrile intermediate, an isonitrile-free variant of the GBB-3CR according to DÖMLING *et al.* was performed in which the isonitrile is generated *in situ* through dehydration of the formamide using triphosgene and triethylamine and subsequent addition of the remaining components.[85] The synthesis route is displayed in **Scheme 11**.
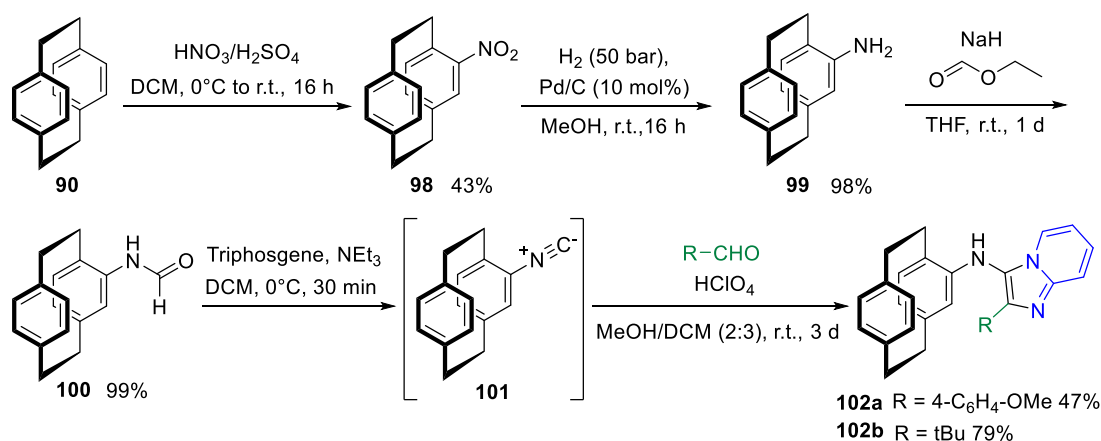
Scheme 11. Preparation of PCP-formamide and its utilization in an isonitrile-free GBB-3CR.

Since the synthesized substrates exhibited a bright blue fluorescent in solution and solid-state, their fluorescence properties were investigated. The normalized emission spectra of selected compounds are displayed in **Figure 22** and the maximum wavelengths are listed in **Table 1**. The fluorescence emission wavelengths could be tuned by variation of the individual precursor components.
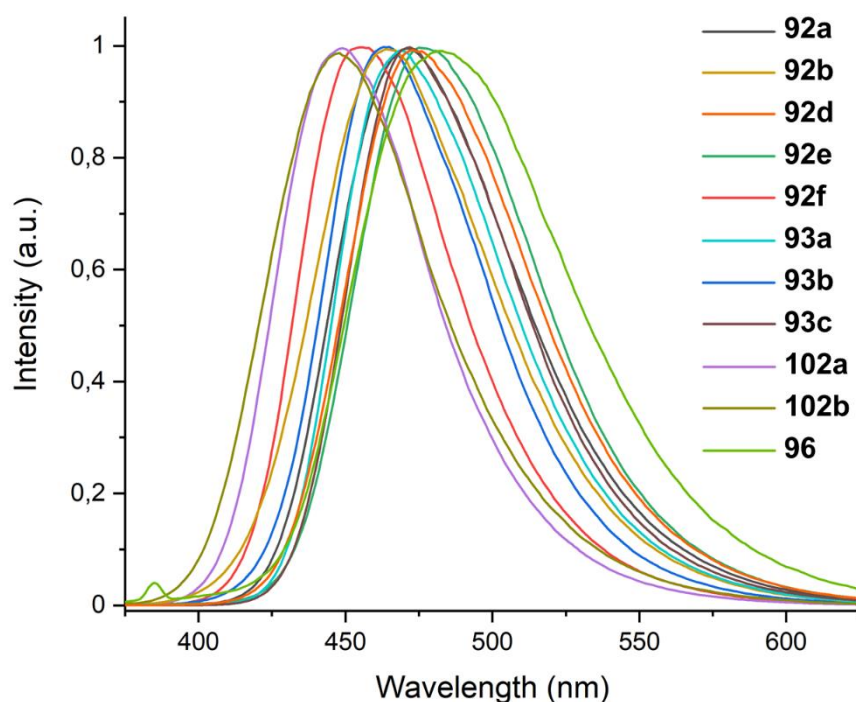
Figure 22. Normalized emission spectra of selected compounds in ethyl acetate, λ_{exc} = 345 nm.

Table 1. Maximum absorption and emission wavelength of selected compounds in ethyl acetate, λ_{exc} = 345 nm.

entry	λ_{abs} [nm]	λ_{em} [nm]	STOKES Shift [nm]	entry	λ_{abs} [nm]	λ_{em} [nm]	STOKES Shift [nm]
92a	343	471	128	**93a**	350	469	119
92b	335	464	129	**93b**	340	464	124
92d	334	473	139	**93c**	350	471	121
92e	343	476	133	**102a**	319	449	130
92f	356	456	100	**102b**	328	447	119
96	351	483	132	-	-	-	-

The amidine component does not substantially influence the emission wavelength, whereas the STOKES shift was reduced slightly for the pyrazine derivatives. Strongly electron-donating isonitrile residues like 4-methoxyphenyl (**92f**) also decrease emission wavelength and STOKES shift. Bis-imidazo[1,2-*a*]pyridine **96** shows a similar absorption and emission profile, with slightly increased emission wavelength and Stokes shift and broadening of the emission peak. The PCP-isonitrile-derived imidazo[1,2-*a*]pyridines **102a** and **102b** exhibit a lower emission wavelength. By employing different π-extended or substituted components, the fluorescence properties of the GBB-products could be varied even more. Functionalization of the other deck could lead to interesting effects due to the transannular communication.

Moreover, the pH-dependency of the fluorescence exemplary for the PCP-derived imidazo[1,2-*a*]pyridine **92f** was investigated(**Figure 23**). Compared to the spectra recorded in ethyl acetate, a bathochromic shift of 16 nm

is observed in water at pH = 7. This solvatochromic effect suggests a larger charge separation in the excited state which is stabilized in more polar solvents. In acidic solution, however, the fluorescence intensity is significantly decreased. Presumably, the protonation of the nitrogen atom of the imidazole ring leads to fluorescence quenching. In contrast, the fluorescence intensity increases in basic solutions, which is also accompanied by a hypsochromic shift. One possible explanation for this could be the decreased stabilization of the excited state in basic media.
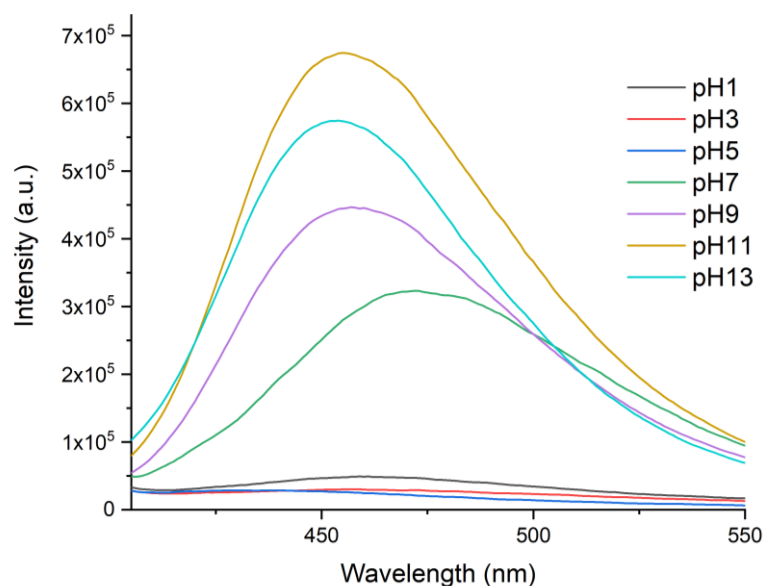
Figure 23. Quantitative emission spectra of **92f** in aqueous solutions of different pH values (8 µM), λ_{exc} = 345 nm-

To demonstrate the utilization of the cyclophanyl imidazole ligands, an exemplary *N,C*-palladacycle was synthesized using a regioselective ortho-palladation method for amine-functionalized [2.2]paracyclophanes reported by Zippel *et al.* in 2021.[116] Palladacycle-directed various synthetic transformations to control regioselectivity are well documented, and could overcome certain synthetic hurdles and drawbacks associated with conventional approaches for regioselective transformations.[117] Through treatment with palladium acetate, followed by lithium chloride and triphenylphosphine, *N,C*-palladacycle **103** was obtained in 37% yield. The regioselectivity of ortho-palladation was examined *via* NMR spectroscopic techniques, confirming the coordination of the secondary amine to the palladium rather than the nitrogen of the imidazole ring.

The catalytic reactivity of PCP-derived palladacycle **103** was examined in a Suzuki-Miyaura cross-coupling reaction using 4-halotoluenes (**104**) and phenylboronic acid (**105**) as reaction components under standard reaction conditions (**Scheme 12**).
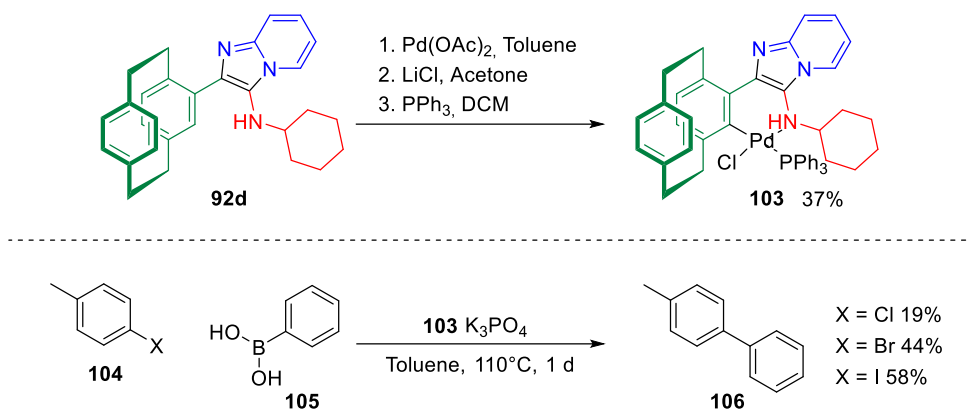
Scheme 12. Synthesis of PCP-derive *N,C*-palladacycle **103** and its synthetic application in a Suzuki-Miyaura reaction.

4-Methyl biphenyl **106** was obtained in good yields from 19% to 58% (I>Br>Cl). The preliminary results obtained for the biaryl coupling product suggest potential applications of PCP-palladacycle 16 as a catalyst. To identify the specific role of the substituents grafted onto the imidazo[1,2-a]heterocycles for chelating ability or enabling higher stability and exploring their catalytic utility in other synthetic transformations, some further studies are certainly needed.

3.2   Design of Imidazo[1,2-*a*]pyridine-based Donor-Acceptor Chromophores

Preface. The synthesis and characterization of all precursors and emitters were done by the author and M. Mergel in the context of her Bachelor thesis. The DFT calculations and the following characterization were performed by J. M. Dos Santos who also provided the corresponding images.

Introduction. Although imidazopyridines are well-explored substrates in medicinal chemistry, examples for their application in material science remain relatively scarce. However, due to their strong luminescent properties, we aimed to explore their potential as potent fluorophores and eventually TADF-emitters.

In 2020, Lee *et al.* reported on the first series of TADF-emitters containing the imidazopyridine motif.[118] Nitrile groups were grafted onto the scaffold to enhance the electron withdrawing properties and combined it as an acceptor with two different donors (**Figure 24**).
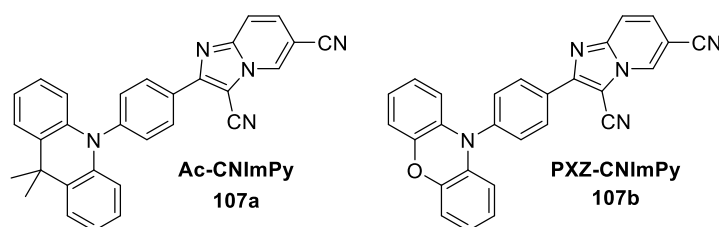
Figure 24. TADF emitters reported by Lee et al. containing a nitrile-substituted ImPy-acceptor.

As this demonstrates the suitability of imidazo[1,2-*a*]pyridines for the design of TADF-emitters, we planned to further explore this scaffold. Grafting the ImPy-moiety *via* a GBB-3CR-based synthesis strategy onto other TADF building blocks would also provide a facile, modular access to a variety of different TADF-architectures. The secondary amino substituent originating from the isonitrile employed in the GBB-3CR increases the electron density of the imidazopyridine. Thus, it might very well be also suited as a TADF-donor rather than an acceptor. Based on these considerations, we aimed to design novel TADF-emitters featuring an ImPy-based donor proofing the chimeric nature of this scaffold.

Theoretical considerations. Prior to synthesis, the general feasibility of the 3-amino imidazo[1,2-*a*]pyridine moiety for TADF-emitters was evaluated. Therefore, DFT calculations were performed in cooperation with the University of St. Andrews by Dr. John Marques Dos Santos. For an initial overview, a set of potential structures were calculated with 3-*tert*-butyl imidazo[1,2-*a*]pyridine as the donor, a mesitylene bridge and several donors of different strengths. The results are listed in **Table 2**.

Table 2. DFT-calculations of ImPy donors with different acceptor types.
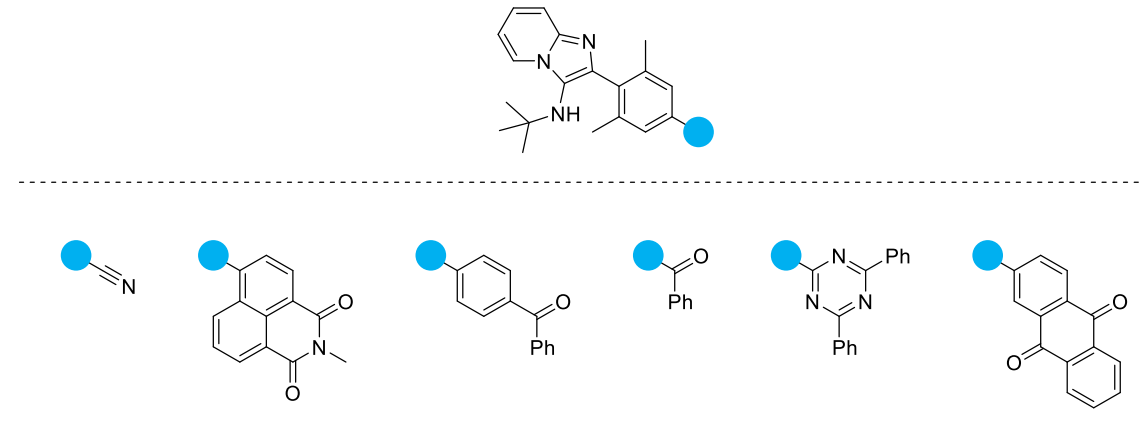
ImPy-CN	ImPy-NPI	ImPy-Ph.Bs.	ImPy-Baz	ImPy-Try	ImPy-Aq
0.92 eV	0.73 eV	0.65 eV	0.63 eV	0.40 eV	**0.18 eV**
389 nm (UV)	389 nm(UV)	343 nm (UV)	339 nm (UV)	361 nm (UV)	**450 nm**

Top row: ΔE_{ST}, bottom row: g_{em}

According to these calculations, the lowest ΔE_{ST} value was obtained for the combination of ImPy and anthraquinone. The ImPy-group seems to be a relatively weak donor, thus pairing it with a strong acceptor gave the best results. Additionally, most of the valuated structures showed emission maxima located in the UV-region. Expanding the imidazo[1,2-*a*]pyridine to an imidazo[1,2-*a*]quinoline shifted the emission wavelength above 400 nm. However, the ΔE_{ST} value increased simultaneously.

Based on these results, we tried to improve the donor strength by attaching two ImPy residues to a central phenyl spacer. A series of target emitters with different geometries was designed: *ortho-*, *meta-* and *para*-ImPyAq. For the *para*-emitter, the location of the methyl groups on the phenyl spacer was inverted because the respective aldehyde component for the GBB-3CR synthesis of this building block is more easily available.

The energy levels of the frontier orbitals of the three isomers and their localization on the optimized structures are presented in **Figure 25**.
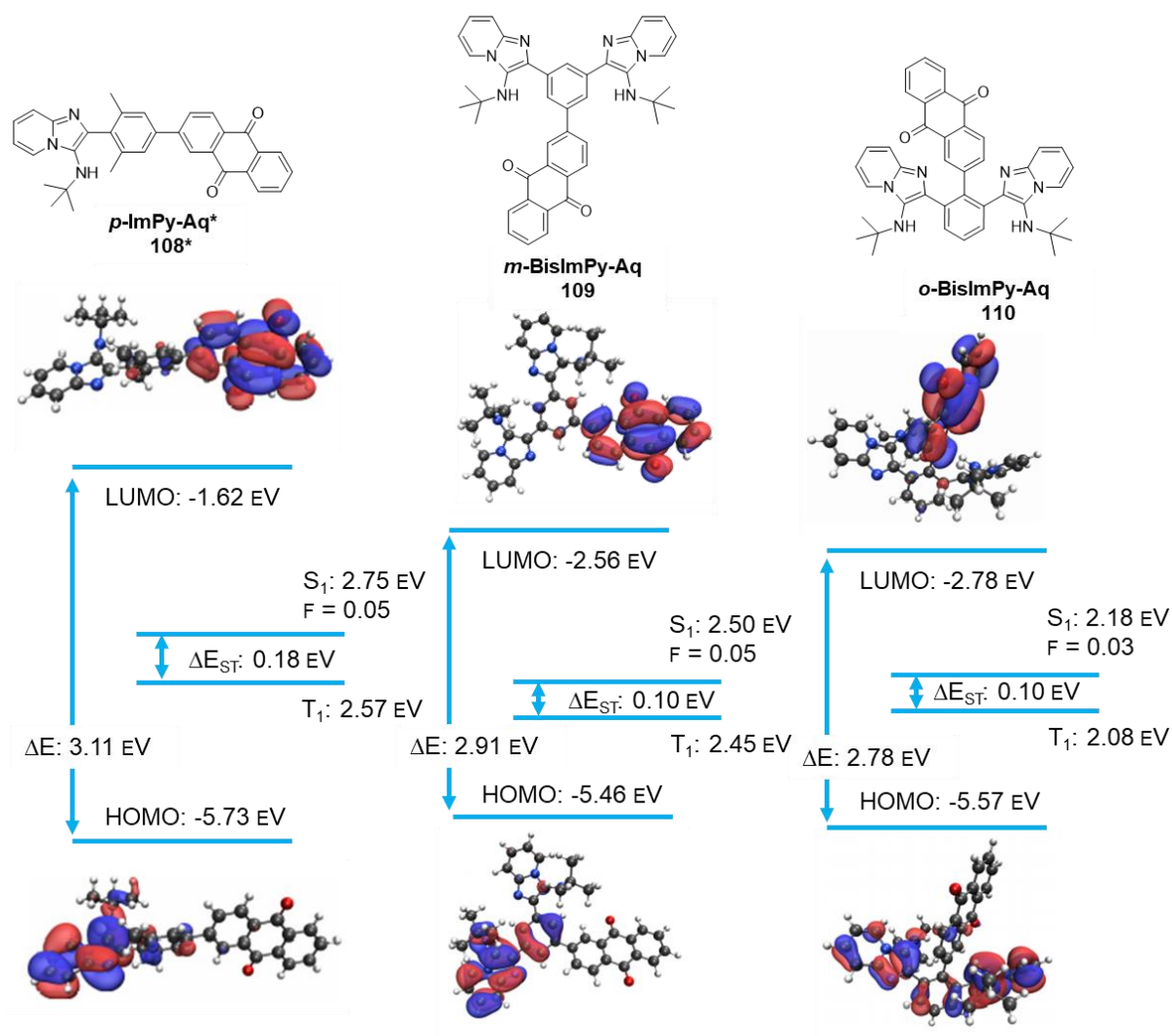
Figure 25. DFT calculations of *p*-ImPyAq* (**108***), *m*-BisImPyAq (**109**) and *o*-BisImPyAq; results provided by J. M. Dos Santos, St. Andrews University.

For all the proposed compounds, the estimated ΔE_{ST} values are in range for possible TADF effects, with *p*-ImPyAq exhibiting the largest ΔE_{ST} with 0.18 eV The bis-ImPyAq isomers both show a ΔE_{ST} of 0.10 eV. The LUMOs of all structures are almost exclusively located on the anthraquinone acceptor, while the HOMOs span over the imidazo[1,2-*a*]pyridine moiety and the central phenyl ring. In the case of *p*-ImPyAq, the biggest extension of the LUMO onto the saver is observed, corresponding to its comparably high ΔE_{ST}. For the *o*-bisImPyAq, the HOMO spans over both imidazo[1,2-*a*]pyridine residues, whereas for the *meta*-isomer, the HOMO is located on only one of the imidazo[1,2-*a*]pyridines and the central phenyl ring instead of being delocalized over both donors, whereas

The HOMO-LUMO gaps was calculated to range from 2.78 eV to 3.11 eV, resulting in a cyan to green emission profiles. However, the singlet oscillator strength of all compounds is relatively low.

Synthesis. To access the proposed structures starting from a set of donors and acceptors, a modular synthesis approach was developed by dissecting the emitters into individual building blocks. The donor building blocks, comprising the ImPy moiety and the phenylene spacer, were prepared *via* a GBB-3CR from the respective brominated benzaldyhdes (**Scheme 13**).
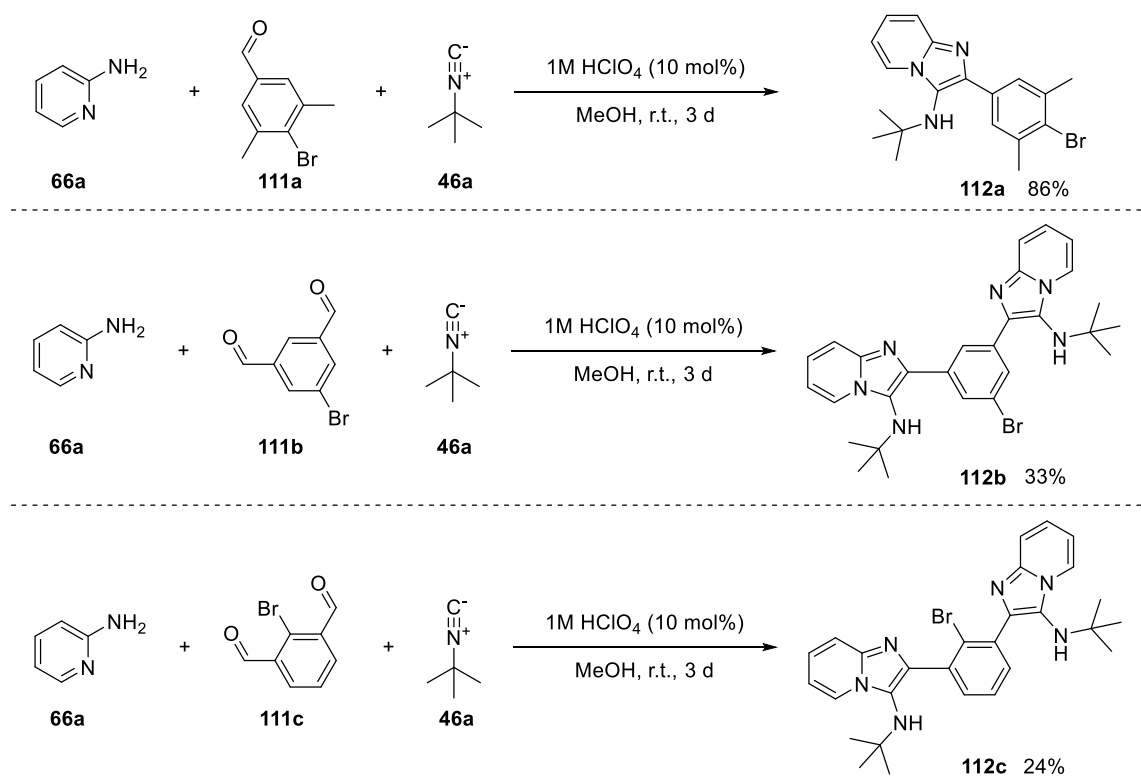
Scheme 13. Synthesis of the ImPy-donor building blocks *via* GBB-3CRs.

The yields of the mono-imidazo[1,2-*a*]pyridine donor **112a** was significantly better than for the bis-imidazo[1,2-*a*]pyridines due to their additional reactive site and the steric congestion in case of **112c**.

The donor building block, anthraquinone pinacol borate was prepared *via* MIYAURA borylation according to a procedure by LIU *et al.* using a Pd(dppf)Cl$_2$ catalyst and potassium acetate as base.[119] The desired product was obtained in quantitative yield (**Scheme 14**).
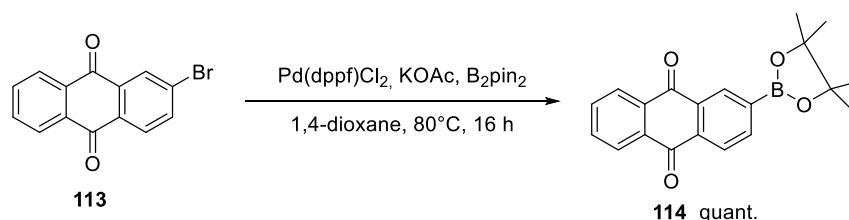
Scheme 14. Synthesis of anthraquinone pinacol borate *via* MIYAURA borylation.

After obtaining the individual building blocks, they should be connected *via* SUZUKI-MIYAURA coupling. To find the best reaction conditions for this key step an optimization was performed using the synthesis of *p*-ImPyAq as a

model system. The conversion was determined *via* NMR analysis by comparison of the integrals of characteristic signals. The results are displayed in **Table 3**.

Table 3. Optimization of the reaction condition for the Suzuki-Miyaura coupling of **112a** and **114**.
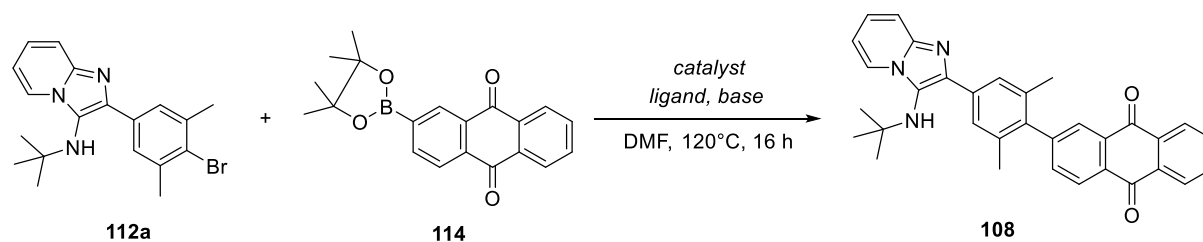
entry	catalyst	mol%	ligand	mol%	base	conversion (%)[a]
1	Pd(dba)$_2$	5	XPhos	10	K$_2$CO$_3$	53
2	Pd$_2$(dba)$_3$	5	XPhos	10	K$_2$CO$_3$	44
3	Pd(PPh$_3$)$_4$	5	XPhos	10	K$_2$CO$_3$	62
4	Pd-Peppsi-iPr	5	XPhos	10	K$_2$CO$_3$	24
5	Pd(OAc)$_2$	5	XPhos	10	K$_2$CO$_3$	64
6	Pd(OAc)$_2$	10	XPhos	20	K$_2$CO$_3$	55
7	Pd(OAc)$_2$	2	XPhos	4	K$_2$CO$_3$	25
8	Pd(OAc)$_2$	5	XPhos	10	KOAc	39
9	Pd(OAc)$_2$	5	SPhos	10	KOAc	51
10	Pd(OAc)$_2$	5	CataCXium A	10	KOAc	36
11	Pd(OAc)$_2$	5	RuPhos	10	KOAc	51
13	Pd(OAc)$_2$	5	none	-	KOAc	3
14	Pd(OAc)$_2$	5	RuPhos	10	KO^{t}Bu	>99
15	Pd(OAc)$_2$	5	RuPhos	10	KOH	>99
16	**Pd(OAc)$_2$**	**5**	**RuPhos**	**10**	**Cs$_2$CO$_3$**	**>99**

112a (1.00 equiv), **114** (1.10 equiv), catalyst, ligand, base (3.00 equiv), solvent: toluene/water (4:1), 110 °C, 16 h.

[a] determined *via* NMR.

Among the tested Pd sources, palladium acetate performed best. For the optimization of the ligand, potassium acetate was used as a base instead of potassium carbonate due to the better functional group tolerance. The best results were obtained from RuPhos and SPhos (**Entries 9, 11**). Without any ligand, only traces of the product could be detected (**Entry 13**). Using stronger bases like potassium *tert*-butoxide, potassium hydroxide or cesium carbonate led to a significantly improved conversion as in all three cases, no residual starting material was present (**Entries 14-16**). Considering the overall purity of the ^{1}H NMR spectra, cesium carbonate was chosen.

Using these optimized conditions, the target *ortho*-, *meta*- and *para*-emitters were synthesized from the respective building blocks (**Scheme 15**).
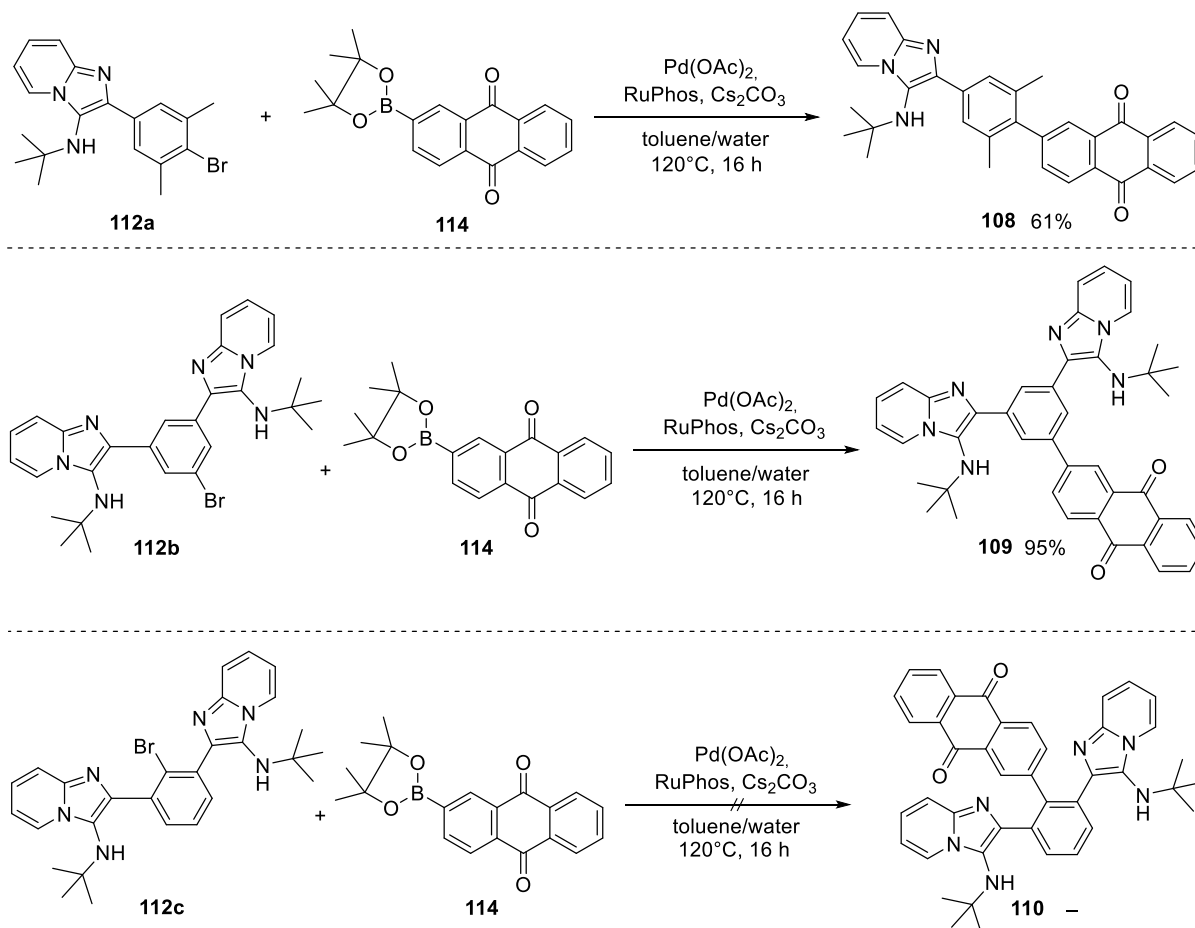
Scheme 15. Synthesis of the *ortho- meta-* and *para-*ImPyAq through Suzuki-Miyaura coupling of the donor and acceptor building blocks.

After flash chromatography, *p*-ImPyAq (**108**) was obtained in a good yield of 61%. For *m*-BisImPyAq (**109**), the yield was even better with 95%, most likely due to the reduced steric hindrance of the bromide. The structure of **109** could be verified unambiguously through single crystal X-ray crystallography (**Figure 26**).
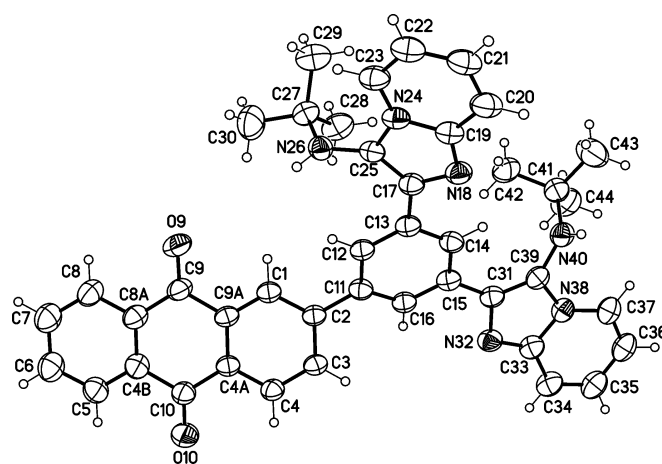
Figure 26. Single-crystal X-Ray structure of 4b (displacement parameters are drawn at 50% probability level).

On the other hand, *o*-BisImPyAq (**110**) could not be obtained. Instead, protodeboronation of the anthraquinone pinacol borate was observed while the ImPy building block remained unconverted. Addressing positions between sterically hindered residues is quite challenging and only a few procedures have been reported, e.g., using AntPhos as a ligand.[25] While this catalytic system is feasible for adjacent phenyl substituents, no reaction was observed for imidazo[1,2-*a*]pyridines. Hence, *o*-BisImPyAq needed to be accessed *via* a different route. Therefore, the acceptor unit was attached to the bridging aldehyde prior to the synthesis of the imidazo[1,2-*a*]pyridine moieties. The synthetic approach is depicted in **Scheme 16**.
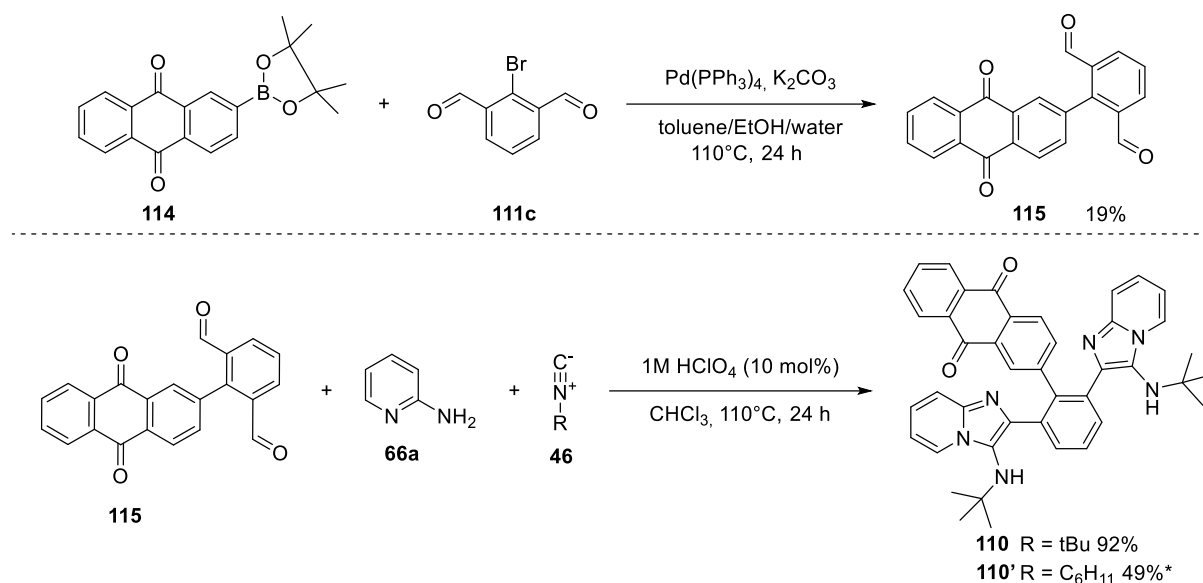
Scheme 16. Synthesis of **115** (top) and **110** and **110'** (bottom). * The reaction was performed in MeOH at r.t. for 3 d.

2-Bromoisophthalaldehyde **111c** was coupled to anthraquinone pinacol borate **114** in a Suzuki-Miyaura reaction. The desired coupling product **115** was obtained in a yield of 19%. Presumably, the losses are due to side reactions like decarbonylation of the neighboring formyl groups as a significant evolution of gas was observed during the reaction. Subsequently, the formyl groups were transformed into 3-amino imidazo[1,2-*a*]pyridines in a GBB-3CR. Initially, standard conditions were applied. However, even after a prolonged reaction time of ten days, the conversion remained incomplete. Thus, the solvent was changed to chloroform and the temperature was elevated to 60 °C to accelerate the reaction. Through this, an excellent yield of 92% for **110** could be achieved.

Photophysical Properties. The synthesized compounds were measured by Dr. J. M. Dos Santos to assess their photophysical properties and evaluate whether the emitters exhibit TADF properties. For this, absorption and emission spectra of the compounds were recorded at ambient temperature (**Figure 27**, **Table 4**), and at 77 K over different time scales (**Figure 28**).
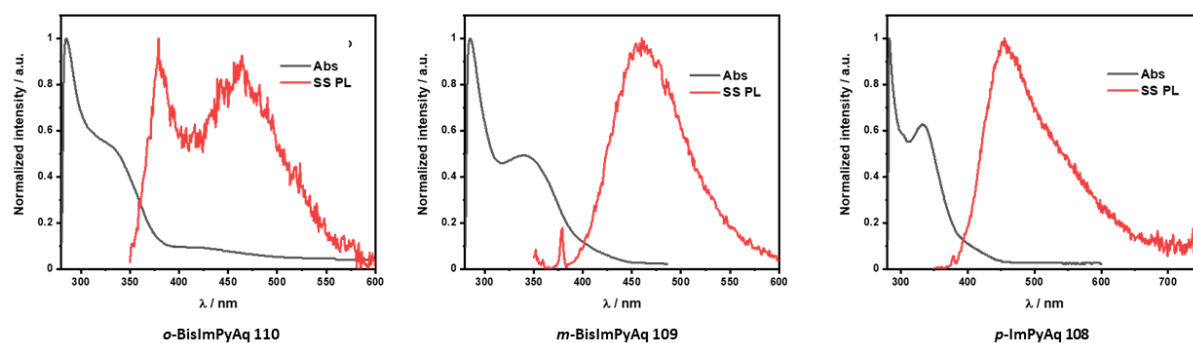
Figure 27. Normalized absorption (black) and emission spectra (red) of **110**, **109** and **108** (from left to right) measured in toluene (10 μM) at r.t.
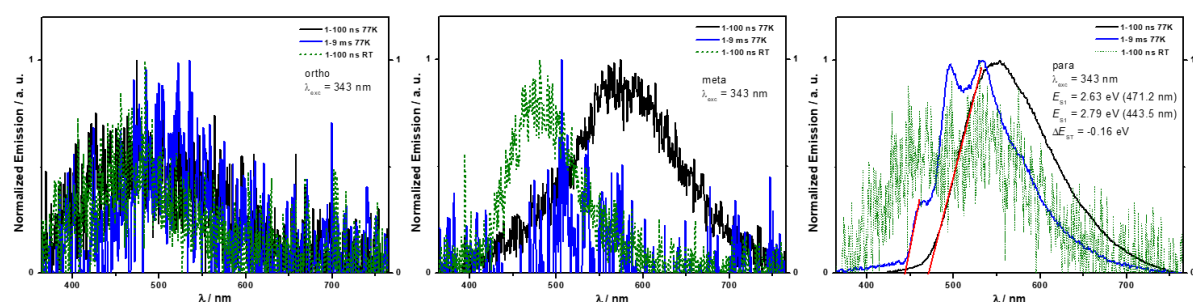
Figure 28. Normalized emission spectra of **110**, **109** and **108** (from left to right) measured in toluene (10 μM) at different time scales and temperatures: 1 – 100 ns at 77 K (black), 1 – 9 ms at 77 K (blue), 1 – 100 ns at r.t. (green).

Overall, the samples are not very emissive, resulting in spectra with poor signal-to-noise ratios. The small peaks at around 375 nm in **Figure 27** stem from reabsorption processes. In *o*-ImPyAq **110**, the reabsorption peak is very intense compared to the emission band due to the low intensity of the emission of this sample.

Low temperature measurements were performed to investigate the fundamental luminescent mechanisms of the samples. For *o*-ImPyAq **110**, the signal-to-noise ratio remained poor, showing almost no emission at all. For *m*-ImPyAq **109**, a bathochromic shift was observed for the prompt fluorescence at 77 K. No delayed luminescence was observed.

In contrast to this, the emission intensity of *p*-ImPyAq **108** was significantly increased upon cooling to 77 K. Aside from the prompt fluorescence, a delayed luminescent was also observed. Surprisingly, the maximum emission wavelength of the delayed fluorescence shows a hypsochromic shift. A potential reason might be that the sample was flash-frozen, thus the conformations of the individual molecules are not in an equilibrium. Presumably, while the singlet emission from all molecules, whereas triplet emission might only occur from certain geometries,

resulting in an unexpected emission profile. Further studies are needed to clarify the underlaying complex phosphorescence mechanism.

Table 4. Photophysical properties of the synthesized emitters.

entry	$l_{max/abs}$ (nm)[a]	e_{max} (M^{-1} cm^{-1})[a]	$l_{max/emi}$(nm)[a]
o-BisImPyAq 110	285 / 335	27,828 / 13,664	463
m-BisImPyAq 109	285/340	32,545 / 15,717	460
p-ImPyAq 108	283 / 332	18,432 / 11,424	455

[a] Measured in Toluene.

Cyclic Voltammetry. To calculate the energies of the frontier molecular orbitals, cyclic voltammetry measurements were performed. The cyclovoltagrams are displayed in **Figure 29** against the ferrocene/ferrocenium (Fc/Fc⁺) redox couple, and in **Figure 30** against standard calomel electrode (SCE). The energy levels of the frontier molecular orbitals (FOMOs) were calculated from the redox potentials (**Table 5** and **Table 6**).
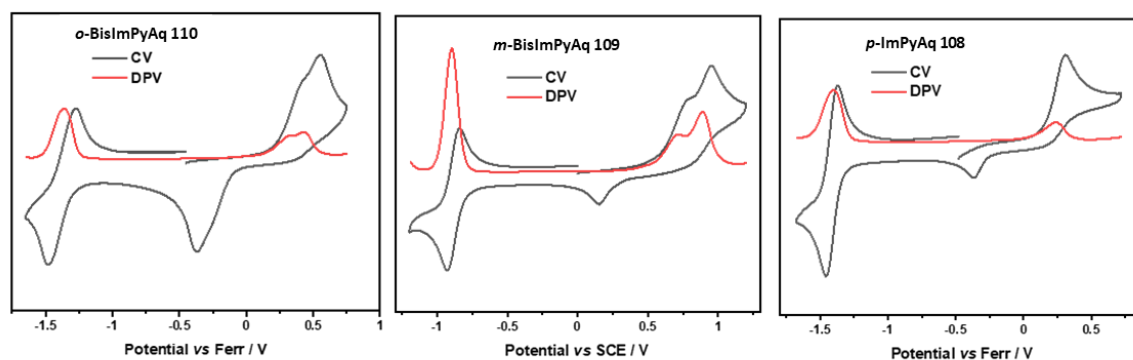
Figure 29. Cyclic voltammetry measurements of **108**, **109** and **110** in dichloromethane and calibrated versus the ferrocene/ferrocenium (Fc/Fc⁺) redox couple (DPV in red).

Table 5. FOMO energy levels were calculated from the redox potentials against the ferrocene/ferrocenium (Fc/Fc⁺) redox couple.

entry	$E_{1/2\ ox}$ (V)[a]	$E_{1/2\ red}$ (V)[a]	HOMO (eV)[b]	LUMO (eV)[c]	E_{gap} (eV)[d]
o-BisImPyAq 110	0.31	-1.36	-5.11	-3.44	1.67
m-BisImPyAq 109	0.25	-1.36	-5.05	-3.44	1.61
p-ImPyAq 108	0.24	-1.40	-5.04	-3.40	1.64

[a] Measured in dichloromethane and calibrated versus the ferrocene/ferrocenium (Fc/Fc⁺) redox couple. [b] Calculated using the formula HOMO = -[E_{ox} + 4.8] eV. [c] Calculated using the formula LUMO = [E_{red} + 4.8] eV. [d] Calculated using the formula E_{gap} = [HOMO − LUMO] eV.
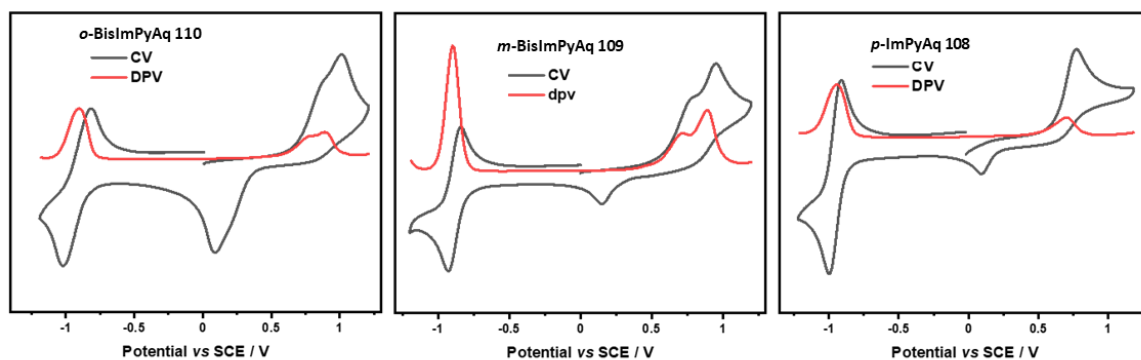
Figure 30. Cyclic voltammetry measurements of **108**, **109** and **110** in dichloromethane and calibrated versus standard calomel electrode (SCE) (DPV in red).

Table 6. FOMO energy levels were calculated from the redox potentials standard calomel electrode (SCE).

entry	$E_{1/2\ ox}$ (V)[a]	$E_{1/2\ red}$ (V)[a]	HOMO (eV)[b]	LUMO (eV)[c]	E_{gap} (eV)[d]
o-BisImPyAq 110	0.77	-0.90	-5.11	-3.44	1.67
m-BisImPyAq 109	0.71	-0.90	-5.05	-3.44	1.61
p-ImPyAq 108	0.70	-0.92	-5.04	-3.40	1.64

[a] Measured in dichloromethane and calibrated versus standard calomel electrode (SCE). [b] Calculated using the formula HOMO = -[E_{ox} + 4.8] eV. [c] Calculated using the formula LUMO = [E_{red} + 4.8] eV. [d] Calculated using the formula E_{gap} = [HOMO – LUMO] eV.
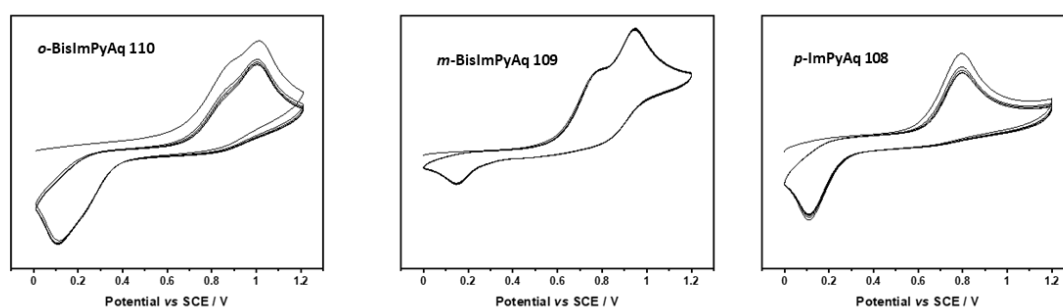
Figure 31. Cyclic voltammetry measurements of **108**, **109** and **110** in dichloromethane over multiple sweeps.

Upon the first oxidation event taking place, a cathodic peak at circa 0.1 V for the three samples can be observed, even when recording on a reversed scan. Potential reasons could be the formation of new species, *e.g.*, dimers or polymers, or decomposition. However, this is unlikely, as recording multiple sweeps did not change the peaks considerably (**Figure 31**), hinting towards a reversible event. Changing the scan rate also does not change the profile or make the oxidation more reversible. Cleaning the surface of the electrode does not influence the measurements either, which means that there is no adsorption taking place. Hence, the peaks originate from the compounds themselves.

Overall, the series of ImPyAq compounds exhibits unusual spectroscopic and electronic properties. The origin of this behavior could not be identified within the context of this work, but will be subject of further studies.

3.2 Imidazo[1,2-*a*]pyridines as Fluorophore Tags for Bioimaging of Steroids

Preface. A manuscript for the following chapter is currently in preparation. The project was done in collaboration with N. Rosenbaum, who also discussed parts of it in his dissertation.[120] The synthesis and characterization of all precursors were done by N. Rosenbaum and the author. Synthesis and characterization of the fluorophore-steroid conjugates were done by N. Rosenbaum, J. Hohmann and the author. UV/Vis-absorption and fluorescence emission spectra were recorded by the author. Cytotoxicity assay and co-localization studies were performed by D. Feser. Cell experiments are currently performed by the Guse Group at the University of Heidelberg.

Introduction. Gorgosterol (**116**), first isolated by Bᴇʀɢᴍᴀɴɴ *et al.* in 1943, belongs to the class of marine steroids found in the soft coral *plexaura flexosa* and its symbionts (**Figure 32**).[121] Exploring the yet unknown role of Gorgosterol in the symbiosis of corals and algae can help elucidate relationships between them. This is crucial for the protection of marine wildlife, especially in respect of the growing stress on marine ecosystems through the effects of climate change. In cooperation with the Gᴜꜱᴇ group at the University of Heidelberg, we aimed to perform cell localization studies of Gorgosterol-derived steroids to gain insight into the relevance of these substances for different metabolic processes. Since steroids do not exhibit any intrinsic luminescence, conjugation of a fluorophore tag is necessary to visualize them in fluorescence microscopy.

R = Me - Gorgosterol
R = H - Demethylgorgosterol

116
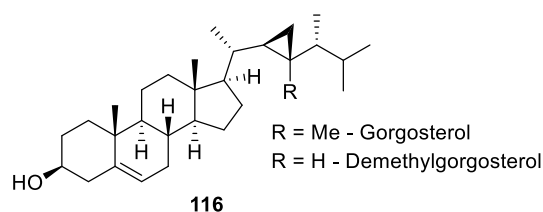
Figure 32. Molecular structure of Gorgosterol and Demethylgorgosterol.

Commercial dyes commonly employed in the fluorescent labeling of biomolecules (e.g., proteins) like rhodamine or fluorescein were not found suitable for the labeling of the present compounds due to their size compared to the relatively small steroid scaffold. Additionally, most dyes are highly polar or ionic. These factors could alter the conjugate properties and behavior. Therefore, size, polarity and fluorescence profile must be carefully balanced to prevent the falsification of intercellular localization and ligand binding.[37b] In contrast to this, the imidazo[1,2-*a*]pyridine moiety is comparably small, thus reducing the risk of dominating the conjugate's properties. Moreover, a steroidal aldehyde intermediate, formed during the semisynthesis of Demethylgorgosterol,[122] lends itself perfectly for the facile assembly of an imidazo[1,2-*a*]pyridine *via* a GBB-3CR. This de novo synthesis strategy of the tag can be considered a fluorophore approach (*cf.* **Chapter 1.2.2**).

Synthesis. The steroidal aldehyde intermediate **117**, provided by Dr. N. ROSENBAUM, was transformed in a GBB-3CR with different amidines and isonitriles. To maximize the conversion of the aldehyde component, an excess of the other components was employed. The reaction was performed using a 1 M solution of perchloric acid in methanol as the catalyst in a mixture of dichloromethane and methanol to synthesize a small library of five steroid-fluorophore conjugates (**Scheme 17**).
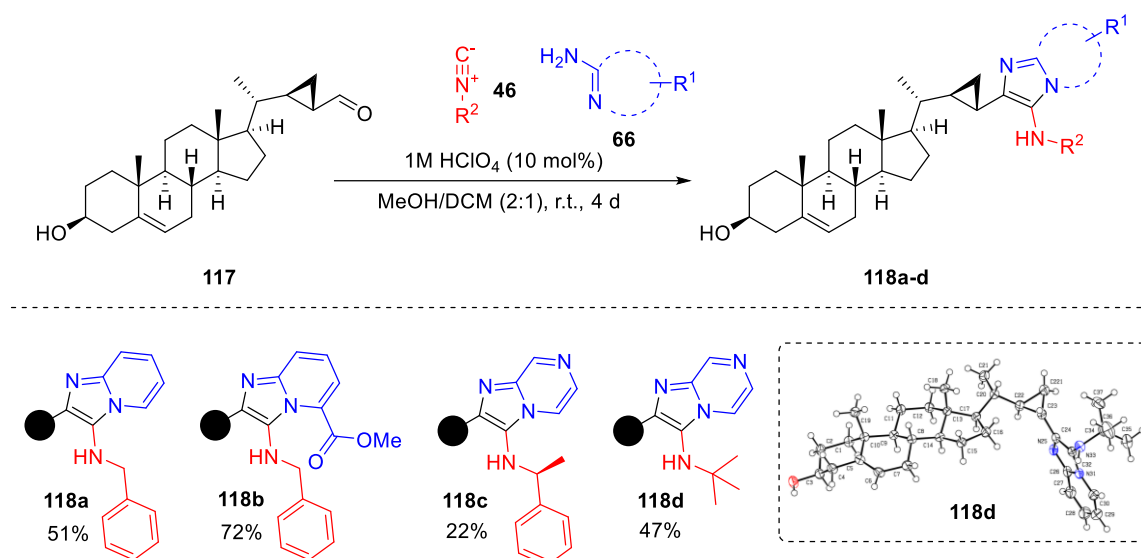
Scheme 17. Side-chain functionalized imidazo[1,2-*a*]heterocyclic Demethylgorgosterol derivatives synthesized *via* GBB-3CR and Single-crystal X-Ray structure of 4b (displacement parameters are drawn at 50% probability level).

The desired conjugates were isolated in yields of up to 72%. No epimerization was observed. The structure of conjugate **118d** was verified *via* single crystal X-Ray analysis.

To retain the characteristic aliphatic cyclopropyl sidechain of the Gorgosterol family, another derivative, termed "inverse" fluorophore-steroid conjugate, was synthesized in a GBB-3CR (**Scheme 18**). The fluoro-tag was attached through a methylene linker. The inverse conjugate **120** was obtained in an excellent yield of 89%.
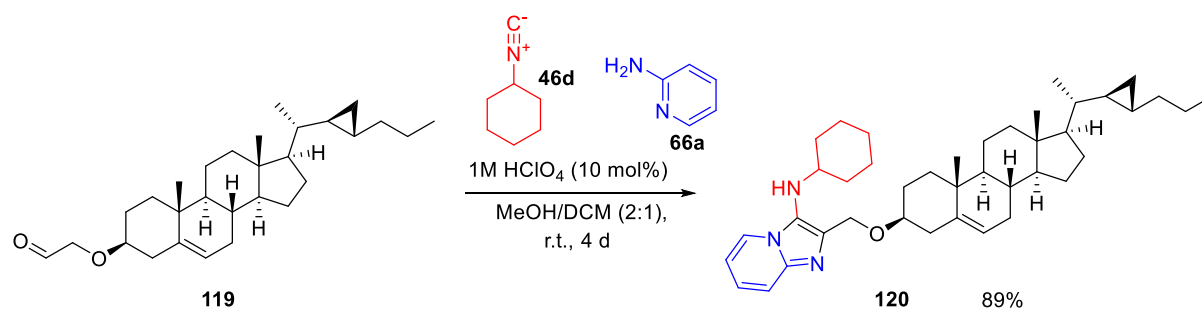
Scheme 18. Scaffold functionalized imidazo[1,2-*a*]heterocyclic Demethylgorgosterol derivatives synthesized *via* GBB-3CR.

Fluorescence properties. UV/Vis absorption and fluorescence emission spectra of the synthesized conjugates were recorded in chloroform. The normalized spectra are depicted in **Figure 33**. Upon prolonged irradiation, some of the compound solutions turned brown. This could either indicate a reduced photostability of the compounds or originate from the photo-induced generation of phosgene from chloroform.
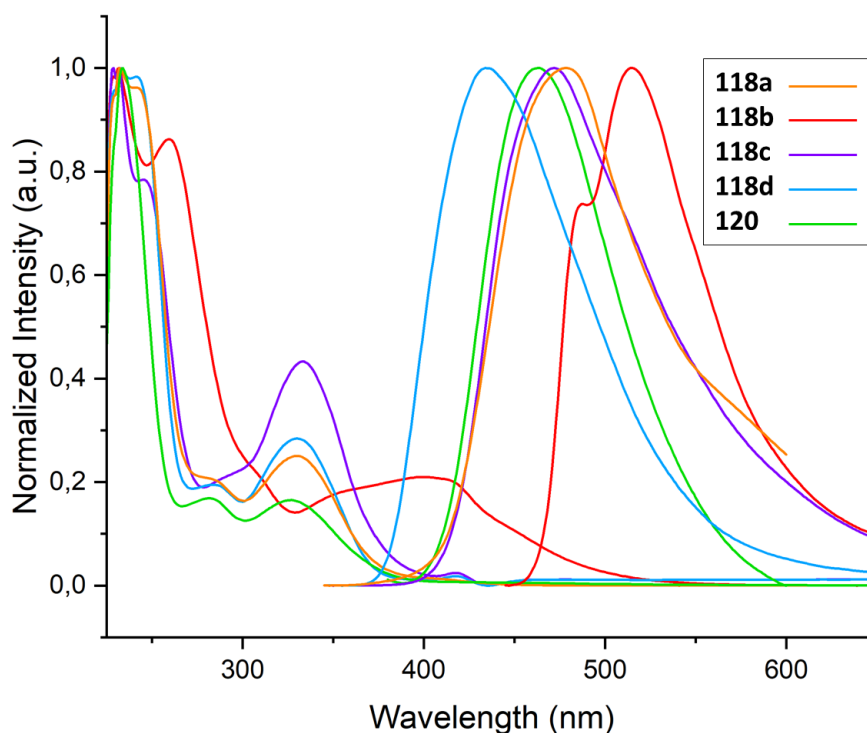
Figure 33. Normalized absorption and emission spectra of the synthesized fluorophore-steroid conjugates measured in CHCl₃.

Table 7. Maximum absorption and emission wavelength of the conjugates in chloroform.

entry	λ_{abs} [nm]	λ_{em} [nm]	Stokes Shift [nm]
118a	330	480	150
118b	400	474 / 502	74 / 102
118c	333	467	134
118d	332	435	103
120	327	458	132

All fluorophore-steroid conjugates show two distinct absorption bands around 250 nm and 330 nm. For the methyl picolinate-derived compound **118b**, a significant bathochromic shift of the second absorption maximum to 400 nm was observed. The emission maxima range from 410 nm to 510 nm. The pyridine derivate **118a** shows the lowest emission wavelength while the pyrazines **118b** and **118c** exhibit a slight bathochromic shift. A similar trend was also observed for the PCP-derived imidazo[1,2-*a*]heterocycles (see **Chapter 3.1**). The picolinate is

significantly red-shifted and shows a shoulder peak at 490 nm. This could indicate an underlaying ESIPT mechanism between the secondary amine proton and the carbonyl oxygen atom of the adjacent methyl ester.

Cytotoxicity. The synthesized compounds were evaluated in an MTT-assay to determine their cytotoxicity. The results are shown in **Figure 34**.
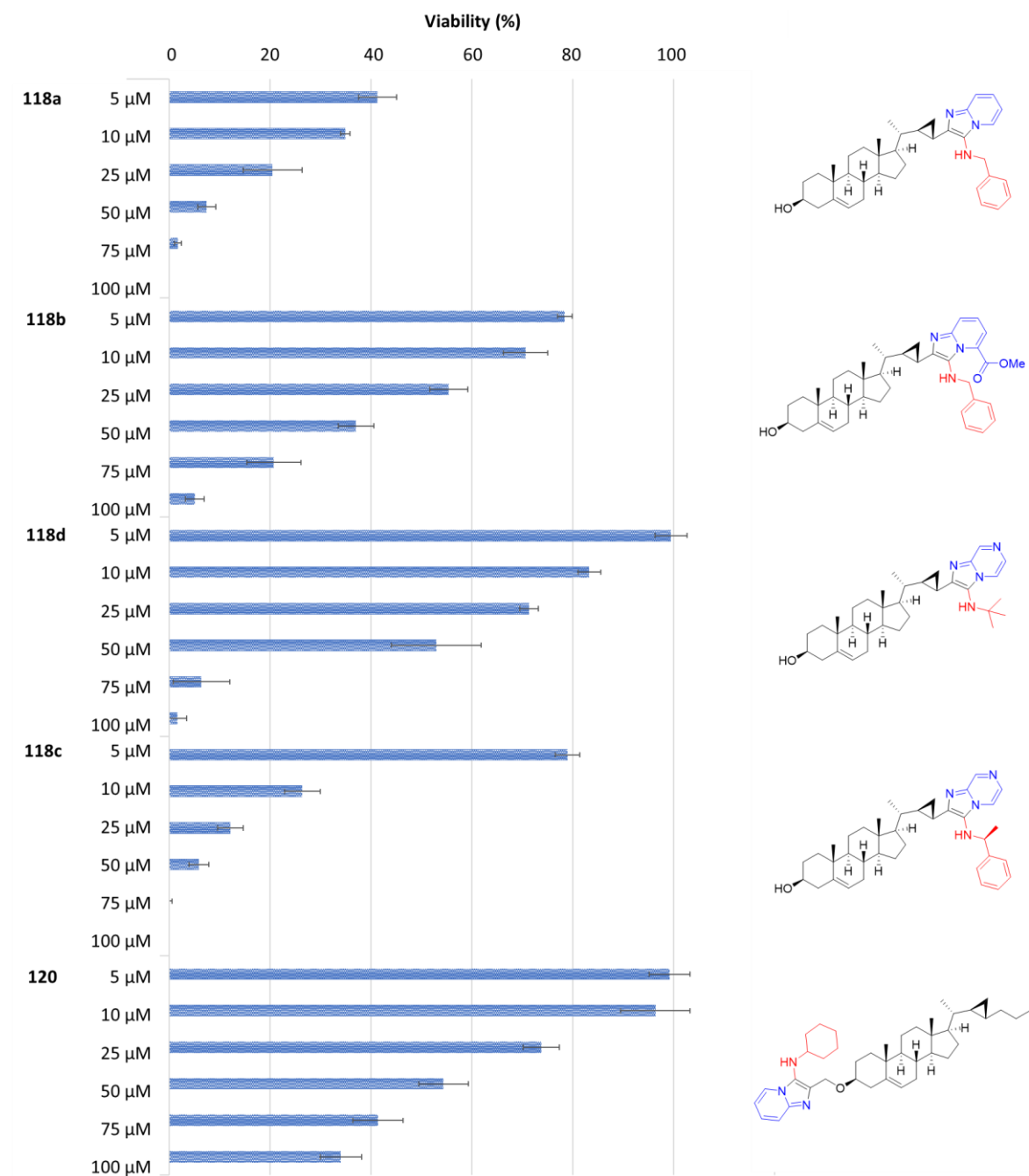
Figure 34. Cytotoxicity studies of the fluorophore-steroid conjugates in HeLa cells. The cells were incubated with solutions of different analyte concentrations. The viability was calculated through the comparison with untreated cells.

Among the synthesized fluorophore-steroid conjugates, **118a** shows the highest cytotoxicity, reducing the cell viability to 40% at the lowest tested concentration of 5 µM, followed by **118b** and **118c**, which at 5 µM reduce the viability to around 80%. **118a**, **118b** and **118dc** bear a phenyl ring in the 3-amino side chain derived from benzyl isonitrile and α-methyl benzyl isonitrile, respectively. The aromatic 3-amino side chain is integral for the cytotoxicity of the conjugates. The compounds **118c** and **120**, which do not bear this side chain, exhibit significantly lower toxicity, reducing the viability to around 50% at 50 µM. **118d** bears a *tert*-butyl side chain and is, apart from this, identical to **118c**. This further supports the assumption that the aromatic isonitrile-derived residue has a significant influence on the cytotoxic profile. The comparably low toxicity of the inverse fluorophore-steroid conjugate **120**, which has a cyclohexyl amino residue, could also be attributed to the missing aromatic side chain. The position of the fluorescence tag is seemingly less important to the cell viability.

To determine the overall influence of the imidazo[1,2-*a*]heterocyclic tag on the cytotoxic profile, complementing studies of differently substituted Gorgosterol derivatives should be conducted.

Bioimaging Studies. The fluorophore-steroid conjugates were investigated in cell co-localization studies in cooperation with DOMINIK FESER from the SCHEPERS group. HeLa cells were treated with 5 µM solutions of the compounds. Mitotracker Red was used as a counter stain for mitochondria. The images are displayed in **Figure 35**.

In the blue channel, signals are observed for conjugates **118b** and **118c**, with **118c** showing the brightest fluorescence. Conjugates **118a**, **118d** and **120**, unfortunately, did not show any considerable signals. Structurally, the imidazo[1,2-a]heterocyclic moieties of the visible compounds both bear a benzyl or methyl benzyl side chain in the 3-position. Concerning the amidine component, **118b** is derived from 6-amino methyl picolinate, whereas the brighter **118c** bears an imidazo[1,2-*a*]pyrazine. The other 2-aminopyrazine derived conjugate **118d**, however, was not fluorescent enough. Hence, the pyrazine ring is not the solely decisive structural feature for the *in vivo* visibility. An aromatic side chain seems to also be important for the fluorescence of the compounds. The imidazo[1,2-*a*]pyridines **118a** and **120** did not give any signals at all, thus this scaffold is not suitable as a fluorescent tag.

The overlay of the blue and red channels suggests an accumulation of the compounds in the mitochondria, regardless of the residues. This result is supported by reports describing mitochondrial accumulation for similar hydrophobic small molecules.[123]

These results showcase the suitability of the imidazo[1,2-*a*]heterocyclic fluorescent tag for the labeling of bioactive small molecule analytes. Namely, the 3-(methylbenzyl)amino imidazo[1,2-*a*]pyrazine tag can be employed as a blue dye. Currently, the respective fluorophore-steroid conjugate **118c** is investigated in other *in vivo* assays using corral cells instead of human cell lines like HeLa. Due to the visibility of the conjugate, these studies should reveal more about the cellular mechanisms in which Gorgosterol-derived steroids are involved.
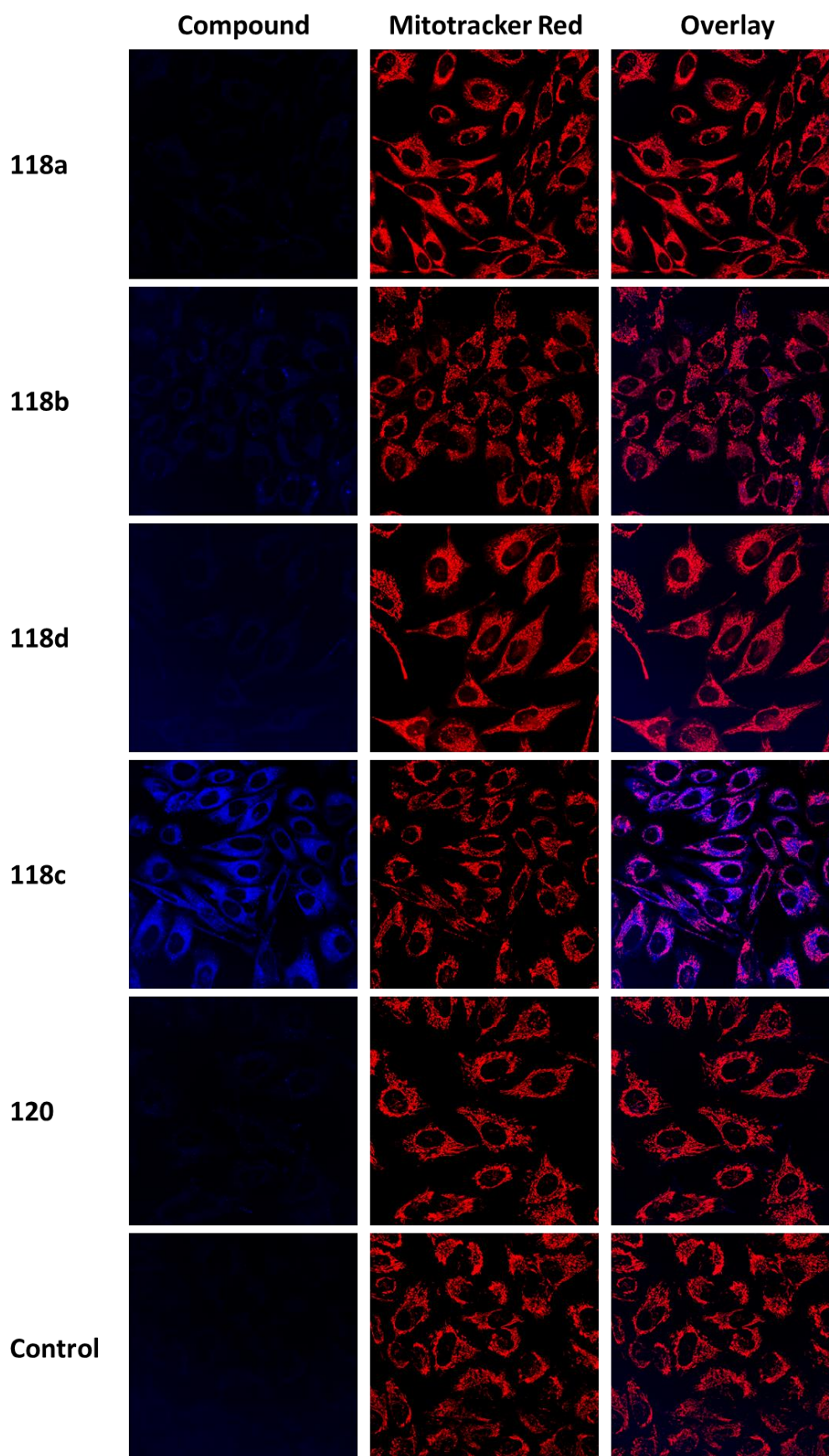
Figure 35. Localization study of the fluorophore-steroid conjugates in HeLa cells using 5 μM solutions of the analytes. The cells were incubated for 5 h. Left: Luminescence of the analytes; middle: counter staining of mitochondria with Mitotracker Red; right: merge of the channels.

3.3   Flat *N*-rich Heterocycles as DNA-Intercalating Agents

Preface. Parts of the following chapter were published in Organic and Biomolecular Chemistry (RSC Publishing).

M. Stahlberger, O. Steinlein, C. R. Adam, M. Rotter, J. Hohmann, M. Nieger, B. Köberle and S. Bräse, Fluorescent Annulated Imidazo[4,5-*c*]isoquinolines *via* a GBB-3CR/Imidoylation Sequence – DNA-Interactions in pUC-19 Gel Electrophoresis Mobility Shift Assay, *Org. Biomol. Chem.* **2022**, 20, 3598.

3.3.1   Post-Modification of GBB-Scaffolds *via* Imidoylative Amination Reactions

Motivation. Regarding the development of new bioactive structures, MCRs excel due to their unmatched potential in establishing large and diverse compound libraries. However, medicinal chemistry, in particular, demands an even higher level of variability, *e.g.*, for high throughput screenings and lead structure optimization. To achieve an even higher degree of diversification, post-modification strategies have been developed to convert MCR products into various kinds of more drug-like, heterocyclic scaffolds.[124] Post-MCR transformations are quite elegant since they offer short synthetic pathways to complex structural motifs and enlarge the accessible chemical space. Due to its widespread applications and high functional group tolerance, most post-MCR strategies have emerged around the UGI-4CR.[125] Among these, ring closure *via* palladium-catalyzed cross coupling reactions are quite prominent.[125j] Ring expansion can be achieved by inserting C_1-synthons like carbon monoxide or isonitriles into the newly coupled bond.[73c-g, 126] CHAUHAN *et al.* applied this methodology to post-modify UGI scaffolds and converted these into isoquinolin-1(2H)-ones.[127] However, post-cyclization strategies of the imidazo[1,2-*a*]pyridine scaffolds accessible *via* the GBB-3CR remain scarce, despite their biological relevance. Reported post-modification procedure of GBB-scaffolds include *N*-arylations (e.g. ULLMAN coupling),[128] PICTET-SPENGLER reactions,[128b] STRECKER-type cyclizations,[129] oxidative ring closures[130] or simple intramolecular condensation reactions.[131] An overview of the accessible scaffolds is presented in **Scheme 19**. In most reports, no further studies of these compound classes were conducted to investigate possible bio-applications. Polyheterocycles are promising scaffolds showing various bioactive properties such as anticancer or DNA-intercalation activity.[132]
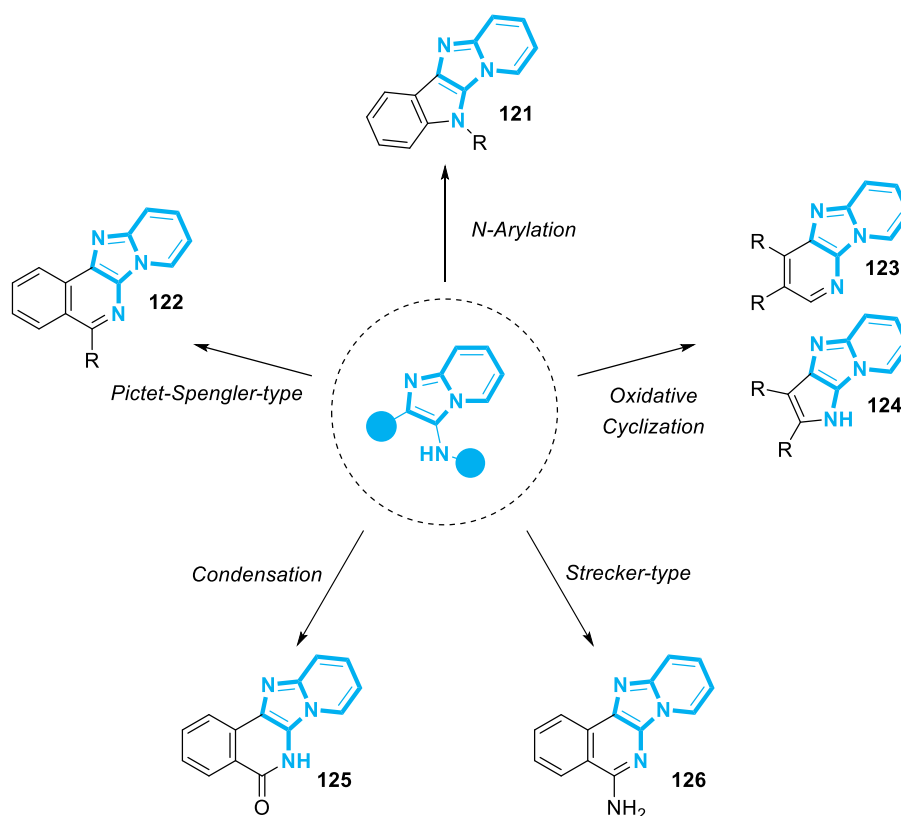
Scheme 19. Selected post-cyclization methods of imidazo[1,2-*a*]scaffolds accessible through the GBB-3CR.

Thus, we aimed to develop a novel sequential synthesis route to convert the GBB-3CR products into more sophisticated, polycyclic systems. Inspired by the sequential UGI-4CR/imidoylation reaction by CHAUHAN *et al.*,[127] we planned to synthesize polyheterocycles *via* a GBB-3CR/imidoylation sequence.

It should be noted that nomenclature concerning such sequential reaction processes is not used consistently in literature and the terms sequential or consecutive transformation and tandem, domino or cascade reaction are often confused. Hence, TIETZE proposed the following definitions to classify chemical reaction sequences.[133] A tandem reaction is considered a one-pot process involving two or more individual reactions taking place under the same reaction conditions. However, these reactions do not occur in parallel, but rather in a linear fashion with the subsequent reaction resulting from the functionalities formed in the previous reaction. Also, the terms domino and cascade reaction describe this case and are thus used synonymously. In a consecutive reaction, on the other hand, the following reaction requires the addition of a catalyst, a mediator, or another reagent. Hence, the whole process remains a one pot-procedure with individual reactions taking place after another while the reaction conditions change throughout the procedure. Sequential reactions form the third reaction class. In contrast to tandem and consecutive reactions, these cannot be conducted as one-pot procedures and require the isolation of the intermediate product.

Synthesis. The precursors were synthesized in a GBB-3CR using perchloric acid or glacial acetic acid as the catalyst. In total, a set of seven GBB-precursors were obtained (**Scheme 20**). Overall, the 3-(*o*-bromophenyl)imidazo[1,2-*a*]heterocycle precursors **128a-g** were obtained in moderate to excellent yields, ranging from 19% to 96%. Considering the mechanism of the GBB-3CR discussed in **Chapter 1.2.3**, the yields of the aminopyridine reactions are significantly lower as the electron-withdrawing nature of the additional nitrogen atom decreases the nucleophilicity of the amine, thus hampering the imine formation. Similarly, electron-donating substituents on the aldehyde component also decrease the yields due to the reduced electrophilicity of the carbonyl carbon atom. Moreover, electron-donating substituents on the amidine component increase the nucleophilicity of the amine, leading to higher yields.
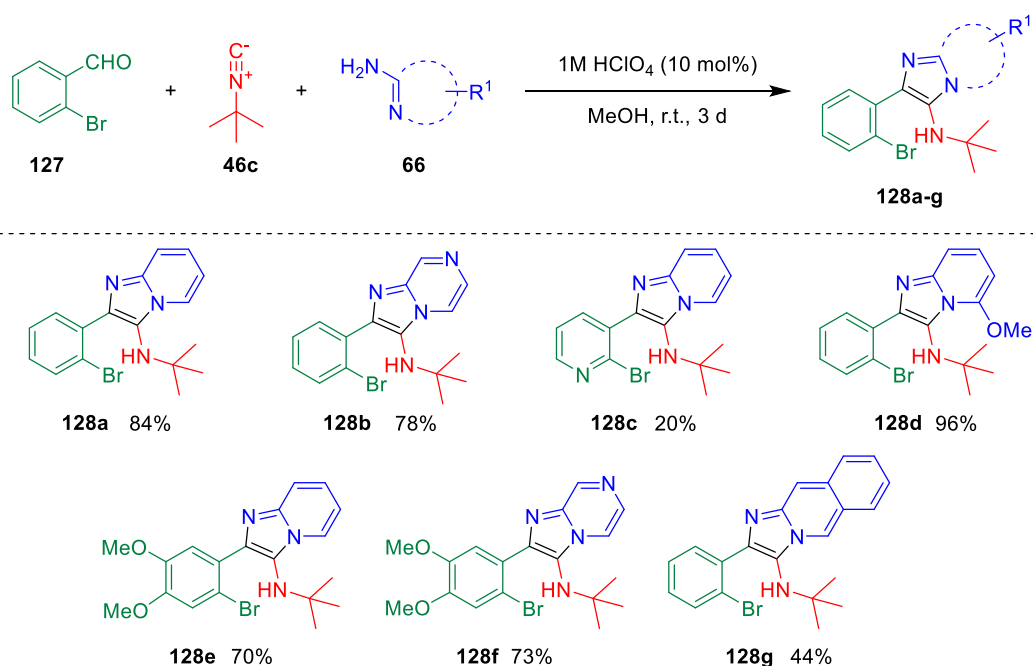
Scheme 20. Synthesis of the 3-(*o*-bromophenyl)imidazo[1,2-*a*]heterocyclic precursors *via* a GBB-3CR. *2.00 equiv of glacial acetic acid were used instead of perchloric acid.

Subsequently, these precursors should be intramolecularly cyclized in an imidoylative HARTWIG-BUCHWALD amination reaction to form annulated imidazo[4,5-*c*]isoquinoline ring systems. In this process, another isonitrile component is inserted between the bromide and the secondary amine. The resulting imine could not be isolated as it immediately undergoes an imine-enamine tautomerization and aromatization overpaid by the elimination of gaseous *iso*-butene. Thereby, the π-system is extended to span over the four rings. A mechanistic rationale is described in **Scheme 21.**
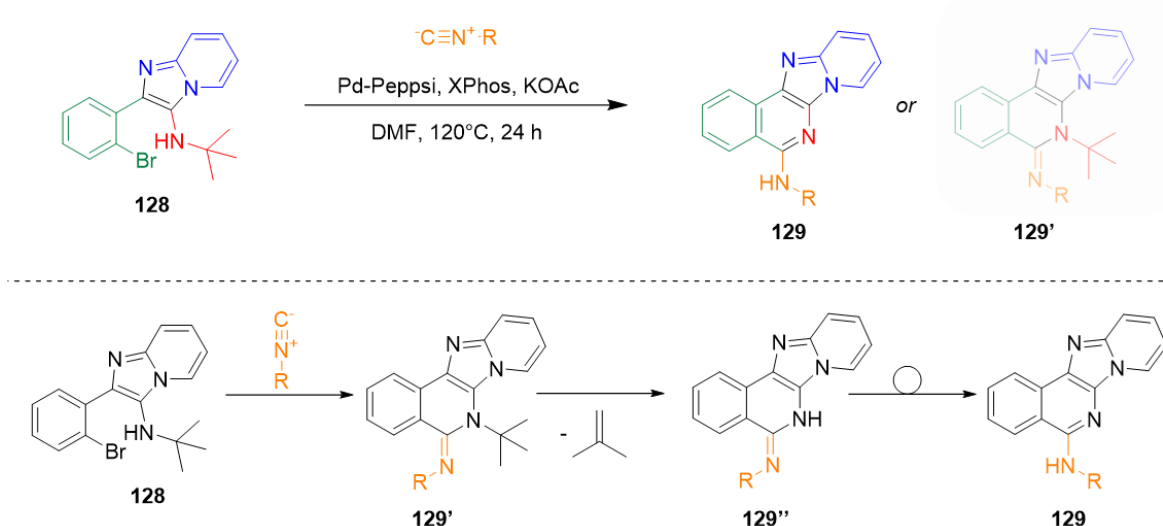
Scheme 21. Proposed mechanistic rationale for the formation of **129**.

The proposed structure of the insertion products **129ad** and **129ba** were verified through single crystal X-Ray analysis (**Figure 36**).
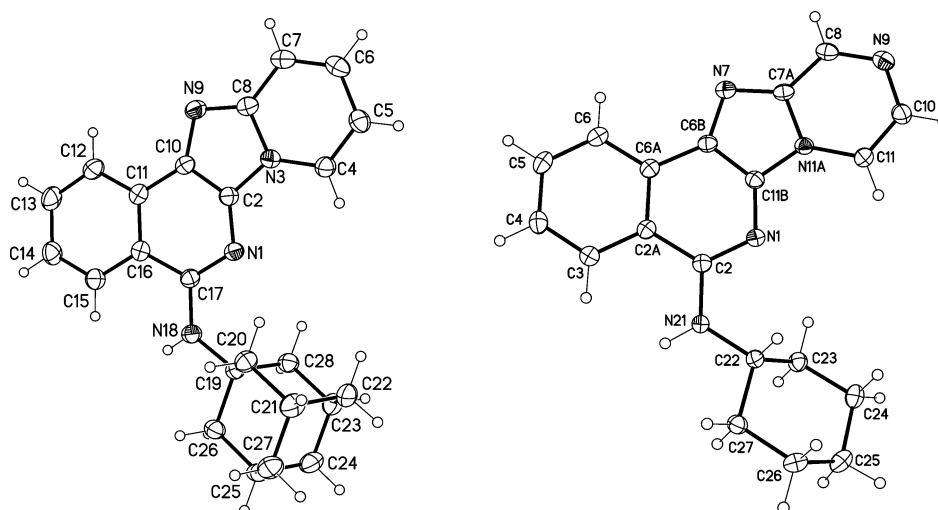
Figure 36. Single-crystal X-Ray structure of **129ad** and **129ba** (displacement parameters are drawn at 30% probability level for **120ad** and 50% probability level for **129ba**).

To optimize this reaction step, several conditions were screened for the insertion of cyclohexyl isonitrile into **128a**. (**Table 8**). The desired insertion product was obtained in 83% yield under imidoylation conditions first reported by Orru *et al.* for the synthesis of 4-amino quinazolines.[134] Using Pd-Peppsi-iPr as the pre-catalyst, the yield was increased to 94%. Under ligand-free conditions, the yield decreased significantly. In most reactions, potassium acetate was used as the base. Stronger bases were not employed as these would accelerate the addition of the amine to the intermediate palladium complex which would compete with the insertion of the isonitrile into the carbon-palladium bond, leading to a non-imidoylative Hartwig-Buchwald amination process affording the respective five-membered ring.

Table 8. Optimization of the intramolecular imidoylative HARTWIG-BUCHWALD coupling using cyclohexyl isonitrile.
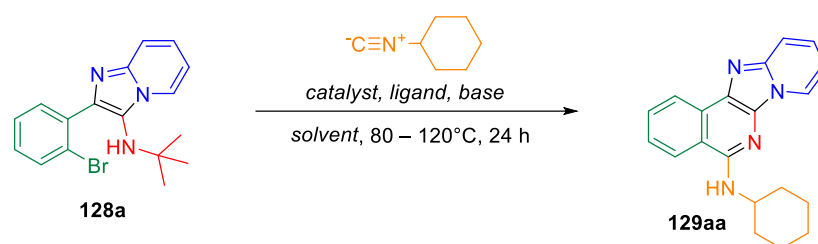
entry	catalyst	ligand	base	solvent	T (°C)	yield (%)^c
1	Pd(OAc)$_2$	*none*	Cs$_2$CO$_3$	DMF	80	0
2	Pd$_2$(dba)$_3$	PPh$_3$	KOAc	DMF	120	0
3	Pd(dba)$_2$	XPhos	KOAc	DMF	120	83
4	**Pd-Peppsi-iPr**	**XPhos**	**KOAc**	**DMF**	**120**	**94**
5	Pd-Peppsi-iPr	*none*	KOAc	DMF	120	38

128a (1.00 equiv), RNC isonitrile (1.3 equiv), ligand (5 mol%), ligand (10 mol%).

Using the optimized reaction conditions, the *p*-bromophenyl imidazopyridines were subjected to imidoylation with various aliphatic isonitriles. The results are depicted in **Scheme 22.**

The insertion products were obtained in moderate to excellent yields, ranging from 20% to 94%. The best results were obtained with precursor **128a**. The more electron-poor pyrazine analogue **128b** was less reactive, resulting in lower yields for **129ba** and **129bb**. This trend was also observed for the methoxy-substituted precursors **128e** and **128f**. The yield is decreased for **128c**, probably because of the slightly basic pyridine nitrogen atom which is easily protonated by silica during chromatographic work-up. Similarly, the benzannulated precursor **128g** was challenging in purification due to π–π stacking, leading to tailing effects.

Among the aliphatic isonitriles inserted into **128a**, cyclohexyl isonitrile performed best, followed by pentyl and 1-adamantyl isonitrile while *tert*-butyl isonitrile afforded the respective insertion product **129ab** in only 24% yield. Presumably, this could be due to the increased steric demand of the *tert*-butyl residue whereas the 1-adamantyl residue is more rigid. Attempts to incorporate aromatic isonitriles were mostly unsuccessful, except for 2,6-dimethylphenyl isonitrile (**129ag**). A plausible reason for the reduced reactivity of aromatic isonitriles is the formation of more stable palladium complexes. Due to the stronger donating character of aromatic isonitriles, these have a stronger affinity to palladium leading to the formation of cationic species with multiple isonitrile ligands.[135] Additionally, their ability for π-stacking adds to this effect. This leads to deactivation of the catalytically active species, reducing the overall reactivity. On the other side, these multiply coordinated complexes can engage in insertion reactions, affording multiple insertion products or isonitrile polymers.[136] Another trend is polarity, resulting in a more difficult purification due to tailing effects during column chromatography. Especially using 2-morpholinoethyl isonitrile, a significant amount of the product could only be obtained in mixed fractions, thus reducing the overall yield of **129ae**.
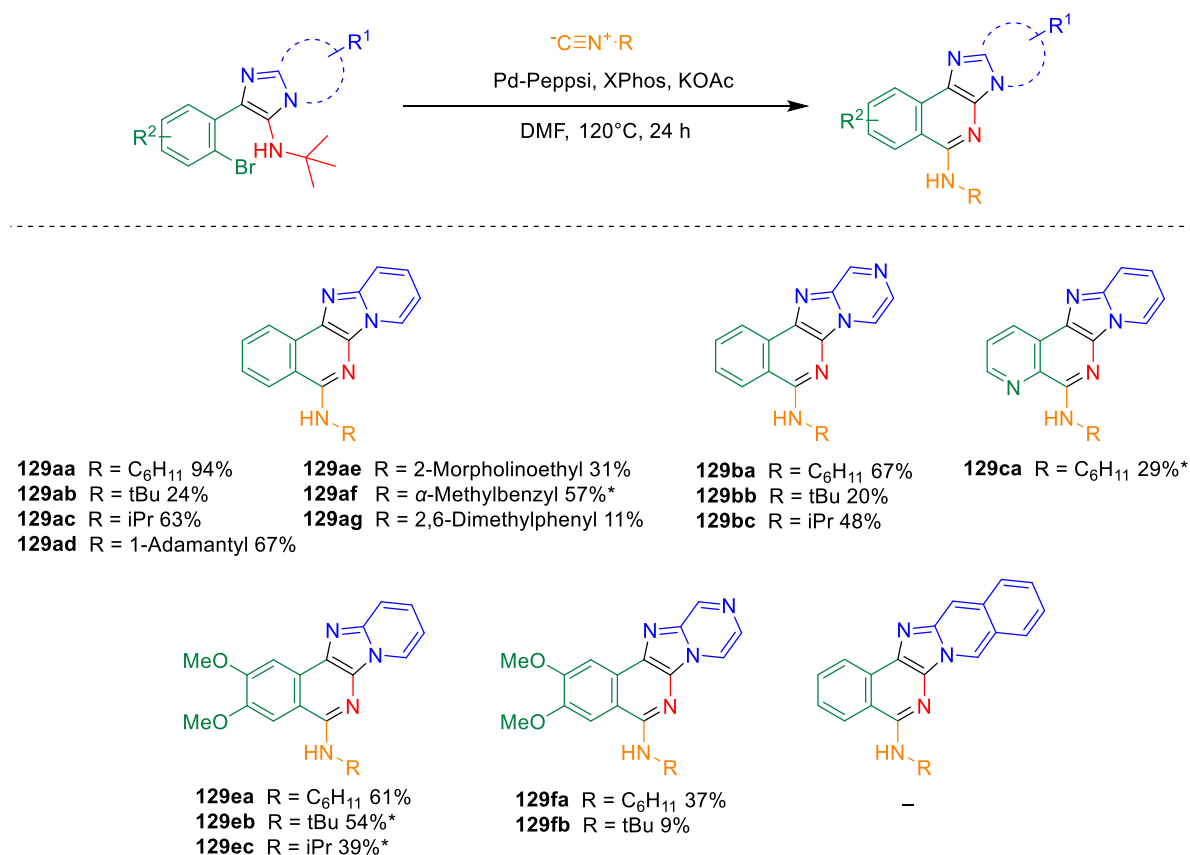
Scheme 22. Synthetic scope of the post-modification of GBB-scaffolds *via* an imidoylative Hartwig Buchwald amination. Reaction conditions: **128** (1.00 equiv), RNC (1.30 equiv), Pd-Peppsi-iPr (5 mol%), XPhos (10 mol%), base (3.00 equiv). *Pd(dba)$_2$ (5 mol%) was used as the Pd-source.

Fluorescence Properties. The insertion products exhibit a strong blue fluorescent under irradiation with UV light. Thus, the fluorescent properties of the insertion products were investigated. UV/Vis absorption and fluorescence emission spectra were recorded. The normalized spectra are shown in **Figure 37** and the maximum absorption and emission wavelengths are listed in **Table 9**.
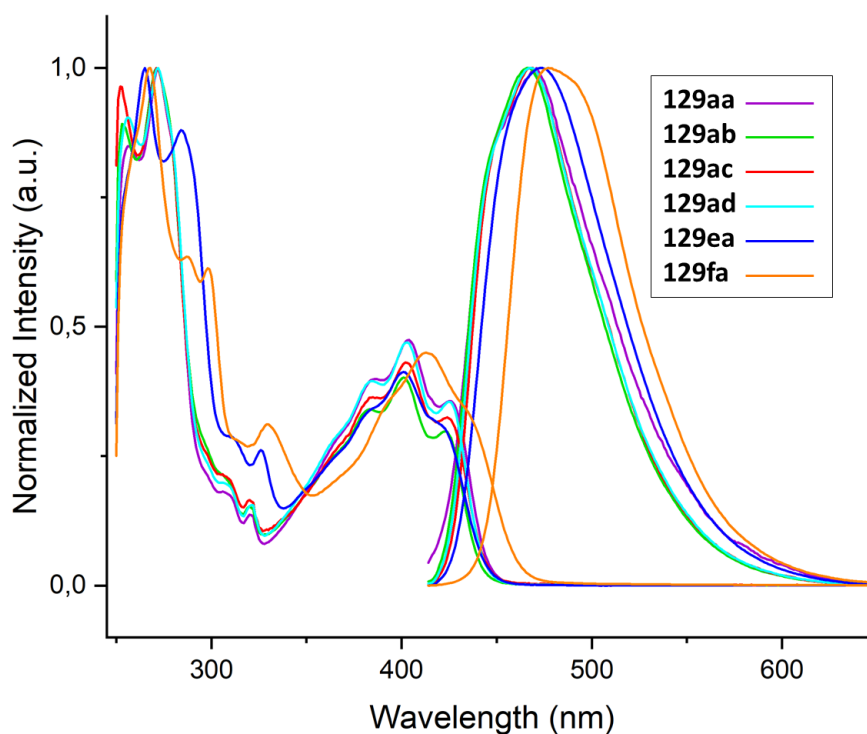
Figure 37. Normalized absorption and emission spectra of selected compounds in CHCl$_3$. λ_{exc} = 395 nm.

Table 9. Maximum absorption and emission wavelength of selected compounds in CHCl$_3$. λ_{exc} = 345 nm.

entry	λ_{abs} [nm]	λ_{Em} [nm]	Stokes Shift [nm]	entry	λ_{abs} [nm]	λ_{em} [nm]	Stokes Shift [nm]
129aa	257/**272** 404	471	67	**129ad**	257/**271** 403	468	65
129ab	254/**272** 401	467	66	**129ea**	**265**/285 403	473	70
129ac	253/**271** 403	468	65	**129fa**	**268**/298 412	476	64

The insertion products exhibit a strong blue fluorescence under irradiation with UV light. The normalized spectra are shown in **Figure 37**. The selected compounds show similar absorption profiles with two bands at around 250 – 280 nm and 375 – 430 nm, which consist of several overlapping bands. The emission spectra all show a maximum emission at around 475 nm. Both absorption and emission profiles are slightly bathochromically shifted for the methoxy substituted substrates.

Unlike the imidazo[1,2-*a*]pyridine system investigated in **Chapter 3.1**, the annulated imidazo[4,5-*c*]isoquinolines do not exhibit significant shifts in absorption and emission wavelengths upon the introduction of substituents or additional nitrogen atoms within the scaffold. Generally, substituent effects seem to have a smaller influence on the fluorescence properties of this system.

ESIPT Side Product. Performing the insertion reaction with GBB-precursor **128d** afforded an unexpected insertion product, an 11-amino-6-imino pyrido[2',1':2,3]imidazo[5,1-*a*]isoindol-1-one (**130**, **Scheme 23**).
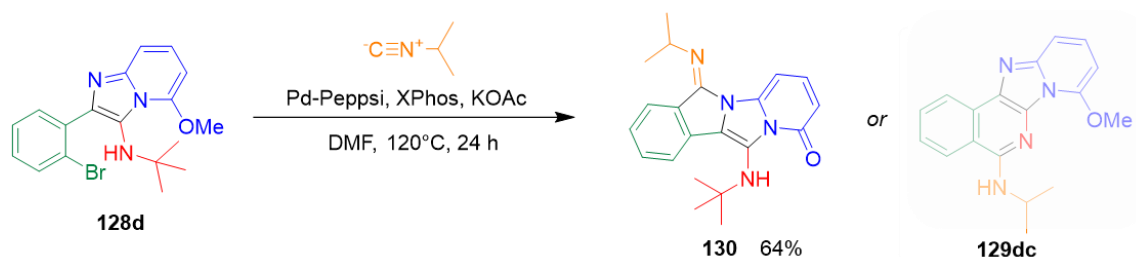
Scheme 23. Imidoylative amination of **128d** affording an unexpected demethylated insertion product.

NMR analysis indicated that the *tert*-butyl residue was not removed and, instead, both isonitrile derived residues are present in the product while cleavage of the methoxy ether was observed. The proposed structure could be verified *via* single crystal X-ray analysis (**Figure 38**).
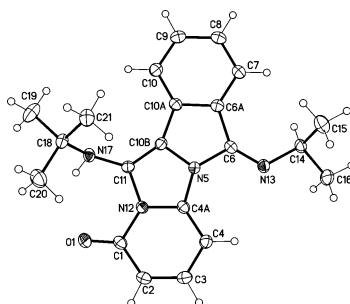
Figure 38. Molecular structure of **130** (displacement parameters are drawn at 50% probability level).

A proposed mechanistic rationale for the formation of the unexpected insertion product **130** is shown in **Scheme 24**. Upon cleavage of the methyl ether, the 4-hydroxy imidazo[1,2-*a*]pyridine **131** tautomerizes to **132**. The secondary amine in the 9-position is then able to nucleophillically attack the intermediary palladium imidoyl in species in **133** to give **130**.
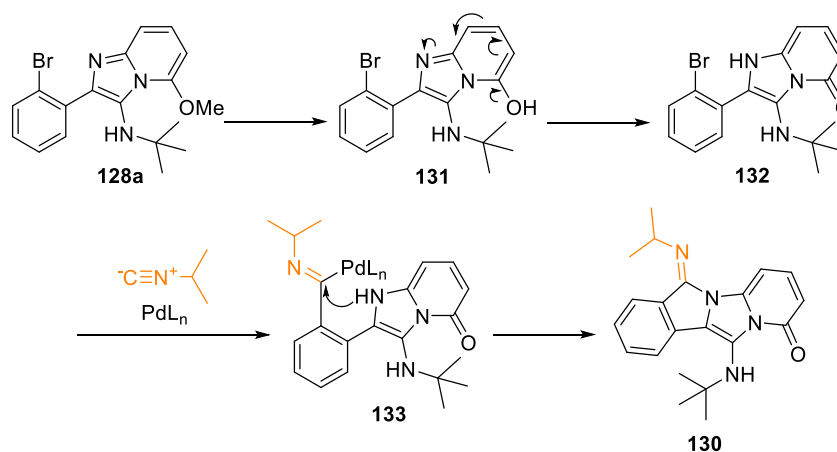
Scheme 24. Mechanistic rationale for the formation of the unexpected insertion product **130**.

Absorption and emission spectra of the 11-amino-6-imino pyrido[2',1':2,3]imidazo[5,1-*a*]isoindol-1-one reveal a strong bathochromic shift of both absorption and emission maxima, indicating an ESIPT process (**Figure 39**). Compared to the imidazo[4,5-*c*]isoquinolines **129**, the unexpected insertion product **130** exhibits a strong bathochromic shift of both absorption and emission, showing a bright green fluorescence upon irradiation. The emission profile shows two overlapping emission bands, which suggests two underlaying fluorescence mechanisms. Due to the proximity of the carbonyl oxygen and the secondary amine in **130**, an ESIPT process may be a plausible cause for the dual emission.[137]
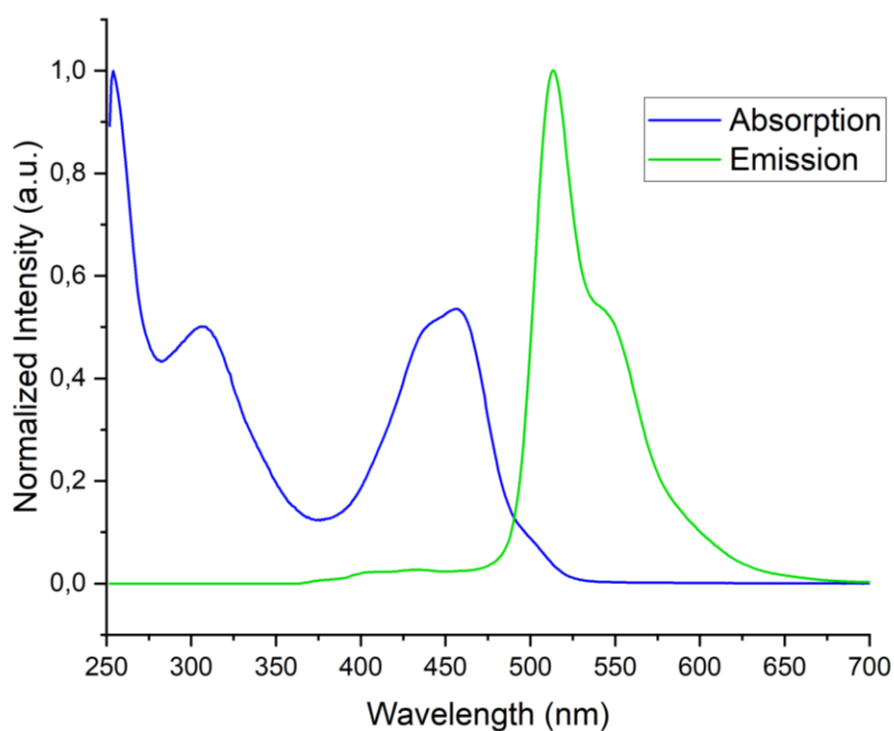
Figure 39. Normalized absorption and emission spectra of **130** measured in CHCl₃.

Overall, this unexpected reaction gives facile access to the pyrido[2',1':2,3]imidazo[5,1-a]isoindol-1-one ring system. Thus, future studies will aim towards expanding the scope of this imidoylative cyclization reaction and establishing of a compound library to further investigate the putative ESIPT properties and assess possible applications as fluorophores.

3.3.2 Investigation of DNA-Interaction

DNA-Binding. The interaction of small molecules with DNA is one of the most important targets for the development of novel chemotherapeutic drugs. Depending on drug's properties, there are different modes of non-covalent DNA binding, for instance, major or minor groove binding, unspecific binding to the phosphate backbone, or DNA-intercalation (**Figure 40**). Flat conjugated molecules, in particular, are often capable of sliding in between the base pairs of double-stranded nucleic acids through π-stacking. Most intercalators are – at least to some extent – sequence-specific. The intercalation results in an unwinding, elongation and rigidification of the double-strand and consequently in a change in the physical properties of the DNA, such as melting point or viscosity. Moreover, these structural changes interfere with the transcription and replication processes, specifically by inhibiting topoisomerase activity.[138] This makes DNA-intercalators both possible mutagens and potentially cytostatic compounds for inhibiting cell growth in tumors. Marketed chemotherapeutics like the anthracyclines doxorubicin and daunorubicin (**140**) rely on this effect. This group of drugs is also referred to as cytostatic antibiotics or tumor antibiotics due to their antibiotic properties. Moreover, the ability to intercalate DNA has been discussed in the context of antiviral drugs to combat diseases like Covid-19.[139]
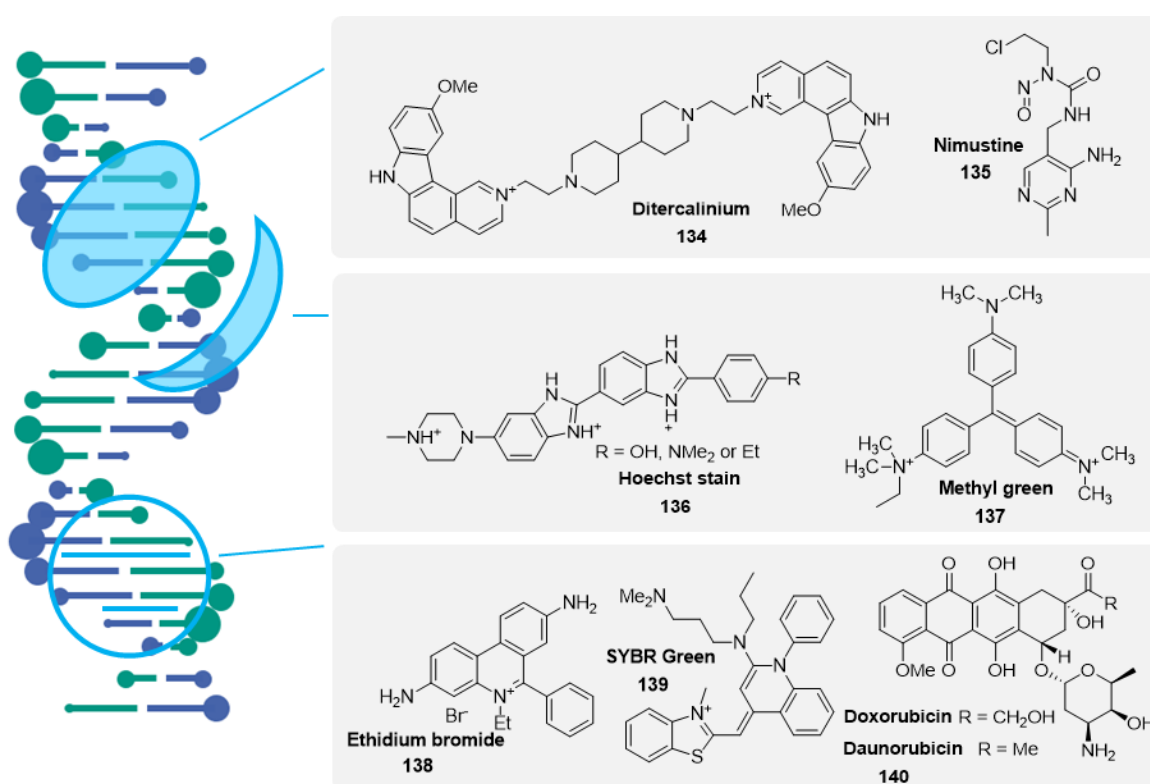
Figure 40. DNA-binding modes and selected examples of the three binder types.

Another widespread application of DNA-intercalating agents is as DNA-affine stains for the detection and visualization of nucleic acids in gel-electrophoresis, real-time quantitative PCR, or the microscopic imaging of cells.[140] Prominent examples of ds-DNA binding stains include the intercalators ethidium bromide (**138** and derived structures, *e.g.*, GelRed) and SYBR Green (**139**), as well as the major groove binder methyl green (**137**).

Since X-ray single crystal analysis revealed a flat geometric structure for the synthesized poly heterocycles, we planned to investigate their DNA-binding properties and identify possible trends in structure-activity relationships. In cooperation with DR. BEATE KÖBERLE and OSKAR STEINLEIN, a selection of the synthesized compounds was investigated (**Figure 41**).[141] Additionally, GBB-precursor **128a**, as well as the PCP-derived compounds **92b** and **92f** were selected as a comparison to assess the interactions of non-cyclized imidazo[1,2-*a*]pyridines. Ethidium bromide (**138**) was chosen as a positive control in the following assay due to its thoroughly studied mode of DNA intercalation.[142] Cisplatin (**141**), a common chemotherapeutic, was used as a negative control as it does not intercalate between base pairs. Instead, cisplatin covalently binds to guanine or adenine by crosslinking the strands, thus interfering with DNA-replication, and inducing apoptosis in fast growing cells.[143]
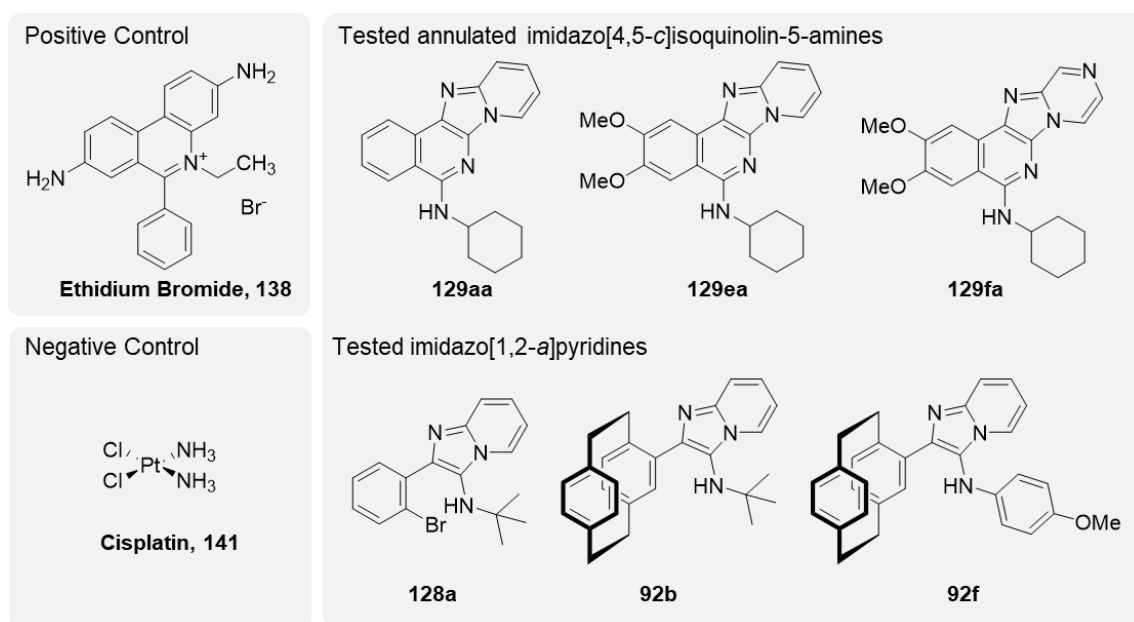
Figure 41. Substances evaluated in electrophoresis mobility shift assays.

DNA Staining. Commonly, ethidium bromide is replaced by other fluorescent stains in agarose or polyacrylamide gel electrophoresis experiments to visualize DNA-bands due to its alleged toxicity.[142, 144] For instance, the GelRed stain is an ethidium bromide analog containing two ethidium bromide moieties while exhibiting fewer toxic effects. The synthesized polyheterocycles were evaluated in a gel electrophoresis experiment without any additional stain to investigate their DNA-affinity and assess their suitability as DNA-stains. A selection of the synthesized compounds was incubated with pUC-DNA and applied onto a gel containing no DNA-stain like ethidium bromide or GelRed. The result is depicted in **Figure 42**. In lanes 3, 5, 7, 9, 11 and 12, the DNA bands could be visually stained. Lanes 2, 4, 6, 8 and 10, which do not contain DNA did not show any band. Thus, the band is unambiguously attributed to the pUC-DNA. Interestingly, lane 1 also shows a band even though the DNA in this lane was not treated with any dye. Potentially, the synthesized dyes can diffuse within the gel and small amounts of diffusing dye suffice to visibly stain DNA bands at other locations.
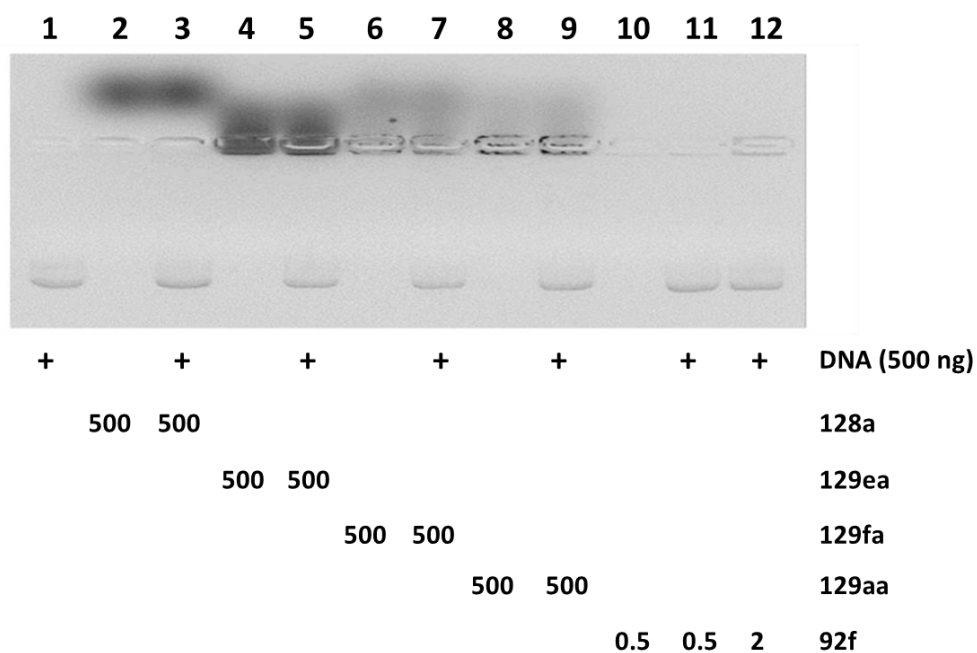
Figure 42. Staining of DNA with selected substrates. pUC19 DNA was treated with 2 mM of selected substrates in. sc and oc pUC DNA were detected by agarose gel electrophoresis.

pUC19-DNA Electrophoretic Mobility Shift Assay. A selection of the synthesized compounds was tested as dyes in an electrophoretic mobility shift assay (EMSA) to assess their effect on the properties of plasmid DNA. Previously, this assay has been established to investigate the strand-break induction capacity of DNA-damaging substances like transition metal compounds. In principle, plasmids of supercoiled DNA are subjected to the substance of interest.[145] Induction of single strand breaks converts the supercoiled (sc) plasmid DNA into open circular (oc), double strand breaks lead to the formation of linear DNA, which can both be separated from sc DNA by gel electrophoresis (**Scheme 25**).[146] In recent reports, this assay is performed with PM2-DNA, a 10 kbp plasmid isolated from the PM2-bacteriophage.[147] However, as the isolation of PM2-DNA is a more elaborate process, using different, more easily accessible plasmids would simplify this assay. For example, pUC19 DNA, a small *E. coli* plasmid of only 2686 bp in length, could provide a more inexpensive and easily obtainable alternative to PM2-DNA. The presented experiments are part of investigations by KÖBERLE and STEINLEIN aiming to establish the use of pUC19 DNA in electrophoretic mobility shift assays and expand the scope of this assay to intercalating substances.
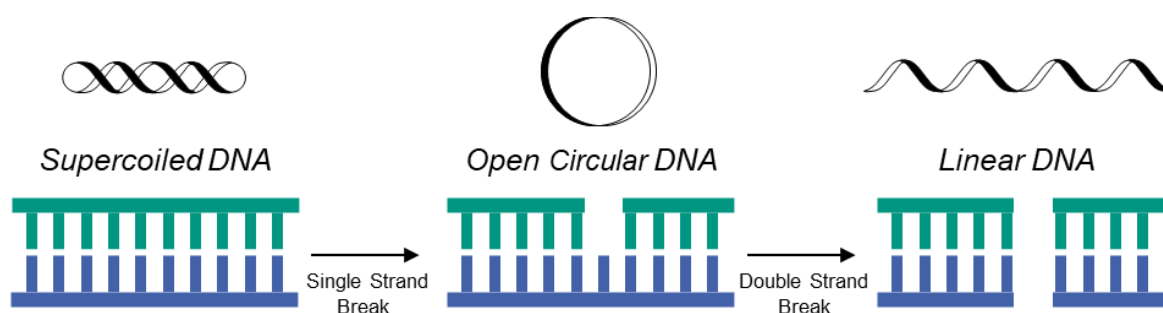
Scheme 25. Influence of DNA single and double strand breaks on the 3D structure of plasmids.

Figure 43 shows the results of treatment of pUC19 DNA with $NiCl_2/H_2O_2$ as DNA strand break inducing agent.[148] DNA intercalating agent ethidium bromide was used as a positive control, which on its own did not affect the migration of pUC19 DNA (**Figure 43, lane 3**). However, in combination with $NiCl_2/H_2O_2$ ethidium bromide affected the formation of oc DNA. Pre-incubation of pUC19 DNA with ethidium bromide for 1 hour and subsequent treatment with $NiCl_2/H_2O_2$ for 1 hour reduced the amount of oc DNA dose-dependently (**Figure 43, lanes 7-9**), while post-incubation with ethidium bromide did not influence the formation of oc DNA (**Figure 43, lanes 4-6**).
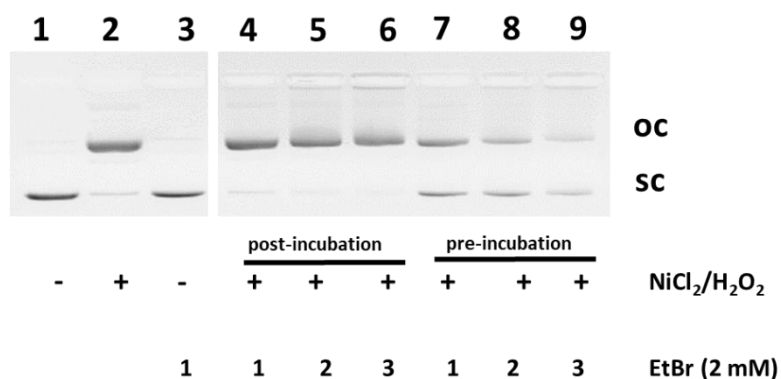
Figure 43. Treatment of pUC19 DNA with $NiCl_2/H_2O_2$ and EtBr. sc and oc pUC DNA were detected by agarose gel electrophoresis. Lane 1: untreated pUC19 DNA; lane 2: pUC19 DNA treated with 50 μM NiCl2 and 0.5 mM H_2O_2 for 1 h; lane 3: pUC19 DNA treated with 1 mM EtBr for 1 h; lanes 4-6: pUC19 DNA treated with 50 μM $NiCl_2$ and 0.5 mM H_2O_2 for 1 h, followed by 1 h treatment with the indicated concentrations of EtBr; lanes 7-9: pUC19 DNA treated with the indicated concentrations of ethidium bromide for 1 h, followed by 1 h treatment with 50 μM $NiCl_2$ and 0.5 mM H_2O_2.

This suggests that the intercalating ethidium bromide prevents the generation of DNA strand breaks. Consequently, the DNA intercalating potential of similar compounds could be assessed in this pUC assay by quantifying their strand break inhibition potential.

pUC19 DNA was treated with 2 mM solutions of the compounds of interest. Similar to the treatment with ethidium bromide, pre-incubation with the compounds prevented the generation of strand breaks, resulting in reduced amounts of oc DNA (**Figure 44, lanes 5, 7, 9**), while post-incubation with the compounds had only little effect on the generation of oc DNA (**Figure 44, lanes 6, 8, 10**).
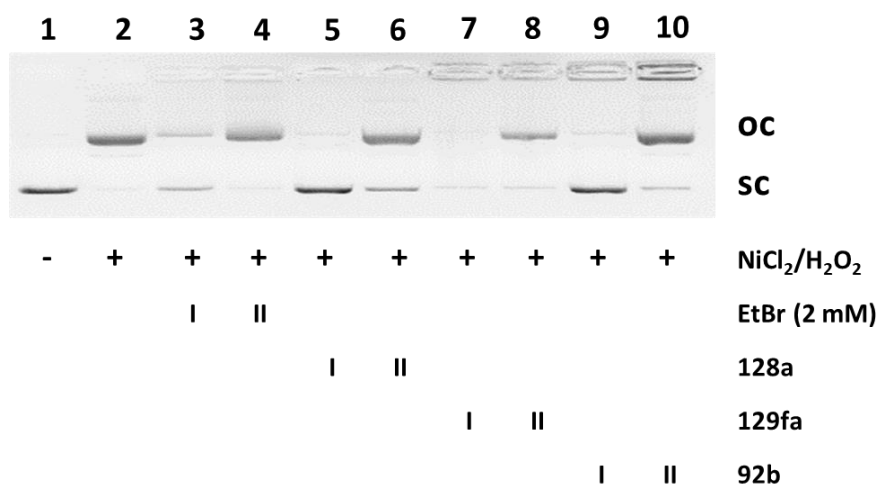
Figure 44. Intercalation of substrates in DNA. pUC19 DNA was treated with 2 mM of selected substrates in combination with NiCl$_2$/H$_2$O$_2$. sc and oc pUC DNA were detected by agarose gel electrophoresis. (I): 1 h pre-treatment of pUC19 DNA with substrate, followed by incubation with NiCl$_2$/H$_2$O$_2$ for 1 h (lanes 5, 7, 9). (II): 1 h post-treatment of pUC19 DNA with substrate, following incubation with NiCl$_2$/H$_2$O$_2$ for 1 h (lanes 6, 8, 10). EtBr was used as a positive control for DNA intercalation.

Pre-treatment of pUC19 DNA with 0.5 mM solutions of the compounds for 1 hour, followed by post-incubation with NiCl$_2$/H$_2$O$_2$ for 1 hour prevented strand breaks and the formation of oc DNA (**Figure 45, lanes 6-10**). However, the negative control cisplatin showed only a small effect on the formation of oc DNA (**Figure 45, lane 5**).
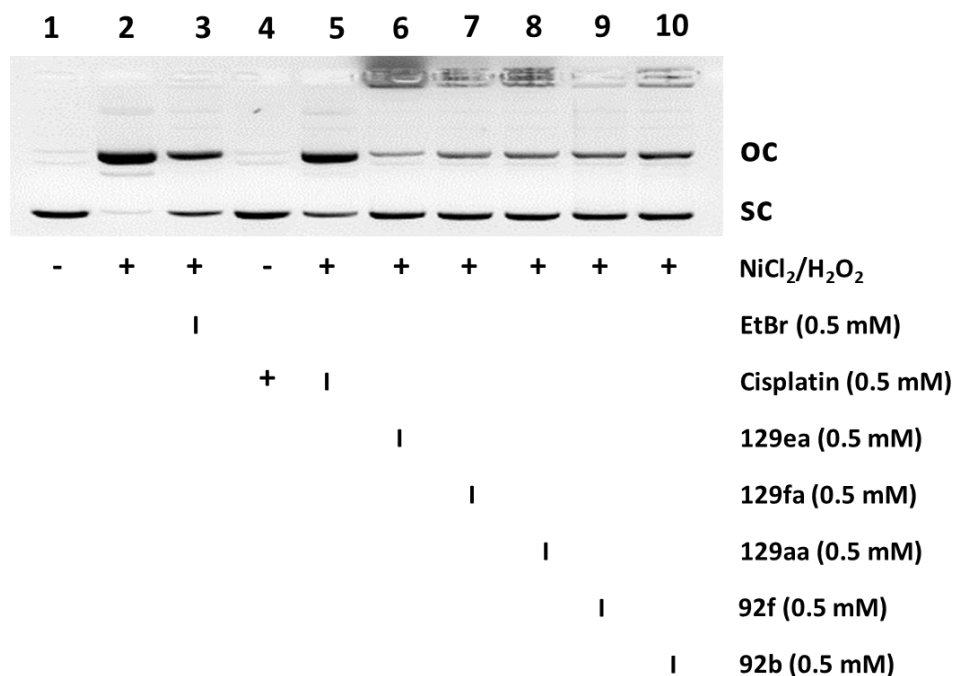
Figure 45. Intercalation of compounds into DNA. pUC19 DNA was pre-treated with 0.5 mM solutions of selected compounds, followed by incubation with NiCl$_2$/H$_2$O$_2$. Supercoiled sc and oc pUC19 DNA were detected by agarose gel electrophoresis. I: pre-treatment. EtBr was used as a positive control for DNA intercalation. Cisplatin was used as negative control.

The formation of oc DNA by treatment with $NiCl_2/H_2O_2$ and its inhibition by the polyheterocyclic compounds was evaluated through semi-quantification of the agarose gel DNA bands (**Figure 46**). The positive intercalating control ethidium bromide prevented the formation of oc DNA by 50% while treatment with the negative control cisplatin resulted in a small reduction of the amount of oc DNA. The synthesized compounds showed scission inhibition of 60 % for **92b** and up to 80% for **129ea**. These results suggests that the synthesized compounds are strong DNA intercalating agents. Surprisingly, the PCP-derived imidazo[1,2-*a*]pyridines show similar strand-breaking inhibition potential despite their sterically demanding, voluminous residues. This could be rationalized by intercalation of the imidazo[1,2-*a*]heterocycle part while PCP-residue is located in the major or minor groove.
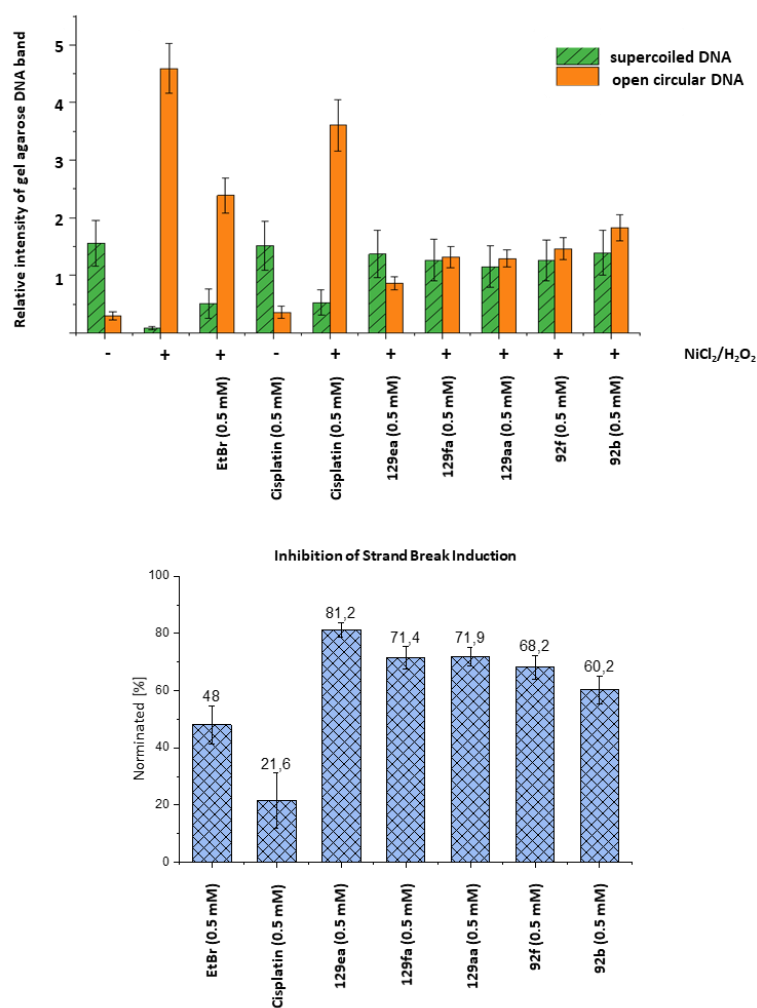
Figure 46. Results of the semi quantification of the agarose gel bands. All compounds were analyzed in three independent experiments, the results are shown as mean values ± standard deviation.

Molecule modelling studies or co-crystallization of DNA-complexes are needed to further elucidate DNA-binding modes. Additionally, cytotoxicity assays should be performed to assess the viability of the compounds for *in vitro* applications.

3.4 Miniaturized Synthesis of Fluorophore Arrays *via* nano3D Printing

Motivation. Extremely miniaturized synthesis, in which reactions are performed on a nanomolar scale in densely packed, confined spaces, allow for facile parallelization of experiments. Currently, most parallelized screening set-ups are using 96- or 384-micro wellplates. A variety of novel concepts and methods for the miniaturized high through-put screening of chemical reactions have been developed, for instance, organic droplet microarrays.[149] Another approach based on nano 3D-printing is currently developed in the Breitling research group. This concept is derived from laser-induced forward transfer (LIFT), a direct laser writing technique, which allows material transfer in defined areas on a surface (**Figure 47**). If different materials are transferred in a consecutive manner, combinatorial stacking patterns can be achieved. Through incubating the surface at elevated temperatures, the transferred materials are able to diffuse and can thus be transformed in a chemical reaction.
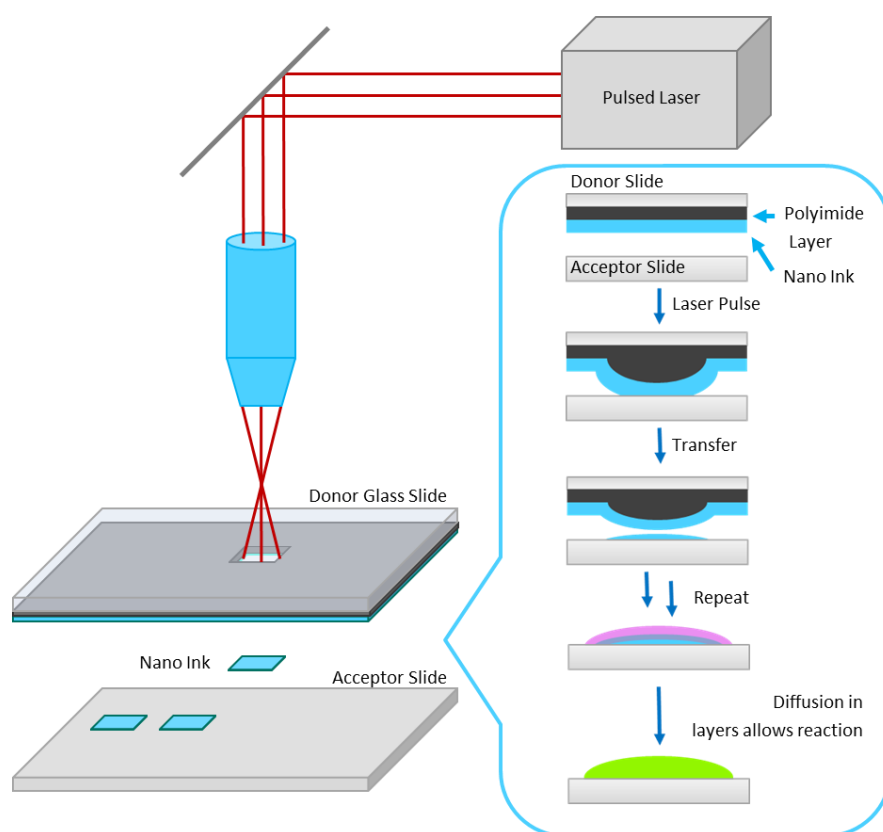
Figure 47. Principle of laser-induced nano3D printing.

In 2017, the BREITLING group first reported the application of the LIFT-method for the synthesis of peptide arrays.[150] By consecutively coupling different activated amino acids to a PEGMA-coated acceptor slide, they managed to synthesize up to nonameric peptides *via* a MERRIFIELD-peptide synthesis protocol. Through either binding of antibodies bearing a fluorescent tag, incorporation of a rhodamine-tagged amino acid or post modification of a propargyl residue *via* 1,3-dipolar cycloaddition with an azide-functionalized dye, the individual peptide spots could be visualized and evaluated using a fluorescence scanner. A density of up to 50.000 material spots on one glass slide was achieved. Since then, continuous efforts were made to further develop the nano 3D-

printing technique and extend its applicability from peptide synthesis to more complex chemical transformations.[151] Dr. Andreas Klinkusch and Robin Rastetter already established the feasibility of this method for Knoevenagel condensations.[152] The evaluation of the reactions was performed *via* fluorescence read-out as well as MALDI-imaging. To prove the generality of the nano3D printing technique for the combinatorial generation of compound libraries and *in situ* synthesis of ultra dense molecule arrays, the method scope must be extended to include a wider variety of transformations. Thus, the objective was to optimize the procedure for more reactions.

Principle. The general idea of nano 3D printing is based on the LIFT concept that revolves around the material transfer from one or more donor slides to an acceptor slide in a specific area.[153] The donor slides are covered with an adhesive polyimide foil. Through spin or blade coating, the polyimide layer is coated with the transfer material layer which is composed of a styrene acrylic copolymer containing 10 wt.-% of the transfer substrate. The acceptor slide is also coated with the polymer matrix. For the automation and a more precise placement of the different donor slides on the acceptor, a robot arm was implemented.

Upon local irradiation with a laser (405 nm), the light energy is absorbed by the Kapton foil, causing it to expand and form a bubble at the interface of the glass slide and the transfer layer. The bubble further expands into the space between donor and acceptor slide, which upon contact results in the deposition of pico- to femtomolar amounts of the transfer substrate on the latter.[154] The laser pattern is provided in the form of Excel files *via* a custom user interface. Usually, the substances are printed in blocks with a gradient of both laser strength and pulse duration in orthogonal directions. Other patterns are also possible by adjusting the laser files. This way, complex patterns can be printed on the microscope slides.

Commonly, the time and thermal energy during the laser impact do not suffice to initiate the reaction of the transferred starting materials. Thus, a separate coupling step is necessary. For this, the slide is incubated in an oven at up to 90 °C under argon atmosphere for a specific period to both provide the activation energy as well as to allow the polymer matrix to become viscous enabling diffusion of the different starting materials.

Evaluation of the reaction outcome is currently mainly performed by fluorescence read-out in the scanner for microscope slides with different channels (488, 532, 635 nm) and cut-off filters that can be fitted to the absorption and emission wavelength of reference material. However, as this hardly suffices as proof for the success of a reaction, further methods are currently implemented, one of them being MALDI-imaging. This technique is usually used for the 2D-analysis of tissue in medical diagnostics. In cooperation with the Hopf group at Hochschule Mannheim, MALDI-imaging analysis of the microscope slides allows for local mass spectrometric evaluation of the compound arrays. Together with the fluorescence results, the reactions on the slides can be monitored and judged thoroughly.

3.4.1 Generation of Fluorophore Libraries

Introduction. The combinatorial generation of compound libraries on a miniature scale is extremely attractive for high throughput screening of reaction conditions, catalysts or properties and can be used for the lead optimization of drugs, pigments, or catalysts. To establish the LIFT method in combinatorial chemistry, we aimed to optimize the procedure for different reaction types and synthesize large compound libraries on the microscope slides. However, there are several prerequisites to be considered when choosing a reaction type. First, as fluorescence read-out is still the main analysis method, the product must be a fluorophore with its absorption maximum being close to the excitation wavelengths of the scanner. Simultaneously, the starting materials should not be fluorescent to avoid overlapping signals. The starting materials should not be sensitive to air and moisture to ensure facile processability. Similarly, the reaction conditions should be relatively mild and not require any sensitive catalysts or additives, low temperatures or protecting gasses. As KNOEVENAGEL reactions could already be successfully performed, other simple chemical transformations like condensation reactions could also be feasible. In addition to this, the reaction should furnish fluorescent products, therefore we chose to evaluate a synthesis method towards flavins. Therefore, a library of reference materials should be synthesized.

Flavins. Flavins are pigments based on the isoalloxazine scaffold. In biological systems, flavins are very abundant, occurring in the form of riboflavin (vitamin B2, **143**), or as the redox active cofactors flavin mononucleotide (FMN, **144**) and flavin adenine dinucleotide (FAD, **145**). These participate in various metabolic processes, such as the citric acid cycle which is an essential element of the respiratory chain.[155] As a result of its reversible redox behavior, the flavin prosthetic group is responsible for enabling enzymatic oxidation and reduction processes. These redox properties have also been exploited in synthetic organic chemistry as redox mediators or sensitizers.[156] In **Figure 48**, the flavin redox behavior and prominent flavins are shown.
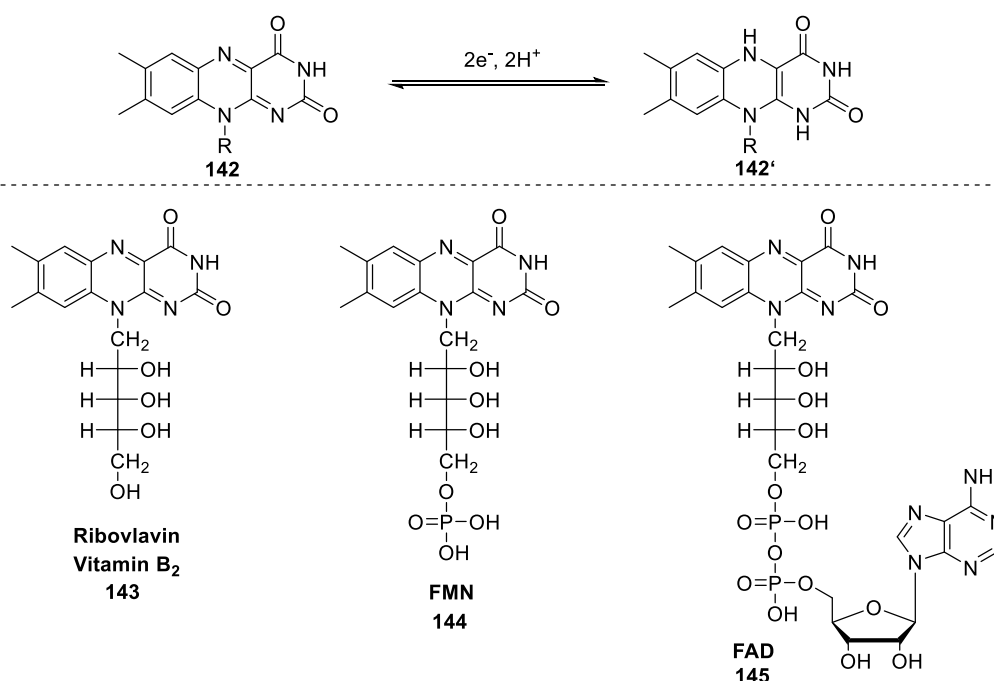
Figure 48. Redox behavior of the flavin group (top) and representative naturally occurring flavins (bottom).

Synthetically, flavins are accessible *via* the acid catalyzed condensation of alloxan and *o*-phenylenediamines. (**Scheme 26**).[157]
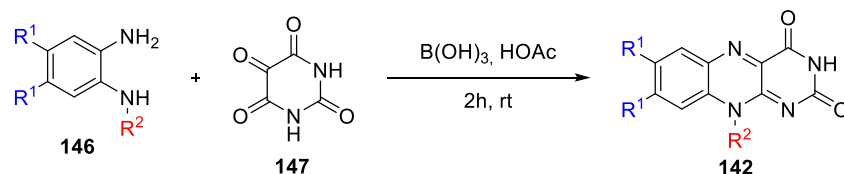
Scheme 26. Flavin synthesis *via* acid-catalyzed condensation of *o*-phenylene diamines and alloxan.

Phenanthrene diamine was synthesized according to a procedure by Colak *et al.* from phenanthrene dione through conversion to the dioxime and subsequent reduction with hydrazine (**Scheme 27**).[158]
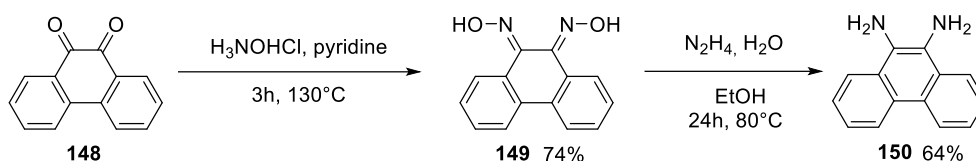
Scheme 27. Synthesis of phenanthrene diamine from phenanthrene dione.

Three diamines were priorly synthesized in two-step procedure (**Scheme 28**). First, the respective amine is coupled to 2-nitro fluorobenzene in a nucleophilic aromatic substitution. The obtained 2-nitro anilines are subsequently reduced to the *N*-alkylated *o*-phenylene diamines.
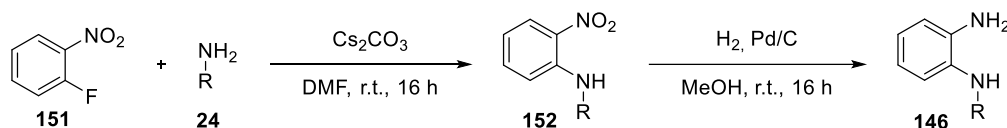
Scheme 28. Synthesis of *N*-substituted *o*-phenylene diamines *via* S_NAr of 2-nitro fluorobenzene and subsequent reduction.

Table 10.

entry	R =	yield (152)	yield (146)
a	4-Methylphenyl	42%	58%
b	1,1'-Biphenyl	19%	72%
c	1-Adamantyl	78%	93%
d	3,5-Dimethylphenyl	33%	86%

A library of flavins from different, mostly commercially available *o*-phenylenediamines was synthesized as reference material to characterize their fluorescent properties (**Scheme 29**).

Over the course of the reaction, the product precipitated and was filtered off. The isolated yields are higher for the small derivatives while the *N*-arylated substrates were obtained in significantly lower yields. Presumably,

based on the reduced nucleophilicity of the secondary amine as well as an increased solubility due to the unpolar substituents, not all the product precipitates and the majority remains in solution. Through alternative purification methods, *e.g.*, phase separation, more of the flavin product could potentially be recovered. The *N*-1-adamantyl substituted *o*-phenylenediamine did not afford any flavin as steric hindrance further decreases the reactivity.
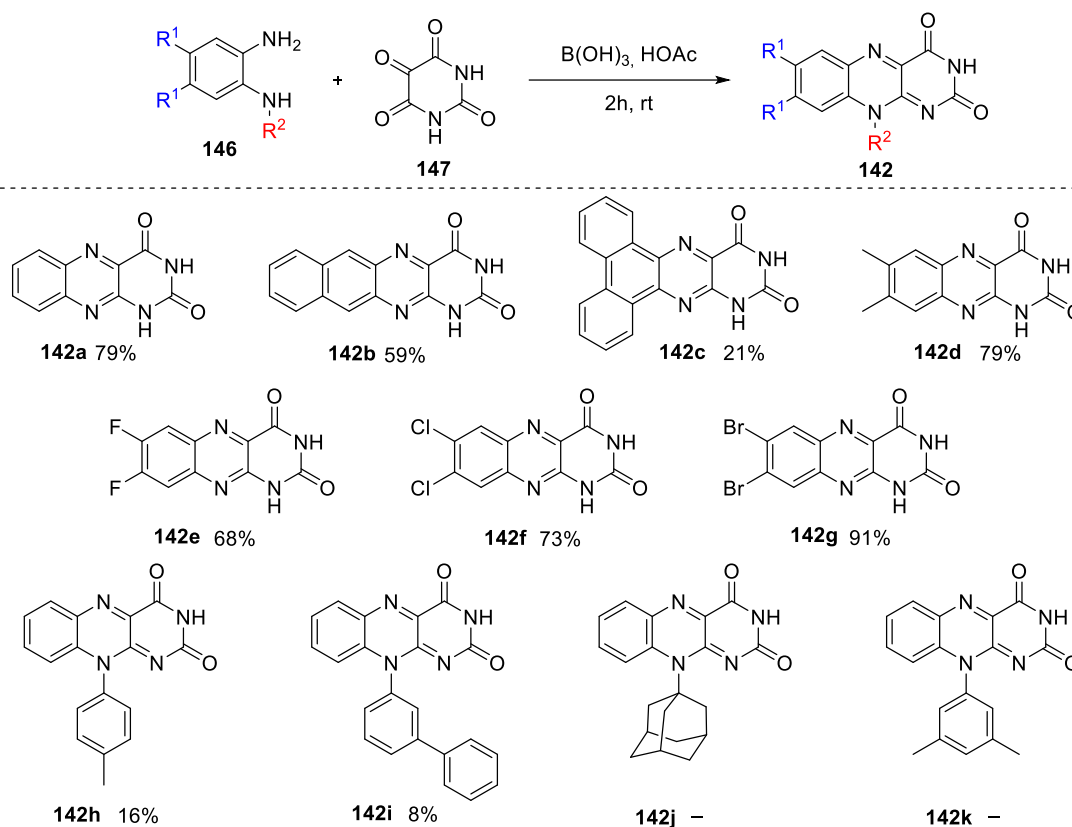
Scheme 29. Synthesis of a library of flavin derivatives.

All flavins were fluorescent upon irradiation. To estimate their emission profiles under the scanner wavelengths, fluorescent spectra were recorded with an excitation wavelength of 350 nm (**Figure 49**). Most flavins show similar absorption and emission profiles with absorption bands from 250 – 300 nm and 350 – 430 nm and an emission band at around 450 nm. Some derivatives, however, differ from this trend. **142b** shows dual emission with a second emission band at around 600 nm. **142h** and **142i** exhibit a strong bathochromic shift in their absorption, and especially in their emission, shifting the emission maxima to around 500 nm. Based on these results, **142b**, **142h** and **142i** were selected for further experiments as their absorption at the scanner excitation wavelength of 488 nm is sufficient and their emission is within the range of the scanner filters. To prove that the fluorescence signals can be unambiguously attributed to the product flavines, the starting materials were transferred individually to a slide and scanned. Unfortunately, in the green channel all three diamines showed signals. Supposedly, this can be rationalized by the photo-induced dimerization of *o*-phenylenediamines. In the blue channel, only diamine **146b** did not show a signal, thus, the reaction to **142i** was selected for an on-slide synthesis. The result is displayed in **Figure 50**.
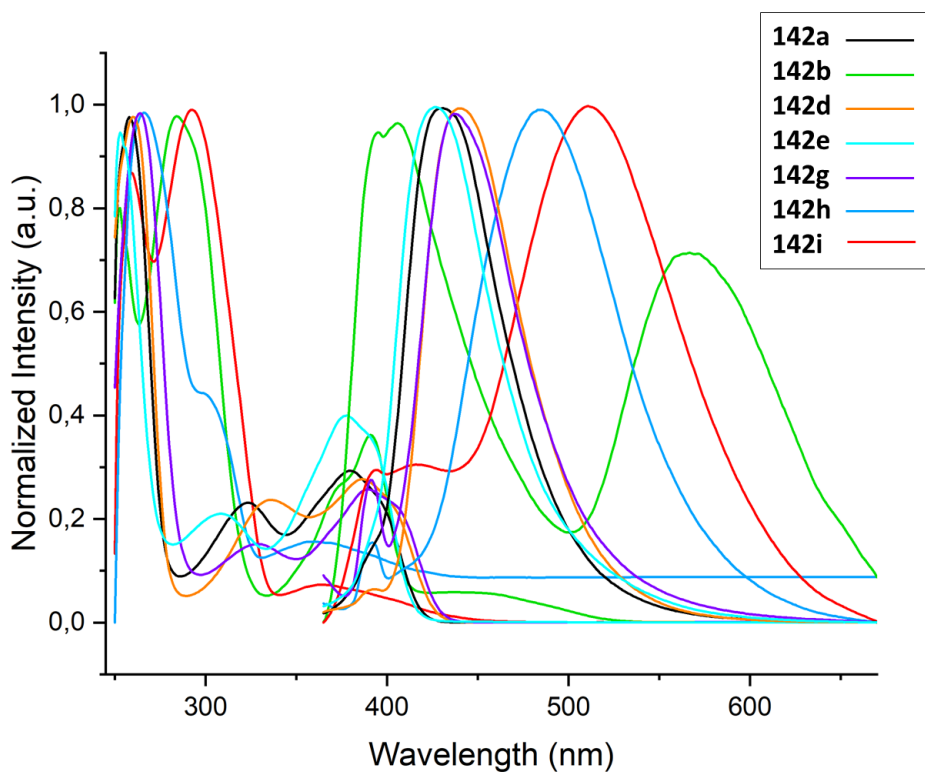
Figure 49. Normalized absorption and emission spectra of selected compounds in DMSO. λ_{exc} = 350 nm.

The laser pattern for one block in which the materials are transferred is presented in **Figure 50**. One block consists of squares of 16 dots. Laser power is increased horizontally from 130 – 200 mW, and pulse duration vertically from 6 – 10 ms.
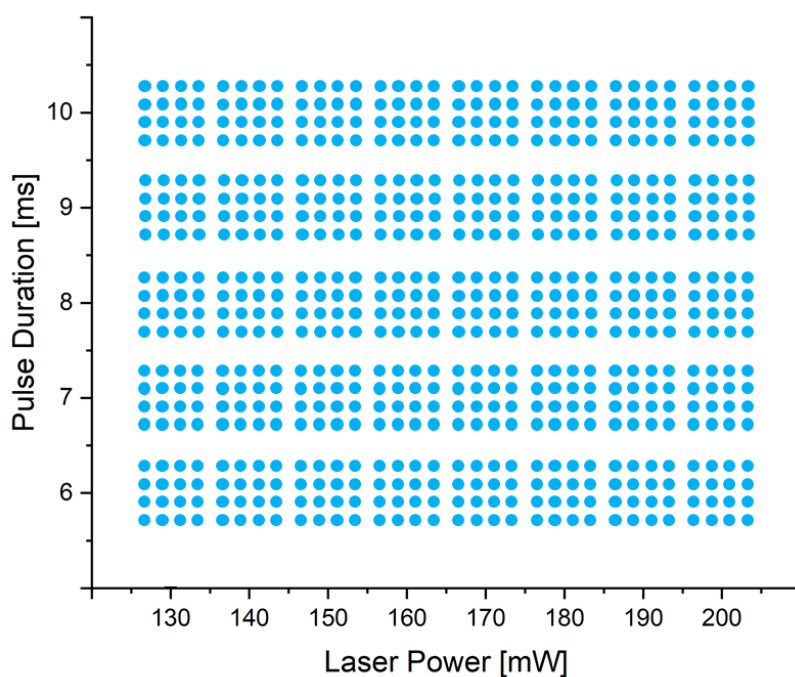
Figure 50. Schematic representation of the laser pattern in which the individual blocks are printed onto the glass slides.
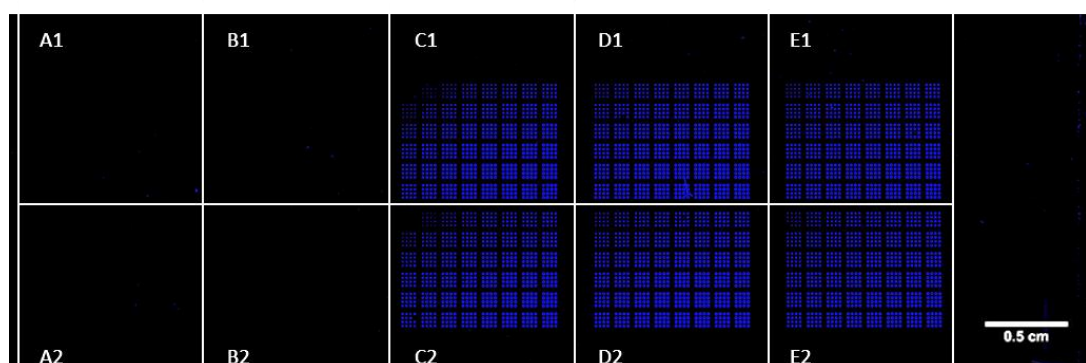
Figure 51. Fluorescence image of an array of flavin **142i** synthesized on a microscope slide after material transfer *via* nano3D printing. Row A: **146b**; row B: alloxan; row C: reference material; row B: **146b**, alloxan; row D: alloxan, **146b**; row E: **146b**, alloxan. Row 1 also contains boric acid. Image acquisition parameters: λ_{exc} = 488 nm; emission filter (504 +- 12), resolution 5 μm. The image's brightness and contrast were adjusted.

While the starting materials printed in the A and B rows do not show any signal in the blue channel, the blocks where flavins are formed are clearly visible. Due to the poor solubility, no reference material of **142i** could be transferred *via* nano3D printing, thus, no comparison can be depicted. However, as none of the starting materials and possible side-products show any fluorescence in the blue channel, the signal most likely stems from the desired flavin.

Thus, the synthesis of a flavin derivative *via* the nano 3D printing method could be demonstrated. Based on these results, a combinatorial library will be synthesized by derivatization of **142i**. Overall, this is a step towards combinatorial assembly of different kinds of fluorophores. The inherent redox activity of flavins could further be exploited in the screening of reaction conditions of photo redox transformations and towards the long-term goal of the photocatalytic reduction of CO_2. and the on-slide assembly of an artificial photosystem.

GBB-3CR. Multicomponent reactions stand out for their unmet potential in generating large numbers of combinations through the variation of the individual components as well as their facile handling and mild reaction conditions. Additionally, the GBB-3CR furnishes fluorescent imidazo[1,2-*a*]heterocycles from non-fluorescent starting materials. Heaven, by implementation of this reaction in the nano3D printing approach, a high degree of diversification of the combinatorial molecular arrays could be achieved.

A model reaction of 2-aminopyrazine (**66a**), *N*,*N*-dimethylamino cinnamaldehyde (**153**) and 1-adamantyl isonitrile (**44**) was selected because of the intense fluorescence of the respective imidazo[1,2-*a*]pyrazine and the facile handling of the solid starting materials. Before evaluating the model reaction on the slide, the transformation was conducted in solution to assess its performance and obtain reference material. Normally, BRØNSTED acids like glacial acetic acid or perchloric acid would be applied as catalysts. In the nano 3D-printer, however, liquids are difficult to process. Thus, different catalysts are necessary. The also commonly used Lewis acidic rare earth triflates are also not applicable as inorganic salts do not transfer in nano 3D printing. Therefore, trichloroacetic acid was used as the catalyst in sub-stoichiometric amounts (**Scheme 30**). GBB-product **154** was obtained in a good yield of 82%.
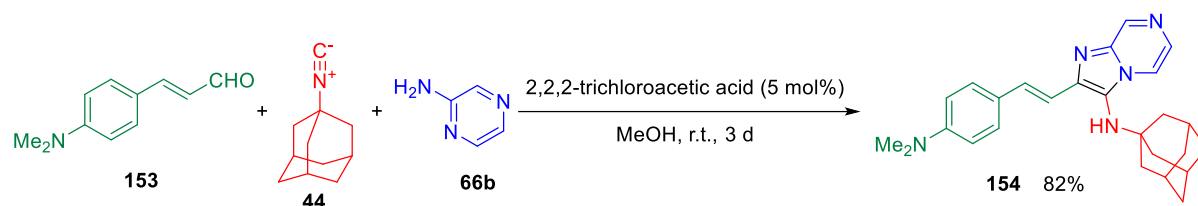
Scheme 30. Synthesis of reference material *via* a 2,2,2-trichloroacetic acid -catalyzed GBB-3CR.

The absorption and emission spectra of the obtained reference material **154** were measured (**Figure 52**). While the emission fits into the desired range for detection of the fluorescence signal with the slide reader, the absorption at 488 nm is quite low, thus, hampering detection with the slide reader. Therefore, an alternative camera setup had to be used for the image acquisition.
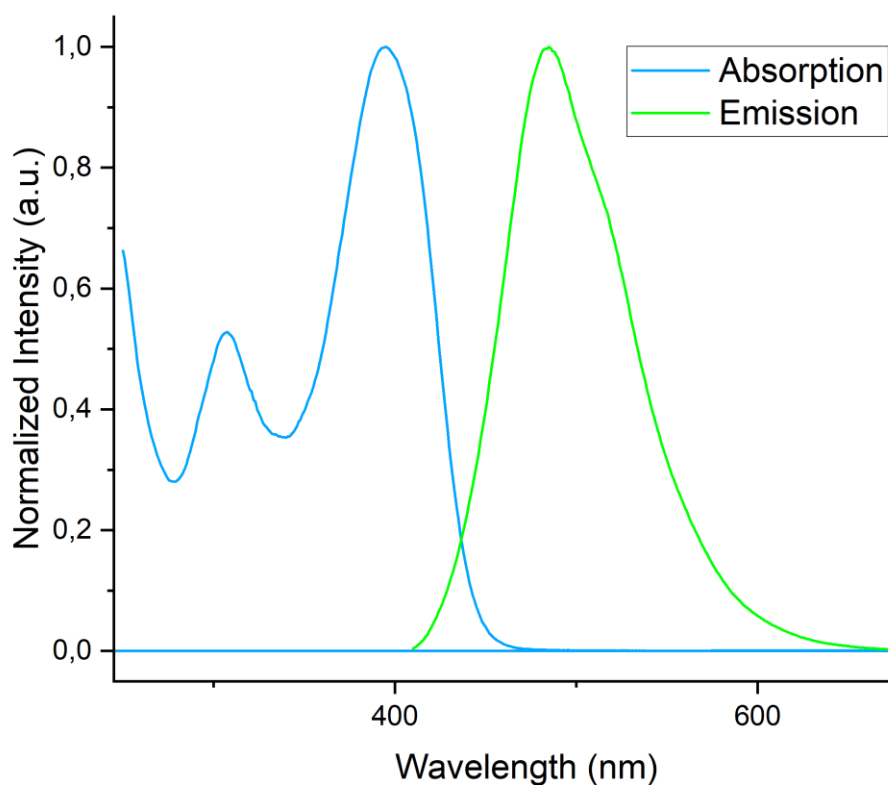
Figure 52. Normalized absorption and emission spectra of **154** in CH_2Cl_2 (λ_{exc} = 395 nm).

The starting materials and reference material of **154** was printed on to the slide and the slide was incubated at 98 °C for 24 hours. The images of the slide under irradiation with 360 nm (top), 488 nm (middle) and 532 nm (bottom) are displayed in **Figure 53**. As the UV-pictures were recorded in a different camera setup instead of the slide reader, thus, only cut outs of the laser pattern can be displayed.
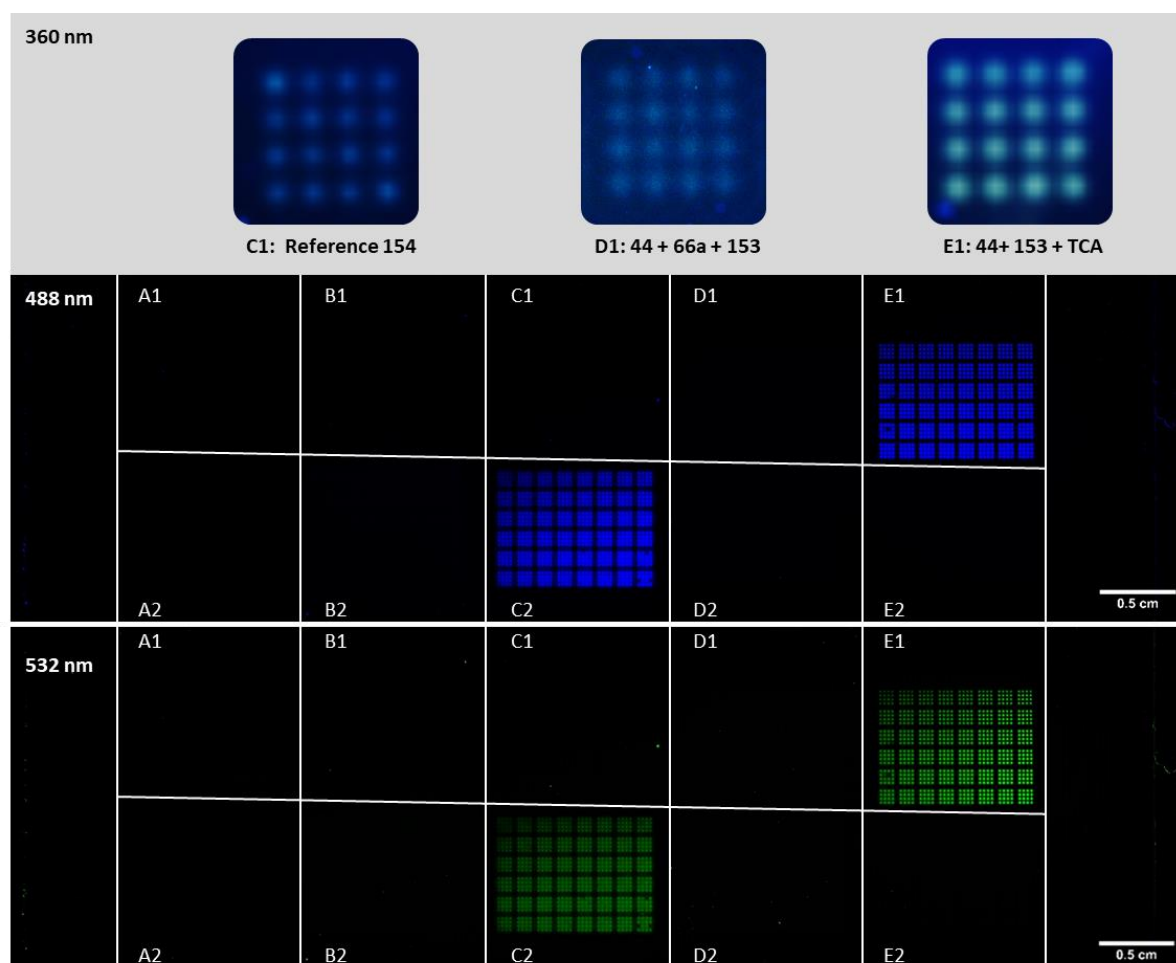
Figure 53. Fluorescence images of an array of **154** synthesized on a microscope slide after material transfer *via* nano3D printing. A1: *N,N*-dimethylamino cinnamaldehyde, A2: trichloro acetic acid, B1: 1-adamantyl isonitrile, B2: 2-aminopyrazine C1: reference material; C2: *N,N*-dimethylamino cinnamaldehyde, trichloro acetic acid, 1-adamantyl isonitrile, 2-aminopyrazine; D1: *N,N*-dimethylamino cinnamaldehyde, trichloro acetic acid, 1-adamantyl isonitrile, 2-aminopyrazine; D2: 1-adamantyl isonitrile, 2-aminopyrazine; E1: *N,N*-dimethylamino cinnamaldehyde, trichloro acetic acid, 1-adamantyl isonitrile; E2: *N,N*-dimethylamino cinnamaldehyde, 1-adamantyl isonitrile. Image acquisition parameters: λ_{exc} = 360 nm (top), 488 nm (middle), 532 nm (bottom); emission filter (blue: 504 ± 12; green: 582 ± 75), resolution 5 µm. The image's brightness and contrast were adjusted.

The starting materials were printed in the four left squares (A1, A2, B, and B2). Under all wavelengths, no luminescence of the starting materials was observed. In position C1, the reference GBB-product **154** was printed, which is only visible under UV-irradiation. Combinations of the starting materials were printed in the remaining positions. D1 and D2 both contain three component mixtures of amidine, aldehyde and isonitrile without any acidic catalyst. Under UV-light, a similar blue fluorescence to C1 is observed. The four-component mixture in C2 additionally contains trichloro acetic acid as a catalyst. Compared to the reference in C1, the mixture shows a significantly altered fluorescence which is very intense and visible under all wavelengths. The combination in position E1 exhibits the same fluorescence, which is unexpected as it only contains acid, aldehyde and isonitrile. These observations suggest the occurrence of a different reaction instead of the desired GBB-3CR.

One reason for the side reactions which are observed on the slide but not in the bulk reaction could be that in nano3D printing, there is no control over the transferable amount. Thus, trichloro acetic acid is also transferred

in stoichiometric rather than catalytic amounts. So far, identification of the side-product was not possible. In the future, with the implementation of MALDI analysis, it should be possible to thoroughly investigate competing processes.

3.4.2   Development of a Fluorescent CO_2-Probe

Introduction. The rapid generation of compound libraries is perfectly suited for high-throughput screening setups.[159] One of our goals with the LIFT method is to scout for reaction conditions to convert CO_2 into value-added chemicals by either incorporating CO_2 into more complex product molecules or by the reduction to CO, formic acid, or formaldehyde. CO_2 is the most prevalent human greenhouse gas, and its emissions predominantly contribute to the rapid climate change. Thus, the development of new methods to synthetically access atmospheric CO_2 and upconvert it to recycled chemical feedstock can contribute to the overall reduction of air pollution as well as creating a more sustainable industry and closed-loop production cycles.[160]

To reduce CO_2 to more valuable base chemicals, a wide variety of concepts exists and is currently in the focus of global research efforts including photocatalytic and electrochemical reduction, artificial photosynthesis, reduction or the incorporation of CO_2 in organic syntheses as a C_1 synthon.[161] One way to contribute to these efforts with the nano 3D printing method could be the screening of possible catalysts or reaction conditions for CO_2 conversion in a microarray format by incubating slides bearing a variety of possible reagents under CO_2 atmosphere. However, due to the current limitation in analytical methods, especially in quantification, this undergoing can not be realized quite yet.

To reach this goal overall, we needed to prove the feasibility of the nano 3D printing method and the possibility of reacting surface-mounted substrates with gaseous CO_2. The idea is to find a reaction in which CO_2 is converted into a product that can be evaluated by the already established methods of fluorescence read-out or MALDI-imaging. For fluorescence, the ideal solution would be a reaction in which CO_2 is incorporated into a newly built fluorescent scaffold to meet the prerequisite of having non-fluorescent starting materials. In literature, several reaction types have been reported. However, most of them are not feasible as they require sensitive metalorganic reagents or catalysts which are not compatible with the nano 3D printing procedure. The most promising reaction is the synthesis of phthalimides (**157**) from an aryne precursor (**155**), an isonitrile (**46**) and CO_2, reported by KAICHARLA *et al.* in 2014.[162] This transformation is illustrated in **Scheme 31**.
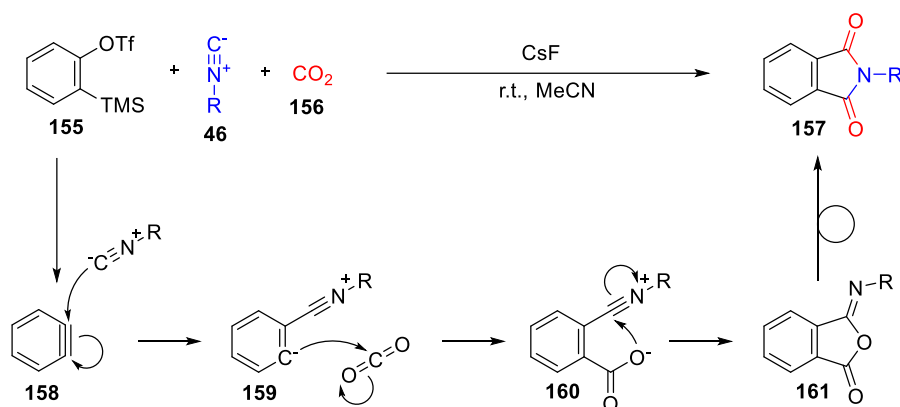
Scheme 31. 3-Component reaction of a Kobayashi aryne precursor, an isonitrile and CO_2 furnishing phthalimides.

In this approach, a Kobayashi aryne precursor,[29] an *o*-trimethylsilyl phenyl triflate (**155**), is deprotected using cesium fluoride to generate the aryne (**158**) *in situ*. Subsequently, the isonitrile attacks the aryne, which in turn attacks CO_2, affording an intermediate *N*-alkyl isoimide (**161**) upon ring closure. Through a fluorine-mediated rearrangement, the phthalimide **157** is formed. According to Orita *et al.*, unsubstituted *N*-alkyl phthalimides do not exhibit any emission, but substitution with an electron-donating residue such as pyrrolidinyl or piperidyl in the 3- or 4-position leads to strong blue fluorescence in the range of 425 to 550 nm, depending on the solvent polarity.[163] To apply in nano 3D printing, the residue must not be grafted onto the phthalimide core in a post-modification step as described by Orita *et al.* Instead, it should already be present in the respective starting materials, in this case, the modified aryne precursor. The synthetic idea is depicted in **Scheme 32**.
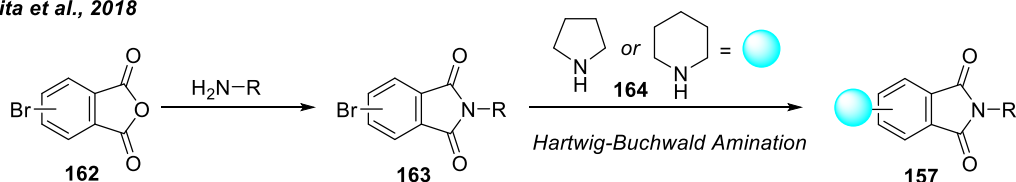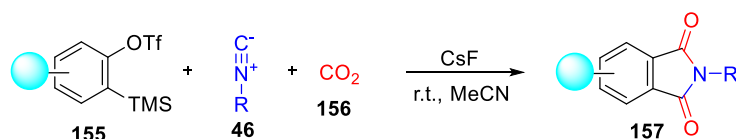
Scheme 32. Synthesis strategy for donor-substituted phthalimides *via* Hartwig-Buchwald amination (top) and CO_2-based 3CR.

Synthesis. The piperidyl-substituted aryne precursor was synthesized in three steps according to modified literature procedures by Fukino *et al.*, and Hallani *et al.* (**Scheme 33**).[164]
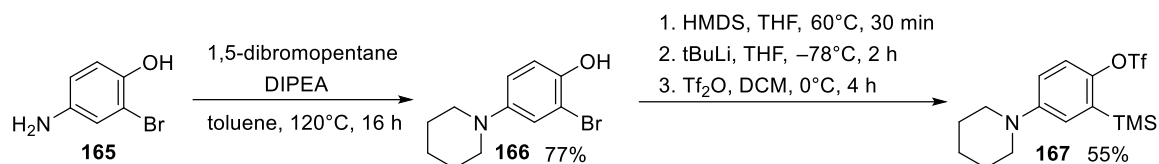
Scheme 33. Synthesis of Kobayashi aryne prevursor **167** from 2-bromo-4-amino phenol. 55% yield!

Initially, 2-bromo-4-amino phenol (**165**) was reacted with 1,5-dibromohexane to build up the piperidyl residue, affording 2-bromo-4-(piperidin-1-yl)phenol (**166**) in 77% yield. Subsequently, **166** was subjected to a three-step transformation to synthesize the desired aryne precursor, **167**. First, the phenolic hydroxy function was protected with a TMS-group using HMDS in THF at 60 °C. Afterwards, the TMS-group was transferred to the adjacent position by lithiation using *t*BuLi. Finally, the hydroxy function was converted into a triflate with triflic anhydride. The desired aryne precursor was isolated in 42% yield over the two separate steps.

Currently, no reliable analysis method for nano3D printed compounds excited at under 400 nm is available. Thus, further experiments are postponed until the implementation of the appropriate analysis tools.

3.5 Development of a Novel Route towards Bemotrizinol

Preface. Parts of the following chapter were published in a patent submitted to the German patent office.

Motivation. To protect human skin as well as outdoor surfaces and coatings, a variety of UV-absorbing substances have been developed for sunscreen applications (cf. **Chapter 1.3 – Optical and UV-Absorbers**). However, as new UV-absorbers rarely get approved by the FDA and related authorities, research nowadays has shifted from the development of novel substances to improving the synthesis of existing, marketed products.

Several compound classes, especially hydroxy benzophenones, pose severe drawbacks in terms of efficacies or photostability, as well as their similarity to estrogen, rendering them endocrine disruptors.[47b] One design particularly well-suited to circumvent these issues is the class of *ortho*-hydroxyphenyl-1,3,5-triazines.[165] In 1996, bis-resorcinyl triazines were first patented as UV-absorbing substances, one of which is Bemotrizinol (**1**, BMT or BEMT, also Tinosorb S, Neoheliopan, **Figure 54**).[166] Since then, it is widely used in sunscreen formulations as a broad band UV-filter, as well as to prevent photodegradation of other UV-absorbers.[46]
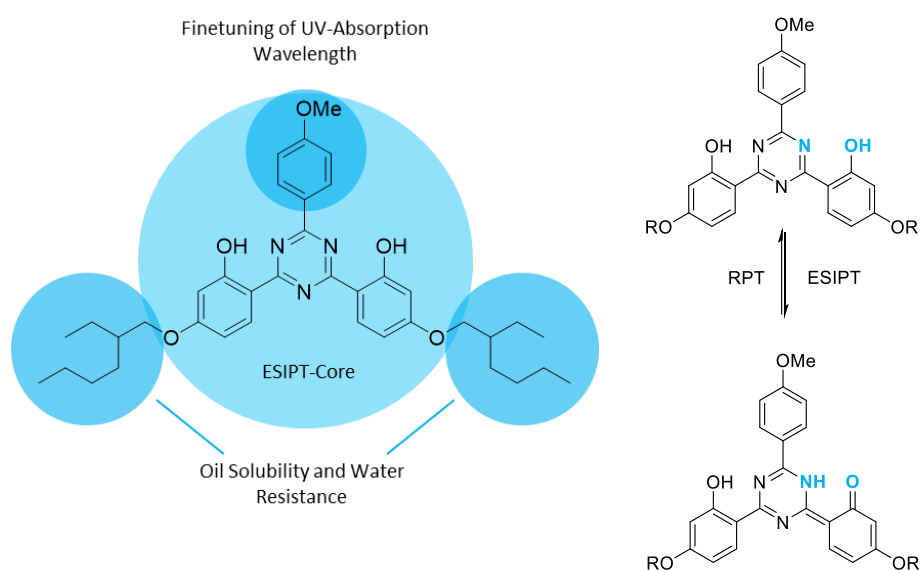
Figure 54. Structure of Bemotrizinol **1** (left) and its ESIPT behavior (right).

Their UV-absorbing properties originate from the ESIPT occurring after irradiation with UV-light.[167] In the excited state, a proton is shifted from the phenolic hydroxy group to the neighboring triazine nitrogen atoms. *Via* vibronic relaxation, the energy is again released in the form of thermal energy followed by the back transfer of the proton to its original position. The other structural features of BMT contribute to its absorption wavelength and its solubility in oil, respectively.

Synthetically, Bemotrizinol is accessible through the three-step route depicted in **Scheme 34**.
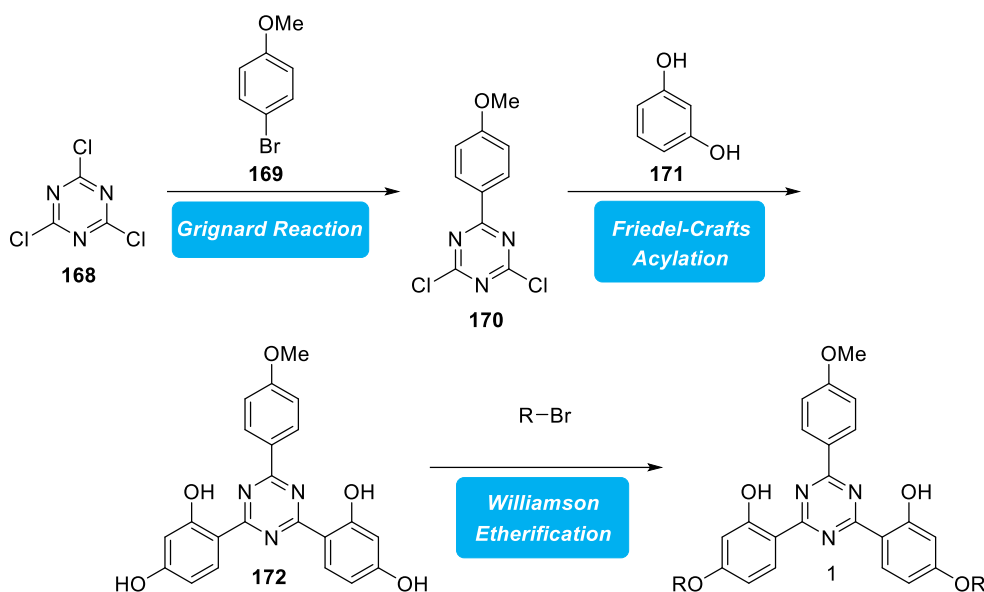
Scheme 34. Established three-step synthetic route towards Bemotrizinol. R = isooctyl

Initially, the 4-methoxyphenyl moiety is attached to cyanuric chloride (**168**) in a GRIGNARD reaction with 4-bromo anisole (**169**). The resulting intermediate **170** is employed in a double FRIEDEL-CRAFTS acylation of two equivalents of resorcinol (**171**). In the final step, the para-hydroxy groups are etherificated with an iso-octyl halide to furnish Bemotrizinol.

While linear and concise, this route poses several drawbacks. For instance, the initial GRIGNARD reaction is considered a safety concern as the reactive intermediates might react heavily with water. This is highly unfavorable, particularly for industrial scale processes. In 2008, JIANG *et al.* reported a slightly modified route in which the GRIGNARD step is replaced by a FRIEDEL-CRAFTS acylation of cyanuric chloride and anisole using aluminum chloride as the Lewis acid catalyst.[168] While this route poses fewer safety concerns, the need for stoichiometric amounts of catalyst results in large amounts of aluminum salt waste which is both environmentally hazardous and expensive in disposing of. Another problem arising from the established synthesis route is the low solubility of the bis-resorcinyl triazine intermediate, termed diopat (di-*ortho*-hydroxyphenyl asymmetric triazine) in conventional solvents. Thus, high boiling polar solvents like methylcellosolve are needed for further processing, decreasing the overall sustainability of the entire synthesis even more.

In particular, considering the increasingly more important aspect of sustainability in research and industry, redesigning the synthesis is desirable from both an ecological as well as an economic perspective. Key points to improve upon are the substitution of potentially dangerous reaction steps, reducing the amounts of catalyst needed for the respective transformations or replacing these entirely and switching to more environmentally benign reagents and solvents throughout the whole process. The different approaches developed to meet these objectives are presented in the following chapters.

3.5.1 Friedel-Crafts Acylation of Cyanuric Chloride: Lewis Acid Screening

Friedel-Crafts Acylation. The first step towards BMT is the synthesis of 2,4-dichloro-6-(4-methoxyphenyl)triazine (**170**). To realize this without resorting to Grignard reagents, Friedel-Crafts acylation was chosen. A set of Lewis acids was screened for their catalytic activity.[169] To avoid over acylation, the reactions were conducted at ambient temperature and with one equivalent of anisole (**173**). The results are listed in **Table 11**.

Table 11: Results of the Lewis-acid screening.
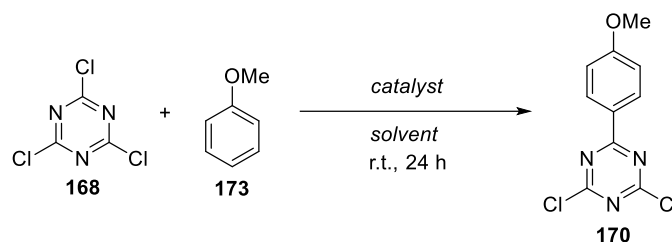
Lewis acid	solvent	result[a]	Lewis acid	solvent	result[a]
AlCl$_3$[b]	CH$_2$Cl$_2$	10%	Sc(OTf)$_3$	MeCN	+
AlCl$_3$[b]	toluene	21%[c]	Y(OTf)$_3$	MeCN	*n.d.*
AlCl$_3$	CH$_2$Cl$_2$	*n.d.*	La(OTf)$_3$	MeCN	*n.d.*
FeF$_3$[b]	CH$_2$Cl$_2$	+	Fe(OTf)$_3$	MeCN	*n.d.*
FeCl$_3$[b]	CH$_2$Cl$_2$	69%	Zn(OTf)$_2$	MeCN	*n.d.*
FeBr$_3$[b]	CH$_2$Cl$_2$	+[c]	Cu(OTf)$_2$	MeCN	*n.d.*
FeI$_3$[b]	CH$_2$Cl$_2$	+	In(OTf)$_3$	MeCN	*n.d.*
CeCl$_3$	CH$_2$Cl$_2$	*n.d.*	Fe(acac)$_3$	CH$_2$Cl$_2$	*n.d.*
TiCl$_4$	CH$_2$Cl$_2$	23%	BF$_3$·OEt$_2$	CH$_2$Cl$_2$	*n.d.*
CuCl$_2$	CH$_2$Cl$_2$	*n.d.*	TfOH	CH$_2$Cl$_2$	+
ZnCl$_2$	CH$_2$Cl$_2$	*n.d.*	Nafion™	DCB	30%
ZrCl$_4$	CH$_2$Cl$_2$	*n.d.*	Zeolithe-H$^\beta$	CH$_2$Cl$_2$	+
SnCl$_2$	CH$_2$Cl$_2$	*n.d.*	Mont. KSF	CH$_2$Cl$_2$	+

[a] The conversion was monitored *via* HPLC analysis. Percentages indicate isolated yields.

[b] Catalyst was used in stoichiometric amounts.

[c] Side reactions were observed.

n.d.: not detected

Aluminum chloride only afforded the acylation product when used in stoichiometric amounts. Considering the low yields, optimizations regarding solvents and reaction conditions are necessary to further improve this catalytic system. When the reaction was performed in toluene, competing acylation of the solvent was observed.

Similarly, iron salts were also successful if used in stoichiometric amounts. With iron chloride, a good yield of 69% was obtained. The stronger Lewis acid iron bromide even resulted in full conversion of anisole; however, over-substitution of cyanuric chloride was observed. Other chlorides did not show any conversion except for titanium chloride which was not pursued further due to the challenging handling. In literature, triflate Lewis acids are often reported as efficient Friedel-Crafts catalysts that are effective even in sub-stoichiometric amounts.[170] However, most triflates evaluated were not successful in the target system. Applying these catalysts in stoichiometric amounts was not investigated owing to their costs.

Among the heterogeneous catalysts,[171] Zeolithe-H$^\beta$ and montmorillonite KSF showed the formation of small amounts of the acylation product, however, even after a prolonged reaction time of three days, the conversion was still too low to further pursue these attempts. Different solvents and elevated temperatures would be subjects of further optimization studies to increase the catalytic activity.

Beads of the acidic, perfluorinated polymer Nafion™ were also employed, affording the product in 30% yield. The use of Nafion could be beneficial since it enables facile removal and recycling of the catalyst. However, due to the high proof of Nafion™, the reaction needs to be optimized to produce higher yields in order to ensure good rentability. For instance, continuous flow reactions using Nafion™ membranes could improve the overall process.[172]

Since substoichiometric catalytic systems are not suitable for the present system, resorting to stochiometric catalysts is necessary. Among these, aluminum and iron chloride performed best. The heterogeneous Nafion might provide a more benign alternative upon further optimization.

3.5.2 Selective Synthesis of Resorcinol Monoether and Cyclohexenone Route

Introduction. Moreover, the synthesis of isooctyloxy resorcinol itself also proves to be challenging. Economically, resorcinol would be an ideal starting material as it is relatively cheap. However, the desymmetrization of resorcinol is not trivial.[173] The most obvious route, the etherification of resorcinol with one equivalent of either isooctanol or the respective halide, always leads to mixtures of resorcinol, its desired monoether as well as the diether. Isolation of the monoether from these mixtures in an industrial scale is difficult because during distillation, resorcinol is prone to sublime and crystallize in the distillation column.

Thus, we aimed to find a more selective route towards the monoether. To circumvent the selectivity issues arising from the desymmetrization of resorcinol, the conversion of unsymmetric starting materials seemed favorable. Thus, two-step synthetic routes were explored in which at first isooctyloxy precursor **176** was synthesized from a 3-substituted phenol (**174**). Subsequently, the functional group in the 3-position needed to be converted into a hydroxyl group.

Hydroxylation. The respective precursor was synthesized in a WILLIAMSON ether synthesis starting from 3-bromophenol (**174**) and isooctanol (**175**), affording 3-bromo isooctyloxy benzene (**176**) in an excellent yield of 91% (**Scheme 35**).
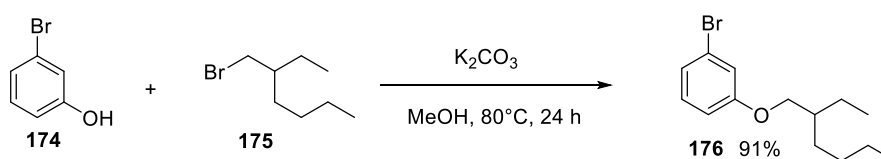
Scheme 35. WILLIAMSON ether synthesis of 3-bromo isooctyloxy benzene.

´

Next, the hydroxy group should be installed in a metal-catalyzed hydroxylation reaction. Several literature-known protocols were applied to the present system. The results are listed in **Table 12.**

Table 12. Metal-catalyzed hydroxylation protocols tested for the hydroxylation of 3-bromo isooctyloxy benzene.
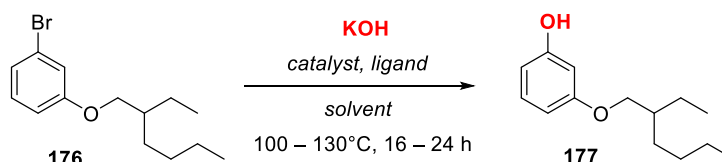
entry	catalyst	ligand	Additive	solvent	T / °C	yield / %
1	Cu(OAc)$_2$	-	Glucose	DMSO/H$_2$O (1:1)	130	*n.d.*
2	CuI	DMEDA	NaI	1,4-Dioxane/H$_2$O (4:1)	120	*n.d.*
3	CuI	L-Proline	Bu$_4$NBr	H$_2$O	120	*n.d.*
4	**Pd$_2$dba$_3$.**	**XPhos**	**-**	**1,4-Dioxane/H$_2$O (4:1)**	**100**	**75**

In most cases, the desired phenol **177** was not formed, and no conversion of the starting material was observed. Only through a method originally reported by BUCHWALD *et al.* the resorcinol monoether **177** would be obtained in a good yield of 75%.

However, the need for both expensive palladium catalysts as well as sophisticated phosphine ligands significantly hamper the feasibility of this approach. Applying this method to the less expensive, more benign 3-chloro isooctyloxy benzene did not afford the desired phenol as no conversion of the starting material was observed.

Direct *O*-arylation of isooctanol using transition-metal catalyzed methods was not possible. As a result of the increased nucleophilicity of the phenolic hydroxyl group, only dimerization and oligomerization of the 3-bromophenol was observed. Protecting group strategies were generally ruled out for their low atom economy.

As most of the unsymmetric approaches towards the resorcinol monoether either did not work at all or were laving in terms of economic efficiency, a different route was pursued.

Cyclohexenone Route. To provide a more easily obtainable, *O*-alkylated resorcinol surrogate, a saturated cyclohexenone monoether system (**180**) was taken into consideration. Cyclohexanedione (**178**) can be easily desymmetrized through the acid catalyzed etherification on one of the carbonyl oxygen atoms while the other carbonyl oxygen stays intact. The enol ether can also be interpreted as a vinylogous ester. For the synthesis of the enol ether **180**, methanesulfonic acid was employed as the catalyst (**Scheme 36**).
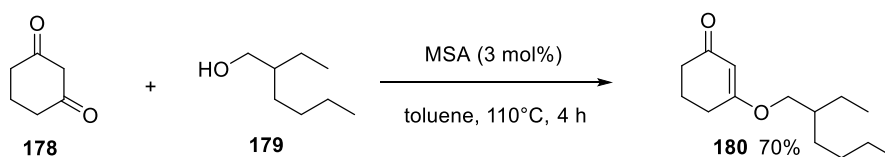
Scheme 36. Synthesis 3-isooctyloxy cyclohexenone *via* an acid-catalyzed condensation.

The desired isooctyloxy cyclohexenone **180** was obtained in a maximum yield of 70%. The reaction could be scaled up to a multigram scale. Facile purification is possible *via* distillation under reduced pressure to remove residual starting material.

With the cyclohexenone monoether at hand, two possible routes open towards the target BMT. The cyclohexenone monoether can either be oxidized to the 3-isooctyloxy phenol building block (**177**) or attached to the triazine core prior to oxidation of the entire system.

3.5.3 Alternative Methods for C-C-Bond Formation on the Triazine Core

Introduction. For the synthesis of triaryl triazines (**181**), different concepts exist (**Scheme 37**). On the one hand, the triazine core can be synthesized *de novo* through the Lewis-acid catalyzed trimerization of nitriles (**182**).[174] However, as this process is statistical, the selective one-pot synthesis of differently substituted triazines with a distinct substitution pattern is not possible. Switching to a consecutive reaction method, AB_2-triazines can be synthesized by modifying one of the nitriles with triflic anhydride and, subsequently, adding the other nitrile component.[175] For the synthesis of BMT, however, the *de-novo* route was not considered as the synthesis of the individual nitrile precursors itself would have already been too elaborate.

Alternatively, triaryl triazines are accessible *via* nucleophilic substitution of the chlorine atoms of cyanuric chloride (**168**).[176] Depending on the degree of substitution, the reactivity of the chlorine atom varies. Thus, each chlorine is substituted under increasingly harsh conditions, with the first one reacting at 0 °C, the second one at ambient temperatures and the third substitution occurring above 60 °C. Commonly used carbon nucleophiles used in the S_NAr of chlorotriazines are GRIGNARD reagents or electron-rich aromatic compounds in FRIEDEL-CRAFTS reactions.[177]
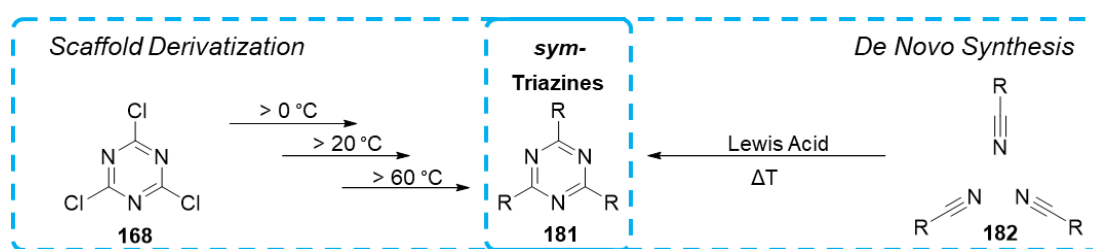
Scheme 37. Synthesis strategies towards triaryl *sym*-triazines.

Li-Enolates. In the original BMT-synthesis, the second step would be another FRIEDEL-CRAFTS acylation of resorcinol with 2,4-dichloro-6-(4-methoxyphenyl)triazine (**170**) obtained from step one. Aside from the aforementioned issues arising from the utilization of stoichiometric amounts of LEWIS acid catalyst, this strategy poses several disadvantages. For instance, the resulting diopat (**172**) is practically insoluble in most solvents and the subsequent alkylation to BMT is therefore performed in extremely polar, possibly toxic solvents like methylcellosolve, thus significantly hampering the processability and purification. Additionally, the poor solubility of diopat leads to residues of this strongly colored intermediate in industrial apparatuses. Hence, we aimed to synthetically bypass the intermediate diopat. One approach would be to attach the isooctyl residues to the resorcinol prior to the FRIEDEL-CRAFTS acylation. However, applying the acylation conditions tested for step one to this system lead to no conversion in every case except for aluminum chloride.

Thus, we aimed to explore different methods for the C-C-bond formation between the triazine core and resorcinol or its surrogates. Among the possible carbon nucleophiles to attach to the triazine ring *via* nucleophilic aromatic substitution, enols or enolates have not been explored yet. To investigate this approach, test reactions were performed using 2-chloro-4,6-diphenyltriazine (**183**) and the commercially available 4-methoxy acetophenone (**184a**) and 3-ethyloxy-2-cyclohexenone (**184b**) (**Scheme 38**).
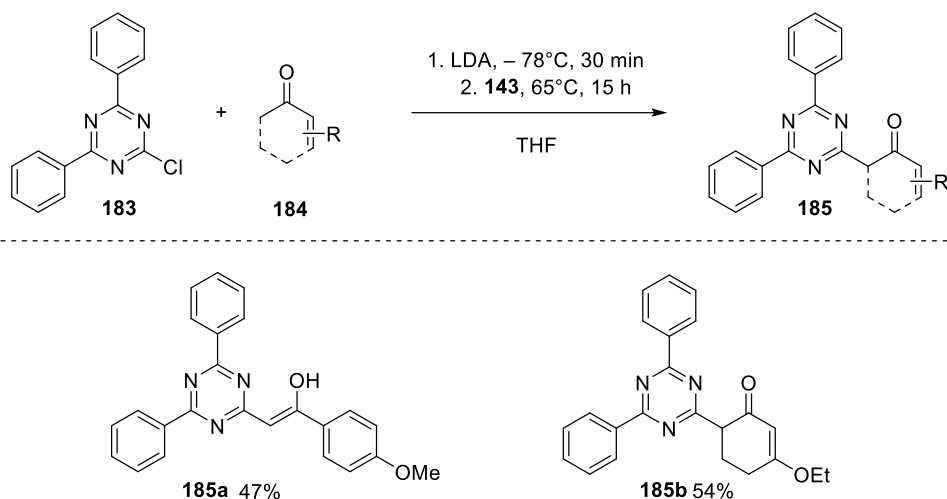
Scheme 38. Reaction of 2-chloro-4,6-diphenyltriazine with different lithium enolates.

First, the ketone was treated with a set of different strong bases (LDA, LiHMDS, NaNH$_2$ and KO^{t}Bu) at −78 °C in anhydrous THF to generate the enolate. Upon addition of the base, the solution turned a yellow color. Subsequently, the triazine was added and the now orange colored mixture was stirred at room temperature for another 16 to 24 hours. Among the strong bases tested in this reaction, only LDA, which is commonly the base of choice for enolate reactions, afforded the desired enol addition product **185a** and **185b** in yields of 47% and 54%, respectively. Possible side products reducing the yields may arise from aldol reaction or condensation.

To investigate the keto-enol tautomerism of the obtained α-triazinyl carbonyl compounds,[178] ^{1}H NMR spectra were recorded in solvents of different polarity. In **Figure 55** and **Figure 56**, the ^{1}H NMR spectra of **185a** and **185b** in benzene-d_6, chloroform-d_1, tetrahydrofuran-d_8, methanol-d_4 and dimethylsulfoxide-d_6 are presented. For both compounds, two tautomers are visible in the less polar solvents. The signals at around 13 ppm can be attributed to the hydrogen bridge of the enol tautomer. Transitioning towards more polar solvents, the amount of enol decreases significantly. In THF and DMSO, only small amounts of enol are observed while the ketone form dominates. The enol form is not present in methanol as protic solvents are also able to form hydrogen bridges, thus further stabilizing the ketone form. With increasing polarity, the overall signal-to-noise ratio decreased due to the reduced solubility of the compounds in more polar solvents.

Comparing the proton spectra, conclusions about the keto enol equilibrium can be drawn. In highly polar solvents like DMSO or methanol, only little to no hydrogen bridges can be observed in the range from 12 ppm to 16 ppm. In apolar solvents, However, the signals of the hydrogen bridges increase with decreasing polarity. By integration of the signals, the ratio of keto- to enol-tautomer can be calculated. In apolar solvents, the enol-form is present in up to 60%, whereas in polar solvents, the keto-form is predominant. Solvent molecules capable of coordinating to the carbonyl group and the triazine nitrogen intercept the formation of hydrogen bond bridges.
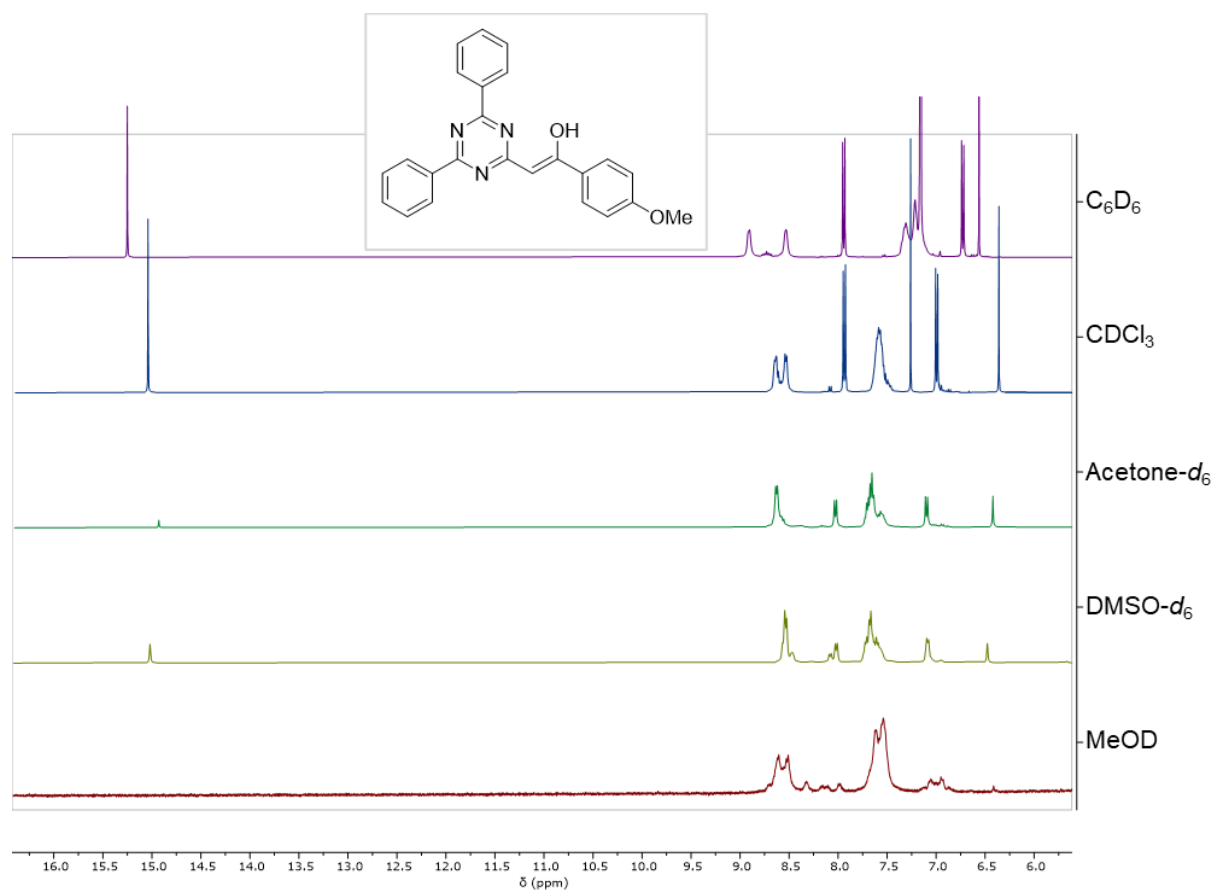
Figure 55. Comparison of th ¹H NMR spectra of **185a** in benzene-d_6, chloroform-d_1, tetrahydrofuran-d_8, dimethylsulfoxide-d_6, and methanol-d_4 (top to bottom).
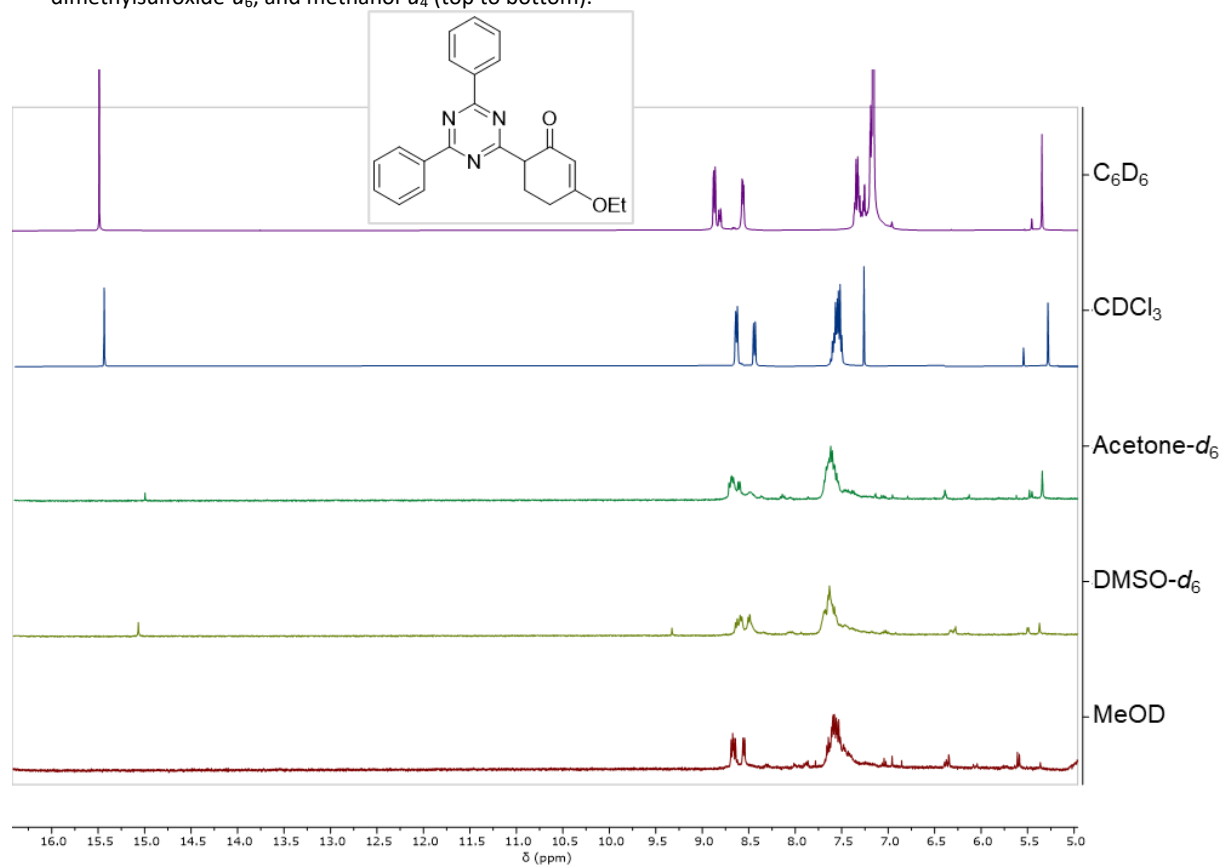
Figure 56. Comparison of th ¹H NMR spectra of **185b** in benzene-d_6, chloroform-d_1, tetrahydrofuran-d_8, dimethylsulfoxide-d6, and methanol-d_4 (top to bottom).

The enolate addition conditions were then applied to the BMT building blocks (**Scheme 39**). Initially, 3-isooctyloxy cyclohexenone (**180**) was treated with LDA and subsequently, 2,4-dichloro-6-(4-methoxyphenyl)triazine (**168**) was added. The desired double adduct **186**, termed tetrahydro-Bemotrizinol, was isolated in 28% yield.
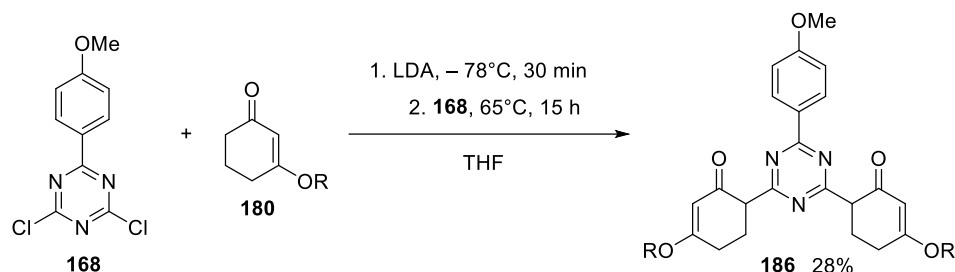
Scheme 39. Reaction of 2-chloro-4,6-diphenyltriazine with a Li-enolate derived from 3-isooctyl oxy cyclohexenone. R = isooctyl.

The losses may be attributed to side reactions like aldol addition or condensation, as well as the formation of regio- and stereoisomers. Complete removal of any excess starting material from the cyclohexenone ether is crucial as residual isooctanol will react with the triazine faster than the enolate, leading to *O*-alkylated side products.

Tetrahydro-BEMT was characterized thoroughly using various spectroscopic and spectrometric methods, proofing the proposed structure. In FAB mass spectrometry, the exact mass of the oxidized BMT is found instead of THBMT, suggesting autoxidation of THBMT under ionizing conditions.

In **Figure 57**, the ^{1}H NMR spectra of BMT (**1**) and tetrahydro-BMT (**186**) are displayed. According to the ^{1}H spectrum, tetrahydro-BMT is not a single substance and instead consists of a mixture of different isomers. On the one hand, there are diastereomers present due to the chiral isooctyl residues and the newly formed stereogenic center on the α-position of the ketone. On the other hand, the equilibrium of the keto-enol-tautomerism is shifted significantly towards the enol, resulting in the formation of tautomers (4:1 ketone/enol). In the lowfield region, signals corresponding to the hydrogen bridge between the triazine nitrogen, and the enol-hydroxy group can be observed. FAB-MS analysis, however, did not show the exact mass of tetrahydro-BEMT but of BEMT. This hints towards facile oxidation under ionizing conditions. Possibly, this effect could be exploited for aerobic oxidation of tetrahydro-BMT to BMT.
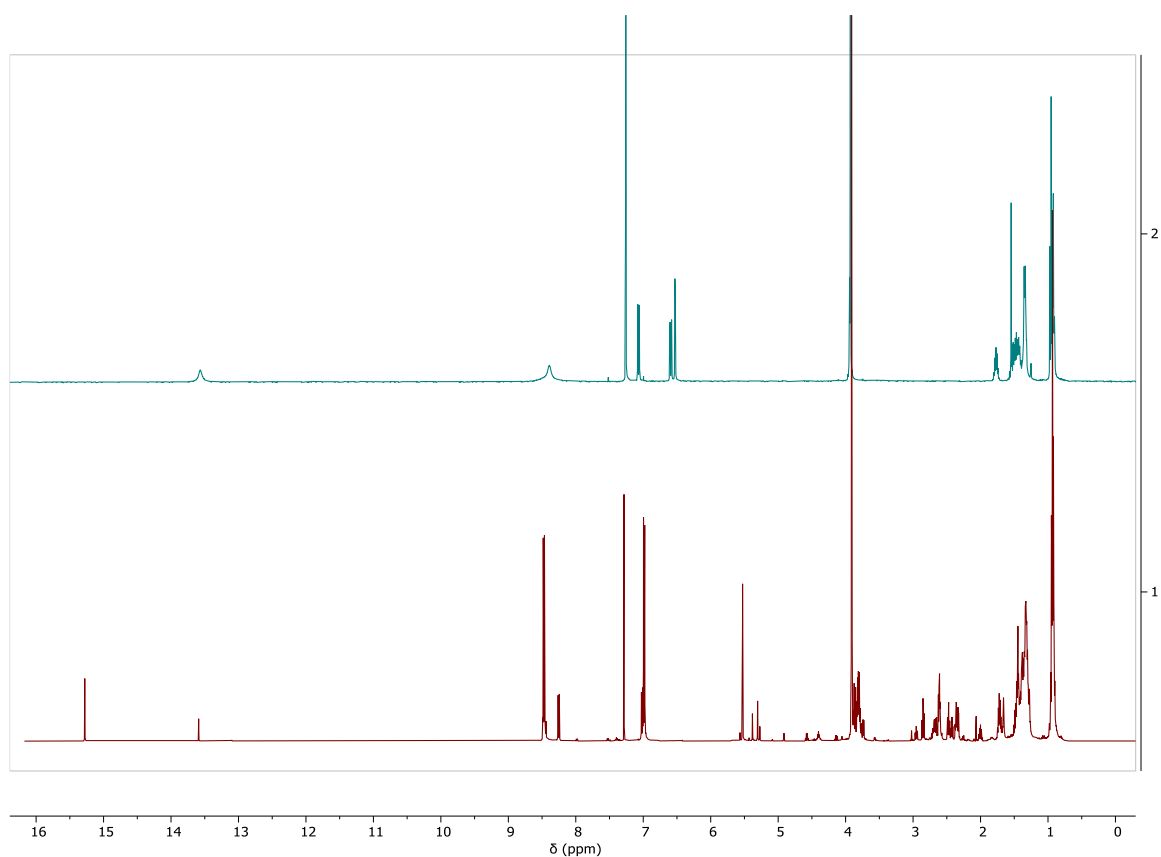
Figure 57. Comparison of the ^{1}H NMR spectra of BMT (top) and THBMT (bottom) In CDCl$_3$.

The effect of the keto enol tautomerism on the photophysical properties was investigated by measuring UV/Vis spectra of THBMT and BMT in different solvents (**Figure 58**).
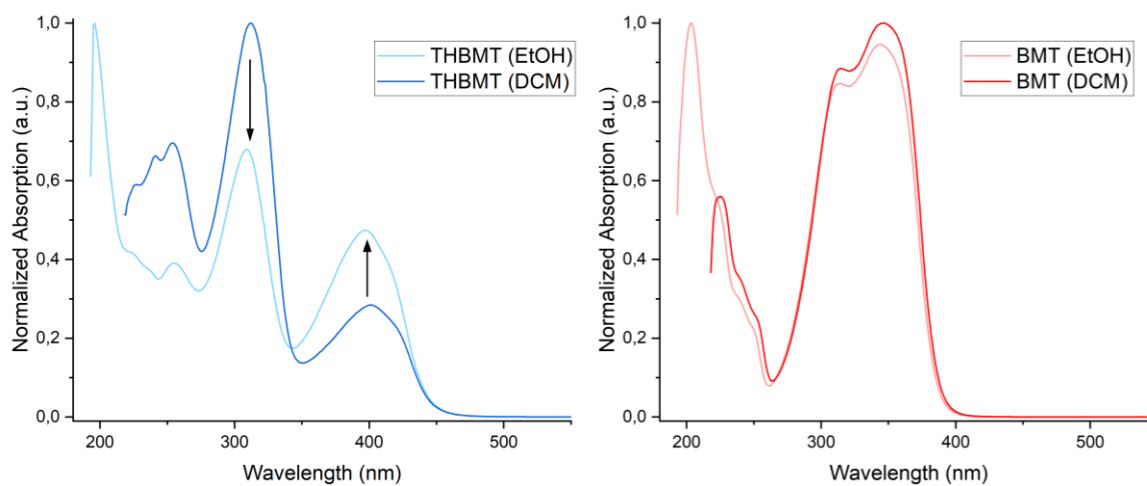
Figure 58. Normalized absorption spectra of THBMT (left) and BMT (right) in ethanol and dichloromethane.

The absorption profiles of tetrahydro-BMT in ethanol and dichloromethane are quite similar and no pronounced solvatochromic shift can be observed. In both spectra, there are two absorption bands at 300 nm and 400 nm.

In dichloromethane, the band at 300 nm is more intense than the band at 400 nm. In ethanol the 300 nm band intensity is decreased while the band intensity at 400 nm is increased. These results can be rationalized by taking the results of the NMR studies into account. According to this, in less polar, aprotic solvents like dichloromethane the enol form is dominant while in protic solvents, the equilibrium is exclusively shifted to the ketone form. Both tautomer forms exhibit different absorption profiles. In contrast to tetrahydro-BMT, the spectra of BMT in these solvents are almost identical (**Figure 58**) since the structure is not able to perform tautomerism in the different solvents. A direct comparison of the UV/Vis spectra of tetrahydro-BMT and BMT in ethanol is shown in **Figure 59.** The commercial UV-filter BMT shows two absorption bands in the UV range between 250 nm and 400 nm and is thus an efficient filter for both the UV-A and UV-B range. Thus, it is considered a broad-band UV-filter. In the UV-B region of 280 – 315 nm, tetrahydro-BMT also shows an absorption band. However, tetrahydro-BMT is missing the absorption band in the UV-A region of 315 – 400 nm.
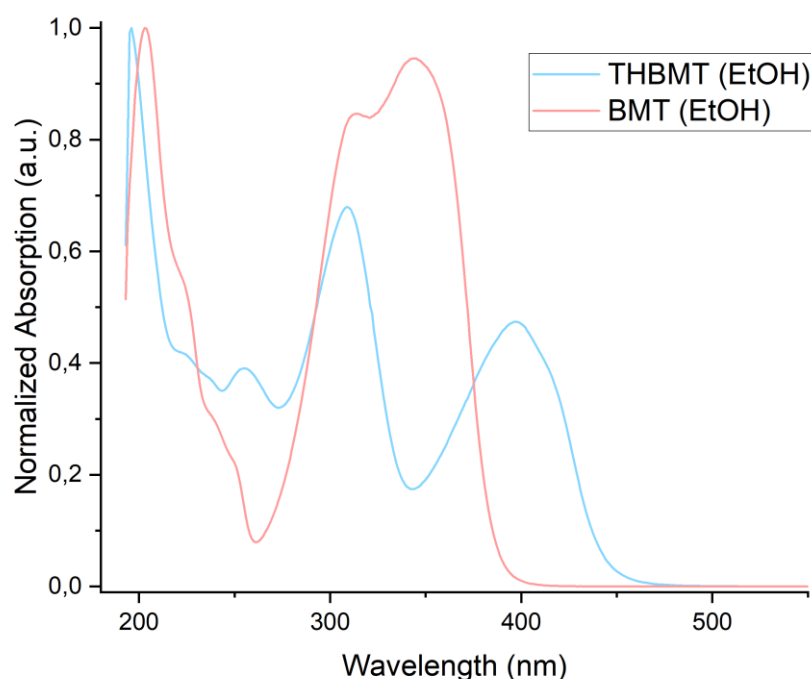
Figure 59. Comparison of the normalized absorption spectra of THBMT (blue) and BMT (red) in ethanol.

As a result, tetrahydro-BMT, unlike BMT, cannot be applied as a broad-band UV-filter. However, its absorption in the UV-B region is quite pronounced, rendering it an interesting candidate for UV-absorbing compounds. Additionally, its suggested autoxidation behavior renders tetrahydro-BMT a potential BMT surrogate converted through *in situ* oxidation in sunscreen formulations. Determination of the sun protection factor of tetrahydro-BMT and photostability measurements are necessary to assess its viability as a sunscreen ingredient.

In the following chapter, the oxidation behavior of tetrahydro-BMT to BMT is investigated in more detail.

3.5.4 Desaturation of Cyclohexenone Monoether

Introduction. Methods to synthesize meta-substituted phenols are sought after because, in contrast to ortho- and para-substitution, the reactivity of electron-rich aromatics disfavors *meta*-substitution. Thus, alternative routes have been developed in which the desired residues are attached to cyclohexanones or cyclohexenone which are subsequently desaturated and oxidatively aromatized to substituted phenols (**Scheme 40**). For the oxidative aromatization of such systems, several different methodologies have been reported. Stoichiometric oxidants like iodine or iodine-DMSO systems,[179] DDQ,[180] IBX[181] have been employed. In terms of catalytic oxidative aromatization, the STAHL group investigated several Pd-based catalytic systems.[182] However, all these reactions do not include substrates in which the cyclohexenone double bond bears an ether substituent. Similar concepts have been developed for dihydropyridines, including photocatalytic oxidation methods using oxygen in combination with photosensitizers.
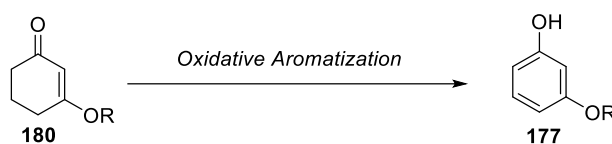
Scheme 40. Oxidative aromatization of cyclohexenone monoethers.

Oxidative Aromatization. In order to oxidize the cyclohexenone monoether to the resorcinol monoether, a variety of different methods were explored. An overview is given in **Table 13**. The methods can be categorized as conventional methods in which the oxidant is applied in stochiometric amounts in excess, or catalytic methods in waive oxygen or hydrogen are used as the oxidizing agent in combination with a transition metal catalyst. Moreover, photocatalysis *via* photosensitizers was explored.

Out of the stochiometric methods, full conversion to the resorcinol monoether was achieved using iodine or IBX. For the oxidation with iodine, water was chosen as the solvent to avoid the formation of unsymmetric resorcinol dieters. Additionally, a system in which DMSO is used as a sacrificial co-solvent to regenerate iodine *in situ*, enabling the use of substoichiometric amounts of iodine, was evaluated. However, only incomplete conversion was observed corresponding to the actual amount of iodine used. Other oxidants did not convert the cyclohexanone monoether.

Catalytic conditions reported by STAHL *et al*. were also evaluated. Unfortunately, these methods could not be applied to the present system. While the scope of these methods does include cyclohexenone substituted in the 3-position, alkoxy substituents were never mentioned. Hence, it is plausible, that the ether residue in this position inhibits the desaturation. A different catalytic system by KIKUSHIMA and NISHINA using copper or iron halides in combination with hydrochloric or hydrobromic acid was also evaluated.[183] Mechanistically, bromine is generated *in situ* and adds to the double bond. Upon double elimination of HBr, the desaturated product is formed. Applying this method to the cyclohexenone monoether, only resorcinol could be detected. While the aromatization did take place, the isooctyl ether was cleaved during the reaction.

Photocatalytic methods with different photosensitizers did not show any conversion, independent of the sensitizers, additives or solvents employed.

Table 13: Oxidative aromatization methods tested for 3 isooctyloxy cyclohexenone.
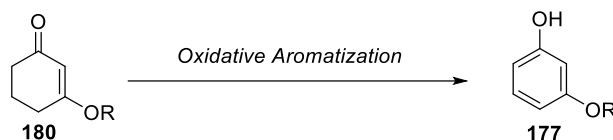
method	oxidant	additive	base	solvent	T / °C	result*
Stoichiometr.[179b, 179d]	I_2 (1.2 eq.)	-	-	H_2O	100	**Full conversion**
Stoichiometr.[179c]	I_2 (0.2 eq.)	DMSO (1.2 eq.)	-	H_2O	120	Incomplete conversion
Stoichiometr.[181]	IBX (4.0 eq.)	-	-	DMSO/PhF (1:1)	85	**Full conversion**
Stoichiometr.[180]	DDQ (3.3 eq.)	-	-	1,4-Dioxane	100	No conversion
Stoichiometr.	H_2O_2	-	-	H_2O	100	No conversion
Catalyt.[184]	Pd/C	H_2/Ar (1 atm,1:3)	K_2CO_3	DMF	120	No conversion
Catalyt.	Pd(OAc)$_2$	-	K_2CO_3	MeCN	85	Traces
Catalyt.	Pd(TFA)$_2$	-	Pyridine	EtOAc	80	Traces
Catalyt.[183]	CuX (0.1 eq.)	HX (0.4 eq.) X = Cl, Br O_2 (1 atm)	-	Dioxan	100	Ether cleavage
Photo.	Rose Bengal / Eosin Y / Riboflavin	O_2 (1 atm)	-	MeCN	r.t.	No conversion

* Conversion was monitored by GC/MS

In general, cyclohexenone monoethers are not easily oxidized. Only two methods were successful. Since both approaches require stoichiometric amounts of halogen-based oxidants, these methods are not feasible for an application on an industrials scale. Consequently, we decided to explore different methods.

Electrochemically Driven Desaturation. Electrochemical methods like electrolysis pose one of the simplest, yet most efficient approaches to perform redox transformations as no additional oxidizing or reducing agents are needed. Harnessing the unexplored potential of electrochemical transformations for industrial chemical synthesis would pose several advantages.[185]

In 2020, Baran *et al.* reported on a versatile and robust electrochemically driven desaturation (EDD) of TMS-protected carbonyl compounds including cyclohexanone substrates.[186] Previously, similar approaches have been described by Shono *et al.* and Moeller *et al*.[187]

The application of electrochemical methods in organic chemistry is not overly common. Unpredicted reactivity, as well as specialized and DIY equipment have hampered its applicability and made many chemists refrain from diving into this field. However, recently the launch of commercial electrochemistry systems like the IKA Electrasyn, co-developed by Phil Baran, made electrochemistry more accessible for organic chemists and resulted in a surge of novel methodologies. In a recent guide, Baran *et al.* gave a comprehensive overview on general considerations for experimental setups.[188] In general, there are always two reactions occurring in an electrochemical cell, an oxidation taking place at the anodes and a reduction at the cathode. The electrode on which the desired reaction occurs is also called a working electrode, the other one a counter electrode. If the reactions on both electrodes are desired, it is a paired electrolysis. The experiment can be performed in an undivided cell or a divided cell in which the half cells are connected through a semipermeable membrane or a salt bridge to enable ion mobility and close the electrochemical cycle. Other parameters to adjust to every experiment are electrode material, solvent and voltage or current. In case of a constant cell volatge, the electrolysis is performed under potentiostatic conditions, and under galvanostatic conditions in case of constant current. To improve the conductivity, an electrolyte is added to the organic solvent, for instance insert salts like tetrafluoroborates or hexafluorophosphates. Electrolysis is either potentiostatic or galvanostatic. Redox potential of substrates can be obtained from cyclic voltammetry measurements.

Initially, cyclic voltammetry measurements were performed by Dr. Philipp Röse to assess the redox potential of both the cyclohexenone monoether **180** and tetrahydro-BMT (**186**). Results are displayed in **Figure 60** for cyclohexenone monoether and **Figure 61** for THBMT.
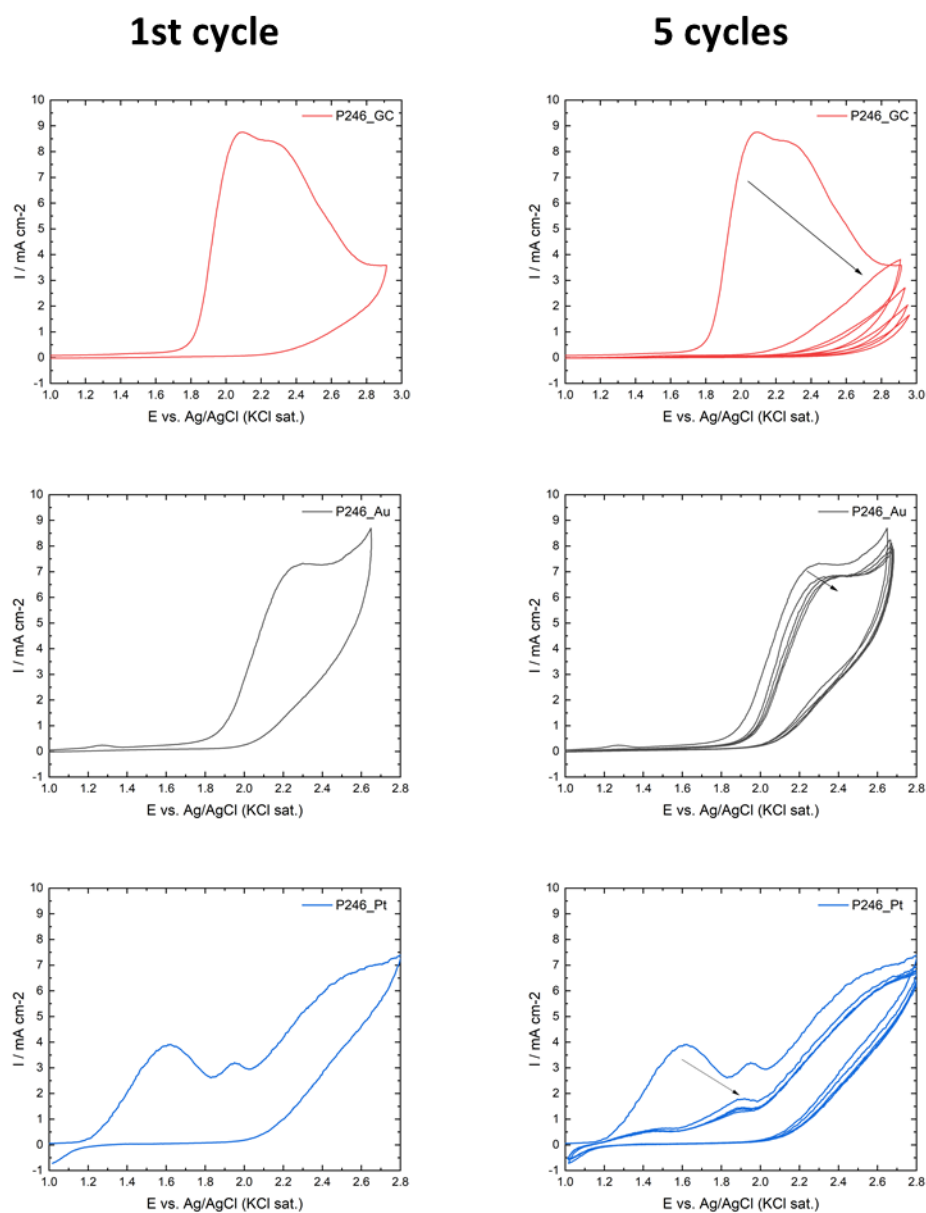
Figure 60. Cyclic voltammetry measurements of cyclohexenone monoether **180** in dichloromethane and calibrated versus a Ag/AgCl (KCl_sat in water) reference electrode.

Each maximum corresponds to oxidation processes occurring at the indicated voltage. The incline of the curve towards higher voltage is caused by the oxidation of the solvent. As no minima occur during the back cycle, the oxidation process is irreversible. Upon repeated cycles, passivation of the electrodes is observed, decreasing intensity over multiple cycles. The highest intensity was observed using glassy carbon electrodes, however, they also showed the most pronounced passivation after the first cycle. In the case of the platinum electrode, the intensity of the oxidation is lower, and a second oxidative process arises. For both peaks, passivation is observed after one cycle. Almost no passivation occurs using gold electrodes.
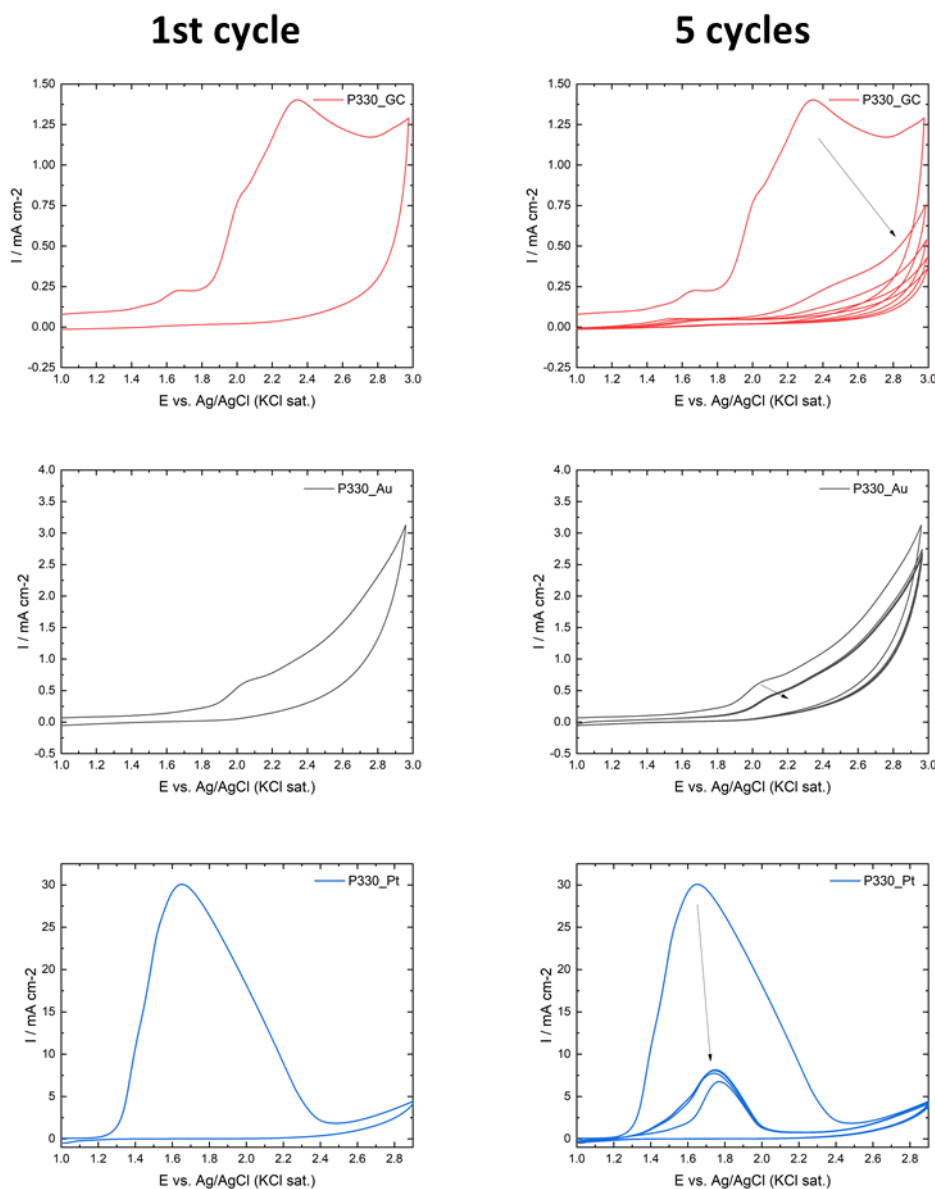
Figure 61. Cyclic voltammetry measurements of tetrahydro-BMT **186** in dichloromethane and calibrated versus a Ag/AgCl (KCl$_{sat}$ in water) reference electrode.

The cyclic voltammetry results for tetrahydro-BMT show significantly different redox behavior for different electrode materials. For glassy carbon, the overall intensity is quite low compared to the spectra of cyclohexenone monoether. Additionally, a strong passivation is observed after the first cycle. For gold, the overall intensity is also relatively low, and no distinct oxidation peak occurs. In the case of a platinum electrode, a significant maximum at 1.8 V with a relatively highest intensity of up to 30 mA/cm² is present. After the first cycle, the intensity is reduced due to passivation, however, remaining constant over the following cycles.

According to these results, preliminary experiments were performed in a potentiostatic system using a platinum anode and a graphite cathode. Electrolyte was a 0.1 M solution of tetrabutylammonium tetrafluoroborate. Formation of the target BMT (**1**) was only observed using dichloromethane as solvent. Presumably, this is due to

the reduction of dichloromethane which functions as an electron sink. Plausible half reactions for anode and cathode are displayed in **Scheme 41**.
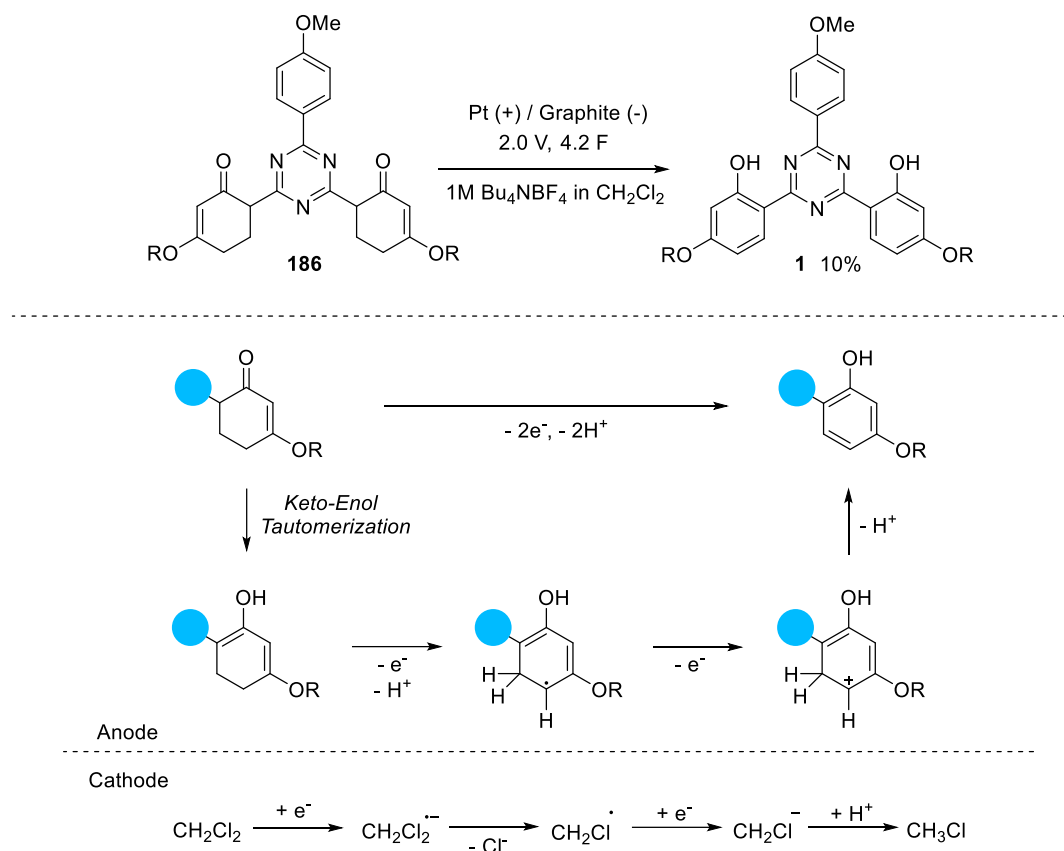
Scheme 41. Proposed electrode processes for the oxidative aromatization of THBMT.

The proposed mechanism for the two-electron oxidative aromatization process of one cyclohexenone moiety involves an initial keto-enol tautomerization. The resulting enol is then oxidized at the anode to a radical cation, followed by the loss of a proton to give a radical. After another oxidation step, a second proton is abstracted to enable aromatization to the desired phenol. On the counter electrode, a one-electron reduction of dichloromethane to chloromethane likely takes place. In this process, chloride anions are generated. This hypothesis is supported by the decreasing cell resistance over the course of the reaction due to the increasing presence of ions. However, the generation of chloride anions poses a major drawback. Reaction progress leads to corrosion of the platinum electrode. Chloride ions lower the redox potential of platinum and enable concurring anodic oxidation under the formation of chloroplatinate species. This is highly disadvantageous considering the costs of platinum electrodes. Additionally, undesired side-reactions were observed during the reaction as indicated by the formation of highly polar side products. Therefore, further optimization and adjustments are necessary to minimize side reactions and increase the yield of the desired oxidative aromatization. Scavenging or masking of the chloride ions would be a possible solution, however, not feasible in an industrial context as stoichiometric amounts of silver salts would be necessary. Instead, performing the reaction in a divided cellular setup could help circumvent unwanted redox processes (**Figure 62**).
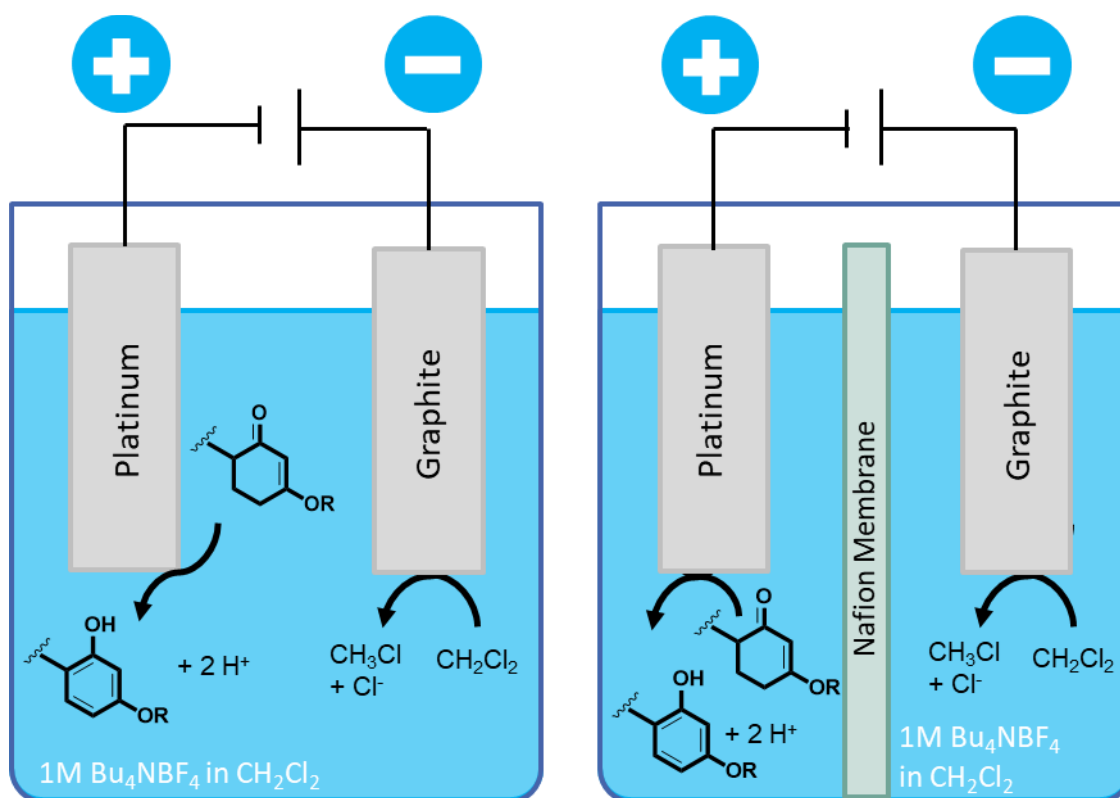
Figure 62. Undivided cell setup (left), divided cell setup (right).

While there certainly is still room for optimizations and improvements, these results indeed prove the feasibility of the transformation. Compared to the method by BARAN *et al.*, no preceding formation TMS-enol ether is needed as hydrogen bonding between the carbonyl and the adjacent triazine promotes enolization. Thus, the herein developed method could complement existing approaches to the electrochemical desaturation of carbonyl compounds.

3.5.5   Summary

Synthesis. To sum up all synthetic efforts of the previous chapters, the improved synthesis route towards Bemotrizinol is depicted in **Scheme 42**. In contrast to the linear state-of-the-art method, the newly developed process presents a convergent approval in which the triazine core and substituted resorcinol or its surrogate are synthesized separately and then combined to the AB$_2$-triazine scaffold.
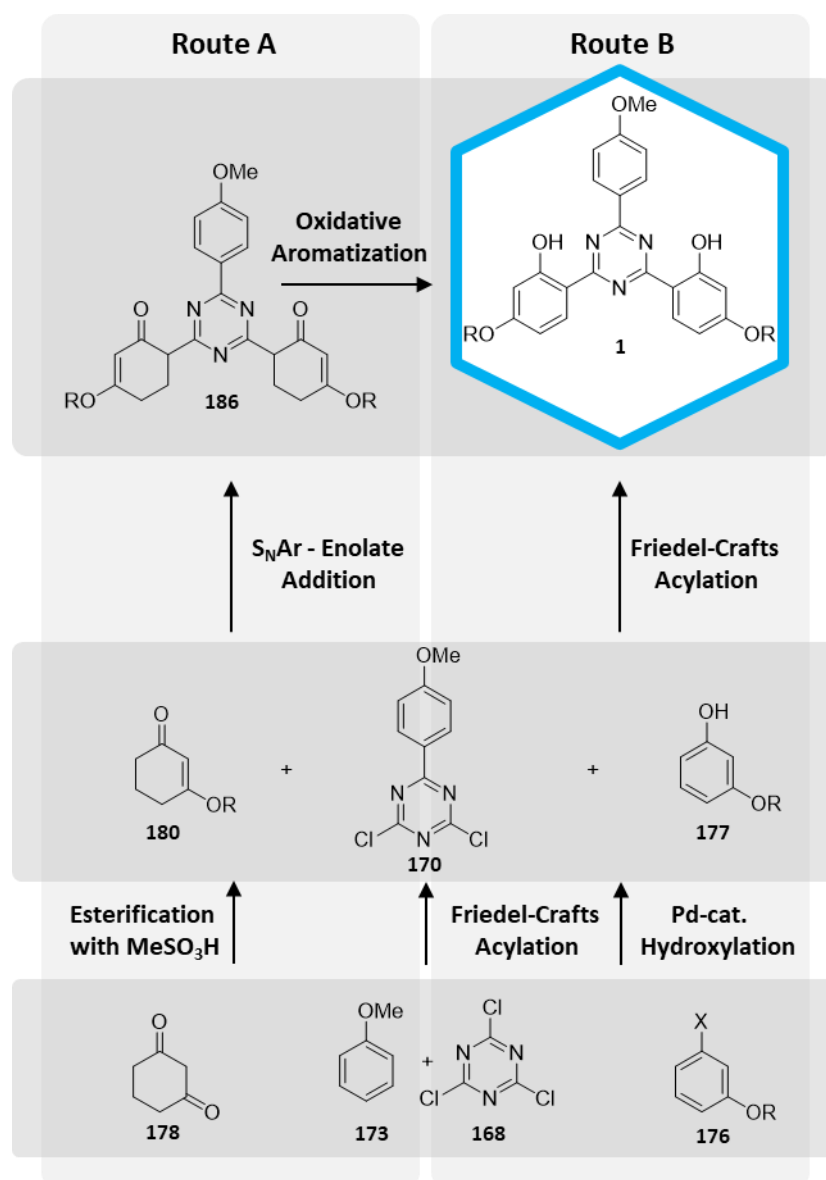
Scheme 42. Overview of the developed synthetic routes towards Bemotrizinol.

For the coupling of cyclohexenone monoethers as resorcinol surrogates to chlorotriazines, a novel protocol was established. The cyclohexenone is converted into an enolate through a strong base which then engages in a nucleophilic substitution. The transfer of this method to other ketones was demonstrated. The resulting α-triazinyl carbonyl compounds are interesting intermediates exhibiting a solvent-dependent tautomerism

which influences their absorption and emission profiles. Tetrahydro-BMT. The target BMT is then obtained through an electrochemical oxidative aromatization of the tetrahydro-BMT intermediate.

The cyclohexenone monoether can also be oxidized to the resorcinol monoether prior to attachment to the triazine core. Among the tested oxidants, only iodine in stochiometric amounts proved to be suitable. Alternatively, the resorcinol monoether is accessible through the palladium catalyzed hydroxylation of 3-bromo phenol ethers.

The resorcinol monoether can either be attached to 2,4-dichloro-6-(4-methoxyphenyl)triazine in a FRIEDEL-CRAFTS acylation, leading directly to BMT. Alternatively, the resorcinol monoether and the triazine can be connected *via* a nucleophilic substitution to obtain an *O*-arylated intermediate. Potentially, this could be converted to BMT in a photo-FRIEß rearrangement. However, selectivity issues arise upon irradiation with UV-light and BMT was only formed in trace amounts. Through optimization and fine-tuning of the reaction conditions, this route could be improved in the future.

Overall, the individual routes offer various advantages over the existing method. However, further optimization is certainly needed to ensure a good rentability of the entire process.

4 Summary and Outlook

In this thesis, a set of methodologies revolving around the imidazo[1,2-*a*]heterocyclic scaffold accessible *via* the GBB-3CR were developed (**Figure 63**). In this context, the GBB-3CR was used for the modification of both [2.2]paracyclophane scaffolds, as well as steroidal aldehydes derived from the marine steroid Gorgosterol. The obtained fluorophores were investigated as pH-sensitive probes and in bio-imaging experiments.

Moreover, sequential synthesis strategies for the modification of the imidazo[1,2-*a*]pyridine scaffold itself were explored. Through intramolecular cross coupling reactions of ImPy building blocks, donor-acceptor fluorophores were synthesized and investigated for potential TADF properties. In an intramolecular imidoylative coupling reaction, the imidazo[1,2-*a*]pyridines were post-cyclized to afford fused polyheterocyclic systems capable of interacting with double-stranded DNA.
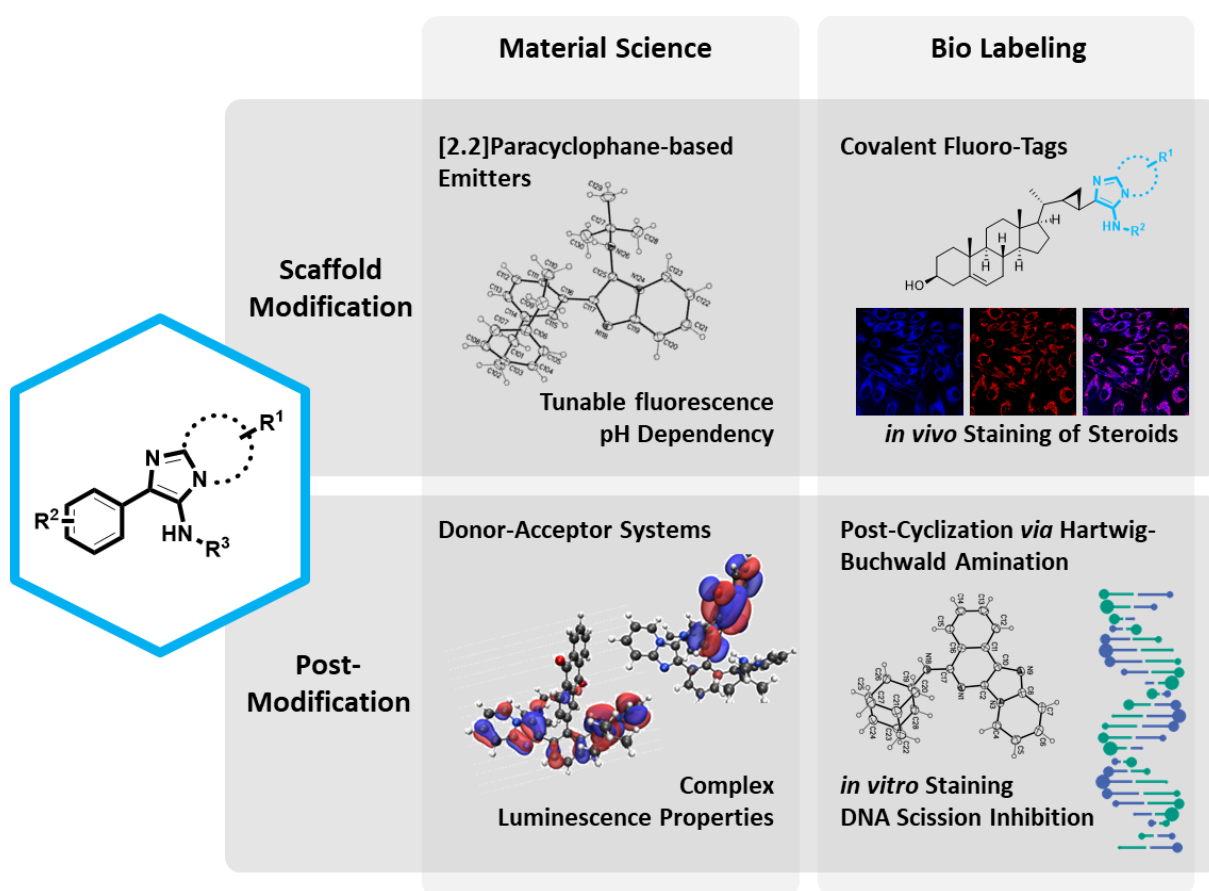
Figure 63. Finished projects for the development of novel imidazo[1,2-*a*]heterocyclic functional fluorophores.

The GBB-3CR was explored in combinatorial 3D-printing to enlarge the scope of reactions. Moreover, flavin synthesis was explored. To prove the feasibility of on-slide transformations of CO_2, a fluorescent probe for CO_2 was developed.

An alternative synthesis route for the commercial UV-filter Bemotrizinol was established, improving the overall sustainability of the process. Key step is the nucleophilic aromatic substitution of chloro-1,3,5-triazines with lithium enolates, followed by an electrochemical oxidative aromatization.

4.1 PCP-based Imidazo[1,2-a]heterocycles as Fluorophores and Ligands

A facile, modular method for the modification of the [2.2]paracyclophane scaffold was developed, affording PCP-based mono- and bis-imidazo[1,2-*a*]pyridines and -pyrazines. For this, PCP-aldehydes, as well as isonitrile were utilized, marking its first application in IMCRs (**Figure 64**).

The fluorescence properties of these substrates have been studied thoroughly, exploring the effect of varying the individual components as well as the pH-dependence of the fluorescence. Moreover, their applicability as ligands for palladium complexes was established and their catalytic activity was assessed in a Suzuki-Miyaura cross coupling reaction.
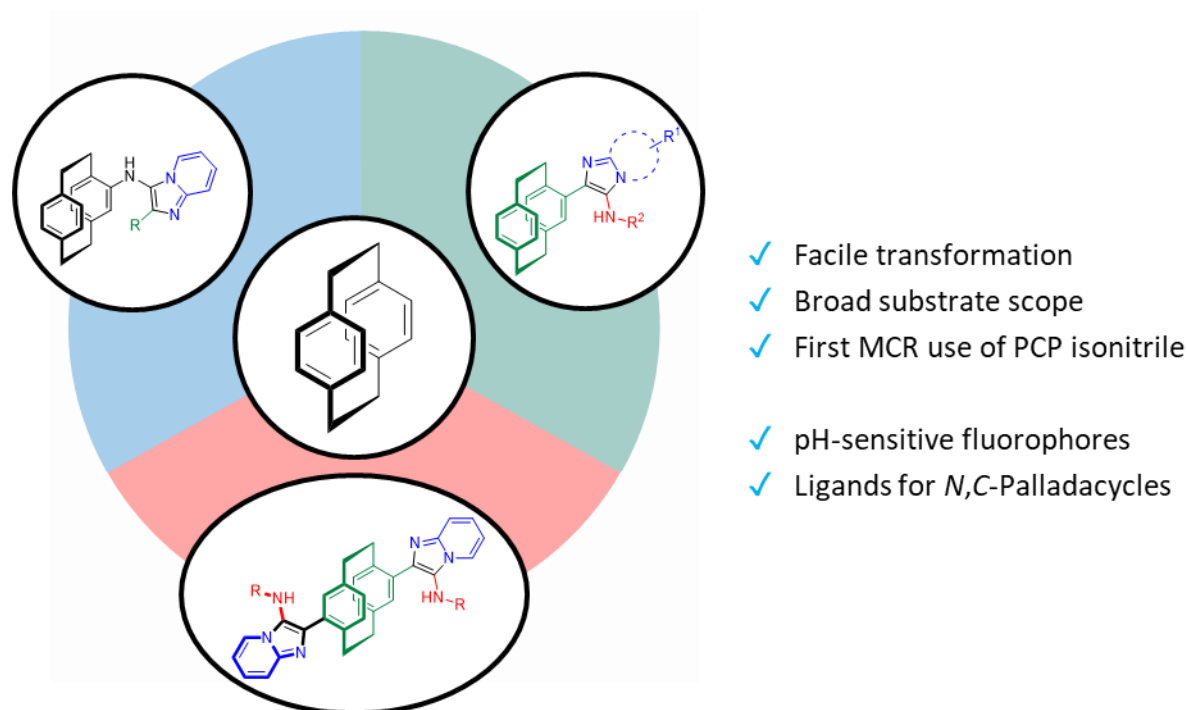
Figure 64. Overview of the PCP-based imidazo[1,2-a]heterocycles accessed *via* GBB-3CR.

This methodology gives access to an interesting substituent motive for the PCP-scaffold, as well as enabling facile introduction of chiral elements into imidazo[1,2-*a*]heterocyclic fluorophores which could be interesting for non-linear optics. Through the combination of the MCR approach and other modifications of the PCP scaffold, diversely substituted [2.2]paracyclophanes could be accessed.

4.2   Design of Imidazo[1,2-*a*]pyridine-based Donor-Acceptor Chromophores

A series of donor-acceptor chromophores were synthesized bearing a 3-amino imidazo[1,2-*a*]pyridine donor motive. The emitters were designed to complement a study by L\ᴇᴇ *et al.* showing the chimeric nature of imidazo[1,2-*a*]pyridines (**Figure 65**).

Through DFT-Calculations, different combinations of the ImPy donor motive and different acceptor were assessed. In combination with anthraquinone acceptor, the calculated ΔE_{ST} values were in range for possible TADF effects. Based on these findings, a series of ImPy-Aq emitters were synthesized with different geometries and substitution patterns.
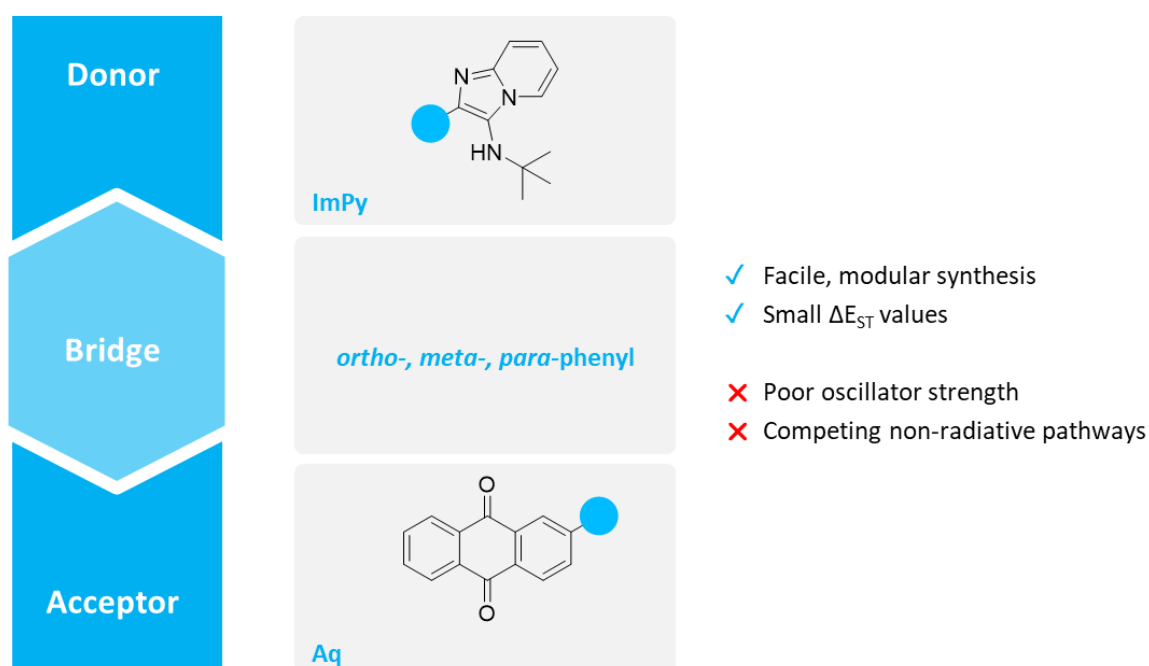
Figure 65. Overview of the imidazo[1,2-a]pyridine donor-acceptor chromophore series

The photophysical properties are currently investigated by the Zʏsᴍᴀɴ-Cᴏʟᴍᴀɴ group at the University of St. Andrews. According to preliminary experimental data, the compounds were only slightly emissive at ambient temperatures due to a low oscillator strength and possible competing non-radiative deactivation pathways. Further photophysical characterizations will be performed to investigate the underlaying luminescence mechanism.

To improve the performance of the emitters, adjustments and optimizations of the structures are necessary to suppress non-radiative effects and improve oscillator strength. Moreover, different combinations of donor and acceptor motives need to be assessed.

Inspired by the work of Sᴘᴜʟɪɴɢ *et al.*, the combination of the ImPy-donor motive and the MCR-based concept for the functionalization of the PCP scaffold would provide a versatile synthetic platform for the development of novel through space emitters.

4.3   Imidazo[1,2-*a*]pyridines as Fluorophore Tags for Bioimaging of Steroids

The imidazo[1,2-*a*]heterocyclic scaffold was established as a covalent fluorescent tag for the bioimaging of steroids. Aldehyde-functionalized derivatives of the marine steroid Demethylgorgosterol were reacted in a GBB-3CR in a fluorophore approach. A small library of five fluorophore-steroid conjugates was synthesized and spectroscopically characterized. The compounds showed mediocre cytotoxicity in an MTT-assay. Two derivatives were investigated in co-localization studies using HeLa cells, showing good visibility. Localization of the steroids in the mitochondria was observed (**Figure 66**).
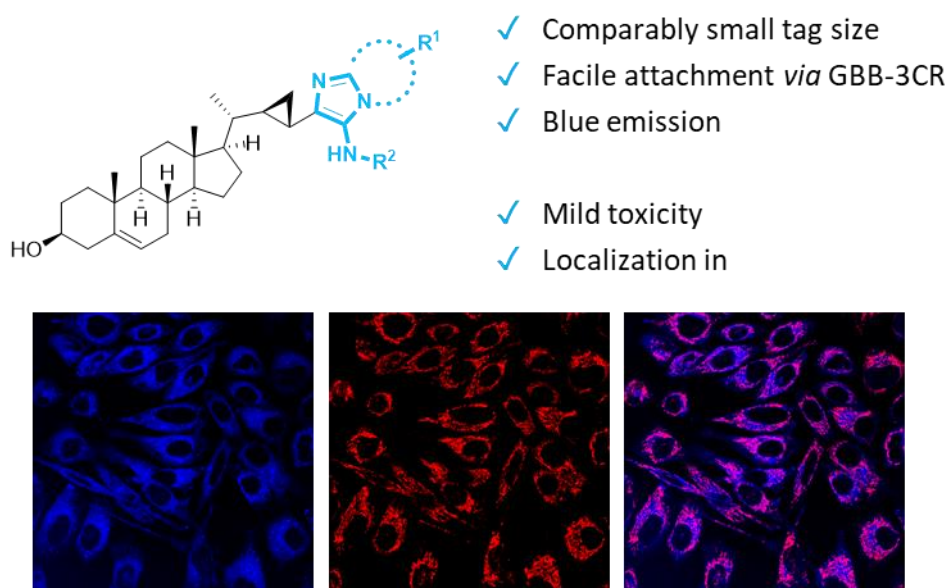
Figure 66. Overview of the fluorophore-steroid conjugates investigated in bioimaging experiments.

The GBB-3CR was established as an efficient method for fluorescent labeling, offering a plethora of advantages like the facile attachment of the tag through mild reaction conditions without the need for additional coupling agents, and facile purification as no fluorescent by-products arise. Due to its broad functional group tolerance, the reaction is orthogonal and could easily be transferred to other analytes. The ImPy tag itself is a blue dye of compact size and thus ideal for the labeling of small molecules to avoid falsification of ligand binding and intracellular affinity.

Currently, the fluorophore-steroid conjugates are investigated in *in vivo* experiments with corral cells by the Guse group at the University of Heidelberg. In future studies, the ImPy tag could be employed in bioimaging studies of other compound classes to prove its general applicability.

4.4   Flat *N*-rich Heterocycles as DNA-Intercalating Agents

A sequential synthesis strategy comprising a GBB-3CR and an intramolecular imidoylative HARTWIG-BUCHWALD coupling was developed and the resulting polyheterocycles were investigated for their DNA-intercalating properties (**Scheme 43**).
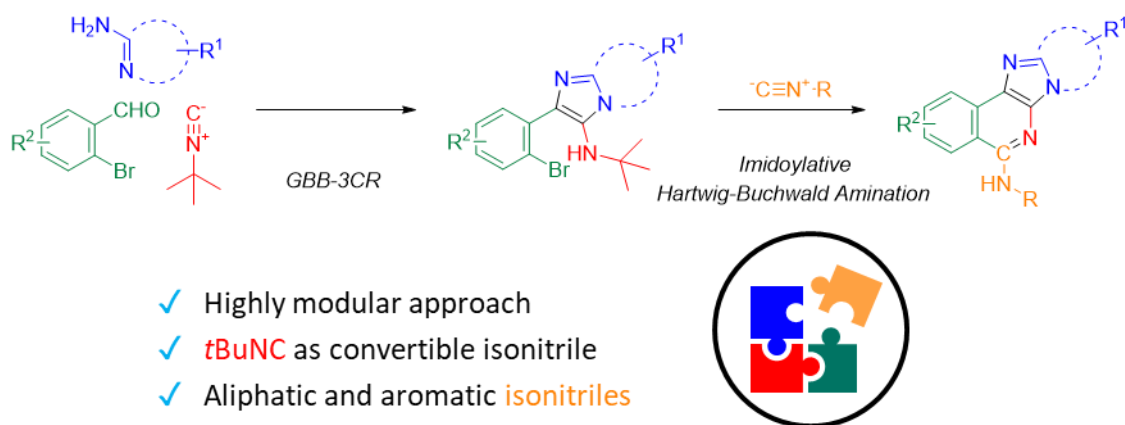
Scheme 43. Synthesis of flat *N*-rich heterocycles *via* reaction sequence of GBB-3CR and imidoylative amination.

A set of GBB-precursors were synthesized in excellent yields and different aliphatic and aromatic isonitriles were inserted, affording a library of isoquinolinones. Their absorption and fluorescence spectra were evaluated, revealing a bright blue fluorescence.

In one case, the formation of an unusual demethoxylated coupling product was observed. The obtained highly fluorescent compound exhibits a pronounced bathochromic shift, most likely originating from an ESIPT process. To investigate this unexpected scaffold, the scope of this reaction will be expanded in future studies.

Selected compounds were examined for their interaction with double strand DNA in a pUC-19 electrophoresis mobility shift assay which was established as a method to quantify ds-DNA scission inhibition. For the investigated compounds, a stabilizing effect on the double strand against oxidative conditions was observed, hinting towards DNA-intercalating properties. DNA-intercalating agents often exhibit antiproliferative effects due to their inhibition of replication mechanisms. Thus, further investigations of potential cytostatic properties should be pursued.

4.5 Miniaturized Synthesis of Fluorophore Arrays *via* nano3D Printing

In a set of experiments, the practicability of different aspects of the miniaturized reaction screening via the nano 3D-printing method has been demonstrated. The miniaturized synthesis of both flavins and imidazo[1,2-*a*]pyridines was achieved (**Figure 67**). Aiming towards the surface-based conversion of CO_2, a fluorescent probe was synthesized which can contribute to developing a screening setup for the photocatalytic conversion of chemicals including CO_2.
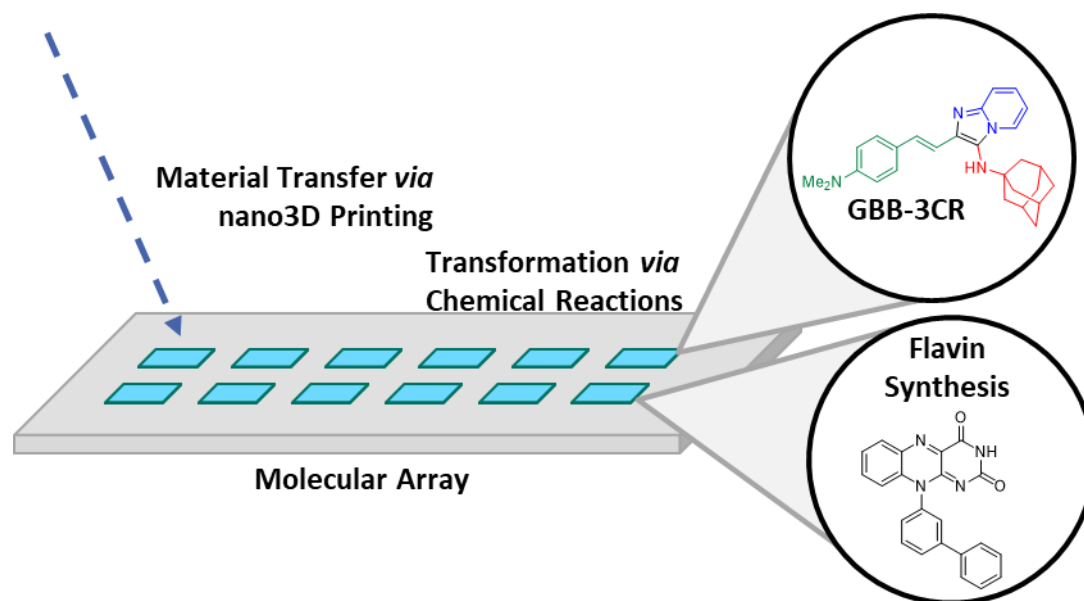
Figure 67. Overview of the miniaturized GBB-3CR and flavin array synthesis *via* nano3D printing.

With the GBB-3CR and a flavin synthesis, two new reaction types were successfully implemented in combinatorial nano3D printing. To fully demonstrate the parallelization potential, libraries of imidazo[1,2-*a*]pyridines and flavins will be synthesized in further experiments. For this, more reference material will be synthesized *via* conventional methods on a milligram scale and spectroscopically characterized. For the characterization of the individual compounds on the slide aside from fluorescent spectroscope, more conclusive, unambiguous analysis should be implemented. Currently, efforts are working to establish MALDI and MALDI-imaging methods.

As all reaction types that are now established for 3D-nano printing are based on condensation reactions, other types have to be explored to enlarge the scope of the method and improve its applicability. Possible alternative transformations could be nucleophilic substitutions, cycloadditions, alkene/alkyne additions, or possibly even robust, non-sensitive cross coupling protocols.

A novel fluorescent chemical probe for CO_2 was designed. The sensor is based on a three-component reaction of an aryne, an isonitrile and CO_2 furnishing *N*-alkyl phthalimides. Therefore, a Kobayashi aryne precursor with an electron-donating piperidyl residue was synthesized. As soon as suitable analysis methods are implemented, the on-slide reaction of the probe with CO_2 will be investigated.

4.6 Development of a Novel Route towards Bemotrizinol

An alternative, convergent synthesis route towards the UV-absorber and sunscreen ingredient Bemotrizinol was developed. By substituting waste-intense and potentially hazardous reaction steps and implementing greener methodologies, the sustainability and rentability of the overall process were improved (**Figure 68**).
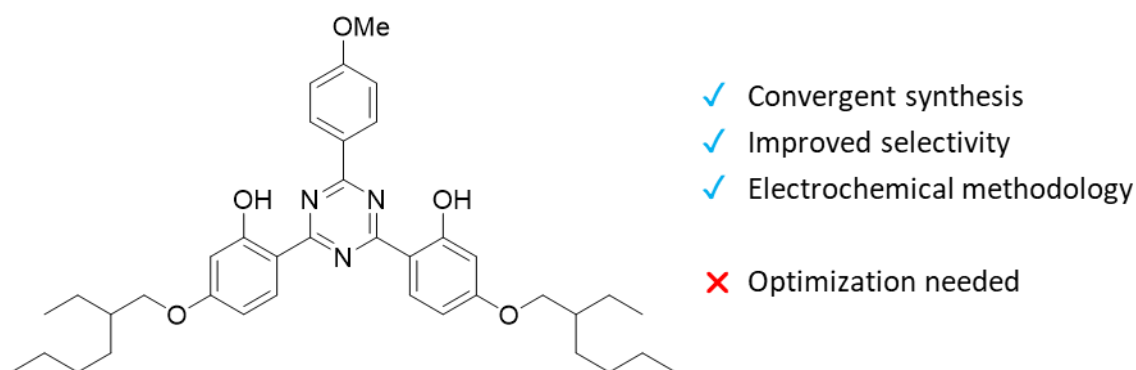
Figure 68. Overview of the improved synthesis method towards Bemotrizinol.

In the first step, a Friedel-Crafts protocol was investigated for the monoacylation of cyanuric chloride using a variety of different LEWIS acid catalysts. Furthermore, a new approach for the synthesis of α-triazinyl carbonyl compounds *via* nucleophilic aromatic substitution utilizing lithium enolates as carbon nucleophiles was developed (**Scheme 44**). Through NMR studies, the solvent-dependent equilibrium of the ketone enol tautomerism was investigated. In further studies, the substrate scope of this method will be expanded.
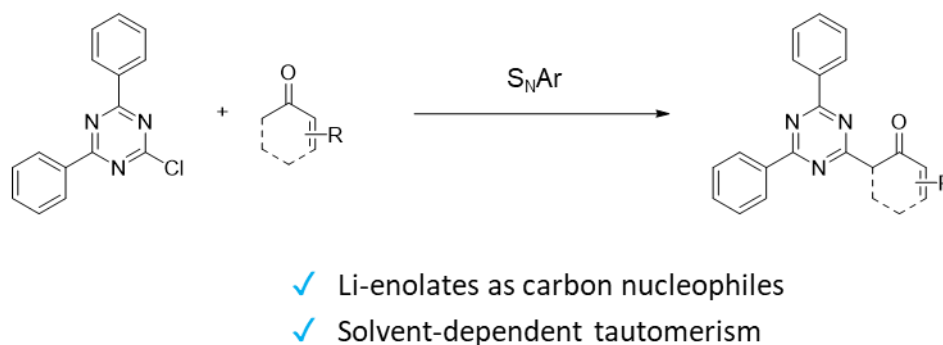
Scheme 44. Synthesis of α-triazinyl carbonyl compounds *via* nucleophilic aromatic substitution with Li-enolates.

The resulting Bemotrizinol surrogate, termed tetrahydro-Bemotrizinol, was characterized intensively, revealing strong UV-B absorption properties and potential autoxidative behavior. Therefore, tetrahydro-Bemotrizinol itself will also be assessed as a potential UV-absorber and sunscreen ingredient. The saturated THBMT intermediate was converted to the target BMT *via* an unprecedented electrochemical oxidative aromatization protocol.

5 Experimental Section

5.1 General Remarks

Parts of the general information are standardized descriptions and were adapted from previous group members.[120, 152, 189]

Materials and Methods

The starting materials, solvents and reagents were purchased from Abcr, Acros, Alfa Aesar, Apollo Scientific, Carbolution, ChemPUR, Fluka, Fluorochem, Merck, Riedel-de Haën, Sigma Aldrich, Strem, TCI, or Thermo Fisher Scientific and used without further purification unless stated otherwise.

Solvents of technical quality were purified by distillation or with the solvent purification system MB SPS5 (acetonitrile, dichloromethane, diethyl ether, tetrahydrofuran, toluene) from MBraun. Solvents of *p.a.* quality were purchased from Acros, Fisher Scientific, Sigma Aldrich, Roth or Riedel-de Haën and were used without further purification. *n*-Pentane was distilled over sodium and benzophenone. Other solvents were obtained from commercial suppliers: anhydrous benzene (Sigma Aldrich, <0.005% water), anhydrous *N,N*-dimethylformamide (Sigma Aldrich, <0.005% water), anhydrous 1,4-dioxane (Sigma Aldrich, <0.005% water), anhydrous dimethyl sulfoxide (Sigma Aldrich, <0.005% water), anhydrous ethanol (Sigma Aldrich, <0.005% water), anhydrous methanol (Sigma Aldrich, <0.005% water), anhydrous isopropanol (Sigma Aldrich, <0.005% water).

Oxygen-free solvents were obtained by freeze-pump-thaw (three cycles) technique.

Air- and moisture-sensitive reactions were carried out under argon atmosphere in oven-dried glassware using standard Schlenk techniques.

For reaction set-ups under high pressure, a Berghof BR100 pressure reactor was used.

For certain reactions, flat-bottom crimp neck vials from ChromaGlobe with aluminum crimp caps were used.

Liquids were added with a stainless-steel cannula and solids were added in powdered shape.

Reactions at low temperature were cooled using flat dewars produced by Isotherm (Karlsruhe) with water/ice or isopropanol/dry ice mixtures.

Solvents were evaporated under reduced pressure at 45 °C using a rotary evaporator. For solvent mixtures, each solvent was measured volumetrically.

Flash column chromatography was performed using Merck silica 60 (0.040 × 0.063 mm, 230–400 mesh ASTM) and quartz sand (glowed and purified with hydrochloric acid).

The Rayonet reactor Model RPR-100 with (16) 14W light bulbs (254 nm) was used for the irradiation with UV light.

Visible-light catalysis was run in a photoreactor made from LED strips (RGB LEDs, 30 W) with an adhesive back, attached to a crystallization dish (190 × 90 mm). Cooling was provided by a fan powered by a battery pack placed

on the bottom of the crystallization dish. Reactions were run with green LEDs at 524 nm (peak wavelength) and blue LEDs at 471 nm (peak wavelength).

For the irradiation with LED UV light (385 nm, 8 × 8 W), an LZC-ICH2 photoreactor from Luzchem was used.

Reaction Monitoring

All reactions were monitored by thin-layer chromatography (TLC) using silica coated aluminum plates (Merck, silica 60, F254). UV active compounds were detected with a UV-lamp at 254 nm and 366 nm excitation. When required, vanillin, basic potassium permanganate, ninhydrin or Seebach solution was used as TLC-stain.

GC-MS (gas chromatography–mass spectrometry) measurements were performed on an Agilent Technologies model 6890N (electron impact ionization), equipped with an Agilent 19091S-433 column (5% phenyl methyl siloxane, 30 m, 0.25 µm) and a 5975B VL MSD detector with a turbo pump. Helium was used as a carrier gas.

Melting Point

Melting points were detected on an OptiMelt MPA100 device from Stanford Research System.

Optical Rotation

Optical rotation was measured with a Perkin Elmer 241 Polarimeter using a 100 mm glass cell and a suitable solvent, at the sodium-D-lines (589.0 and 589.6 nm) and a constant temperature of 20 °C.

Nuclear Magnetic Resonance Spectroscopy (NMR)

NMR spectra were recorded on a Bruker Avance 400 NMR instrument at 400 MHz for ^{1}H NMR, 101 MHz for ^{13}C NMR, 376 MHz for ^{19}F NMR and 162MHz for ^{31}P NMR, or a Bruker Avance 500 NMR instrument at 500 MHz for ^{1}H NMR, 126 MHz for ^{13}C NMR and 470 MHz for ^{19}F NMR and 202 MHz for ^{31}P NMR.

The NMR spectra were recorded at room temperature in deuterated solvents acquired from Eurisotop, Sigma Aldrich or Deutero. The chemical shift δ is displayed in parts per million [ppm] and the references used were the ^{1}H and ^{13}C peaks of the solvents themselves:

d_1-chloroform (CDCl$_3$): 7.26 ppm for ^{1}H and 77.16 ppm for ^{13}C

d_6-dimethyl sulfoxide (DMSO-d_6): 2.50 ppm for ^{1}H and 39.52 ppm for ^{13}C

d_6-benzene (C$_6$D$_6$): 7.16 ppm for ^{1}H and 128.06 ppm for ^{13}C.

d_8-toluene: 2.08 ppm for ^{1}H and 137.48 ppm for ^{13}C

d_4-methanol (CD$_3$OD): 3.31 ppm for ^{1}H and 49.00 ppm for ^{13}C

d_8-tetrahydrofuran (THF-d_8): 1.73 ppm for ^{1}H and 67.57 ppm for ^{13}C

d_3-acetonitrile (CD$_3$CN): 1.94 ppm for ^{1}H and 118.26 ppm for ^{13}C

d_6-acetone: 2.05 ppm for ^{1}H and 206.26 ppm for ^{13}C

For the characterization of centrosymmetric signals, the signal's median point was chosen, for multiplets the signal range. The following abbreviations were used to describe the proton splitting pattern: d = doublet,

t = triplet, m = multiplet, dd = doublet of doublet, ddd = doublet of doublet of doublet, dddd = doublet of doublet of doublet of doublet, dt = doublet of triplet. Absolute values of the coupling constants "J" are given in Hertz [Hz] in absolute value and decreasing order. Signals of the ^{13}C spectrum were assigned by phase edited heteronuclear single quantum coherence (HSQC) and were specified in the following way: C_q = quaternary carbon atoms (no signal).

Infrared Spectroscopy (IR)

The infrared spectra were recorded with a BRUKER, Alpha P instrument. All samples were measured by attenuated total reflection (ATR). The positions of the absorption bands are given in wavenumbers $\tilde{v}$ in cm^{-1} and were measured in the range from 3600 cm^{-1} to 500 cm^{-1}.

Characterization of the absorption bands was done in dependence of the absorption strength with the following abbreviations: vs (very strong, 0–9%), s (strong, 10–39%), m (medium, 40–69%), w (weak, 70–89%), vw (very weak, 90–100%).

Mass Spectrometry (MS)

Electron ionization (EI) and fast atom bombardment (FAB) experiments were conducted using a FINNIGAN, MAT 90 (70 eV) instrument, with 3-nitrobenzyl alcohol (3-NBA) as matrix and reference for high resolution. For the interpretation of the spectra, molecular peaks [M]$^+$, peaks of protonated molecules [M+H]$^+$ and characteristic fragment peaks are indicated with their mass-to-charge ratio (m/z) and their intensity in percent, relative to the base peak (100%) is given. In case of high-resolution measurements, the maximum tolerated error is ±5 ppm.

ESI experiments were recorded on a Q-Exactive (Orbitrap) mass spectrometer (THERMO FISHER SCIENTIFIC, San Jose, CA, USA) equipped with a HESI II probe to record high resolution. The tolerated error is ±5 ppm of the molecular mass. The spectra were interpreted by molecular peaks [M]$^+$, peaks of protonated molecules [M+H]$^+$ and characteristic fragment peaks and indicated with their mass-to-charge ratio (m/z).

Elemental Analysis (EA)

Elemental analysis was done on an ELEMENTAR vario MICRO instrument. The weight scale used was a SARTORIUS M2P. Calculated and found percentage by mass values for carbon, hydrogen, nitrogen, and sulfur are indicated in fractions of 100%.

High Performance Liquid Chromatography (HPLC)

Analysis of the enantiomeric excess was conducted using an AGILENT HPLC 1100 series system with a G1322A degasser, a G1211A pump, a G1313A autosampler, a G1316A column oven and a G1315B diode array system using a DAICEL Chiralpak® AD-H (4.6 × 250 mm, 5 µm particle size), DAICEL Chiralpak® OD-H (4.6 × 250 mm, 5 µm particle size), DAICEL Chiralpak® OJ-H (4.6 × 250 mm, 5 µm particle size), or YMC CHIRAL ART Amylose-SA column (4.6 × 250 mm, 5 µm particle size) columns were used with HPLC-grade n-hexane/isopropanol as mobile phase, respectively.

X-Ray Analysis

X-Ray analysis of single crystals were performed by Dr. Martin Nieger (University of Helsinki, Finland) on a Kappa-CCD-diffractometer by Bruker-Nonius at 123(2) K using MoKα-radiation (λ = 0.71073 Å) or on a SuperNova dual X-ray diffractometer by Agilent at 120(2) K using CuKα-radiation (λ = 1.54178 Å).

Cyclic Voltammetry

Cyclic voltammograms (CVs) Cyclic voltammetry measurements were carried out on a Gamry 600+ and a Gamry 3000 potentiostat (Gamry Instruments) using a Teflon cell and an MSR electrode rotator (Pine Research) equipped with a disc electrode (Pt, Au or glassy carbon, 0.5 mm diameter) and a platinum wire counter electrode. The potentials were normalized to a Ag/AgCl (KCl$_{sat}$ in water) reference electrode (Meisenberger GmbH). A 1.0 M Bu$_4$NBF$_4$ in CH$_2$Cl$_2$ electrolyte was used for all electrochemical experiments. Before each measurement, the solution was purged with argon (99.999%, Air Liquide). Cyclic voltammetry experiments were carried out at ambient temperature. The potential window ranged from 0.05 to 1.6 V vs Ag/AgCl. Measurements were performed sequentially at scan rates of 200, 100, 50, 25, and 200 mV s^{-1}, with three cyclic voltammograms per scan rate. were recorded under argon atmosphere using a Gamry Instrument Interface 1010B potentiostat.

The CV measurements in **Chapter 3.2** were performed on an Electrochemical Analyzer potentiostat model 620D from CH Instruments. The samples were prepared in CH$_2$Cl$_2$ solutions. All measurements were performed using 0.1 M Bu$_4$NPF$_6$ in CH$_2$Cl$_2$. An Ag/Ag$^+$ electrode was used as the reference electrode, a platinum electrode (active diameter of 2 mm) was used as the working electrode and a platinum wire electrode was used as the counter electrode.

Electrochemistry

All the electrochemical oxidations were performed in an IKA ElectraSyn 2.0 equipped with electrodes (each 0.8 × 3.0 cm^2). Electrodes were purchased from IKA and used as received. Reference electrodes were filled with fresh 3 M aqueous KCl solution.

Absorption Spectroscopy

UV/Vis spectra were recorded either on an Analytik Jena Specord 50/plus or on a Perkin-Elmer Lambda 650 spectrometer.

Emission Spectroscopy

Emission spectra were recorded on a Horiba Scientific fluoromax-4 spectrofluorometer or Agilent Cary Eclipse fluorescent spectrometer both equipped with a Czerny-Turner-type monochromator and an R928P PMT detector.

Advanced Photophysical Characterization

Optically dilute solutions of concentrations on the order of 10^{-5}-10^{-6}M were prepared in HPLC grade solvent for absorption and emission analysis. Absorption spectra were recorded at room temperature on a Shimadzu UV-1800 double beam spectrophotometer. Aerated solutions were bubbled with compressed air for 5 min, whereas degassed solutions were prepared *via* three freeze-pump-thaw cycles prior to emission analysis using an in-house

adapted fluorescence cuvette, itself purchased from Starna. Steady-state emission and time-resolved emission spectra were recorded at 298 K using an Edinburgh Instruments FLS980 fluorimeter. Samples were excited at 360 nm for steady-state measurements and at 378 nm for time-resolved measurements. Time-resolved spectra were obtained from dilute solutions of samples in toluene using a gated intensified charge coupled device (iCCD camera) from Stanford Computer Optics under laser excitation at 343 nm (100 Hz) at 77 K. For ΔE_{ST} measurements prompt emission spectra were collected using 1 ns time delay and 100 ns integration time window, while phosphorescence spectra were collected using 1 ms time delay and 9 ms integration time window.

DFT Calculations

DFT calculations were performed with the Gaussian 09 revision D.018 suite. Initially the geometries of both emitters in the ground state in the gas phase were optimized employing the PBE0 functional with the standard Pople 6-31G(d,p) basis set. Time-dependent DFT calculations were performed using the Tamm–Dancoff approximation (TDA). The molecular orbitals were visualized using GaussView 5.0 software.

5.2 Biological Methods and Assays

pUC-DNA Relaxation Assay

DNA intercalation was assessed using the pUC-DNA relaxation assay. Briefly, 500 ng pUC19 DNA was dissolved in enzyme buffer (40 mM sodium phosphate, 100 mM NaCl, pH 7.4) and incubated with the respective compounds for 1 h at 37 °C in the dark. Supercoiled (sc) and open circular (oc) forms of pUC19 DNA were separated by electrophoresis in a 1% agarose gel containing GelRed (1/10 000) for 2.5 h at 90 V. The density of the bands was quantified using a Herolab gel detection system (EASY win 32).

MTT-Assay

Cytotoxicity was assessed in an MTT-Assay (Promega) in 96-well plates using human cervix carcinoma epithelial cell (HeLa cells). The intracellular reaction of 3-(4,5-dimethylthiazol-2-yl)-2,5-diphenoltetrazoliumbromide (MTT) was monitored with a SpectraMax ID3 at 595 nm. As the reaction only occurs in living cells, the absorption intensity is proportional to cell viability.

A 5 mM solution of the compounds in DMSO was diluted with culture medium (DMEM + 10% FBS buffer + 1% P/s) to concentrations from 5 μM to 100 μM to not exceed a DMSO concentration of 0.05%.

1.0×10^4 HeLa-cells per well were cultivated in 100 μl DMEM and incubated for 24 h at 37 °C and 5% CO_2. The cells were treated with the test solutions by removal of the incubation medium and addition of the compound solutions in DMEM. The cells were incubated at 37 °C and 5% CO_2 for 72 h. The dead control was treated with 5 μl Triton-X100 (20% in ddH_2O). 15 μl of MTT per well were added. The cells were incubated another 3 h. Afterwards, 100 μl of stop solution were added and the cells were again incubated for 24 h. The absorption was measured at 595 nm in a SpectraMax ID3.

Intracellular Co-Localization Studies and Microscopy

The intracellular localization in HeLa cells was evaluated with a confocal fluorescence microscope (Stellaris 5). For the staining of the mitochondria, Mitotracker™ Red CMXRos was used

1.5×10^4 HeLa-cells per well were cultivated in 200 µl DMEM on an 8 well IBIDI µ-slide for 24 h at 37 °C and 5% CO_2. The cells were treated with 5 µM solutions of the compounds by removal of the incubation medium and addition of the compound solutions in DMEM. The cells were incubated at 37 °C and 5% CO_2 for 24 h. The medium was removed and 200 µl fresh DMEM solution with 125 nm of Mitotracker™ Red CMXRos (1 µL of a 25 µM stock solution). The cells were incubated another 30 min. Afterwards, the cells were washed three times with DBPS buffer. Images were recorded with a Stellaris 5.

5.3 nano3D Printing

nano3D Printer

The laser apparatus was constructed by Dr. Laura Weber (IMT/Karlsruhe) and is based on the cLift-system by Dr. Tobias Foertsch and Dr. Felix Löffler. It contains a 405 nm laser (300 mW, IBEAM-SMART-405-S-HP, Toptica Photonics), which is deflected to the laser stage *via* a scan head (intelliSCAN III 10, Scanlabs) and focused *via* a FΘ-lense (S4LFT5110/322, Sill Optics). The donor slides can be automatically transferred onto the acceptor slide using a robot arm (SCARA Robot SR-6iA, Fanuc).

Laminator

The donor slides were covered with the Kapton-foil using a LM 330 Laminator by Vogt Papiertechnik (Böblingen-Altdorf/Germany).

Blade Coating

The automatic blade coating device AB3655 was purchased from TQC Sheen (Hilden/Germany).

Slide Readout *via* Fluorescence Scanner

Fluorescence read-out of the slides were performed using an InnoScan1100-AL by InnopSys (Carbonne/France). For the excitation, 488 nm, 532 nm, or 635 nm lasers were used. The slides were read out using the simultaneous scan mode. The scan resolution was 5.00 µm. The fluorescence images were edited and analyzed by Mapix software.

Polymer Matrix

The matrix (S-LEC-P LT 7552) was purchased from Sekisui Chemical Co. Ltd. (Osaka/Japan).

Glass Slides

The microscope slides were purchased from Paul Marienfeld GmbH & Co. KG (Lauda-Königshafen/Germany).

Polyimide Foil

The Kapton® foil (polyimide) type 70110 (25,0 µm carrier material; 60,0 µm overall thickness) was purchased from CMC Klebetechnik GmbH (Frankenthal/Germany).

General Procedure for nano3D Printing

Preparation of donor slides: Standard microscope glass slides were sonicated for 5 min in a soap solution, deionized water, isopropanol, and acetone. Subsequently, the slides were dried in an argon stream. The cleaned slides were then laminated with an adhesive Kapton foil. Blade-Coating: The Kapton-slides were mounted on the blade coating device, 70 µL of the coating solution were pipetted under the doctor's blade (Hight: 1500 µm) and the surface was coated with a blade speed of 10 mm/s.

Preparation of the coating solution: 15 mg of the transfer substance and 135 mg S-LEC polymer matrix were dissolved in 1 ml of dichloromethane.

Preparation of acceptor slides: Standard microscope glass slides were sonicated for 5 min in a soap solution, deionized water, isopropanol, and acetone. Subsequently, the slides were dried in an argon stream. The cleaned slides were stored in a dust-free container. For coated, the slides were mounted on the blade coating device, 70 µL of a 10 – 100 mg/mL solution of S-LEC polymer matrix in dichloromethane were pipetted under the doctor's blade (Height: 1500 µm) and the surface was coated with a blade speed of 10 mm/s.

Laser Transfer *via* nano3D-printing: First, the acceptor slide was mounted on the laser stage and fixated. The donor slide was put on top of the acceptor slide with the coated side facing downwards. The desired laser pattern was entered through a custom software in form of an Excel table. After the transfer, the used donor was removed, and the process was repeated for different donors until all materials were transferred in the desired combination. Lastly, the acceptor slide was removed and stored in a dust-free container until further processing.

Reaction coupling: After the material transfer, the acceptor slides were put into a container and incubated in an oven at 90 °C for 1 d.

5.4 Syntheses and Spectroscopic Characterization

Parts of the were published in the Bachelor theses and Vertieferarbeiten of M. ROTTER, N. SCHWARZ, C. R. ADAM. A. VRANIĆ AND M. MERGEL. The experiments were performed according to procedures developed by the author and carried out under the supervision of the author. The fluorophore-steroid conjugates in Chapter 5.4.3 were synthesized in cooperation with N. Rosenbaum who also published their synthesis and spectroscopic characterization in his dissertation.

5.4.1 PCP-based Imidazo[1,2-*a*]heterocycles as Fluorophores and Ligands

2-(1,4(1,4)-Dibenzenacyclohexaphane-1²-yl)-*N*-benzylimidazo[1,2-*a*]pyridin-3-amine (92a)
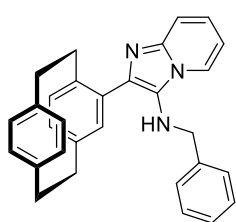
2-Aminopyridine (100 mg, 1.06 mmol, 1.00 equiv) and 4-formyl[2.2]paracyclophane (251 mg, 1.06 mmol, 1.00 equiv) were dissolved in a mixture of 6 mL of dichloromethane and 4 mL of methanol. Subsequently, a 1 M solution of perchloric acid in methanol (10.7 mg, 106 µL, 106 µmol, 0.10 equiv) and benzyl isonitrile (124 µL, 124 mg, 1.06 mmol, 1.00 equiv) were added. The mixture was stirred at r.t. for 72 h. The solvent was removed under reduced pressure and the residue was purified *via* flash chromatography (SiO$_2$, CH/EtOAc/NEt$_3$ 4:1:0.01 to 1:1:0.01). **92a** was isolated as a yellow solid (311 mg, 724 µmol, 68%).

R_f (SiO$_2$, CH/EtOAc 1:1) = 0.45.

¹H NMR (400 MHz, CDCl$_3$) δ [ppm] = 8.08 (dt, J = 6.8, 1.3 Hz, 1H, CH_{Ar}), 7.72 (d, J = 9.0 Hz, 1H, CH_{Ar}), 7.25 − 7.14 (m, 6H, CH_{Ar}), 6.99 (d, J = 1.9 Hz, 1H, CH_{Ar}), 6.81 (td, J = 6.8, 1.1 Hz, 1H, CH_{Ar}), 6.72 (dd, J = 7.9, 1.7 Hz, 1H, CH_{Ar}), 6.68 (dd, J = 7.8, 1.8 Hz, 1H, CH_{Ar}), 6.63 (dd, J = 7.7, 1.7 Hz, 1H, CH_{Ar}), 6.60 − 6.54 (m, 2H, CH_{Ar}), 6.51 (dd, J = 7.8, 1.9 Hz, 1H, CH_{Ar}), 3.97 − 3.86 (m, 2H, CH_2-Ph), 3.58 (t, J = 6.5 Hz, 1H, NH), 3.38 − 3.28 (m, 1H, CH_2-PCP), 3.26 − 2.98 (m, 5H, CH_2-PCP), 2.94 − 2.81 (m, 2H, CH_2-PCP).

¹³C NMR (101 MHz, CDCl$_3$) δ [ppm] = 141.5 (C$_q$), 140.1 (C$_q$), 139.6 (C$_q$), 139.5 (C$_q$), 139.0 (C$_q$), 137.4 (C$_q$), 136.9 (C$_q$), 135.4 (CH$_{Ar}$), 133.5 (CH$_{Ar}$), 133.2 (CH$_{Ar}$), 133.0 (CH$_{Ar}$), 132.7 (CH$_{Ar}$), 132.3 (CH$_{Ar}$), 132.1 (CH$_{Ar}$), 128.6 (CH$_{Ar}$), 128.1 (CH$_{Ar}$), 127.9 (C$_q$), 127.6 (CH$_{Ar}$), 126.5 (C$_q$), 123.3 (CH$_{Ar}$), 122.6 (CH$_{Ar}$), 117.8 (CH$_{Ar}$), 111.7 (CH$_{Ar}$), 52.2 (CH$_2$, CH$_2$-Ph), 35.5 (CH$_2$, CH$_2$-PCP), 35.5 (CH$_2$, CH$_2$-PCP), 35.4 (CH$_2$, CH$_2$-PCP), 34.3 (CH$_2$, CH$_2$-PCP).

IR (ATR) $\tilde{v}$ [cm^{-1}] = 3026 (vw), 3005 (vw), 2922 (w), 2850 (vw), 1628 (vw), 1539 (vw), 1501 (w), 1435 (w), 1346 (w), 1234 (w), 1198 (w), 1095 (vw), 1027 (vw), 900 (w), 866 (vw), 808 (vw), 794 (vw), 773 (vw), 755 (m), 739 (w), 725 (w), 701 (w), 607 (w), 513 (w), 483 (w), 442 (w).

FAB-MS *m/z* (%): 430 [M + H]$^+$ (100), 429 [M]$^+$ (53), 338 [M − C$_7$H$_7$]$^+$ (36), 91 [C$_7$H$_7$]$^+$ (91).

HRMS-FAB (*m/z*): [M + H]$^+$ calcd. for C$_{30}$H$_{28}$N$_3$, 430.2283; found, 430.2285.

2-(1,4(1,4)-Dibenzenacyclohexaphane-1²-yl)-*N*-(*tert*-butyl)imidazo[1,2-*a*]pyridine-3-amine (92b)
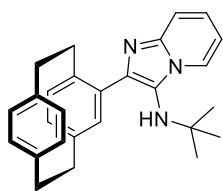
2-Aminopyridine (150 mg, 1.59 mmol, 1.00 equiv) and 4-formyl[2.2]paracyclophane (377 mg, 1.59 mmol, 1.00 equiv) were dissolved in a mixture of 6 mL of dichloromethane and 4 mL of methanol. Subsequently, a 1 M solution of perchloric acid in methanol (10.7 mg, 106 μL, 106 μmol, 0.10 equiv) Subsequently, glacial acetic acid (0.18 mL, 191 mg, 3.19 mmol, 2.00 equiv) and *tert.*-butyl isonitrile (0.18 mL, 133 mg, 1.59 mmol, 1.00 equiv) was added. The mixture was stirred at r.t. for 72 h. The solvent was removed under reduced pressure and the residue was purified *via* flash chromatography (SiO$_2$, CH/EtOAc/NEt$_3$ 8:1:0.01 to 2:1:0.01). **92b** was isolated as a beige solid (241 mg, 604 μmol, 38%).

R$_f$ (SiO$_2$, CH/EtOAc 1:1) = 0.57.

¹H NMR (400 MHz, CDCl$_3$) δ [ppm] = 8.27 (d, *J* = 6.9 Hz, 1H, C*H*$_{Ar}$), 7.68 (d, *J* = 9.1 Hz, 1H, C*H*$_{Ar}$), 7.15 (ddd, *J* = 9.1, 6.6, 1.3 Hz, 1H, C*H*$_{Ar}$), 7.04 (d, *J* = 1.8 Hz, 1H, C*H*$_{Ar}$), 6.80 – 6.75 (m, 2H, C*H*$_{Ar}$), 6.73 (dd, *J* = 7.8, 1.8 Hz, 1H, C*H*$_{Ar}$), 6.62 (dd, *J* = 7.8, 1.8 Hz, 1H, C*H*$_{Ar}$), 6.57 (dd, *J* = 7.8, 1.9 Hz, 1H, C*H*$_{Ar}$), 6.50 (d, *J* = 7.8 Hz, 1H, C*H*$_{Ar}$), 6.47 (dd, *J* = 7.8, 1.9 Hz, 1H, C*H*$_{Ar}$), 3.27-2.84 (m, 8H, C*H*$_2$-PCP), 0.77 (s, 9H, C*H*$_3$).

¹³C NMR (101 MHz, CDCl$_3$) δ [ppm] = 142.5 (C$_q$), 140.1 (C$_q$), 139.6 (C$_q$), 139.3 (C$_q$), 136.9 (C$_q$), 135.0 (*C*H$_{Ar}$), 134.7 (C$_q$), 134.0 (*C*H$_{Ar}$), 133.3 (C$_q$), 133.2 (*C*H$_{Ar}$), 132.8 (*C*H$_{Ar}$), 132.5 (*C*H$_{Ar}$), 131.8 (*C*H$_{Ar}$), 124.4 (*C*H$_{Ar}$), 123.8 (*C*H$_{Ar}$), 123.3 (*C*H$_{Ar}$), 121.0 (C$_q$) 117.6 (*C*H$_{Ar}$), 111.0 (*C*H$_{Ar}$), 56.4 (*C*$_q$), 35.6 (CH$_2$, *C*H$_2$-PCP), 35.6 (CH$_2$, *C*H$_2$-PCP), 35.4 (CH$_2$, *C*H$_2$-PCP), 33.9 (CH$_2$, *C*H$_2$-PCP), 29.9 (3C, CH$_3$).

IR (ATR) ν̃ [cm^{-1}] = 3353 (vw), 2850 (vw), 2952 (w), 2925 (w), 1628 (vw), 1594 (vw), 1541 (vw), 1500 (w), 1412 (vw), 1362 (w), 1341 (w), 1271 (vw), 1200 (w), 1093 (vw), 937 (vw), 900 (w), 863 (vw), 806 (w), 757 (w), 736 (w), 711 (w), 666 (w), 632 (vw), 606 (vw), 585 (vw), 511 (w), 449 (vw), 428 (vw).

FAB-MS *m/z* (%): 396 [M + H]$^+$ (100), 395 [M]$^+$ (73), 338 [M – C$_4$H$_9$]$^+$ (26), 291 [M – C$_8$H$_8$]$^+$ (7).

HRMS-FAB (*m/z*): [M + H]$^+$ calcd. for C$_{27}$H$_{30}$N$_3$, 396.2440; found, 396.2440.

2-(1,4(1,4)-Dibenzenacyclohexaphane-1²-yl)-*N*-(adamantyl)imidazo[1,2-*a*]pyridine-3-amine (92c)
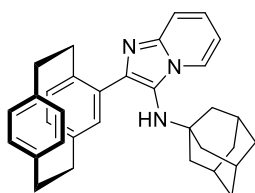
2-Aminopyridine (100 mg, 1.06 mmol, 1.00 equiv) and 4-formyl[2.2]paracyclophane (251 mg, 1.06 mmol, 1.00 equiv) were dissolved in a mixture of 6 mL of dichloromethane and 4 mL of methanol. Subsequently, a 1 M solution of perchloric acid in methanol (0.11 mL, 10.7 mg, 0.11 mmol, 0.10 equiv) and adamantane-1-isonitrile (171 mg, 1.06 mmol, 1.00 equiv) were added. The mixture was stirred at r.t. for 72 h. The solvent was removed under reduced pressure and the residue was purified *via* flash chromatography (SiO$_2$, CH/EtOAc/NEt$_3$ 8:1:0.01 to 2:1:0.01). **92c** was isolated as a beige solid (436 mg, 922 μmol, 87%).

R$_f$ (SiO$_2$, CH/EtOAc 1:1) = 0.50.

¹H NMR (500 MHz, CDCl₃) δ [ppm] = 8.32 (dd, J = 6.8, 1.5 Hz, 1H), 7.68 (d, J = 9.0 Hz, 1H), 7.15 (t, J = 7.9 Hz, 1H), 7.04 (d, J = 2.0 Hz, 1H), 6.78 (t, J = 6.8 Hz, 2H), 6.69 (dd, J = 7.8, 1.9 Hz, 1H), 6.62 (dd, J = 7.8, 1.9 Hz, 1H), 6.56 (dd, J = 7.7, 1.9 Hz, 1H), 6.50–6.44 (m, 2H), 3.24 (ddd, J = 12.9, 9.3, 4.1 Hz, 1H, N*H*), 3.16–3.09 (m, 2H), 3.09–3.00 (m, 2H), 2.99–2.92 (m, 2H), 2.84 (t, J = 7.2 Hz, 2H), 1.79 (p, J = 3.0 Hz, 3H), 1.43 (s, 6H), 1.37–1.29 (m, 6H).

¹³C NMR (126 MHz, CDCl₃) δ [ppm] = 142.3 (C_q), 139.9 (C_q), 139.6 (C_q), 139.3 (C_q), 136.8 (C_q), 135.0 (CH_Ar), 134.5 (C_q), 134.0 (CH_Ar), 133.4 (CH_Ar), 133.3 (CH_Ar), 132.7 (CH_Ar), 132.6 (CH_Ar), 131.8 (CH_Ar), 124.0 (CH_Ar), 123.4 (CH_Ar), 123.2 (C_q), 123.2 (C_q), 117.5 (CH_Ar), 111.0 (CH_Ar), 56.6 (C_q), 43.4 (CH₂), 36.2 (2C, CH₂), 35.6 (CH₂, *C*H₂-PCP), 35.6 (CH₂, *C*H₂-PCP), 35.5 (CH₂, *C*H₂-PCP), 34.0 (CH₂, *C*H₂-PCP), *29.7 (3C, CH), 27.1 (3C, CH₂)*.

IR (ATR) $\tilde{v}$ [cm⁻¹] =2904 (vs), 2849 (s), 1663 (s), 1622 (m), 1591 (m), 1547 (m), 1502 (m), 1480 (m), 1452 (m), 1429 (m), 1358 (m), 1305 (m), 1261 (vs), 1204 (s), 1089 (vs), 1018 (vs), 938 (w), 902 (m), 863 (m), 799 (vs), 755 (vs), 735 (vs), 718 (vs), 674 (s), 629 (s), 569 (s), 511 (vs), 496 (s), 442 (s), 384 (s).

FAB-MS *m/z* (%): 475 (32), 474 [M + H]⁺ (100), 473 [M]⁺ (19), 207 (22), 154 (23), 149 (26), 147 (49), 136 (36), 135 (32), 133 (94), 91 (32), 90 (22), 89 (30).

HRMS-FAB (*m/z*): [M + H]⁺ calcd. for C₃₃H₃₆N₃, 474.2904; found, 474.2904.

2-(1,4(1,4)-Dibenzenacyclohexaphane-1²-yl)-*N*-cyclohexylimidazo[1,2-*a*]pyridin-3-amine (92d)
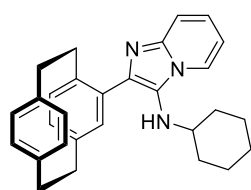
2-Aminopyridine (100 mg, 1.06 mmol, 1.00 equiv) and 4-formyl[2.2]paracyclophane (251 mg, 1.06 mmol, 1.00 equiv) were dissolved in a mixture of 6 mL of dichloromethane and 4 mL of methanol. Subsequently, a 1 M solution of perchloric acid in methanol (10.7 mg, 106 µL, 106 µmol, 0.10 equiv) and cyclohexyl isonitrile (132 µL, 116 mg, 1.06 mmol, 1.00 equiv) were added. The mixture was stirred at r.t. for 72 h. The solvent was removed under reduced pressure and the residue was purified *via* flash chromatography (SiO₂, CH/EtOAc/NEt₃ 4:1:0.01 to 2:1:0.01). **92d** was isolated as a yellow solid (321 mg, 761 µmol, 72%).

R$_f$ (SiO₂, CH/EtOAc 2:1) = 0.28.

¹H NMR (400 MHz, CDCl₃) δ [ppm] = 8.07 (d, J = 6.8 Hz, 1H, C*H*_Ar), 7.70 (d, J = 9.1 Hz, 1H, C*H*_Ar), 7.14 (ddd, J = 9.0, 6.7, 1.3 Hz, 1H, C*H*_Ar), 7.06 (d, J = 1.9 Hz, 1H, C*H*_Ar), 6.83 – 6.76 (m, 2H, C*H*_Ar), 6.69 (dd, J = 7.8, 1.9 Hz, 1H, C*H*_Ar), 6.63 (dd, J = 7.8, 1.9 Hz, 1H, C*H*_Ar), 6.57 (dd, J = 7.8, 1.9 Hz, 1H, C*H*_Ar), 6.53 (d, J = 7.9 Hz, 1H, C*H*_Ar), 6.48 (dd, J = 7.8, 1.9 Hz, 1H, C*H*_Ar), 3.30 – 2.96 (m, 6H, C*H*₂-PCP), 2.92 – 2.79 (m, 2H, C*H*₂-PCP), 2.65 – 2.53 (m, 1H, C*H*), 1.80 – 1.70 (m, 1H, C*H*₂), 1.66 – 1.52 (m, 1H, C*H*₂), 1.45 – 1.28 (m, 3H, C*H*₂), 1.16 – 0.82 (m, 4H, C*H*₂), 0.71 – 0.58 (m, 1H, C*H*₂).

¹³C NMR (101 MHz, CDCl₃) δ [ppm] = 141.7 (C_q), 140.0 (C_q), 139.6 (C_q), 139.3 (C_q), 136.7 (C_q), 135.7 (C_q), 135.2 (CH_Ar), 133.9 (C_q), 133.8 (CH_Ar), 133.1 (CH_Ar), 133.1 (CH_Ar), 132.6 (CH_Ar), 132.5 (CH_Ar), 131.9 (CH_Ar), 125.9 (C_q), 122.9 (CH_Ar), 122.8 (CH_Ar), 117.7 (CH_Ar), 111.4 (CH_Ar), 56.2 (CH), 35.6 (CH₂, *C*H₂-PCP), 35.5 (CH₂, *C*H₂-PCP), 35.4 (CH₂, *C*H₂-PCP), 34.3 (CH₂, *C*H₂-PCP), 34.1 (CH₂), 33.6(CH₂), 25.7 (CH₂), 25.0 (CH₂), 24.6 (CH₂).

IR (ATR) ῦ [cm⁻¹] = 3287 (vw), 3017 (vw), 2923 (w), 2846 (w), 1740 (vw), 1633 (vw), 1589 (vw), 1559 (w), 1536 (w), 1448 (w), 1362 (w), 1284 (w), 1232 (w), 1184 (w), 1145 (w), 933 (w), 899 (w), 862 (vw), 811 (w), 774 (vw), 748 (m), 729 (w), 712 (w), 674 (w), 644 (w), 593 (w), 512 (w), 442 (w).

FAB-MS *m/z* (%): 422 [M + H] (100), 421 [M]⁺ (75), 318 (11).

HRMS-FAB (*m/z*): [M + H]⁺ calcd. for $C_{29}H_{32}N_3$, 422.2596; found, 422.2595.

2-(1,4(1,4)-Dibenzenacyclohexaphane-1²-yl)-*N*-pentylimidazo[1,2-*a*]pyridin-3-amine (92e)[190]
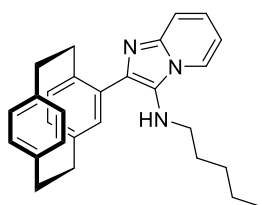
2-Aminopyridine (150 mg, 1.59 mmol, 1.00 equiv) and 4-formyl[2.2]paracyclophane (376 mg, 1.59 mmol, 1.00 equiv) were dissolved in a mixture of 6 mL of dichloromethane and 4 mL of methanol. Subsequently, glacial acetic acid (0.18 mL, 191 mg, 3.19 mmol, 2.00 equiv) and 1-pentyl isonitrile (0.20 mL, 155 mg, 1.59 mmol, 1.00 equiv) were added. The mixture was stirred at r.t. for 72 h. The solvent was removed under reduced pressure and the residue was purified *via* flash chromatography (SiO₂, CH/EtOAc/NEt₃ 4:1:0.01 to 1:1:0.01). **92e** was isolated as a yellow solid (400 mg, 970 μmol, 61%).

R_f (SiO₂, CH/EtOAc 1:1) = 0.48.

¹H NMR (400 MHz, CDCl₃) *δ* [ppm] = 8.05 (d, *J* = 6.8 Hz, 1H, C*H*_Ar), 7.77 (d, *J* = 9.1 Hz, 1H, C*H*_Ar), 7.17 (ddd, *J* = 9.1, 6.6, 1.4 Hz, 1H, C*H*_Ar), 7.03 (d, *J* = 1.8 Hz, 1H, C*H*_Ar), 6.84 (td, *J* = 6.8, 1.1 Hz, 1H, C*H*_Ar), 6.78 (dd, *J* = 7.8, 1.9 Hz, 1H, C*H*_Ar), 6.68 – 6.61 (m, 2H, C*H*_Ar), 6.58 (dd, *J* = 7.8, 1.9 Hz, 1H, C*H*_Ar), 6.55 (d, *J* = 7.8 Hz, 1H, C*H*_Ar), 6.49 (dd, *J* = 7.8, 1.9 Hz, 1H, C*H*_Ar), 3.29 – 3.18 (m, 2H, C*H*₂-PCP), 3.18 – 2.96 (m, 4H, C*H*₂-PCP), 2.93 – 2.82 (m, 2H, C*H*₂-PCP), 2.82 – 2.70 (m, 2H, C*H*₂) , 1.40 – 1.21 (m, 2H, C*H*₂), 1.21 – 1.05 (m, 4H, C*H*₂), 0.81 – 0.73 (m, 3H, C*H*₃).

¹³C NMR (101 MHz, CDCl₃) *δ* [ppm] = 141.4 (C_q), 140.2 (C_q), 139.6 (C_q), 139.4 (C_q), 137.1 (C_q), 135.4 (CH_Ar), 135.0 (C_q), 133.6 (CH_Ar), 133.3 (C_q) 133.2 (CH_Ar), 133.0 (CH_Ar), 132.6 (CH_Ar), 132.3 (CH_Ar), 132.1 (CH_Ar), 127.2 (C_q), 123.4 (CH_Ar), 122.6 (CH_Ar), 117.6 (CH_Ar), 111.8 (CH_Ar), 47.9 (CH₂), 35.6 (CH₂, *C*H₂-PCP), 35.5 (CH₂, *C*H₂-PCP), 35.4 (CH₂, *C*H₂-PCP), 34.2 (CH₂, *C*H₂-PCP), 30.1 (CH₂), 29.1 (CH₂), 22.5 (CH₂), 14.1 (CH₃).

IR (ATR) ῦ [cm⁻¹] = 3326 (vw), 2925 (w), 2853 (w), 1627 (vw), 1588 (vw), 1555 (w), 1500 (vw), 1441 (vw), 1411 (vw), 1345 (w), 1272 (vw), 1186 (w), 1116 (vw), 937 (vw), 905 (vw), 860 (vw), 805 (w), 744 (w), 729 (w), 715 (w), 648 (w), 613 (vw), 590 (vw), 513 (w), 442 (vw), 385 (vw).

FAB-MS *m/z* (%): 410 [M + H]⁺ (100), 409 [M]⁺ (69), 352 [M − C₄H₉]⁺ (13), 306 [M − C₈H₈ + H]⁺ (13).

HRMS-FAB (*m/z*): [M + H]⁺ calcd. for $C_{28}H_{32}N_3$, 410.2596; found, 410.2566.

2-(1,4(1,4)-Dibenzenacyclohexaphane-1²-yl)-*N*-(4-methoxyphenyl)imidazo[1,2-*a*]pyridin-3-amine (92f)[190]
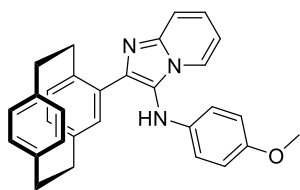
2-Aminopyridine (150 mg, 1.59 mmol, 1.00 equiv) and 4-formyl[2.2]paracyclophane (377 mg, 1.59 mmol, 1.00 equiv) were dissolved in a mixture of 6 mL dichloromethane of and 4 mL of methanol. Subsequently, glacial acetic acid (0.18 mL, 191 mg, 3.19 mmol, 2.00 equiv) and 4-methoxyphenylisonitrile (212 mg, 1.59 mmol, 1.00 equiv) were added. The mixture was stirred at r.t. for 72 h. The solvent was removed under reduced pressure and the residue was purified *via* flash chromatography (SiO$_2$, CH/EtOAc/NEt$_3$ 8:1:0.01 to 1:1:0.01). **92f** was isolated as a brown solid (295 mg, 668 µmol, 42%).

R$_f$ (SiO$_2$, CH/EtOAc 1:1) = 0.43.

^{1}H NMR (400 MHz, CDCl$_3$) δ [ppm] = 7.78 – 7.71 (m, 2H, C*H*$_{Ar}$), 7.23 (ddd, *J* = 9.0, 6.7, 1.4 Hz, 1H, C*H*$_{Ar}$), 6.95 (d, *J* = 1.9 Hz, 1H, C*H*$_{Ar}$), 6.81 – 6.75 (m, 3H, C*H*$_{Ar}$), 6.61 – 6.58 (m, 3H, C*H*$_{Ar}$), 6.57 – 6.53 (m, 1H, C*H*$_{Ar}$), 6.52 – 6.48 (m, 2H, C*H*$_{Ar}$), 6.47 (d, *J* = 2.3 Hz, 1H, C*H*$_{Ar}$), 6.44 (dd, *J* = 7.8, 1.9 Hz, 1H, C*H*$_{Ar}$), 5.52 (s, 1H, N*H*), 3.75 (s, 3H, OC*H*$_3$), 3.63 – 3.53 (m, 1H, C*H*$_2$-PCP), 3.21 – 2.77 (m, 7H, C*H*$_2$-PCP).

^{13}C NMR (101 MHz, CDCl$_3$) δ [ppm] = 153.6 (C$_q$), 142.5 (C$_q$), 139.9 (C$_q$), 139.6 (C$_q$), 139.5 (C$_q$), 139.1 (C$_q$), 138.6 (C$_q$), 137.9 (C$_q$), 135.7 (CH$_{Ar}$), 133.4 (C$_q$), 133.1 (CH$_{Ar}$), 133.0 (CH$_{Ar}$), 133.0 (CH$_{Ar}$), 132.76 (CH$_{Ar}$), 132.4 (CH$_{Ar}$), 131.8 (CH$_{Ar}$), 124.1 (CH$_{Ar}$), 123.4 (CH$_{Ar}$), 120.0 (C$_q$), 118.0 (CH$_{Ar}$), 115.3 (CH$_{Ar}$), 115.0 (CH$_{Ar}$), 111.9 (CH$_{Ar}$), 55.8 (CH$_3$, OC*H*$_3$), 35.6 (CH$_2$, *C*H$_2$-PCP), 35.4 (CH$_2$, *C*H$_2$-PCP), 35.4 (CH$_2$, *C*H$_2$-PCP), 34.7 (CH$_2$, *C*H$_2$-PCP).

IR (ATR) $\tilde{v}$ [cm^{-1}] = 2922 (w), 2890 (w), 2849 (w), 1629 (vw), 1594 (vw), 1565 (w), 1506 (vs), 1462 (w), 1451 (w), 1441 (w), 1411 (w), 1370 (w), 1346 (m), 1283 (w), 1231 (vs), 1177 (m), 1109 (w), 1033 (s), 1007 (w), 901 (w), 868 (w), 822 (s), 803 (m), 754 (s), 734 (vs), 714 (s), 677 (w), 656 (w), 637 (m), 609 (w), 592 (w), 571 (m), 545 (w), 513 (vs), 493 (m), 460 (w), 441 (m), 424 (m), 408 (w), 392 (w), 384 (w).

FAB-MS *m/z* (%): 446 [M + H]$^+$ (100), 445 [M]$^+$ (89), 342 [M – C$_8$H$_8$H]$^+$ (19), 311 (13), 207 (15).

HRMS-FAB (*m/z*): [M + H]$^+$ calcd. for C$_{30}$H$_{27}$N$_3$O, 446.2232; found, 446.2234.

2-(1,4(1,4)-Dibenzenacyclohexaphane-1²-yl)-*N*-benzylimidazo[1,2-*a*]pyrazin-3-amine (93a)[190]
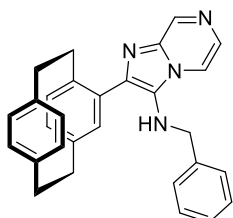
2-Aminopyrazine (150 mg, 1.58 mmol, 1.00 equiv) and 4-formyl[2.2]paracyclophane (373 mg, 1.58 mmol, 1.00 equiv) were dissolved in a mixture of 6 mL of dichloromethane and 4 mL of methanol. Subsequently, glacial acetic acid (0.18 mL, 189 mg, 3.15 mmol, 2.00 equiv) and benzyl isonitrile (0.19 mL, 185 mg, 1.58 mmol, 1.00 equiv) were added. The mixture was stirred at r.t. for 72 h. The solvent was removed under reduced pressure and the residue was purified *via* flash chromatography (SiO$_2$, CH/EtOAc/NEt$_3$ 4:1:0.01 to 1:1:0.01). **93a** was isolated as a yellow solid (325 mg, 758 µmol, 48%).

R$_f$ (SiO$_2$, CH/EtOAc 1:1) = 0.14.

^{1}H NMR (400 MHz, CDCl$_3$) δ [ppm] = 9.10 (d, J = 1.5 Hz, 1H, CH_{Ar}), 7.90 (dd, J = 4.7, 1.5 Hz, 1H, CH_{Ar}), 7.82 (d, J = 4.6 Hz, 1H, CH_{Ar}), 7.26 – 7.18 (m, 3H, CH_{Ar}), 7.13 (dd, J = 6.7, 2.9 Hz, 2H, CH_{Ar}), 6.88 (d, J = 1.7 Hz, 1H, CH_{Ar}), 6.71 – 6.60 (m, 3H, CH_{Ar}), 6.60 – 6.53 (m, 3H, CH_{Ar}), 4.05 – 3.91 (m, 2H, CH_2-Ph), 3.75 (t, J = 6.5 Hz, 1H, NH), 3.31 – 2.83 (m, 8H, CH_2-PCP).

^{13}C NMR (101 MHz, CDCl$_3$) δ [ppm] = 161.0 (C$_q$) 143.5 (CH$_{Ar}$), 140.4 (C$_q$), 139.6 (C$_q$), 139.4 (C$_q$), 138.6 (C$_q$), 138.4 (C$_q$), 137.8 (C$_q$), 136.9 (C$_q$), 135.5 (CH$_{Ar}$), 133.7 (CH$_{Ar}$), 133.4 (CH$_{Ar}$), 133.3 (CH$_{Ar}$), 132.8 (CH$_{Ar}$), 132.6 (CH$_{Ar}$), 132.2 (CH$_{Ar}$), 132.1 (CH$_{Ar}$), 128.9 (C$_q$), 128.8 (CH$_{Ar}$), 128.8 (CH$_{Ar}$), 128.2 (CH$_{Ar}$), 127.9 (CH$_{Ar}$), 127.8 (CH$_{Ar}$), 115.4 (CH$_{Ar}$), 51.6 (CH$_2$, CH$_2$-Ph), 35.5 (CH$_2$, CH$_2$-PCP), 35.5 (CH$_2$, CH$_2$-PCP), 35.4 (CH$_2$, CH$_2$-PCP), 34.2 (CH$_2$, CH$_2$-PCP).

IR (ATR) $\tilde{\upsilon}$ [cm^{-1}] = 3219 (w), 3021 (w), 2923 (w), 1666 (w), 1540 (w), 1494 (w), 1430 (w), 1383 (w), 1348 (w), 1288 (w), 1181 (w), 1059 (w), 1013 (w), 936 (w), 900 (w), 868 (w), 809 (w), 778 (w), 732 (m), 696 (m), 604 (w), 512 (w), 496, (w) 467 (w), 420 (w).

FAB-MS m/z (%): 431 [M + H]$^+$ (100), 430 [M]$^+$ (46), 339 (16), 327 (11), 235 (11), 91 (19).

HRMS-FAB (m/z): [M + H]$^+$ calcd. for C$_{29}$H$_{27}$N$_4$, 431.2236; found, 431.2238.

2-(1,4(1,4)-Dibenzenacyclohexaphane-1^2-yl)-*N*-(tert-butyl)imidazo[1,2-*a*]pyrazin-3-amine (93b)[190]
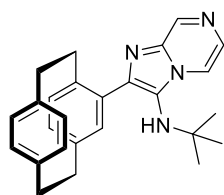
2-Aminopyrazine (150 mg, 1.58 mmol, 1.00 equiv) und 4-formyl[2.2]paracyclophane (373 mg, 1.58 mmol, 1.00 equiv) was dissolved in a mixture of 6 mL of dichloromethane and 4 mL of methanol. Subsequently, glacial acetic acid (0.18 mL, 189 mg, 3.15 mmol, 2.00 equiv) und *tert.*-butyl isonitrile (0.18 mL, 131 mg, 1.58 mmol, 1.00 equiv) was added. The mixture was stirred at r.t. for 72 h. The solvent was removed under reduced pressure and the residue was purified *via* flash chromatography (SiO$_2$, CH/EtOAc/NEt$_3$ 4:1:0.01 to 1:1:0.01). **93b** was isolated as a beige solid (73 mg, 190 µmol, 12%).

R$_f$ (SiO$_2$, CH/EtOAc 1:1) = 0.24.

^{1}H NMR (400 MHz, CDCl$_3$) δ [ppm] = 9.13 (d, J = 1.5 Hz, 1H, CH_{Ar}), 8.16 (dd, J = 4.6, 1.5 Hz, 1H, CH_{Ar}), 7.86 (d, J = 4.6 Hz, 1H, CH_{Ar}), 6.97 (d, J = 1.4 Hz, 1H, CH_{Ar}), 6.71 (s, 2H, CH_{Ar}), 6.64 – 6.55 (m, 2H, CH_{Ar}), 6.53 (s, 2H, CH_{Ar}), 3.27 – 2.83 (m, 8H, CH_2-PCP), 0.77 (s, 9H, CH_3).

^{13}C NMR (101 MHz, CDCl$_3$) δ [ppm] = 143.5 (CH$_{Ar}$), 142.9 (C$_q$), 140.4 (C$_q$), 139.6 (C$_q$), 139.2 (C$_q$), 137.9 (C$_q$), 137.1 (C$_q$), 135.1 (CH$_{Ar}$), 133.8 (CH$_{Ar}$), 133.8 (CH$_{Ar}$), 133.6 (CH$_{Ar}$), 133.5 (C$_q$), 132.7 (CH$_{Ar}$), 132.5 (CH$_{Ar}$), 132.0 (CH$_{Ar}$), 128.7 (CH$_{Ar}$), 126.1 (C$_q$), 116.7 (CH$_{Ar}$), 57.0 (C$_q$), 35.6 (CH$_2$, CH$_2$-PCP), 35.5 (CH$_2$, CH$_2$-PCP), 35.4 (CH$_2$, CH$_2$-PCP), 33.8 (CH$_2$, CH$_2$-PCP), 29.9 (3C, CH$_3$).

IR (ATR) $\tilde{\upsilon}$ [cm^{-1}] = 3351 (vw), 2952 (w), 2927 (w), 1685 (vw), 1594 (vw), 1523 (w), 1476 (w), 1419 (w), 1379 (w), 1362 (w), 1341 (w), 1285 (w), 1198 (w), 1012 (vw), 934 (vw), 903 (w), 863 (vw), 809 (w), 712 (w), 669 (w), 639 (w), 617 (w), 550 (vw), 512 (w), 450 (vw), 416 (w), 384 (vw).

FAB-MS m/z (%): 397 [M + H]$^+$ (100), 396 [M]$^+$ (54), 340 [M + H − C$_4$H$_9$]$^+$ (28), 339 [M − C$_4$H$_9$]$^+$ (12).

HRMS-FAB (m/z): [M + H]$^+$ calcd. for C$_{26}$H$_{29}$N$_4$, 397.2392; found, 397.2394.

2-(1,4(1,4)-Dibenzenacyclohexaphane-1²-yl)-*N*-isopropylimidazo[1,2-*a*]pyrazin-3-amine (93c)[190]
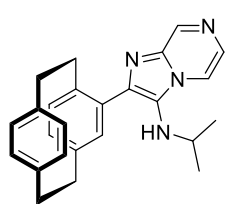
2-Aminopyrazine (150 mg, 1.58 mmol, 1.00 equiv) and 4-formyl[2.2]paracyclophane (373 mg, 1.58 mmol, 1.00 equiv) were dissolved in a mixture of 6 mL of dichloromethane and 4 mL of methanol. Subsequently, glacial acetic acid (0.18 mL, 189 mg, 3.15 mmol, 2.00 equiv) and isopropyl isonitrile (0.15 mL, 109 mg, 1.58 mmol, 1.00 equiv) were added. The mixture was stirred at r.t. for 72 h. The solvent was removed under reduced pressure and the residue was purified *via* flash chromatography (SiO$_2$, CH/EtOAc/NEt$_3$ 4:1:0.01 to 1:1:0.01). **93c** was isolated as a yellow solid (208 mg, 553 µmol, 35%).

R$_f$ (SiO$_2$, CH/EtOAc 1:1) = 0.16.

¹H NMR (400 MHz, CDCl$_3$) δ [ppm] = 9.12 (d, *J* = 1.4 Hz, 1H, C*H*$_{Ar}$), 7.97 (dd, *J* = 4.6, 1.5 Hz, 1H, C*H*$_{Ar}$), 7.86 (d, *J* = 4.6 Hz, 1H, C*H*$_{Ar}$), 6.99 (d, *J* = 1.7 Hz, 1H, C*H*$_{Ar}$), 6.74 – 6.67 (m, 2H, C*H*$_{Ar}$), 6.63 (dd, *J* = 7.8, 1.7 Hz, 1H, C*H*$_{Ar}$), 6.57 (dd, *J* = 7.8, 1.7 Hz, 1H, C*H*$_{Ar}$), 6.56 – 6.52 (m, 2H, C*H*$_{Ar}$), 3.28 – 2.80 (m, 9H, C*H*$_2$-PCP, C*H*), 0.95 (d, *J* = 6.3 Hz, 3H, C*H*$_3$), 0.71 (d, *J* = 6.2 Hz, 3H, C*H*$_3$).

¹³C NMR (101 MHz, CDCl$_3$) δ [ppm] = 143.6 (CH$_{Ar}$), 140.4 (C$_q$), 139.7 (C$_q$), 139.6 (C$_q$), 139.2 (C$_q$), 137.2 (C$_q$), 137.2 (C$_q$), 135.3 (CH$_{Ar}$), 133.7 (CH$_{Ar}$), 133.6 (CH$_{Ar}$), 133.5 (CH$_{Ar}$), 132.9 (C$_q$), 132.7 (CH$_{Ar}$), 132.3 (C$_q$), 132.1 (CH$_{Ar}$), 128.8 (CH$_{Ar}$), 127.7 (CH$_{Ar}$), 115.6 (CH$_{Ar}$), 49.1 (CH), 35.6 (CH$_2$, *C*H$_2$-PCP), 35.4 (CH$_2$, *C*H$_2$-PCP), 34.7 (CH$_2$, *C*H$_2$-PCP), 34.1 (CH$_2$, *C*H$_2$-PCP), 23.6 (CH$_3$), 23.3 (CH$_3$).

IR (ATR) $\tilde{\upsilon}$ [cm^{-1}] = 3316 (vw), 2966 (w), 2923 (w), 1655 (w), 1529 (m), 1496 (w), 1428 (w), 1377 (w), 1352 (m), 1290 (w), 1227 (w), 1170 (w), 1013 (vw), 933 (w), 902 (w), 867 (w), 815 (w), 789 (w), 752 (w), 716 (w), 680 (vw), 635 (w), 606 (w), 588 (w), 512 (w), 443 (vw), 415 (w), 386 (w).

FAB-MS *m/z* (%): 383 [M + H]$^+$ (100), 382 [M]$^+$ (47), 339 [M − C$_3$H$_7$] (9), 279 [M − C$_8$H$_8$ + H]$^+$ (18), [M − C$_8$H$_8$]$^+$ (7).

HRMS-FAB (*m/z*): [M + H]$^+$ calcd. for C$_{25}$H$_{27}$N$_4$, 383.2236; found, 382.2237.

1,4(1,4)-Dibenzenacyclohexaphane-1²,4³-dicarbaldehyde (95)
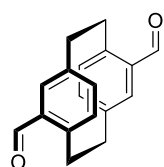
trans-Dibromo[2.2]paracyclophane (5.00 g, 13.7 mmol, 1.00 equiv) was dissolved in anhydrous THF (400 mL) under an argon atmosphere. The solution was cooled to -78°C. A 1.6 M solution of ^{t}BuLi in hexane (3.50 g, 34.1 mL, 54.6 mmol, 1.60M, 4.00 equiv) was added, and the solution was stirred for 1 h. Subsequently, it was allowed to warm up to 0°C and stirred for 1 h. Afterwards, *N*,*N*-dimethylformamide (9.98 g, 10.5 mL, 137 mmol, 10.0 equiv) was added in one portion, and the solution was stirred for 16 h. The mixture was quenched with an aqueous NH$_4$Cl solution, extracted with dichloromethane, and dried over Na$_2$SO$_4$. The residue was purified *via* flash chromatography (SiO$_2$, CH/EtOAc 20:1 to 4:1). **95** was isolated as a beige solid (2.20 g, 8.32 mmol, 61%).

R$_f$ (SiO$_2$, CH/EtOAc 1:1) = 0.45.

¹H NMR (400 MHz, CDCl₃) δ [ppm] = 9.94 (s, 2H), 7.05 (d, *J* = 2.0 Hz, 2H), 6.63 (dd, *J* = 7.8, 2.1 Hz, 2H), 6.52 (d, *J* = 7.8 Hz, 2H), 4.13 (ddd, *J* = 13.1, 10.5, 2.4 Hz, 2H), 3.29 (ddd, *J* = 13.2, 10.6, 2.4 Hz, 2H), 3.16 (ddd, *J* = 13.4, 10.5, 5.9 Hz, 2H), 3.01 (ddd, *J* = 13.3, 10.7, 5.8 Hz, 2H).

¹³C NMR (126 MHz, CDCl₃) δ [ppm] = 192.1 (2C, CH, *C*HO), 143.1 (2C, C_q), 140.7 (2C, C_q), 137.1 (2C, CH_Ar), 136.9 (2C, C_q), 136.7 (2C, CH_Ar), 135.4 (2C, CH_Ar), 34.5 (2C, CH₂, CH₂-PCP), 33.0 (2C, CH₂, *C*H₂-PCP).

IR (ATR) ṽ [cm⁻¹] = 2925 (w), 2854 (w), 2826 (w), 2748 (w), 1670 (vs), 1587 (s), 1550 (m), 1485 (w), 1451 (w), 1436 (w), 1411 (w), 1394 (w), 1281 (w), 1248 (w), 1224 (s), 1200 (m), 1181 (m), 1163 (w), 1137 (s), 1086 (w), 970 (w), 945 (m), 901 (m), 880 (m), 863 (m), 789 (m), 747 (m), 721 (s), 698 (w), 649 (vs), 616 (s), 526 (m), 497 (w), 486 (w), 448 (m), 388 (w).

FAB-MS *m/z* (%):265 (29), 155 (39), 154 (100), 139 (30), 138 (43), 137 (68), 136 (81), 131 (34), 119 (28), 109 (45), 107 (42), 105 (43), 97 (44), 95 (68), 93 (30), 91 (54).

HRMS-FAB (*m/z*): [M + H]⁺ calcd. for C₁₈H₁₇O₂, 265.1223; found, 265.1221.

2,2'-(1,4(1,4)-Dibenzenacyclohexaphane-12,43-diyl)bis(*N*-pentylimidazo[1,2-*a*]pyridin-3-amine) (96)
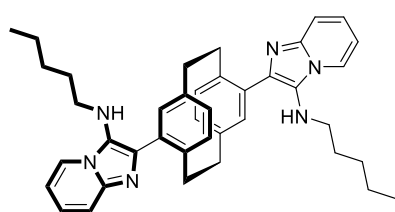
2-Aminopyridine (142 mg, 1.51 mmol, 2.00 equiv) and **95** (200 mg, 757 µmol, 1.00 equiv) were dissolved in a mixture of 6 mL of dichloromethane and 4 mL of methanol. Subsequently, a 1 ᴍ solution of perchloric acid in methanol (15.2 mg, 151 µL, 151 µmol, 0.20 equiv) and pentyl-1-isonitrile (147 mg, 147 µL, 1.51 mmol, 2.00 equiv) were added. The mixture was stirred at r.t. for 6 d. The solvent was removed under reduced pressure and the residue was purified *via* flash chromatography (SiO₂, CH/EtOAc/NEt₃ 4:1:0.01 to 1:1:0.01). **96** was isolated as an orange solid (200 mg, 326 µmol, 43%).

R_f (SiO₂, CH/EtOAc 1:2) = 0.10.

¹H NMR (500 MHz, CDCl₃) δ [ppm] = 8.09 (d, *J* = 6.8 Hz, 2H, C*H*_Ar), 7.79 (d, *J* = 9.1 Hz, 2H, C*H*_Ar), 7.20 (t, *J* = 8.0 Hz, 2H, C*H*_Ar), 7.13 (d, *J* = 2.0 Hz, 2H, C*H*_Ar), 6.92 (d, *J* = 7.9 Hz, 2H, C*H*_Ar), 6.86 (t, *J* = 6.7 Hz, 2H, C*H*_Ar), 6.70 (dd, *J* = 7.8, 2.0 Hz, 2H, C*H*_Ar), 3.37 (t, *J* = 6.8 Hz, 2H, N*H*), 3.19 (pt, *J* = 9.3, 5.1 Hz, 4H, C*H*₂-PCP), 2.95 (qdd, *J* = 13.5, 8.9, 5.1 Hz, 4H, C*H*₂-PCP), 2.78 (ddp, *J* = 18.7, 12.5, 6.5 Hz, 4H, C*H*₂), 1.36–1.23 (m, 4H, C*H*₂), 1.13 (tq, *J* = 8.4, 5.2, 4.0 Hz, 8H, C*H*₂), 0.80–0.73 (m, 6H, C*H*₃).

¹³C NMR (101 MHz, CDCl₃) δ [ppm] = 141.2 (2C, C_q), 139.9 (2C, C_q), 136.8 (2C, C_q), 135.8 (2C, CH_Ar), 134.9 (2C, C_q), 132.9 (2C, CH_Ar), 132.5 (2C, CH_Ar), 127.3 (2C, C_q), 123.6 (2C, CH_Ar), 122.7 (2C, CH_Ar), 117.5 (2C, CH_Ar), 111.9 (2C, CH_Ar),111.8 (2C, Cq), 47.9 (2C, CH₂), 35.3 (2C, CH₂, *C*H₂-PCP), 33.5 (2C, CH₂, *C*H₂-PCP,), 30.1 (2C, *C*H₂), 29.1 (2C, *C*H₂), 22.5 (2C, CH₂), 14.1 (2C, CH₃).

IR (ATR) ṽ [cm⁻¹] = 3370 (vw), 3012 (vw), 2949 (m), 2925 (s), 2853 (m), 1628 (w), 1591 (w), 1558 (m), 1500 (w), 1465 (w), 1426 (w), 1374 (w), 1344 (s), 1266 (m), 1235 (m), 1193 (m), 1146 (w), 1123 (w), 1105 (m), 1065 (w),

1041 (w), 1001 (w), 907 (m), 878 (w), 860 (w), 827 (w), 802 (m), 749 (vs), 735 (vs), 674 (s), 626 (w), 602 (m), 574 (w), 510 (vs), 456 (m), 441 (m), 424 (w), 411 (w), 398 (m), 390 (w), 380 (m).

FAB-MS *m/z* (%): 612 (40), 611 (100), 610 (49), 609 (17), 553 (12), 539 (12), 512 (15), 307 (13), 306 (53), 305 (15), 235 (13), 234 (17), 233 (16), 219 (16), 209 (13), 208 (20), 207 (30), 154 (17), 136 (15), 95 (12), 91 (14).

HRMS-FAB (*m/z*): [M + H]$^+$ calcd. for $C_{40}H_{47}N_6$, 611.3857; found, 611.3856.

4^3-(3-(Pentylamino)imidazo[1,2-*a*]pyrazin-2-yl)-1,4(1,4)-dibenzenacyclohexaphane-12-carbaldehyde (97)
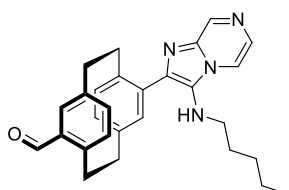
2-Aminopyrazine (53 mg, 567 µmol, 1.00 equiv) and **95** (150 mg, 567 µmol, 1.00 equiv) were dissolved in a mixture of 24 mL of dichloromethane and 16 mL of methanol. Subsequently, a 1 M solution of perchloric acid in methanol (5.7 mg, 57 µL, 57 µmol, 0.10 equiv) and pentyl-1-isonitrile (55 mg, 55 µL, 567 µmol, 2.00 equiv) were added. The mixture was stirred at r.t. for 6 d. The solvent was removed under reduced pressure, and the residue was purified *via* flash chromatography (SiO$_2$, CH/EtOAc/NEt$_3$ 4:1:0.01 to 1:1:0.01). **97** was isolated as an orange solid (33 mg, 75 µmol, 13%).

R_f (SiO$_2$, Cyclohexane/EtOAc 1:2) = 0.15.

^{1}H NMR (500 MHz, CDCl$_3$) δ [ppm] = 10.05 (s, 1H, C*H*O), 9.11 (d, *J* = 1.4 Hz, 1H, C*H*$_{Ar}$), 7.92 (dd, *J* = 4.6, 1.4 Hz, 1H, C*H*$_{Ar}$), 7.87 (d, *J* = 4.6 Hz, 1H, C*H*$_{Ar}$), 7.11 (d, *J* = 1.8 Hz, 1H, C*H*$_{Ar}$), 7.01 (d, *J* = 1.8 Hz, 1H, C*H*$_{Ar}$), 6.93 (dd, *J* = 7.7, 1.8 Hz, 1H, C*H*$_{Ar}$), 6.83 (d, *J* = 7.7 Hz, 1H, C*H*$_{Ar}$), 6.52 (d, *J* = 7.9 Hz, 1H, C*H*$_{Ar}$), 6.43 (dd, *J* = 7.8, 1.9 Hz, 1H, C*H*$_{Ar}$), 4.20–4.10 (m, 1H, C*H*$_2$-PCP), 3.34 (t, *J* = 6.6 Hz, 1H, N*H*), 3.32–3.23 (m, 2H, C*H*$_2$-PCP), 3.11 (dddd, *J* = 13.0, 9.1, 6.2, 4.0 Hz, 4H, C*H*$_2$-PCP), 3.04–2.90 (m, 2H, C*H*$_2$-PCP), 2.83 (dp, *J* = 19.0, 5.9 Hz, 2H, C*H*$_2$), 1.34 − 1.22 (m, 2H, C*H*$_2$), 1.18 − 1.05 (m, 4H, C*H*$_2$), 0.79–0.67 (m, 3H, C*H*$_3$).

^{13}C NMR (101 MHz, CDCl$_3$) δ [ppm] = 192.2 (CH, *C*HO), 143.8 (CH$_{Ar}$), 143.5 (C$_q$), 140.4 (C$_q$), 140.3 (C$_q$), 137.6 (CH$_{Ar}$), 137.6 (C$_q$), 137.4 (C$_q$), 137.0 (C$_q$), 136.6 (CH$_{Ar}$), 136.4 (C$_q$), 136.0 (CH$_{Ar}$), 134.4 (CH$_{Ar}$), 133.7 (CH$_{Ar}$), 133.3 (C$_q$), 133.0 (CH$_{Ar}$), 129.0 (C$_q$), 128.9 (CH$_{Ar}$), 115.4 (CH$_{Ar}$), 47.5 (CH$_2$), 35.2 (CH$_2$), 35.1 (CH$_2$, *C*H$_2$-PCP), 33.3 (CH$_2$, *C*H$_2$-PCP), 33.0 (CH$_2$), 30.1 (CH$_2$), 28.9 (CH$_2$), 22.4 (CH$_2$), 14.0 (CH$_3$).

IR (ATR) $\tilde{v}$ [cm^{-1}] = 3325 (w), 2952 (s), 2924 (vs), 2853 (vs), 2727 (w), 1680 (vs), 1611 (m), 1591 (m), 1538 (vs), 1486 (s), 1462 (s), 1453 (s), 1435 (s), 1354 (vs), 1286 (vs), 1225 (vs), 1190 (vs), 1157 (vs), 1145 (vs), 1125 (vs), 1079 (s), 1051 (s), 1013 (s), 973 (s), 931 (s), 907 (vs), 881 (vs), 781 (vs), 720 (vs), 650 (vs), 606 (vs), 518 (vs), 490 (vs), 445 (vs), 416 (vs), 405 (vs).

HRMS-ESI (*m/z*): [M + H]$^+$ calcd. for $C_{28}H_{31}N_4O_1$, 439.2492; found, 439.2493.

4-Nitro[2.2]paracyclophane (98)
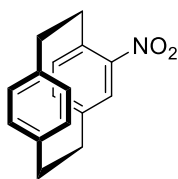
[2.2]Paracyclophane (10.0 g, 48.0 mmol, 1.00 equiv) was dissolved in dichloromethane (950 mL) and cooled to 0 °C. A mixture of sulfuric acid (95% aq. solution, 10.8 mL, 192 mmol, 4.00 equiv) and nitric acid (70% aq. solution, 6.65 mL, 96.0 mmol, 2.00 equiv) was slowly added. The mixture was warmed to room temperature. After 16 h, the reaction mixture was decanted onto ice, leaving any dark orange tar in the reaction vessel. The biphasic mixture was stirred for 15 min and the layers were separated. The aqueous phase was extracted with dichloromethane (3 × 100 mL). The combined organic layers were dried over Na_2SO_4, and the solvent was removed under reduced pressure. The residue was purified by flash column chromatography (SiO$_2$, PE$_{40/60}$/ EtOAc, 10:1). **98** was obtained as an orange solid (5.20 g, 20.5 mmol, 43%).

R_f (SiO$_2$, n-pentane/EtOAc, 10:1) = 0.45.

^{1}H NMR (500 MHz, CDCl$_3$) δ [ppm] = 7.22 (d, J = 1.9 Hz, 1H, CH_{Ar}), 6.79 (dd, J = 7.8, 1.9 Hz, 1H, CH_{Ar}), 6.65 – 6.60 (m, 2H, CH_{Ar}), 6.58 (dd, J = 7.9, 1.9 Hz, 1H, CH_{Ar}), 6.56 (dd, J = 7.8, 1.9 Hz, 1H, CH_{Ar}), 6.48 (dd, J = 7.9, 1.8 Hz, 1H, CH_{Ar}), 4.03 (ddd, J = 13.3, 9.5, 2.0 Hz, 1H, CH_2-PCP), 3.27 – 3.12 (m, 4H, CH_2-PCP), 3.12 – 3.03 (m, 2H, CH_2-PCP), 2.90 (ddd, J = 13.3, 10.0, 7.2 Hz, 1H, CH_2-PCP).

^{13}C NMR (126 MHz, CDCl$_3$) δ [ppm] = 149.4 (C$_q$), 142.2 (C$_q$), 139.9 (C$_q$), 139.4 (C$_q$), 137.9 (CH$_{Ar}$), 137.5 (CH$_{Ar}$), 136.6 (C$_q$), 133.3 (CH$_{Ar}$), 133.2 (CH$_{Ar}$), 132.5 (CH$_{Ar}$), 130.1 (CH$_{Ar}$), 129.7 (CH$_{Ar}$), 36.2 (CH$_2$, CH$_2$-PCP), 35.1 (CH$_2$, CH$_2$-PCP), 34.9 (CH$_2$, CH$_2$-PCP), 34.6 (CH$_2$, CH$_2$-PCP).

IR (ATR) $\tilde{v}$ [cm^{-1}] = 3058 (w), 2924 (w), 2853 (w), 1601 (w), 1591 (w), 1550 (w), 1514 (vs), 1482 (m), 1451 (m), 1436 (m), 1411 (w), 1402 (w), 1333 (vs), 1300 (vs), 1261 (m), 1242 (m), 1201 (m), 1179 (m), 1132 (w), 1095 (m), 1026 (w), 931 (w), 904 (s), 882 (w), 870 (s), 843 (w), 805 (vs), 789 (s), 768 (w), 758 (m), 722 (m), 703 (s), 694 (s), 673 (s), 633 (vs), 582 (m), 564 (w), 509 (vs), 465 (w), 425 (w), 415 (w), 398 (w), 384 (w).

EI-MS m/z (%) = 253 [M]$^+$ (12), 104 [C$_8$H$_9$]$^+$ (100).

HRMS-EI (m/z): [M]$^+$ calcd. for C$_{16}$H$_{15}$O$_2$N, 253.1097, found: 253.1097.

4-Amino[2.2]paracyclophane (99)
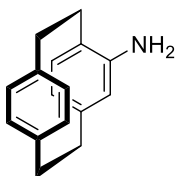
According to a procedure by Zippel,[189B] pressure reactor was charged with 4-nitro[2.2]paracyclophane (3.00 g, 11.8 mmol, 1.00 equiv) and palladium on carbon (10 wt.%, 126 mg, 1.18 mmol, 0.10 mol%). Methanol (40 mL) was added, and the reactor was pressurized with hydrogen (50 bar). The mixture was vigorously stirred (750 rpm) at room temperature for 16 h. The mixture was filtered through a pad of Celite®, and the solvent was removed under reduced pressure. The residue was purified by flash column chromatography (SiO$_2$, n-pentane/EtOAc, 4:1). **99** was obtained as a yellow solid (2.60 g, 11.6 mmol, 99%).

R_f (SiO$_2$, CH/EtOAc 6:1) = 0.26.

¹H NMR (500 MHz, CDCl₃) δ [ppm] = 7.18 (dd, J = 7.8, 2.0 Hz, 1H, CH_{Ar}), 6.59 (dd, J = 7.9, 2.0 Hz, 1H, CH_{Ar}), 6.40 (dt, J = 7.8, 1.8 Hz, 2H, CH_{Ar}), 6.27 (d, J = 7.7 Hz, 1H, CH_{Ar}), 6.14 (dd, J = 7.6, 1.8 Hz, 1H, CH_{Ar}), 5.38 (d, J = 1.8 Hz, 1H, CH_{Ar}), 3.46 (s, 2H, NH_2), 3.16 − 3.07 (m, 3H, CH_2-PCP), 3.07 − 2.92 (m, 3H, CH_2-PCP), 2.87 − 2.79 (m, 1H, CH_2-PCP), 2.72 − 2.62 (m, 1H, CH_2-PCP).

¹³C NMR (126 MHz, CDCl₃) δ [ppm] = 145.1 (C$_q$), 141.2 (C$_q$), 139.1 (C$_q$), 139.0 (C$_q$), 135.4 (CH$_{Ar}$), 133.6 (CH$_{Ar}$), 132.5 (CH$_{Ar}$), 131.6 (CH$_{Ar}$), 126.9 (CH$_{Ar}$), 124.6 (C$_q$), 122.9 (CH$_{Ar}$), 122.4 (CH$_{Ar}$), 35.5 (CH$_2$), 35.1 (CH$_2$), 33.1 (CH$_2$), 32.4 (CH$_2$).

IR (ATR) $\tilde{v}$ [cm^{-1}] = 3472 (w), 3383 (w), 3007 (w), 2919 (vs), 2891 (s), 2850 (s), 1884 (vw), 1693 (vw), 1612 (vs), 1592 (s), 1565 (s), 1497 (vs), 1451 (w), 1438 (m), 1424 (vs), 1322 (w), 1285 (s), 1203 (w), 1183 (w), 1160 (w), 1128 (w), 1095 (w), 980 (w), 938 (w), 922 (vw), 897 (w), 863 (m), 795 (s), 759 (w), 715 (vs), 659 (vs), 586 (m), 557 (w), 530 (w), 510 (vs), 490 (s), 455 (m), 435 (w), 392 (w).

EI-MS m/z (%) = 223 [M]$^+$ (36), 119 [M − C$_8$H$_8$]$^+$ (100).

HRMS-EI (m/z): [M]$^+$ calcd. for C$_{16}$H$_{17}$N, 223.1356, found: 223.1354.

4-Formamido[2.2]paracyclophane (10)

A solution of 4-amino[2.2]paracyclophane (258 mg, 1.15 mmol, 1.00 equiv) and ethyl formate (1.40 mL, 1.28 g, 17.3 mmol, 15.0 equiv) in anhydrous THF (25 mL) was added dropwise to a suspension of NaH (60% in mineral oil, 215 mg, 5.37 mmol) in 25 mL of anhydrous THF. The resulting mixture was stirred at r.t. for 24 h, then the reaction was quenched with water (10 mL). The solvents were removed under reduced pressure, and the residue was dissolved in ethyl acetate/water (400/100 mL). The aqueous phase was extracted with ethyl acetate (2 × 100 mL), the combined organic extracts were dried over Na$_2$SO$_4$, and the solvent was removed under reduced pressure. The residue was purified by flash column chromatography (SiO$_2$, CH/EtOAc, 4:1). **100** was obtained as a brown solid (281 mg, 1.15 mmol, 98%).
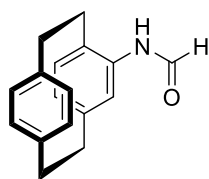
R_f (SiO$_2$, CH/EtOAc 2:1) = 0.25.

¹H NMR (500 MHz, DMSO) δ [ppm] = 9.73 (d, J = 10.9 Hz, 0.35H, NH), 9.50 (s, 0.65H, NH), 8.48 (d, J = 10.9 Hz, 0.33H), 8.27 (d, J = 2.0 Hz, 0.67H), 6.82 (d, J = 1.7 Hz, 0.70H), 6.73 (dd, J = 7.7, 1.9 Hz, 0.70H), 6.69 (dd, J = 7.8, 2.0 Hz, 0.30H), 6.55 (dd, J = 7.8, 1.9 Hz, 0.30H), 6.51 (dd, J = 7.8, 1.9 Hz, 0.72H), 6.48 (d, J = 1.6 Hz, 0.28H), 6.47–6.45 (m, 1H), 6.45–6.43 (m, 0.7H), 6.42–6.41 (m, 0.7H), 6.39 (t, J = 2.3 Hz, 0.62H), 6.37 (t, J = 2.3 Hz, 0.60H), 6.21 (d, J = 1.7 Hz, 0.38H), 3.42–3.27 (m, 1H, CH_2), 3.06–2.85 (m, 6H, CH_2), 2.73–2.62 (m, 1H, CH_2).

¹³C NMR (126 MHz, CDCl₃) δ [ppm] = 159.0 (CH, CHO), 140.2 (C$_q$), 138.8 (C$_q$), 138.7 (C$_q$), 136.5 (C$_q$), 134.9 (CH$_{Ar}$), 133.0 (CH$_{Ar}$), 132.9 (CH$_{Ar}$), 132.0 (CH$_{Ar}$), 130.1 (C$_q$), 128.4 (CH$_{Ar}$), 128.3 (CH$_{Ar}$), 126.4 (CH$_{Ar}$), 34.7 (CH$_2$), 34.5 (CH$_2$), 33.0 (CH$_2$), 32.6 (CH$_2$).

Minor Isomer: **¹³C NMR** (126 MHz, DMSO) δ [ppm] = 164.0 (CHO), 140.9 (C_q), 139.1 (C_q), 138.8 (C_q), 136.6 (C_q), 135.7 (CH_Ar), 133.1 (CH_Ar), 132.9 (CH_Ar), 131.8 (CH_Ar), 130.4 (C_q), 130.1 (CH_Ar), 128.0 (CH_Ar), 123.7 (CH_Ar), 34.6 (CH_2), 34.3 (CH_2), 33.3 (CH_2), 32.1 (CH_2).

IR (ATR) ṽ [cm⁻¹] =3153 (w), 3065 (w), 3031 (w), 3006 (w), 2927 (m), 2900 (w), 2853 (w), 1689 (vs), 1649 (m), 1595 (m), 1568 (w), 1497 (w), 1455 (w), 1445 (w), 1422 (w), 1411 (w), 1385 (w), 1309 (s), 1281 (vs), 1241 (m), 1086 (w), 1038 (w), 945 (w), 898 (m), 878 (m), 830 (w), 805 (vs), 783 (m), 721 (s), 696 (w), 671 (s), 646 (m), 591 (s), 520 (m), 500 (m), 482 (vs), 466 (w), 425 (m).

FAB-MS *m/z* (%) = 252 [M + H]⁺ (27), 251 [M]⁺ (25), 155 (34), 154 (100), 139 (15), 138 (38), 137 (66), 136 (62), 120 (11), 107 (18), 91 (12), 90 (11), 89 (18).

HRMS-FAB (*m/z*): [M]⁺ calcd. for $C_{17}H_{17}NO$, 251.1305, found: 251.1306.

N-(1,4(1,4)-Dibenzenacyclohexaphane-1²-yl)-2-(4-methoxyphenyl)imidazo[1,2-*a*]pyridin-3-amine (102a)[190]
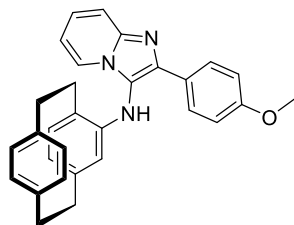
4-Formamido[2.2]paracyclophane (200 mg, 0.80 mmol, 1.00 equiv) was dissolved in dichloromethane (6 mL). At 0 °C, triphosgene (95 mg, 0.32 mmol, 0.40 equiv) and triethylamine (0.26 mL, 193 mg, 1.91 mmol, 2.40 equiv) were added. The reaction mixture was stirred for 30 min. Subsequently, methanol (4 mL), 2-aminopyridine (27 mg, 0.80 mmol, 1.00 equiv), *p*-methoxy benzaldehyde (0.10 mmol, 110 mg, 0.80 mmol, 1.00 equiv), and glacial acetic acid (0.09 mL, 96 mg, 1.59 mmol, 1.00 equiv) were added. The mixture was stirred at r.t. for 72 h. The solvent was removed under reduced pressure and the residue was purified *via* flash chromatography (SiO_2, CH/EtOAc/NEt_3 4:1:0.01 to 1:1:0.01). **102a** was obtained as a yellow solid (165 mg, 376 μmol, 47%).

R_f (SiO_2, CH/EtOAc 1:1) = 0.21.

¹H NMR (400 MHz, CDCl_3) δ [ppm] = 8.08 – 7.99 (m, 2H, CH_Ar), 7.62 – 7.53 (m, 2H, CH_Ar), 7.13 (ddd, *J* = 9.0, 6.8, 1.4 Hz, 1H, CH_Ar), 7.03 – 6.95 (m, 2H, CH_Ar), 6.79 (dd, *J* = 7.9, 1.9 Hz, 1H, CH_Ar), 6.62 (td, *J* = 6.7, 1.2 Hz, 1H, CH_Ar), 6.56 (dd, *J* = 7.8, 1.9 Hz, 1H, CH_Ar), 6.45 (dd, *J* = 7.8, 1.9 Hz, 1H, CH_Ar), 6.34 (d, *J* = 7.7 Hz, 1H, CH_Ar), 6.11 (ddd, *J* = 15.7, 7.8, 1.8 Hz, 2H, CH_Ar), 5.52 (s, 1H, N*H*), 5.10 (d, *J* = 1.8 Hz, 1H, CH_Ar), 3.82 (s, 3H, OC*H*_3), 3.21 – 3.03 (m, 3H, C*H*_2-PCP), 2.93 – 2.74 (m, 4H, C*H*_2-PCP), 2.65 – 2.51 (m, 1H, C*H*_2-PCP).

¹³C NMR (101 MHz, CDCl_3) δ [ppm] =159.6 (C_q), 143.4 (C_q), 142.4 (C_q), 142.0 (C_q), 139.7 (C_q), 139.1 (C_q), 139.0 (C_q), 136.1 (CH_Ar), 133.0 (CH_Ar), 132.96 (CH_Ar), 131.9 (CH_Ar), 129.2 (CH_Ar), 128.4 (CH_Ar), 126.4 (C_q), 124.6 (CH_Ar), 124.6 (CH_Ar), 124.3 (C_q), 123.1 (CH_Ar), 119.5 (CH_Ar), 118.8 (C_q), 117.4 (CH_Ar), 114.0 (CH_Ar), 111.81 (CH_Ar), 55.4 (CH_3, OC*H*_3), 35.3 (CH_2, C*H*_2-PCP), 35.1 (CH_2, C*H*_2-PCP), 33.9 (CH_2, C*H*_2-PCP), 32.0 (CH_2, C*H*_2-PCP).

IR (ATR) ṽ [cm⁻¹] = 3275 (vw), 2919 (vw), 1614 (vw), 1568 (w), 1499 (w), 1467 (w), 1416 (w), 1398 (w), 1343 (w), 1293 (w), 1246 (w), 1173 (w), 1108 (vw), 1030 (w), 877 (vw), 836 (w), 798 (w), 750 (w), 736 (w), 717 (w), 652 (vw), 592 (vw), 560 (w), 514 (w), 492 (w), 449 (vw), 400 (vw).

FAB-MS *m/z* (%): 446 [M + H]⁺ (100), 445 [M]⁺ (79), 341 (14), 211 (37).

HRMS-FAB (*m/z*): [M + H]$^+$ calcd. for $C_{30}H_{28}O_1N_3$, 446.2232; found, 446.2234.

_N_-(1,4(1,4)-Dibenzenacyclohexaphane-1^2-yl)-2-(_tert._-butyl)imidazo[1,2-_a_]pyridin-3-amine (102b)[190]
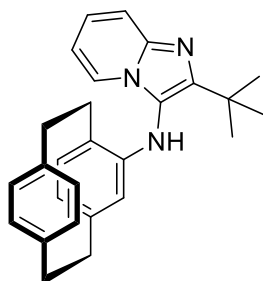
4-Formamido[2.2]paracyclophane (200 mg, 0.80 mmol, 1.00 equiv) was dissolved in dichloromethane (6 mL). At 0 °C, triphosgene (95 mg, 0.32 mmol, 0.40 equiv) and triethylamine (0.26 mL, 193 mg, 1.91 mmol, 2.40 equiv) were added. The reaction mixture was stirred for 30 min. Subsequently, methanol (4 mL), 2-aminopyridine (27 mg, 0.80 mmol, 1.00 equiv), pivaldehyde (0.09 mL, 69 mg, 0.80 mmol, 1.00 equiv), and glacial acetic acid (0.09 mL, 96 mg, 1.59 mmol, 1.00 equiv) were added. The mixture was stirred at r.t. for 72 h. The solvent was removed under reduced pressure and the residue was purified *via* flash chromatography (SiO$_2$, CH/EtOAc/NEt$_3$ 4:1:0.01 to 1:1:0.01). **102b** was obtained as a yellow solid (250 mg, 632 µmol, 79%).

***R**_f_* (SiO$_2$, CH/EtOAc 2:1) = 0.11.

^{1}H NMR (300 MHz, CDCl$_3$) δ [ppm] = 7.98 (s, 1H, C*H*$_{Ar}$), 7.61 – 7.51 (m, 1H, C*H*$_{Ar}$), 7.22 (dd, *J* = 7.9, 1.9 Hz, 1H, C*H*$_{Ar}$), 7.19 – 7.11 (m, 1H, C*H*$_{Ar}$), 6.74 (s, 1H, C*H*$_{Ar}$), 6.67 (dd, *J* = 7.8, 1.9 Hz, 1H, C*H*$_{Ar}$), 6.56 (dd, *J* = 7.8, 1.9 Hz, 1H, C*H*$_{Ar}$), 6.40 (dd, *J* = 7.9, 1.9 Hz, 1H, C*H*$_{Ar}$), 6.35 (d, *J* = 7.7 Hz, 1H, C*H*$_{Ar}$), 6.13 (dd, *J* = 7.7, 1.8 Hz, 1H, C*H*$_{Ar}$), 5.16 (s, 1H, N*H*), 5.11 (s, 1H, C*H*$_{Ar}$), 3.25 – 3.11 (m, 3H, C*H*$_2$-PCP), 3.02 – 2.84 (m, 4H, C*H*$_2$-PCP), 2.68 – 2.51 (m, 1H, C*H*$_2$-PCP), 1.40 (s, 9H, C*H*$_3$).

^{13}C NMR (101 MHz, CDCl$_3$) δ [ppm] = 149.3 (C$_q$), 145.1 (C$_q$) 142.0 (C$_q$), 141.3 (C$_q$), 139.4 (C$_q$), 139.1 (C$_q$), 135.9 (CH$_{Ar}$), 133.4 (CH$_{Ar}$), 133.0 (CH$_{Ar}$), 131.8 (CH$_{Ar}$), 128.3 (CH$_{Ar}$), 124.3 (CH$_{Ar}$), 123.9 (CH$_{Ar}$), 123.5 (C$_q$), 122.3 (CH$_{Ar}$), 119.3 (CH$_{Ar}$), 119.0 (C$_q$) 117.5 (CH$_{Ar}$), 111.6 (CH$_{Ar}$), 35.5 (CH$_2$, *C*H$_2$-PCP), 35.2 (CH$_2$, *C*H$_2$-PCP), 34.3 (CH$_2$, *C*H$_2$-PCP), 33.1 (C$_q$), 31.5 (CH$_2$, *C*H$_2$-PCP), 30.3 (3C, CH$_3$).

IR (ATR) $\tilde{v}$ [cm^{-1}] = 3366 (vw), 2929 (vw), 1631 (vw), 1567 (w), 1546 (w), 1498 (w), 1411 (w), 1372 (vw), 1347 (w), 1271 (w), 1230 (vw), 1192 (vw), 1166 (vw), 931 (vw), 874 (vw), 824 (vw), 796 (w), 755 (w), 738 (w), 715 (w), 654 (w), 588 (vw), 532 (vw), 513 (vw), 413 (w), 386 (vw).

FAB-MS *m/z* (%): 396 [M + H]$^+$ (100), 395 [M]$^+$ (88), 105 [C$_8$H$_8$ + H]$^+$ (20).

HRMS-FAB (*m/z*): [M + H]$^+$ calcd. for $C_{27}H_{30}N_3$, 396.2440; found, 396.2441.

Chloro(*rac*-3-(cyclohexylamino-*κN*-)-2-([2.2]paracyclophan-4-yl-*κC⁵*-)limidazo[1,2-*a*]pyridino) (triphenylphosphine)palladium(II) (103)
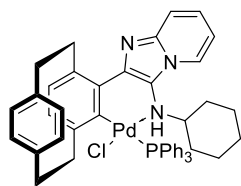
2-(1,4(1,4)-Dibenzenacyclohexaphane-12-yl)-*N*-cyclohexylimidazo[1,2-*a*]pyridine-3-amine (84.0 mg, 199 µmol, 1.00 equiv) and palladium(II) acetate (47.0 mg, 209 µmol, 1.05 equiv) were dissolved in anhydrous toluene (1.6 mL) and heated to 90 °C for 20 min. The solvent was removed under reduced pressure, and the residue was suspended in anhydrous acetone (2.1 mL). Lithium chloride (25.3 mg, 598 µmol, 3.00 equiv) was added. After stirring at r.t. for 16 h, triphenylphosphine (52.3 mg, 199 µmol, 1.00 equiv) was added. After another 16 h, the solvent was removed under reduced pressure, and the residue was purified *via* flash chromatography (SiO$_2$, *n*-pentane/EtOAc 2:1). Compound **103** was isolated as a yellow solid (60 mg, 72.8 µmol, 37%).

R$_f$ (SiO$_2$, CH/EtOAc 1:1) = 0.11.

¹H NMR (500 MHz, CDCl$_3$) δ [ppm] = 8.79 (dt, *J* = 9.0, 1.1 Hz, 1H), 8.24 (dt, *J* = 6.9, 1.2 Hz, 1H), 7.61 (ddd, *J* = 11.3, 8.3, 1.3 Hz, 6H), 7.35–7.28 (m, 4H), 7.21 (td, *J* = 7.7, 2.2 Hz, 6H), 7.01–6.91 (m, 2H), 6.48–6.41 (m, 2H), 6.03 (d, *J* = 7.8 Hz, 1H), 5.83 (dd, *J* = 7.8, 1.7 Hz, 1H), 5.59 (dd, *J* = 7.8, 1.7 Hz, 1H), 3.41 (ddd, *J* = 13.6, 9.4, 4.6 Hz, 1H), 3.32 (ddd, *J* = 12.8, 10.1, 5.4 Hz, 1H), 3.11–3.04 (m, 1H), 3.01–2.95 (m, 2H), 2.94–2.85 (m, 2H), 2.80 (ddd, *J* = 13.7, 9.4, 4.5 Hz, 1H), 2.65 (ddd, *J* = 13.5, 9.2, 5.1 Hz, 1H), 2.09–2.00 (m, 1H), 1.87–1.79 (m, 1H), 1.75–1.63 (m, 2H), 1.50 (dd, *J* = 8.8, 4.3 Hz, 1H), 1.28–1.07 (m, 6H).

¹³C NMR (126 MHz, CDCl$_3$) δ [ppm] = 162.7 (d, *J* = 6.4 Hz, C$_q$), 145.2 (d, *J* = 6.8 Hz, C$_q$), 144.8 (d, *J* = 2.7 Hz, C$_q$), 143.8 (d, *J* = 6.0 Hz, 3C, C$_q$), 141.0 (C$_q$), 140.0 (C$_q$), 138.4 (C$_q$), 135.5 (d, *J* = 11.1 Hz, 6C, CH$_{Ar}$), 134.5 (*C$_q$*), 133.6 (CH$_{Ar}$), 132.6 (d, *J* = 2.7 Hz, C$_q$), 132.6 (CH$_{Ar}$), 132.2 (d, *J* = 5.8 Hz, CH$_{Ar}$), 132.1 (CH$_{Ar}$), 131.0 (CH$_{Ar}$), 130.0 (d, *J* = 2.3 Hz, 3C, CH$_{Ar}$), 129.8 (CH$_{Ar}$), 127.6 (d, *J* = 10.6 Hz, 6C, CH$_{Ar}$), 126.0 (CH$_{Ar}$), 122.6 (CH$_{Ar}$), 121.6 (C$_q$), 118.7 (CH$_{Ar}$), 113.1 (CH$_{Ar}$), 55.3 (CH), 41.7 (d, *J* = 9.4 Hz, CH$_2$, *C*H$_2$-PCP), 36.4 (CH$_2$, *C*H$_2$-PCP), 35.1 (CH$_2$, *C*H$_2$-PCP), 35.0 (CH$_2$, *C*H$_2$-PCP), 33.6 (CH$_2$), 33.3 (CH$_2$), 25.9 (CH$_2$), 24.5 (2C, CH$_2$).

³¹P NMR (202 MHz, CDCl$_3$) δ [ppm] = 31.38 (d, *J* = 12.3 Hz).

IR (ATR) $\tilde{\upsilon}$ [cm⁻¹] = 3278 (w), 3053 (w), 2922 (s), 2850 (m), 1632 (w), 1589 (w), 1499 (m), 1480 (w), 1434 (s), 1363 (w), 1349 (w), 1203 (w), 1188 (w), 1094 (m), 905 (w), 741 (vs), 691 (vs), 530 (vs), 511 (vs), 496 (s), 453 (w), 422 (w).

FAB-MS *m/z* (%):823 (19), 792 (25), 791 (23), 790 (47), 789 (35), 788 (78), 787 (45), 786 (26), 731 (24), 664 (30), 663 (69), 662 (40), 648 (22), 647 (48), 563 (20), 561 (20), 530 (28), 529 (33), 528 (51), 527 (53), 526 (71), 525 (69), 524 (55), 523 (28), 442 (20), 441 (38), 422 (41), 421 (52), 420 (100), 419 (28), 418 (37), 417 (21), 416 (19), 339 (23), 338 (26), 336 (30), 323 (20), 317 (20), 316 (22), 314 (24), 312 (22), 311 (50), 309 (25), 307 (22), 263 (26), 262 (26), 246 (19), 235 (21), 234 (41), 233 (27), 232 (25), 219 (40), 217 (19), 208 (21), 207 (38), 205 (20), 191 (24), 183 (25), 155 (27), 154 (79), 147 (42), 138 (24), 137 (28), 136 (37), 131 (25), 129 (21), 117 (19), 115 (24), 107 (23), 105 (30), 95 (25), 91 (39).

HRMS-FAB (*m/z*): [M + H]⁺ calcd. for C$_{47}$H$_{45}$N$_3$³⁵ClP¹⁰⁶Pd, 823.2069; found, 823.2070.

4-Methyl-1,1'-biphenyl (106)
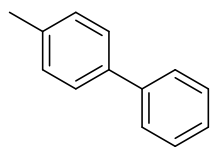
A 4-halotoluene (1.09 mmol, 1.00 equiv), phenylboronic acid (199 mg, 1.63 mmol, 1.50 equiv), palladacycle **16** (9.00 mg, 10.9 µmol, 0.01 equiv) and potassium phosphate (463 mg, 2.18 mmol, 2.00 equiv) were dissolved in anhydrous toluene (5.5 mL). and heated to 110 °C for 1 d. The solvent was removed under reduced pressure, and the residue was purified *via* flash chromatography (SiO$_2$, *n*-pentane/EtOAc 100:1). Biaryl **106** was isolated as a colorless solid.

4-Chlorotoluene (138 mg, 127 µL, 1.09 mmol, 1.00 equiv)   Yield: 35 mg, 208 µmol, 19%

4-Bromotoluene (186 mg, 1.09 mmol, 1.00 equiv)   Yield: 80 mg, 476 µmol, 44%

4-Iodotoluene (238 mg, 1.09 mmol, 1.00 equiv)   Yield: 106 mg, 630 µmol, 58%

The analytical data is in agreement with literature.[117c]

^{1}H NMR (400 MHz, CDCl$_3$) δ [ppm] = 7.62 (dd, *J* = 7.2, 1.3 Hz, 2H, CH$_{Ar}$), 7.53 (d, *J* = 7.9 Hz, 2H, CH$_{Ar}$), 7.46 (t, *J* = 7.5 Hz, 2H, CH$_{Ar}$), 7.42 – 7.31 (m, 1H, CH$_{Ar}$), 7.29 (d, *J* = 7.2 Hz, 2H, CH$_{Ar}$), 2.43 (s, 3H, CH$_3$).

5.4.2 Design of Imidazo[1,2-*a*]pyridine-based Donor-Acceptor Chromophores

2-(4-Bromo-3,5-dimethylphenyl)-*N*-(*tert*-butyl)imidazo[1,2-*a*]pyridin-3-amine (112a)
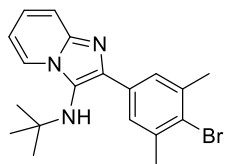
2-Aminopyridine (662 mg, 7.04 mmol, 1.00 equiv), 4-bromo-3,5-dimethylbenzaldehyde (1.50 g, 7.04 mmol, 1.00 equiv), *tert*-butyl isonitrile (585 mg, 802 µL, 7.04 mmol, 1.00 equiv) and a 1M solution of perchloric acid in methanol (70.7 mg, 704 µL, 704 µmol, 0.10 equiv) were dissolved in methanol (15 mL) and stirred at r.t. for 3 d. The solvent was removed under reduced pressure, and the residue was purified *via* flash chromatography (SiO$_2$, CH/EE 10:1 to 2:1). **112a** was isolated as a colorless solid (2.24 g, 6.02 mmol, 86%).

R$_f$ (CH/EtOAc 1:1) = 0.57.

¹H NMR (400 MHz, CDCl3) δ [ppm] = 8.19 (dt, J = 7.0, 1.2 Hz, 1H), 7.70 (s, 2H), 7.52 (dt, J = 9.0, 1.1 Hz, 1H), 7.12 (ddd, J = 9.1, 6.6, 1.3 Hz, 1H), 6.76 (td, J = 6.8, 1.2 Hz, 1H), 3.01 (s, 1H), 2.47 (s, 6H), 1.06 (s, 9H).

¹³C NMR (126 MHz, CDCl$_3$) δ [ppm] = 142.1 (C$_q$), 138.5 (C$_q$), 138.2 (2C, C$_q$), 133.6 (C$_q$), 127.8 (2C, CH$_{Ar}$), 126.8 (C$_q$), 124.4 (CH$_{Ar}$), 123.6 (C$_q$), 123.5 (CH$_{Ar}$), 117.4 (CH$_{Ar}$), 111.6 (CH$_{Ar}$), 56.6 (C$_q$), 27.1 (3C, CH$_3$), 24.0 (2C, CH$_3$).

IR (ATR) $\tilde{v}$ [cm^{-1}] = 3329 (w), 2969 (w), 2956 (w), 2927 (w), 1537 (w), 1504 (w), 1462 (m), 1442 (m), 1385 (m), 1373 (w), 1360 (vs), 1341 (vs), 1283 (w), 1213 (m), 1200 (m), 1181 (s), 1028 (s), 1014 (m), 941 (w), 884 (m), 786 (m), 749 (vs), 730 (vs), 717 (w), 698 (w), 674 (w), 606 (s), 569 (m), 486 (w), 455 (w), 442 (m), 384 (w).

FAB-MS *m/z* (%): 375 (20), 374 (93), 373 (59), 372 (100), 371 (37), 370 (5), 318 (12), 317 (29), 316 (48), 315 (28), 314 (39), 291 (13), 290 (5), 289 (30), 288 (5), 287 (16), 154 (6), 105 (6), 95 (7), 91 (6).

HRMS-FAB (m/z): [M + H]$^+$ calcd. for C$_{19}$H$_{23}$N$_3$Br, 372.1070; found, 372.1069.

2,2'-(2-Bromo-1,3-phenylene)bis(*N*-(*tert*-butyl)imidazo[1,2-*a*]pyridin-3-amine) (112b)
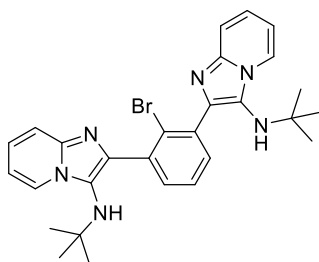
2-Aminopyridine (884 mg, 9.39 mmol, 2.00 equiv), 2-bromobenzene-1,3-dicarbaldehyde (1.00 g, 4.69 mmol, 1.00 equiv), *tert*-butyl isonitrile (781 mg, 1.06 mL, 9.39 mmol, 2.00 equiv) and a 1M solution of perchloric acid in methanol (94.3 mg, 939 µL, 939 µmol, 0.20 equiv) were dissolved in methanol (15 mL) and stirred at *r.t.* for 3 d. The solvent was removed under reduced pressure, and the residue was purified *via* flash chromatography (SiO$_2$, CH/EE 10:1 to 2:1). **112b** was isolated as a colorless solid (600 mg, 1.13 mmol, 24%).

R$_f$ (CH/EtOAc 1:1) = 0.19.

¹H NMR (400 MHz, CDCl$_3$) *δ* [ppm] = 8.30 (dt, J = 7.0, 1.2 Hz, 2H), 7.67 (d, J = 7.6 Hz, 2H), 7.56 (dt, J = 9.1, 1.1 Hz, 2H), 7.51 (t, J = 7.6 Hz, 1H), 7.17 (ddd, J = 9.1, 6.6, 1.3 Hz, 2H), 6.80 (td, J = 6.7, 1.2 Hz, 2H), 3.11 (s, 2H), 0.96 (s, 18H).

¹³C NMR (126 MHz, CDCl₃) δ [ppm] = 142.1 (2C, C$_q$), 139.9 (C$_q$), 137.8 (2C, C$_q$), 133.0 (2C, CH$_{Ar}$), 127.5 (CH$_{Ar}$), 124.9 (2C, C$_q$), 124.2 (2C, CH$_{Ar}$), 123.8 (2C, CH$_{Ar}$), 123.6 (2C, C$_q$), 117.6 (2C, CH$_{Ar}$), 111.5 (2C, CH$_{Ar}$), 56.1 (2C, C$_q$), 30.3 (6C, CH$_3$).

IR (ATR) $\tilde{v}$ [cm⁻¹] = 3336 (w), 2962 (w), 2929 (w), 2866 (w), 1626 (w), 1550 (w), 1494 (w), 1472 (w), 1453 (w), 1363 (vs), 1334 (s), 1272 (w), 1239 (w), 1220 (m), 1210 (vs), 1174 (m), 1150 (w), 1129 (w), 1103 (w), 1020 (w), 1000 (w), 833 (w), 809 (w), 783 (w), 758 (vs), 737 (m), 722 (s), 713 (w), 696 (m), 666 (w), 622 (m), 612 (m), 596 (s), 584 (m), 571 (w), 533 (w), 517 (w), 482 (w), 456 (w), 446 (w), 428 (w), 409 (w), 397 (w), 375 (w).

FAB-MS *m/z* (%): 534 (32), 533 (98), 532 (59), 531 (100), 530 (31), 476 (15), 475 (25), 474 (15), 473 (20), 420 (9), 419 (8), 418 (9), 417 (7), 337 (7), 310 (6), 233 (6), 154 (10), 136 (7).

HRMS-FAB (m/z): [M + H]⁺ calcd. for C$_{28}$H$_{32}$N$_6$⁷⁹Br, 531.1866; found, 531.1867.

2,2'-(5-Bromo-1,3-phenylene)bis(*N*-(*tert*-butyl)imidazo[1,2-*a*]pyridin-3-amine) (112c)
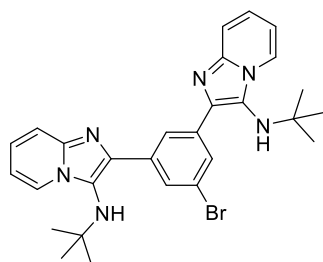
2-Aminopyridine (2.21 g, 23.5 mmol, 2.00 equiv), 5-bromobenzene-1,3-dicarbaldehyde (2.50 g, 11.7 mmol, 1.00 equiv), *tert*-butyl isonitrile (1.95 g, 2.67 mL, 23.5 mmol, 2.00 equiv) and a 1M solution of perchloric acid in methanol (235 mg, 2.35 mL, 2.35 mmol, 0.20 equiv) were dissolved in methanol (25 mL) and stirred at r.t. for 3 d. The solvent was removed under reduced pressure, and the residue was purified *via* flash chromatography (SiO₂, CH/EE/NEt₃ 7:1:0.02 to 1:3:0.02). **112c** was isolated as a colorless solid (2.07 g, 8.89 mmol, 33%).

R$_f$ (SiO₂, CH/EtOAc 1:1) = 0.11.

¹H NMR (500 MHz, CDCl₃) δ [ppm] = 8.52 (t, *J* = 1.5 Hz, 1H), 8.26 (dt, *J* = 6.9, 1.2 Hz, 2H), 8.11 (d, *J* = 1.5 Hz, 2H), 7.57 (dt, *J* = 9.0, 1.1 Hz, 2H), 7.19 (ddd, *J* = 9.0, 6.6, 1.3 Hz, 2H), 6.82 (td, *J* = 6.8, 1.2 Hz, 2H), 3.32 (s, 2H), 1.08 (s, 18H).

¹³C NMR (126 MHz, CDCl₃) δ [ppm] = 141.7 (2C, C$_q$), 136.8 (2C, C$_q$), 130.0 (2C, CH$_{Ar}$), 126.5 (CH$_{Ar}$), 125.0 (2C, CH$_{Ar}$), 124.2 (2C, C$_q$), 124.2 (C$_q$), 123.8 (2C, CH$_{Ar}$), 122.5 (2C, C$_q$), 117.3 (2C, CH$_{Ar}$), 112.0 (2C, CH$_{Ar}$), 56.6 (2C, C$_q$), 30.4 (6C, CH$_3$).

IR (ATR) $\tilde{v}$ [cm⁻¹] = 3353 (w), 2961 (m), 1562 (w), 1503 (w), 1361 (s), 1337 (s), 1204 (s), 1128 (m), 1077 (s), 878 (w), 766 (s), 752 (vs), 738 (vs), 707 (w), 690 (m), 622 (s), 438 (m).

FAB-MS *m/z* (%): 633 (7), 631 (5), 534 (27), 533 (83), 532 (40), 531 (100), 530 (13), 477 (7), 476 (13), 475 (27), 474 (12), 473 (17), 421 (6), 420 (17), 419 (21), 418 (17), 417 (18), 392 (9), 390 (6), 313 (6).

HRMS-FAB (m/z): [M+H]⁺ calcd. for C$_{28}$H$_{32}$N$_6$⁷⁹Br, 531.1866; found, 531.1866.

2-(4,4,5,5-Tetramethyl-1,3,2-dioxaborolan-2-yl)anthraquinone (114)
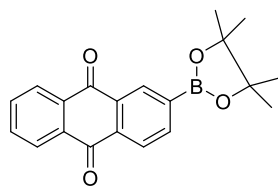
2-Bromoanthraquinone (5.00 g, 17.4 mmol, 1.00 equiv), bis(pinacol)diboron (5.75 g, 22.6 mmol, 1.30 equiv), Pd(dppf)Cl$_2$ CH$_2$Cl$_2$ (711 mg, 0.87 mmol, 5 mol%) and K$_2$CO$_3$ (6.84 g, 69.6 mmol, 4.00 equiv) were dissolved in 1,4-dioxane (125 mL). The mixture was heated to 84 °C for 41 h. Subsequently, the reaction was quenched with water. The resulting mixture was extracted with ethyl acetate and the combined organic phases were dried over Na$_2$SO$_4$. The solvent was removed under reduced pressure, and the residue was purified *via* flash chromatography (SiO$_2$, CH/CHCl$_3$ 10:1 to 4:1). **114** was isolated as a yellow solid (5.80 g, 17.3 mmol, quant.).

R$_f$ (SiO$_2$, CH/EtOAc 4:1) = 0.53.

^{1}H NMR (500 MHz, CDCl$_3$) δ [ppm] = 8.75 (d, J = 1.2 Hz, 1H, CH$_{Ar}$), 8.36–8.29 (m, 2H, CH$_{Ar}$), 8.29–8.27 (m, 1H, CH$_{Ar}$), 8.20 (dd, J = 7.7, 1.2 Hz, 1H, CH$_{Ar}$), 7.85–7.74 (m, 2H, CH$_{Ar}$), 1.38 (s, 12H, CH$_3$).

^{13}C NMR (126 MHz, CDCl$_3$) δ [ppm] = 183.6 (C$_q$, CO), 183.3 (C$_q$, CO), 140.2 (CH$_{Ar}$), 135.2 (C$_q$), 134.3 (CH$_{Ar}$), 134.2 (CH$_{Ar}$), 133.9 (CH$_{Ar}$), 133.7 (C$_q$), 133.7 (C$_q$), 132.6 (C$_q$), 127.4 (CH$_{Ar}$), 127.4 (C$_q$), 127.3 (CH$_{Ar}$), 126.3 (CH$_{Ar}$), 84.7 (2C, C$_q$), 25.1 (4C, CH$_3$).

IR (ATR) $\tilde{\nu}$ [cm^{-1}] = 2979 (w), 2965 (w), 2928 (w), 1673 (vs), 1591 (m), 1489 (m), 1375 (m), 1360 (s), 1332 (vs), 1310 (s), 1276 (vs), 1213 (m), 1169 (s), 1149 (vs), 1125 (vs), 1111 (vs), 1078 (s), 1034 (w), 976 (w), 955 (s), 939 (w), 929 (s), 860 (vs), 840 (m), 826 (m), 789 (w), 775 (w), 707 (vs), 691 (s), 680 (vs), 640 (m), 632 (s), 579 (w), 526 (w), 452 (w), 407 (w), 391 (s).

FAB-MS *m/z* (%): 336 (37), 335 (100), 334 (20), 307 (20), 155 (22), 154 (70), 139 (21), 138 (29), 137 (61), 136 (53), 107 (18).

HRMS-FAB (m/z): [M + H]$^+$ calcd. for C$_{20}$H$_{20}$O$_4$B, 335.1449; found, 335.1449.

2-(9,10-Dioxo-9,10-dihydroanthraquinone-2-yl)isophthalaldehyde (115)
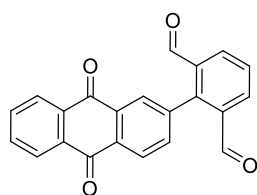
2-Bromobenz-1,3-dialdehyde (1.50 g, 7.04 mmol, 1.00 equiv), anthraquinone-2-pinacol borate (2.59 g, 7.75 mmol, 1.10 equiv), Pd(PPh$_3$)$_4$ (407 mg, 352 µmol, 5 mol%) und K$_2$CO$_3$ (4,87 g, 35.2 mmol, 5.00equiv) were dissolved in a 5:2:1 mixture of toluene, ethanol, and water (120 mL). The solution was reacted at 110 °C under argon atmosphere for 24 h. Subsequently, the solution was extracted with dichloromethane. The combined organic phases were dried over Na$_2$SO$_4$. The solvent was removed under reduced pressure, and the residue was purified *via* flash chromatography (SiO$_2$, CH/EE 10:1 to 3:1). **115** was obtained as a yellow solid (456 mg, 1.34 mmol, 19%).

R$_f$ (SiO$_2$, CH/EtOAc 1:1) = 0.69.

^{1}H NMR (500 MHz, CDCl$_3$) δ [ppm] = 9.83 (d, *J* = 0.7 Hz, 2H, CHO), 8.49 (d, *J* = 7.9 Hz, 1H, CH$_{Ar}$), 8.39 – 8.30 (m, 5H, CH$_{Ar}$), 7.89 – 7.74 (m, 4H, CH$_{Ar}$).

¹³C NMR (126 MHz, CDCl₃) δ [ppm] = 189.9 (2C, CH, CHO), 182.8 (C_q, CO), 182.6 (C_q, CO), 145.5 (2C, C_q), 139.6 (C_q), 135.8 (2C, CH_Ar), 134.7 (C_q), 134.7 (2C, CH_Ar), 133.8 (2C, CH_Ar), 133.6 (C_q), 133.3 (2C, CH_Ar), 129.7 (C_q), 129.0 (C_q), 127.7 (C_q), 127.6 (2C, CH_Ar).

IR (ATR) ṽ [cm⁻¹] = 1721 (w), 1672 (vs), 1589 (s), 1572 (m), 1323 (s), 1290 (s), 1230 (vs), 1177 (w), 1164 (m), 949 (m), 919 (s), 854 (m), 813 (m), 803 (s), 793 (m), 703 (vs), 671 (m), 635 (m), 626 (m), 540 (m), 487 (m), 378 (s).

FAB-MS *m/z* (%): 341 (11), 307 (22), 289 (13), 219 (9), 191 (9), 167 (9), 155 (30), 154 (100), 153 (10), 152 (10), 149 (9), 147 (13), 139 (17), 138 (37), 137 (65), 136 (71), 135 (9), 131 (10), 124 (11), 121 (11), 120 (12), 119 (13), 117 (9), 115 (10), 107 (24), 105 (13), 97 (11), 95 (13), 91 (23), 90 (10), 89 (18).

HRMS-FAB (m/z): [M + H]⁺ calcd. for C₂₂H₁₃O₄, 341.0808; found, 341.0807.

2-(4-(3-(*tert*-Butylamino)imidazo[1,2-*a*]pyridin-2-yl)-2,6-dimethylphenyl)anthraquinone (108)
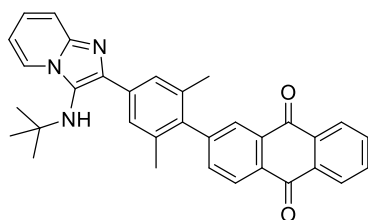
112a (111 mg, 29 µmol, 1.00 equiv), **114** (100 mg, 29 µmol, 1.00 equiv), Pd(OAc)₂ (3.36 mg, 14 µmol, 5 mol%), RuPhos (14 mg, 29 µmol, 1.00 equiv) and Cs₂CO₃ (293 mg, 89 µmol, 3.00 equiv) were dissolved in a mixture of toluene and water (4 mL). The mixture was stirred argon atmosphere for 24 h at 110 °C. The solvent was removed under reduced pressure, and the residue was purified *via* flash chromatography (SiO₂, CH/EE 7:1 to 1:1). **108** was obtained as an orange solid (91 mg, 18 µmol, 61%).

R_f (SiO₂, CH/EtOAc 1:1) = 0.43.

¹H NMR (500 MHz, CDCl₃) δ [ppm] = 8.39 (d, *J* = 7.9 Hz, 1H, CH_Ar), 8.35–8.31 (m, 2H, CH_Ar), 8.23 (dt, *J* = 6.9, 1.2 Hz, 1H, CH_Ar), 8.17 (d, *J* = 1.7 Hz, 1H, CH_Ar), 7.82–7.78 (m, 2H, CH_Ar), 7.76 (s, 2H, CH_Ar), 7.65 (dd, *J* = 7.9, 1.7 Hz, 1H, CH_Ar), 7.55 (dt, *J* = 9.0, 1.2 Hz, 1H, CH_Ar), 7.13 (ddd, *J* = 9.0, 6.6, 1.3 Hz, 1H, CH_Ar), 6.77 (td, *J* = 6.8, 1.2 Hz, 1H, CH_Ar), 3.12 (br, 1H, N*H*), 2.10 (s, 6H, CH₃), 1.11 (s, 9H, CH₃).

¹³C NMR (126 MHz, CDCl₃) δ [ppm] = 183.5 (C_q, CO), 183.2 (C_q, CO), 148.0 (C_q), 142.2 (C_q), 139.1 (C_q), 139.0 (C_q), 135.5 (C_q), 135.4 (CH_Ar), 134.9 (C_q), 134.3 (C_q), 134.2 (CH_Ar), 134.2 (CH_Ar), 133.7 (2C, C_q), 132.2 (C_q), 128.3 (CH_Ar), 127.7 (CH_Ar), 127.4 (CH_Ar), 127.4 (CH_Ar), 127.3 (CH_Ar), 127.3 (2C, CH_Ar), 124.1 (CH_Ar), 123.7 (C_q), 123.6 (CH_Ar), 117.5 (CH_Ar), 111.4 (CH_Ar), 56.3 (C_q), 30.4 (3C, CH₃), 20.8 (2C, CH₃).

IR (ATR) ṽ [cm⁻¹] = 2965 (w), 2921 (w), 1666 (vs), 1588 (s), 1445 (w), 1363 (w), 1343 (m), 1323 (s), 1299 (s), 1286 (s), 1268 (s), 1241 (s), 1214 (m), 1183 (m), 1159 (m), 1037 (w), 1031 (w), 1004 (w), 959 (w), 929 (s), 895 (w), 882 (m), 858 (m), 841 (w), 817 (w), 789 (w), 762 (vs), 741 (w), 731 (m), 710 (vs), 674 (m), 636 (w), 625 (w), 606 (w), 588 (m), 561 (w), 524 (w), 436 (m), 407 (m), 382 (m).

FAB-MS *m/z* (%): 500 (53), 155 (33), 154 (100), 138 (43), 137 (69), 136 (80), 107 (34), 95 (28), 91 (42).

2-(3,5-Bis(3-(*tert*-butylamino)imidazo[1,2-*a*]pyridin-2-yl)phenyl)anthraquinone (109)[191]
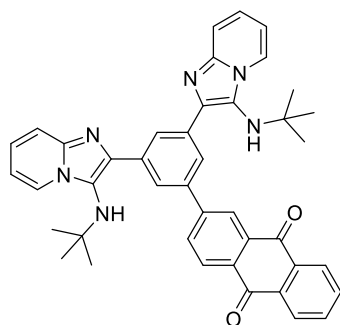
112b (159 mg, 290 µmol, 1.00 equiv), **114** (100 mg, 290 µmol, 1.00 equiv), RuPhos (14.3 mg, 29 µmol, 0.10 equiv), K_2CO_3 (124 mg, 890 µmol, 3.00 equiv) and Pd(OAc)$_2$ (3.36 mg, 14 µmol, 0.05 equiv) were dissolved under argon atmosphere in a mixture of toluene and water (25 mL) and stirred for 24 h at 110 °C. The solvent was removed under reduced pressure, and the residue was purified *via* flash chromatography (SiO$_2$, CH/EE 7:1 to 1:10). **109** was isolated as a red solid (656 mg, 995 µmol, 95%).

R_f (SiO$_2$, CH/EtOAc 1:6) = 0.16.

^{1}H NMR (400 MHz, CDCl$_3$) δ [ppm] = 8.71 (d, *J* = 1.9 Hz, 1H, CH$_{Ar}$), 8.64 (t, *J* = 1.6 Hz, 1H, CH$_{Ar}$), 8.41 (d, *J* = 8.1 Hz, 1H, CH$_{Ar}$), 8.39 – 8.31 (m, 4H, CH$_{Ar}$), 8.31 – 8.20 (m, 2H, CH$_{Ar}$), 7.87 – 7.77 (m, 2H, CH$_{Ar}$), 7.57 (dt, *J* = 9.0, 1.1 Hz, 2H, CH$_{Ar}$), 7.17 (ddd, *J* = 9.0, 6.6, 1.4 Hz, 2H, CH$_{Ar}$), 6.81 (td, *J* = 6.8, 1.2 Hz, 2H, CH$_{Ar}$), 3.34 (s, 2H, N*H*), 1.11 (s, 18H, CH$_3$).

^{13}C NMR (126 MHz, CDCl$_3$) δ [ppm] = 183.4 (2C, C$_q$, CO), 183.2 (2C, C$_q$, CO), 147.2 (C$_q$), 142.3 (2C, C$_q$), 139.2 (2C, C$_q$), 139.1 (C$_q$), 136.4 (2C, C$_q$), 134.3 (CH$_{Ar}$), 134.2 (CH$_{Ar}$), 134.0 (C$_q$), 133.9 (C$_q$), 132.8 (CH$_{Ar}$), 132.3 (C$_q$), 128.5 (CH$_{Ar}$), 128.2 (CH$_{Ar}$), 127.4 (CH$_{Ar}$), 126.3 (2C, CH$_{Ar}$), 125.8 (CH$_{Ar}$), 124.3 (2C, CH$_{Ar}$), 124.1 (2C, C$_q$), 123.7 (2C, CH$_{Ar}$), 117.5 (2C, CH$_{Ar}$), 111.6 (2C, CH$_{Ar}$), 56.8 (2C, C$_q$), 30.6 (6C, CH$_3$).

IR (ATR) ṽ [cm^{-1}] = 2965 (m), 2929 (w), 2904 (w), 2868 (w), 1732 (w), 1672 (vs), 1632 (w), 1591 (vs), 1504 (w), 1473 (w), 1460 (w), 1441 (w), 1390 (w), 1361 (vs), 1323 (vs), 1296 (vs), 1239 (s), 1215 (vs), 1201 (vs), 1162 (m), 1112 (m), 1044 (m), 975 (m), 931 (s), 887 (m), 853 (m), 795 (w), 754 (vs), 732 (vs), 711 (vs), 670 (s), 639 (s), 633 (s), 605 (s), 483 (s), 448 (s), 404 (s), 392 (s), 381 (s).

FAB-MS m/z (%): 661 (19), 660 (55), 659 (100) [M + H]$^+$, 658 (30), 602 (30), 601 (39), 546 (26), 545 (27), 484 (25), 483 (73), 441 (26).

HRMS-FAB (m/z): [M + H]$^+$ calcd. for C$_{42}$H$_{39}$O$_2$N$_6$, 659.3129; found, 659.3130.

2-(2,6-Bis(3-(*tert*-Butylamino)imidazo[1,2-*a*]pyridin-2-yl)phenyl)anthraquinone (110)[191]
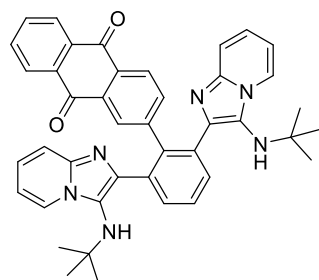
2-Aminopyridine (41.5 mg, 440 µmol, 2.00 equiv), **115** (75 mg, 220 µmol, 1.00 equiv), *tert*-butyl isonitrile (36.6 mg, 50 µL, 440 µmol, 2.00 equiv) and a 1 M solution of perchloric acid in methanol (4.42 mg, 44 µL, 44.0 µmol, 0.20 equiv) were dissolved in Chloroform and stirred at 60 °C for 1 d. The solvent was removed under reduced pressure, and the residue was purified *via* flash chromatography (SiO$_2$, CH/EE 5:1 to 1:10). **110** was isolated as an orange solid (134 mg, 203 µmol, 92%).

R_f (SiO$_2$, CH/EtOAc 1:6) = 0.06.

¹H NMR (500 MHz, CDCl₃) δ [ppm] = 8.71 (d, *J* = 1.9 Hz, 1H, CH$_{Ar}$), 8.64 (t, *J* = 1.6 Hz, 1H, CH$_{Ar}$), 8.39 – 8.31 (m, 4H, CH$_{Ar}$), 8.30 – 8.17 (m, 4H, CH$_{Ar}$), 7.87 – 7.78 (m, 2H, CH$_{Ar}$), 7.57 (dt, *J* = 8.9, 1.1 Hz, 2H, CH$_{Ar}$), 7.25 – 7.13 (m, 2H, CH$_{Ar}$), 6.80 (td, *J* = 6.8, 1.2 Hz, 2H, CH$_{Ar}$), 3.35 (s, 2H, N*H*), 1.10 (s, 18H, CH₃).

¹³C NMR (126 MHz, CDCl₃) δ [ppm] = 182.9 (C$_q$, CO), 181.9 (C$_q$, CO), 147.0 (C$_q$), 142.6 (2C, C$_q$) 139.3 (C$_q$), 137.7, 136.2 (CH$_{Ar}$), 135.2 (2C, C$_q$), 134.2 (2C, C$_q$), 133.2 (2C, CH$_{Ar}$), 133.7 (CH$_{Ar}$), 133.5 (C$_q$), 133.1 (C$_q$), 132.5 (2C, C$_q$), 131.7 (CH$_{Ar}$), 129.1 (CH$_{Ar}$), 128.9 (CH$_{Ar}$), 127.5 (CH$_{Ar}$), 127.3 (CH$_{Ar}$), 127.0 (CH$_{Ar}$), 124.6 (C$_q$), 124.4 (2C, CH$_{Ar}$), 123.5 (2C, CH$_{Ar}$), 117.4 (2C, CH$_{Ar}$), 111.4 (2C, CH$_{Ar}$), 56.7 (2C, C$_q$), 30.6 (6C, CH₃).

IR (ATR) ṽ [cm⁻¹] = 3369 (w), 2958 (w), 2924 (w), 2854 (w), 1672 (vs), 1630 (w), 1591 (m), 1554 (w), 1550 (w), 1500 (w), 1473 (w), 1455 (w), 1441 (w), 1388 (w), 1364 (m), 1339 (m), 1322 (s), 1299 (vs), 1266 (m), 1242 (m), 1221 (s), 1211 (s), 1198 (s), 1173 (m), 1146 (w), 1135 (w), 1081 (w), 972 (w), 962 (w), 952 (w), 931 (m), 907 (w), 857 (m), 817 (m), 756 (vs), 737 (vs), 710 (vs), 673 (m), 646 (w), 633 (w), 612 (w), 572 (w), 458 (w), 428 (w), 401 (w), 382 (s).

FAB-MS m/z (%): 665 (43), 664 (100), 662 (42), 661 (31), 660 (46), 659 (85), 658 (30), 648 (31), 647 (67), 530 (73), 219 (83), 191 (33), 163 (31), 161 (32), 159 (30), 154 (41), 149 (32), 147 (61), 136 (41), 131 (38), 119 (34), 107 (37), 105 (43), 97 (38), 95 (53), 91 (71).

HRMS-FAB (m/z): [M + H]⁺ calcd. for C₄₂H₃₉O₂N₆, 659.3129; found, 659.3127.

2-(2,6-Bis(3-(Cyclohexylamino)imidazo[1,2-*a*]pyridin-2-yl)phenyl)anthraquinone (110')[191]
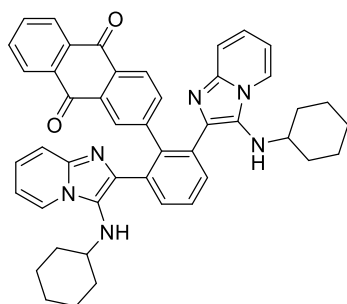
2-Aminopyridine (41.5 mg, 440 µmol, 2.00 equiv), cyclohexyl isonitrile (48.1 mg, 55 µL, 440 µmol, 2.00 equiv), **115** (75 mg, 220 µmol, 1.00 equiv) and a 1M solution of perchloric acid in methanol (4.43 mg, 44 µL, 44 µmol, 0.20 equiv) were dissolved in methanol (5 mL) and stirred at r.t. for 10 d. The solvent was removed under reduced pressure, and the residue was purified *via* flash chromatography (SiO₂, CH/EE 7:1 to 1:10). **110'** was isolated as a deep red solid (76 mg, 0.1 mmol, 49%).

R$_f$ (SiO₂, CH/EtOAc 1:6) = 0.06.

¹H NMR (500 MHz, CDCl₃) *δ* [ppm] = 8.30 – 8.20 (m, 2H, CH$_{Ar}$), 8.17 – 8.11 (m, 1H, CH$_{Ar}$), 8.09 (d, *J* = 1.8 Hz, 1H, CH$_{Ar}$), 7.95 (d, *J* = 8.0 Hz, 1H, CH$_{Ar}$), 7.89 – 7.66 (m, 6H, CH$_{Ar}$), 7.63 (dd, *J* = 8.1, 7.3 Hz, 2H, CH$_{Ar}$), 7.56 – 7.46 (m, 3H, CH$_{Ar}$), 7.10 (ddd, *J* = 9.1, 6.6, 1.3 Hz, 2H, CH$_{Ar}$), 6.65 (td, *J* = 6.7, 1.1 Hz, 2H, CH$_{Ar}$), 2.47 (s, 2H, N*H*), 1.53 – 0.66 (m, 22H).

¹³C NMR (126 MHz, CDCl₃) *δ* [ppm] = 183.0 (C$_q$, CO), 181.1 (C$_q$, CO), 146.9 (C$_q$), 141.9 (2C, C$_q$) 138.2 (C$_q$), 137.0, 136.3 (CH$_{Ar}$), 134.7 (2C, C$_q$), 134.4 (2C, C$_q$), 134.2 (2C, CH$_{Ar}$), 134.1 (CH$_{Ar}$), 133.6 (C$_q$), 133.1 (C$_q$), 132.1 (2C, C$_q$), 131.6 (CH$_{Ar}$), 128.9 (CH$_{Ar}$), 128.8 (CH$_{Ar}$), 127.4 (CH$_{Ar}$), 127.2 (CH$_{Ar}$), 126.9 (CH$_{Ar}$), 125.7 (C$_q$), 123.8 (2C, CH$_{Ar}$), 122.8 (2C, CH$_{Ar}$), 117.5 (2C, CH$_{Ar}$), 111.6 (2C, CH$_{Ar}$), 56.0 (2C, CH), 33.4 (4C, CH₂), 25.4 (2C, CH₂), 24.3 (4C, CH₂).

IR (ATR) $\tilde{v}$ [cm^{-1}] = 2924 (m), 2850 (w), 1670 (s), 1589 (s), 1558 (w), 1500 (w), 1448 (w), 1347 (m), 1322 (s), 1296 (vs), 1269 (s), 1244 (s), 1160 (w), 1146 (w), 1111 (w), 952 (w), 929 (m), 857 (w), 816 (w), 752 (vs), 738 (vs), 708 (vs), 670 (s), 635 (m), 381 (vs).

FAB-MS *m/z* (%): 713 (13), 712 (43), 711 (100) [M + H]$^+$, 710 (54), 709 (10), 137 (11), 136 (13), 95 (22)

HRMS-FAB (m/z): [M + H]$^+$ calcd. for $C_{46}H_{43}O_2N_6$, 711.3442; found, 711.3442.

5.4.3 Imidazo[1,2-*a*]pyridines as Fluorophore Tags for Bioimaging of Steroids

(20*R*)-20-((1*R*,2*S*)-2-(3-(Benzylamino)imidazo[1,2-*a*]pyridin-2-yl)cyclopropyl)pregn-5-en-3*β*-ol (118a)[120]
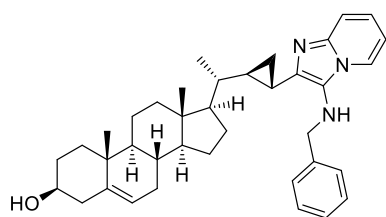
Steroidal aldehyde **117** (52.0 mg, 140 μmol, 1.00 equiv), 2-aminopyridine (26.4 mg, 281 μmol, 2.00 equiv), benzyl isonitrile (32.9 mg, 34.2 μL, 281 μmol, 2.00 equiv) and a 1 M solution of perchloric acid in methanol (14.0 μL, 14.0 μmol, 0.10 equiv) were reacted in 2:1 mixture of MeOH and CH$_2$Cl$_2$ (1.5 mL) for 3 d. The solvent was removed under reduced pressure and the residue was purified *via* flash chromatography (SiO$_2$, *n*-hexane/EtOAc:NEt$_3$ 2:1:0 to 1:2:0.01) and subsequent by recrystallization from iPrOH/water. **118a** was obtained as a yellow solid (40.3 mg, 71.5 μmol, 51%).

***R**$_f$* (SiO$_2$, *n*-pentane/EtOAc 1:2 + 1% NEt$_3$) = 0.43.

^{1}H NMR (500 MHz, CDCl$_3$) δ [ppm] = 7.91 (d, *J* = 6.8 Hz, 1H, CH$_{Ar}$), 7.41 (d, *J* = 8.1 Hz, 1H, CH$_{Ar}$), 7.41 – 7.31 (m, 4H, CH$_{Ar}$), 7.33 – 7.26 (m, 1H, CH$_{Ar}$), 7.03 (t, *J* = 7.9 Hz, 1H, CH$_{Ar}$), 6.67 (t, *J* = 6.8 Hz, 1H, CH$_{Ar}$), 5.31 (dt, *J* = 5.4, 2.3 Hz, 1H), 4.19 (d, *J* = 4.0 Hz, 2H, CH$_2$), 3.52 (tt, *J* = 11.1, 4.7 Hz, 1H), 3.27 (t, *J* = 6.3 Hz, 1H, NH), 2.30 – 2.18 (m, 2H, CH$_2$), 2.01 (dt, *J* = 12.7, 3.5 Hz, 1H), 1.96 – 1.89 (m, 1H), 1.89 – 1.80 (m, 3H), 1.78 (dt, *J* = 9.0, 4.7 Hz, 1H), 1.69 (s, 1H, OH), 1.56 – 1.38 (m, 7H), 1.37 – 1.24 (m, 2H), 1.18 (td, *J* = 12.7, 4.5 Hz, 1H), 1.13 – 0.82 (m, 12H, contains: 1.08 (d, *J* = 6.7 Hz, 3H, CH$_3$), 1.00 (s, 3H, CH$_3$)), 0.67 (s, 3H, CH$_3$), 0.68 – 0.62 (m, 1H, CH$_2$).

^{13}C NMR (126 MHz, CDCl$_3$) δ [ppm] = 141.3 (C$_q$), 140.8 (C$_q$), 140.5 (C$_q$), 139.6 (C$_q$), 128.7 (2C, CH$_{Ar}$), 128.3 (2C, CH$_{Ar}$), 127.6 (CH$_{Ar}$), 125.2 (C$_q$), 122.9 (CH$_{Ar}$), 121.7 (CH$_{Ar}$), 121.6 (CH), 116.7 (CH$_{Ar}$), 111.0 (CH$_{Ar}$), 71.8 (CH), 58.0 (CH), 56.4 (CH), 53.5 (CH$_2$), 50.2 (CH), 42.4 (C$_q$), 42.3 (CH$_2$), 40.5 (CH), 39.6 (CH$_2$), 37.3 (CH$_2$), 36.5 (C$_q$), 31.9 (CH), 31.8 (CH$_2$), 31.7 (CH$_2$), 29.9 (CH), 28.4 (CH$_2$), 24.2 (CH$_2$), 21.1 (CH$_2$), 19.6 (CH$_3$), 19.4 (CH$_3$), 17.6 (CH), 13.2 (CH$_2$), 11.9 (CH$_3$).

IR (ATR) $\tilde{v}$ [cm^{-1}] = 3366 (w), 3312 (w), 3070 (vw), 3020 (vw), 2959 (m), 2949 (m), 2929 (m), 2884 (w), 2847 (m), 1635 (vw), 1579 (m), 1451 (m), 1349 (s), 1232 (w), 1176 (w), 1119 (w), 1058 (s), 1027 (m), 952 (w), 882 (w), 875 (w), 759 (vs), 737 (vs), 694 (s), 459 (m), 411 (w).

FAB-MS m/z (%) = 564 (100) [M+H]$^+$, 563 (46) [M]$^+$, 562 (31) [M–H]$^+$, 546 (7) [M–OH]$^+$, 515 (7), 472 (21), 307 (7), 290 (7).

HRMS-FAB (m/z): [M+H]$^+$calcd. for C$_{38}$H$_{50}$N$_3$O, 564.3948; found: 564.3947.

EA: calcd. for C$_{38}$H$_{49}$N$_3$O, C 80.95, H 8.76, N 7.45; found: C 79.71, H 8.90, N 7.03.

Specific rotation: $[\alpha]_D^{20}$ = –13.1° (c = 0.26, CHCl$_3$).

Methyl 3-(benzylamino)-2-((1S,2R)-2-(3β-hydroxypregn-5-en-20R-yl)cyclopropyl)imidazo[1,2-a]pyridine-5-carboxylate (118b)[120]
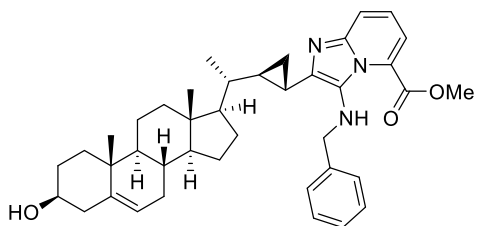
Steroidal aldehyde **117** (95.0 mg, 256 μmol, 1.00 equiv), methyl 6-aminopicolinate (78.0 mg, 513 μmol, 2.00 equiv), benzyl isonitrile (60.1 mg, 62.4 μL, 513 μmol, 2.00 equiv) and a 1 M solution of perchloric acid in methanol (25.6 μL, 25.6 μmol, 0.10 equiv) was reacted in a 2:1 mixture of MeOH and CH₂Cl₂ (1.5 mL). The solvent was removed under reduced pressure and the residue was purified *via* flash chromatography (SiO₂, *n*-hexane/EtOAc/NEt₃ 2:1:0 to 1:2:0.01), and subsequent recrystallization from iPrOH/water. **118b** was obtained as a bright orange solid (115 mg, 184 μmol, 72% yield).

R$_f$ (SiO₂, cyclohexane/EtOAc 1:1) = 0.49.

¹H NMR (500 MHz, CDCl₃) δ [ppm] = 7.60 (dd, *J* = 8.8, 1.2 Hz, 1H, CH$_{Ar}$), 7.25 – 7.21 (m, 4H, CH$_{Ar}$), 7.16 (dd, *J* = 7.5, 2.0 Hz, 2H, CH$_{Ar}$), 7.01 (dd, *J* = 8.8, 7.0 Hz, 1H, 6-H$_{Het}$), 5.30 (d, *J* = 4.9 Hz, 1H, 6-H), 4.12 – 4.00 (m, 2H, CH₂Ar), 3.88 (s, 3H, OCH₃), 3.91 – 3.82 (m, 1H, NH), 3.52 (tt, *J* = 10.6, 4.7 Hz, 1H, 3-H), 2.30 – 2.18 (m, 2H, 4-CH₂), 2.13 (dt, *J* = 9.0, 4.7 Hz, 1H), 2.02 (dt, *J* = 12.7, 3.6 Hz, 1H), 1.95 – 1.77 (m, 4H), 1.59 – 1.39 (m, 8H), 1.35 (q, *J* = 9.7 Hz, 1H), 1.19 (td, *J* = 12.9, 4.6 Hz, 1H), 1.13 – 0.86 (m, 12H, contains: 1.10 (d, *J* = 6.5 Hz, 3H, CH₃), 1.00 (s, 3H, CH₃)), 0.74 (ddd, *J* = 8.7, 6.0, 4.1 Hz, 1H, 3-CH₂), 0.67 (s, 3H, CH₃).

¹³C NMR (126 MHz, CDCl₃) δ [ppm] = 163.6 (C$_q$), 143.8 (C$_q$), 142.3 (C$_q$), 140.9 (C$_q$), 140.0 (C$_q$), 128.6 (2C, CH$_{Ar}$), 128.6 (C$_q$), 128.1 (2C, CH$_{Ar}$), 127.4 (CH$_{Ar}$), 126.4 (C$_q$), 121.8 (CH$_{Ar}$), 120.9 (CH$_{Ar}$), 120.6 (CH$_{Ar}$), 117.5 (CH$_{Ar}$), 71.9 (CH), 58.1 (CH), 56.6 (CH), 53.8 (CH₂), 53.0 (CH₃), 50.3 (CH), 42.6 (C$_q$), 42.5 (CH₂), 40.4 (CH), 39.8 (CH₂), 37.4 (CH₂), 36.6 (C$_q$), 32.1 (CH), 32.0 (CH₂), 31.8 (CH₂), 29.9 (CH), 28.4 (CH₂), 24.4 (CH₂), 21.2 (CH₂), 19.7 (CH₃), 19.5 (CH₃), 17.9 (CH), 14.1 (CH₂), 12.0 (CH₃).

IR (ATR) ṽ [cm⁻¹] = 3376 (w), 3251 (w), 2962 (m), 2924 (s), 2854 (m), 1706 (vs), 1565 (m), 1449 (s), 1434 (s), 1327 (s), 1281 (vs), 1245 (s), 1204 (vs), 1140 (vs), 1072 (vs), 1024 (s), 863 (m), 795 (s), 742 (vs), 694 (s).

HRMS-ESI (m/z): [M + H]⁺ calcd. for C₄₀H₅₂N₃O₃, 622.4003; found: 622.3996.

Specific rotation: $[\alpha]_D^{20}$ = −13.5° (c = 0.51, CHCl₃).

(20R)-20-((1R,2S)-2-(3-(((S)-1-Phenylethyl)amino)imidazo[1,2-a]pyrazin-2-yl)cyclopropyl)pregn-5-en-3β-ol (118c)[120]
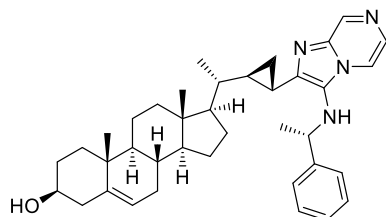
Steroidal aldehyde **117** (100 mg, 270 μmol, 1.00 equiv), 2-aminopyrazine (51.3 mg, 540 μmol, 2.00 equiv), (S)-methyl benzyl isonitrile (70.8 mg, 73.0 μL, 540 μmol, 2.00 equiv) and a 1 M solution of perchloric acid in methanol (27.0 μL, 27.0 μmol, 0.100 equiv) were reacted in a 2:1 mixture of MeOH and CH_2Cl_2 (3 mL). The solvent was removed under reduced pressure and the residue was purified by flash column chromatography (SiO_2, n-hexane/EtOAc 2:1 to 1:2 + 1% NEt_3), and subsequent recrystallization from iPrOH/water. **118c** was obtained as an off-white crystalline solid (35.0 mg, 60.5 μmol, 22% yield).

R_f (SiO_2, n-pentane/EtOAc 1:2 + 1% NEt_3) = 0.31.

^{1}H NMR (500 MHz, $CDCl_3$) δ [ppm] = 8.79 (d, J = 1.5 Hz, 1H, CH_{Ar}), 7.79 (dd, J = 4.6, 1.5 Hz, 1H, CH_{Ar}), 7.70 (d, J = 4.5 Hz, 1H, CH_{Ar}), 7.40 – 7.36 (m, 2H, CH_{Ar}), 7.35 – 7.30 (m, 2H, CH_{Ar}), 7.30 – 7.24 (m, 1H, CH_{Ar}), 5.32 (dt, J = 5.7, 1.9 Hz, 1H, 6), 4.40 (qd, J = 6.6, 4.0 Hz, 1H, CH), 3.57 – 3.43 (m, 1H), 3.30 (d, J = 4.2 Hz, 1H, NH), 2.31 – 2.18 (m, 2H, CH_2), 2.02 (dt, J = 12.7, 3.5 Hz, 1H), 1.94 (dtd, J = 16.7, 4.8, 2.3 Hz, 1H), 1.89 – 1.74 (m, 4H), 1.68 (s, 1H, OH), 1.57 – 1.34 (m, 12H, contains: 1.48 (d, J = 6.6 Hz, 3H, CH_3), 1.34 (q, J = 9.5 Hz, 1H)), 1.20 (td, J = 12.8, 4.5 Hz, 1H), 1.13 – 0.89 (m, 12H, contains: 1.09 (d, J = 6.6 Hz, 3H, CH_3), 1.01 (s, 3H, CH_3)), 0.77 (ddd, J = 8.5, 6.1, 4.1 Hz, 1H, CH_2), 0.68 (s, 3H, CH_3).

^{13}C NMR (126 MHz, $CDCl_3$) δ [ppm] = 145.0 (C_q), 144.3 (C_q), 142.2 (CH_{Ar}), 141.0 (C_q,), 136.9 (C_q), 128.9 (2C, CH_{Ar}), 128.8 (CH_{Ar}), 127.9 (CH_{Ar}), 126.6 (2C, CH_{Ar}), 126.0 (C_q), 121.7 (CH_{Ar}), 115.1 (CH_{Ar}), 71.9 (CH), 58.8 (CH_{Ar}), 58.0 (CH), 56.5 (CH), 50.3 (CH), 42.6 (C_q), 42.4 (CH_2), 40.4 (CH), 39.7 (CH_2), 37.4 (CH_2), 36.6 (C_q), 32.1 (CH), 32.0 (CH_2), 31.8 (CH_2), 30.4 (CH), 28.4 (CH_2), 24.4 (CH_2), 23.2 (CH_3), 21.2 (CH_2), 19.6 (CH_3), 19.5(CH_3), 17.8 (CH), 14.2 (CH_2), 12.0 (CH_3).

IR (ATR) $\tilde{\nu}$ [cm^{-1}] = 3309 (w), 3235 (w), 3030 (vw), 2963 (w), 2945 (m), 2924 (m), 2863 (m), 2827 (w), 1550 (s), 1493 (m), 1455 (m), 1350 (s), 1224 (m), 1179 (m), 1157 (m), 1061 (vs), 1023 (m), 914 (m), 788 (vs), 762 (s), 698 (vs), 541 (m), 407 (m).

HRMS-ESI (m/z): calcd. for $C_{38}H_{51}N_4O$, [M + H]$^+$: 579.4057; found: 579.4054.

EA: calcd. for $C_{38}H_{50}N_4O$, C 78.85, H 8.71, N 9.68; found: C 77.67, H 8.51, N 9.42.

Specific rotation: $[\alpha]_D^{20}$ = −20.2° (c = 0.49, $CHCl_3$).

(20R)-20-((1R,2S)-2-(3-(tert-Butylamino)imidazo[1,2-a]pyridin-2-yl)cyclopropyl)pregn-5-en-3β-ol (118d)[120]
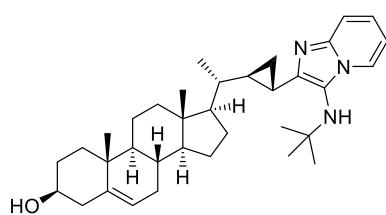
Steroidal aldehyde **117** (95.0 mg, 256 μmol, 1.00 equiv), 2-aminopyridine (48.3 mg, 513 μmol, 2.00 equiv), *tert*-butyl isonitrile (42.6 mg, 58.0 μL, 513 μmol, 2.00 equiv) and a 1 M solution of perchloric acid in methanol (14.0 μL, 14.0 μmol, 0.100 equiv) in a 2:1 mixture of MeOH/CH$_2$Cl$_2$ (3 mL). The solvent was removed under reduced pressure, and the residue was purified by flash column chromatography (SiO$_2$, *n*-hexane/EtOAc/NEt$_3$ 2:1:0 to 1:2:0.01) and subsequent recrystallization from iPrOH/water. **118d** was obtained as colorless crystals (64.3 mg, 121 μmol, 47% yield).

R$_f$ (SiO$_2$, *n*-pentane/EtOAc 1:2 + 1% NEt$_3$) = 0.42.

^{1}H NMR (500 MHz, CDCl$_3$) δ [ppm] = 8.12 (dt, *J* = 6.8, 1.3 Hz, 1H, CH$_{Ar}$), 7.39 (dt, *J* = 9.0, 1.2, 1.2 Hz, 1H, CH$_{Ar}$), 7.02 (ddd, *J* = 9.0, 6.6, 1.4 Hz, 1H, CH$_{Ar}$), 6.68 (td, *J* = 6.8, 1.2 Hz, 1H, CH$_{Ar}$), 5.29 (d, *J* = 5.5 Hz, 1H), 3.53 (tt, *J* = 10.4, 4.6 Hz, 1H), 2.78 (s, 1H, NH), 2.29 – 2.17 (m, 2H, CH$_2$), 2.12 (s, 1H, OH), 2.01 (dt, *J* = 12.7, 3.4 Hz, 1H), 1.97 – 1.70 (m, 5H), 1.56 – 1.34 (m, 9H, contains: 1.32 (q, *J* = 9.5 Hz, 1H)), 1.23 (s, 9H, CH$_3$), 1.22 – 1.13 (m, 1H), 1.12 – 0.88 (m, 12H, contains: 1.07 (d, *J* = 6.5 Hz, 3H, CH$_3$), 1.00 (s, 3H, CH$_3$)), 0.69 (ddd, *J* = 8.6, 6.0, 4.1 Hz, 1H, CH$_2$), 0.67 (s, 3H, CH$_3$).

^{13}C NMR (126 MHz, CDCl$_3$) δ [ppm] = 142.7 (C$_q$), 141.9 (C$_q$), 141.0 (C$_q$), 123.2 (C$_q$), 123.1 (CH$_{Ar}$), 122.9 (CH$_{Ar}$), 121.6 (CH$_{Ar}$), 116.6 (CH$_{Ar}$), 110.7 (CH$_{Ar}$), 71.8 (CH), 58.0 (CH), 56.6 (CH), 55.8 (C$_q$), 50.4 (CH), 42.53 (C$_q$), 42.51 (CH$_2$), 40.4 (CH), 39.7 (CH$_2$), 37.5 (CH$_2$), 36.6 (C$_q$), 32.0 (CH), 31.9 (CH$_2$), 31.7 (CH$_2$), 30.6 (3C, CH$_3$), 29.8 (CH), 28.4 (CH$_2$), 24.4 (CH$_2$), 21.2 (CH$_2$), 19.6 (CH$_3$), 19.5 (CH$_3$), 18.3 (CH), 13.6 (CH$_2$), 12.0 (CH$_3$).

IR (ATR) $\tilde{v}$ [cm^{-1}] = 3339 (w), 3201 (w), 3077 (vw), 2963 (m), 2946 (s), 2925 (s), 2884 (m), 2863 (m), 2827 (w), 1633 (w), 1585 (w), 1506 (w), 1465 (m), 1445 (m), 1373 (m), 1356 (s), 1218 (m), 1203 (m), 1074 (m), 1065 (s), 905 (m), 748 (s), 730 (vs), 497 (m), 458 (m).

HRMS-ESI (m/z): [M + H]$^+$ calcd. for C$_{35}$H$_{52}$N$_3$O, 530.4105; found: 530.4098.

Specific rotation: $[\alpha]_D^{20}$ = +42.3° (c = 0.57, CHCl$_3$).

(20R)-3β-((3-(Cyclohexylamino)imidazo[1,2-a]pyridin-2-yl)methoxy)-20-((1S,2S)-2-propylcyclopropyl)pregn-5-en (120)[120]
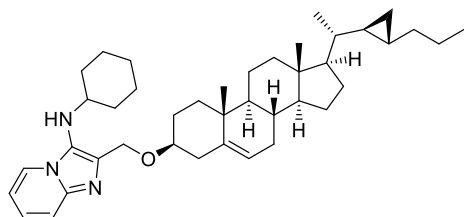
Steroidal aldehyde **119** (52.0 mg, 122 μmol, 1.00 equiv), 2-aminopyridine (22.9 mg, 244 μmol, 2.00 equiv), cyclohexyl isonitrile (26.6 mg, 29.9 μL, 244 μmol, 2.00 equiv) and a 1 M solution of perchloric acid in methanol (12.2 μL, 12.2 μmol, 0.100 equiv) were reacted in a 2:1 mixture of MeOH/CH$_2$Cl$_2$ (1.5 mL). The solvent was removed under reduced pressure and the residue was purified by flash column chromatography (SiO$_2$, n-pentane/EtOAc/NEt$_3$ 1:1:0.01). **120** was obtained as a yellow solid (66.7 mg, 109 μmol, 89%).

R$_f$ (SiO$_2$, n-pentane/EtOAc 1:2 + 1% NEt$_3$) = 0.25.

^{1}H NMR (500 MHz, CDCl$_3$): δ [ppm] = 8.02 (dt, J = 6.9, 1.2 Hz, 1H, CH$_{Ar}$), 7.46 (dt, J = 9.0, 1.2 Hz, 1H, CH$_{Ar}$), 7.07 (ddd, J = 9.1, 6.6, 1.3 Hz, 1H, CH$_{Ar}$), 6.74 (td, J = 6.7, 1.2 Hz, 1H, CH$_{Ar}$), 5.36 (dt, J = 5.6, 2.1 Hz, 1H, 6-H), 4.82 – 4.68 (m, 2H, CH$_2$), 3.35 (tt, J = 11.2, 4.5 Hz, 1H), 3.24 (s, 1H, NH), 2.97 – 2.84 (m, 1H, CH), 2.46 (ddd, J = 13.2, 4.8, 2.4 Hz, 1H, CH$_2$), 2.28 (tq, J = 13.4, 11.4, 2.7 Hz, 1H, CH$_2$), 2.06 – 1.83 (m, 7H), 1.81 – 1.70 (m, 2H), 1.66 – 1.32 (m, 11H), 1.31 – 1.13 (m, 7H), 1.12 – 0.86 (m, 13H, contains: 1.00 (s, 3H, CH$_3$), 0.96 (d, J = 6.6 Hz, 3H, CH$_3$), 0.89 (t, J = 7.4 Hz, 3H, CH$_3$)), 0.82 (dtd, J = 13.3, 8.5, 6.5 Hz, 1H), 0.70 – 0.59 (m, 1H), 0.62 (s, 3H, CH$_3$), 0.59 – 0.52 (m, 1H), 0.19 (tt, J = 9.0, 4.8 Hz, 1H), 0.10 – 0.03 (m, 2H).

^{13}C NMR (126 MHz, CDCl$_3$): δ [ppm] = 141.3 (C$_q$), 140.9 (C$_q$), 134.7 (C$_q$), 127.0 (C$_q$), 123.1 (CH$_{Ar}$), 122.6 (CH$_{Ar}$), 121.7 (CH$_{Ar}$), 117.6 (CH$_{Ar}$), 111.4 (CH$_{Ar}$), 78.8 (CH), 64.1 (CH$_2$), 58.2 (CH), 57.1 (CH), 56.6 (CH), 50.3 (CH), 42.4 (C$_q$), 40.4 (CH), 39.7 (CH$_2$), 39.1 (CH$_2$), 37.2 (CH$_2$), 36.9 (C$_q$), 36.5 (CH$_2$), 34.3 (2C, CH$_2$), 32.0 (2C, CH$_2$ and CH), 28.3 (CH$_2$), 27.8 (CH$_2$), 26.9 (CH), 25.8 (CH$_2$), 25.0 (2C, CH$_2$), 24.4 (CH$_2$), 22.4 (CH$_2$), 21.1 (CH$_2$), 20.5 (CH), 19.9 (CH$_3$), 19.4 (CH$_3$), 14.2 (CH$_3$), 11.9 (CH$_3$), 9.5 (CH$_2$).

IR (ATR) $\tilde{v}$ [cm^{-1}] = 3281 (vw), 3055 (vw), 2927 (vs), 2850 (s), 1632 (vw), 1567 (w), 1504 (w), 1452 (m), 1445 (m), 1336 (s), 1079 (vs), 1017 (m), 803 (w), 752 (s), 735 (vs), 596 (w), 426 (w).

HRMS-ESI (m/z): [M + H]$^+$ calcd. for C$_{41}$H$_{62}$N$_3$O, 612.4887; found: 612.4871.

EA: calcd. for C$_{41}$H$_{61}$N$_3$O C 80.47, H 10.05, N 6.87; found: C 80.11, H 9.99, N 6.73.

Specific rotation: $[\alpha]_D^{20}$ = −13.2° (c = 0.33, CHCl$_3$).

5.4.4 DNA Flat *N*-rich Heterocycles as DNA-Intercalating Agents

2-(2-Bromophenyl)-*N*-(*tert*-butyl)imidazo[1,2-*a*]pyridine-3-amine (128a)
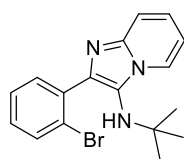
2-Aminopyridine (300 mg, 3.19 mmol, 1.00 equiv), 2-bromobenzaldehyde (590 mg, 0.38 mL, 3.19 mmol, 1.00 equiv), *tert*-butyl isonitrile (265 mg, 0.30 mL, 3.19 mmol, 1.00 equiv) and glacial acetic acid (383 mg, 0.37 mL, 6.37 mmol, 2.00 equiv) were reacted in methanol (10 mL) for 3 d. The solvent was removed under reduced pressure and the residue was purified *via* flash chromatography (SiO$_2$, CH/EtOAc/NEt$_3$ 6:1:0.01 to 0:1:0.04). GBB product **128a** was obtained as a white solid (775 mg, 2.25 mmol, 71%).

R_f (SiO$_2$, CH/EtOAc 1:1) = 0.27.

^{1}H NMR (400 MHz, CDCl$_3$) δ [ppm] = 8.30 (dd, *J* = 6.9, 1.2 Hz, 1H, C*H*$_{Ar}$), 7.64 (ddd, *J* = 7.8, 1.5 Hz, 2H, C*H*$_{Ar}$), 7.53 (dd, *J* = 9.1, 1.1 Hz, 1H, C*H*$_{Ar}$), 7.39 (td, *J* = 7.5 , 1.3 Hz, 1H, C*H*$_{Ar}$), 7.28 – 7.09 (m, 2H, C*H*$_{Ar}$), 6.79 (td, *J* = 6.8, 1.2 Hz, 1H, C*H*$_{Ar}$), 3.21 (s, 1H, N*H*), 0.92 (s, 9H, C*H*$_3$).

^{13}C NMR (101 MHz, CDCl$_3$) δ [ppm] = 157.0 (C$_q$), 142.1 (C$_q$), 139.3 (C$_q$), 137.1 (C$_q$), 133.2 (CH$_{Ar}$), 132.7 (CH$_{Ar}$), 129.5 (CH$_{Ar}$), 127.6 (CH$_{Ar}$), 123.8 (CH$_{Ar}$), 122.2 (C$_q$), 117.5 (CH$_{Ar}$), 111.5 (CH$_{Ar}$), 101.4 (CH$_{Ar}$), 55.9 (C$_q$), 30.1 (3C, CH$_3$).

IR (ATR) $\tilde{v}$ [cm^{-1}] = 3228 (w), 2962 (w), 2861 (w), 1629 (w), 1553 (w), 1500 (w), 1468 (w), 1431 (w), 1384 (m), 1353 (m), 1337 (s), 1271 (w), 1222 (s), 1205 (m), 1197 (m), 1142 (w), 1024 (m), 946 (w), 918 (w), 809 (w), 752 (vs), 738 (vs), 727 (s), 715 (m), 700 (s), 674 (w), 649 (m), 608 (m), 582 (w), 571 (w), 524 (w), 486 (w), 465 (w), 416 (m).

FAB-MS *m/z* (%): 290 (10), 289 (26), 288 (30), 287 (25), 286 (20), 261 (13), 259 (10), 208 (5), 181 (12), 147 (8).

HRMS-FAB (*m/z*): [M + H]$^+$ calcd. for C$_{18}$H$_{18}$N$_4$, 290.1530; found, 290.1531.

2-(2-Bromophenyl)-*N*-(*tert*-butyl)imidazo[1,2-*a*]pyrazine-3-amine (128b)
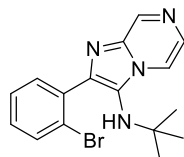
2-Aminopyrazine (300 mg, 3.15 mmol, 1.00 equiv), 2-bromobenzaldehyde (584 mg, 0.37 mL, 3.15 mmol, 1.00 equiv), *tert*-butyl isonitrile (262 mg, 0.36 mL, 3.15 mmol, 1.00 equiv) and glacial acetic acid (378 mg, 0.36 mL, 6.31 mmol, 2.00 equiv) were reacted in methanol (10 mL) for 3 d. The solvent was removed under reduced pressure and the residue was purified *via* flash chromatography (SiO$_2$, CH/EtOAc/NEt$_3$ 6:1:0.01 to 0:1:0.04). GBB product **128b** was obtained as a white solid(134 mg, 0.39 mmol, 12%).

R_f (SiO$_2$, CH/EtOAc 1:2) = 0.21.

^{1}H-NMR (400 MHz, CDCl$_3$) δ [ppm] = 9.00 (d, *J* = 1.5 Hz, 1H, C*H*$_{Ar}$), 8.21 (dd, *J* = 4.7, 1.5 Hz, 1H, C*H*$_{Ar}$), 7.88 (d, *J* = 4.7 Hz, 1H, C*H*$_{Ar}$), 7.66 (dd, *J* = 8.0, 1.2 Hz, 1H, C*H*$_{Ar}$), 7.62 (dd, *J* = 7.7, 1.8 Hz, 1H, C*H*$_{Ar}$), 7.43 (td, *J* = 7.5, 1.2 Hz, 1H, C*H*$_{Ar}$), 7.32 – 7.27 (m, 1H, C*H*$_{Ar}$), 2.97 – 2.85 (s, 1H, N*H*), 0.93 (s, 9H, C*H*$_3$).

¹³C-NMR (101 MHz, CDCl₃) δ [ppm] = 143.7 (CH$_{Ar}$), 142.0 (C$_q$), 137.4 (C$_q$), 135.9 (C$_q$), 133.1 (CH$_{Ar}$), 132.9 (CH$_{Ar}$), 130.2 (CH$_{Ar}$), 129.1 (CH$_{Ar}$), 127.8 (CH$_{Ar}$), 126.3 (C$_q$), 122.7 (C$_q$), 116.7 (CH$_{Ar}$), 56.4 (C$_q$), 30.1 (3C, CH₃).

IR (ATR) $\tilde{\upsilon}$ [cm⁻¹] = 3234 (w), 2962 (m), 1666 (m), 1596 (w), 1538 (w), 1488 (w), 1463 (m), 1433 (m), 1388 (m), 1362 (m), 1343 (m), 1311 (w), 1290 (w), 1209 (m), 1160 (w), 1026 (m), 916 (w), 814 (m), 759 (m), 710 (m), 658 (w), 607 (m), 465 (w), 438 (w), 417 (m).

FAB-MS *m/z* (%): 347 [M(⁸¹Br) + H]⁺ (98), 346 [M(⁸¹Br)]⁺ (49), 345 [M(⁷⁹Br) + H]⁺ (100), 344 [M(⁷⁹Br)]⁺ (24), 290 [M(⁸¹Br) – tBu + H]⁺ (31), 289 [M(⁸¹Br) – tBu]⁺ (24), 288 [M(⁷⁹Br) – tBu + H]⁺ (27).

HRMS-FAB (*m/z*): [M + H]⁺ calcd. for C₁₆H₁₈N₄⁷⁹Br, 345.0715; found, 345.0716.

2-(2-Bromopyridine)-*N*-(*tert.*-butyl)imidazo[1,2-*a*]pyridine-3-amine (128c)
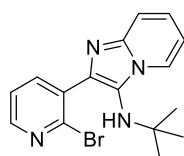
2-Aminopyridine (300 mg, 3.19 mmol, 1.00 equiv), 2-bromo-3-pyridinecarboxaldehyde (593 mg, 0.38 mL, 3.19 mmol, 1.00 equiv), *tert.*-butyl isonitrile (265 mg, 0.36 mL, 3.19 mmol, 1.00 equiv) and glacial acetic acid (383 mg, 0.37 mL, 6.37 mmol, 2.00 equiv) were reacted in methanol (10 mL) for 3 d. The solvent was removed under reduced pressure and the residue was purified *via* flash chromatography (SiO₂, CH/EtOAc/NEt₃ 6:1:0.01 to 0:1:0.04). **128c** was obtained as a white solid (223 mg, 0.65 mmol, 30%).

R_f (SiO₂, CH/EtOAc 1:2) = 0.13.

¹H-NMR (400 MHz, CDCl₃) δ [ppm] = 8.39 (dd, *J* = 4.7, 2.0 Hz, 1H, C*H*$_{Ar}$), 8.32 (dt, *J* = 6.9, 1.2 Hz, 1H, C*H*$_{Ar}$), 8.00 (dd, *J* = 7.6, 2.0 Hz, 1H, C*H*$_{Ar}$), 7.52 (d, *J* = 9.1 Hz, 1H, C*H*$_{Ar}$), 7.38 (dd, *J* = 7.6, 4.7 Hz, 1H, C*H*$_{Ar}$), 7.19 (ddd, *J* = 9.0, 6.6, 1.3 Hz, 1H, C*H*$_{Ar}$), 6.82 (td, *J* = 6.8, 1.1 Hz, 1H, C*H*$_{Ar}$), 3.22 (s, 1H, N*H*), 0.93 (s, 9H, C*H₃*).

¹³C-NMR (101 MHz, CDCl₃) δ [ppm] = 149.4 (CH$_{Ar}$), 142.5 (C$_q$), 141.7 (C$_q$), 141.4 (CH$_{Ar,}$), 137.1 (C$_q$), 134.8 (C$_q$), 125.0 (C$_q$), 124.9 (CH$_{Ar}$), 123.9 (CH$_{Ar}$), 122.9 (CH$_{Ar}$), 117.5 (CH$_{Ar}$), 111.9 (CH$_{Ar}$), 55.9 (C$_q$), 30.2 (3C, CH₃).

IR (ATR) $\tilde{\upsilon}$ [cm⁻¹] = 3227 (vw), 2961 (vw), 1647 (vw), 1550 (w), 1501 (w), 1398 (w), 1376 (w), 1352 (w), 1337 (w), 1224 (w), 1201 (w), 1151 (vw), 1119 (vw), 1047 (w), 918 (vw), 841 (vw), 801 (w), 760 (w), 740 (w), 726 (w), 710 (w), 684 (w), 611 (w), 524 (w), 444 (vw), 414 (w).

FAB-MS *m/z* (%): 347 [M(⁸¹Br) + H]⁺ (97), 346 [M(⁸¹Br)]⁺ (57), 345 [M(⁷⁹Br) + H]⁺ (100), 344 [M(⁷⁹Br)]⁺ (39), 290 [M(⁸¹Br) – tBu + H]⁺ (25), 289 [M(⁸¹Br) – tBu]⁺ (22), 288 [M(⁷⁹Br) – tBu + H]⁺ (24), 287 [M(⁷⁹Br) – tBu]⁺ (12).

HRMS-FAB (*m/z*): [M + H]⁺ calcd. for C₁₆H₁₈N₄⁷⁹Br, 345.0715; found, 345.0716.

EA C₁₆H₁₇N₄Br: calcd., C 55.66, H 4.96, N 16.23; found, C 54.28, H 4.92, N 15.01.

2-(2-Bromophenyl)-*N*-(*tert*-butyl)-5-methoxyimidazo[1,2-*a*]pyridin-3-amine (128d)
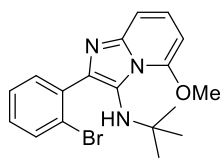
6-Methoxy-2-aminopyridine (300 mg, 3.19 mmol, 1.00 equiv), 2-bromobenzaldehyde (447 mg, 0.38 mL, 3.19 mmol, 1.00 equiv), *tert*-butyl isonitrile (201 mg, 0.36 mL, 3.19 mmol, 1.00 eq.) and glacial acetic acid (290 mg, 0.28 mL, 6.38 mmol, 2.00 equiv) were reacted in methanol (10 mL) for 3 d. The solvent was removed under reduced pressure and the residue was purified *via* flash chromatography (SiO₂, CH/EtOAc/NEt₃ 6:1:0.01 to 0:1:0.04). **128d** was obtained as a colorless solid (865 mg, 2.39 mmol, 95%).

R_f (SiO₂, CH/EtOAc 2:1) = 0.05.

¹H NMR (400 MHz, CDCl₃) δ [ppm] = 7.64 (dd, *J* = 8.1, 1.3 Hz, 1H, C*H*$_{Ar}$), 7.59 (dd, *J* = 7.7, 1.8 Hz, 1H, C*H*$_{Ar}$), 7.33 (td, *J* = 7.5, 1.2 Hz, 1H, C*H*$_{Ar}$), 7.20 – 7.14 (m, 2H, C*H*$_{Ar}$), 7.05 (dd, *J* = 9.0, 7.4 Hz, 1H, C*H*$_{Ar}$), 5.96 (dd, *J* = 7.4, 0.9 Hz, 1H, C*H*$_{Ar}$), 4.03 (s, 3H, C*H*₃), 0.88 (s, 9H, C*H*₃).

¹³C NMR (101 MHz, CDCl₃) δ [ppm] = 152.3 (C$_q$), 143.6 (C$_q$), 138.4 (C$_q$), 136.9 (C$_q$), 133.3 (CH$_{Ar}$), 133.0 (CH$_{Ar}$), 129.1 (CH$_{Ar}$), 127.1 (C$_q$), 126.5 (CH$_{Ar}$), 124.8 (CH$_{Ar}$), 123.9 (C$_q$), 111.0 (CH$_{Ar}$), 88.6 (CH$_{Ar}$), 56.0 (CH₃), 56.0 (C$_q$), 29.9 (3C, CH₃).

IR (ATR) $\tilde{v}$ [cm⁻¹] = 3399 (vw), 2968 (w), 1637 (w), 1597 (w), 1537 (w), 1509 (w), 1439 (w), 1420 (w), 1361 (w), 1308 (w), 1270 (w), 1202 (w), 1109 (w), 1020 (w), 972 (w), 849 (vw), 767 (m), 754 (m), 720 (w), 683 (w), 639 (w), 541 (w), 449 (w).

FAB-MS *m/z* (%): 376 [M(⁸¹Br) + H]⁺ (92), 375 [M(⁸¹Br)]⁺ (100), 374 [M(⁷⁹Br) + H]⁺ (94), 373 [M(⁷⁹Br)]⁺ (89), 319 [M(⁸¹Br) – tBu + H]⁺ (14), 318 [M(⁸¹Br) – tBu]⁺ (36), 317 [M(⁷⁹Br) – tBu + H]⁺ (16), 316 [M(⁷⁹Br) – tBu]⁺ (34).

HRMS-FAB (*m/z*): [M + H]⁺ calcd. for C₁₈H₂₁O₁N₃⁷⁹Br, 374.0868; found, 374.0869.

2-(2-Bromo-4,5-dimethoxyphenyl)-*N*-(*tert*-butyl)imidazo[1,2-*a*]pyridine-3-amine (128e)
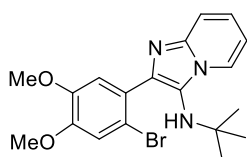
2-Aminopyridine (300 mg, 3.19 mmol, 1.00 equiv), 2-bromo-4,5-dimethoxybenzaldehyde (593 mg, 0.38 mL, 3.19 mmol, 1.00 equiv), *tert*-butyl isonitrile (265 mg, 0.36 mL, 3.19 mmol, 1.00 equiv) and glacial acetic acid (383 mg, 0.36 mL, 6.37 mmol, 2.00 equiv) were reacted in methanol (10 mL) for 3 d. The solvent was removed under reduced pressure and the residue was purified *via* flash chromatography (SiO₂, CH/EtOAc/NEt₃ 6:1:0.01 to 0:1:0.04). GBB product **128e** was obtained as a white solid (223 mg, 0.65 mmol, 30%).

R_f (SiO₂, CH/EtOAc 1:2) = 0.21.

¹H-NMR (400 MHz, CDCl₃) δ [ppm] = 8.30 (dt, *J* = 6.9, 1.2 Hz, 1H, C*H*$_{Ar}$), 7.51 (dd, *J* = 9.0, 1.1 Hz, 1H, C*H*$_{Ar}$), 7.17 (s, 1H, C*H*$_{Ar}$), 7.16 – 7.11 (m, 1H, C*H*$_{Ar}$), 7.06 (s, 1H, C*H*$_{Ar}$), 6.78 (td, *J* = 6.7, 1.2 Hz, 1H, C*H*$_{Ar}$), 3.92 – 3.85 (m, 6H, OC*H*₃), 2.01 (s, 1H, N*H*), 0.94 (s, 9H, C*H*₃).

¹³C-NMR (101 MHz, CDCl₃) δ [ppm] = 149.5 (C$_q$), 148.6 (C$_q$), 142.0 (C$_q$), 139.2 (C$_q$), 129.3 (C$_q$), 124.6 (C$_q$), 124.2 (CH$_{Ar}$), 123.8 (CH$_{Ar}$), 117.4 (CH$_{Ar}$), 115.1 (CH$_{Ar}$), 115.0 (CH$_{Ar}$), 112.8 (C$_q$), 111.4 (CH$_{Ar}$), 56.3 (CH₃), 55.9 (CH₃), 30.1 (3C, CH₃), 27.0 (C$_q$).

IR (ATR) $\tilde{\upsilon}$ [cm⁻¹] = 3344 (vw), 2964 (w), 1740 (w), 1684 (w), 1631 (w), 1604 (w), 1503 (s), 1462 (m), 1440 (m), 1405 (m), 1341 (m), 1249 (m), 1205 (s), 1172 (m), 1026 (m), 952 (w), 912 (w), 861 (w), 833 (w), 756 (m), 728 (m), 642 (w), 599 (w), 498 (w), 418 (w).

FAB-MS *m/z* (%): 406 [M(^{81}Br) + H]⁺ (99), 405 [M(^{81}Br)]⁺ (63), 404 [M(^{79}Br) + H]⁺ (100), 403 [M(^{79}Br)]⁺ (39), 349 [M(^{81}Br) − tBu + H]⁺ (12), 348 [M(^{81}Br) − tBu]⁺ (21), 347 [M(^{79}Br) − tBu + H]⁺ (12), 346 [M(^{79}Br) − tBu]⁺ (18).

HRMS-FAB (*m/z*): [M + H]⁺ calcd. for $C_{19}H_{23}O_2N_3{}^{79}Br$, 404.0974; found, 404.0972.

2-(2-Bromo-4,5-dimethoxyphenyl)-*N*-(*tert.*-butyl)imidazo[1,2-*a*]pyrazine-3-amine (128f)
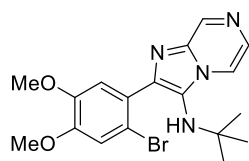
2-Aminopyrazine (200 mg, 2.10 mmol, 1.00 equiv), 2-bromo-4,5-dimethoxybenzaldehyde (515 mg, 0.35 mL, 2.10 mmol, 1.00 equiv), *tert*-butyl isonitrile (175 mg, 0.24 mL, 2.10 mmol, 1.00 equiv) and glacial acetic acid (253 mg, 0.24 mL, 4.21 mmol, 2.00 equiv) were reacted in methanol (10 mL) for 3 d. The solvent was removed under reduced pressure and the residue was purified *via* flash chromatography (SiO₂, CH/EtOAc/NEt₃ 6:1:0.01 to 0:1:0.04) GBB product **128f** was obtained as a white solid (312 mg, 0.77 mmol, 38%).

R_f (SiO₂, CH/EtOAc 1:1) = 0.40.

¹H-NMR (400 MHz, CDCl₃) δ [ppm] = 8.98 (d, *J* = 1.5 Hz, 1H, C*H*$_{Ar}$), 8.20 (dd, *J* = 4.7, 1.5 Hz, 1H, C*H*$_{Ar}$), 7.87 (d, *J* = 4.7 Hz, 1H, C*H*$_{Ar}$), 7.13 (s, 1H, C*H*$_{Ar}$), 7.08 (s, 1H, C*H*$_{Ar}$), 3.92 (s, 3H, OC*H*₃), 3.90 (s, 3H, OC*H*₃), 3.32 (s, 1H, N*H*), 0.94 (s, 9H, C*H*₃).

¹³C-NMR (101 MHz, CDCl₃) δ [ppm] = 150.0 (C$_q$), 148.8 (C$_q$), 143.5 (CH$_{Ar}$), 142.1 (CH$_{Ar}$), 141.9 (C$_q$), 137.4 (C$_q$), 134.4 (CH$_{Ar}$), 132.7 (CH$_{Ar}$), 129.1 (CH$_{Ar}$), 128.1 (C$_q$), 126.1 (C$_q$), 116.6 (CH$_{Ar}$), 115.2 (CH$_{Ar}$), 114.9 (CH$_{Ar}$), 112.8 (C$_q$), 60.5 (C$_q$), 56.4 (CH₃), 56.3 (CH₃), 30.1 (3C, CH₃).

IR (ATR) $\tilde{\upsilon}$ [cm⁻¹] = 3334 (vw), 2962 (vw), 1736 (vw), 1604 (w), 1537 (vw), 1501 (w), 1462 (w), 1441 (w), 1408 (w), 1365 (w), 1349 (w), 1249 (w), 1203 (m), 1173 (w), 1018 (w), 952 (w), 858 (w), 823 (w), 779 (w), 699 (vw), 646 (w), 611 (w), 584 (vw), 421 (w).

FAB-MS *m/z* (%): 407 [M(^{81}Br) + H]⁺ (97), 406 [M(^{81}Br)]⁺ (62), 405 [M(^{79}Br) + H]⁺ (100), 404 [M(^{79}Br)]⁺ (43).

HRMS-FAB (*m/z*): [M + H]⁺ calcd. for $C_{18}H_{22}O_2N_4{}^{79}Br$, 405.0926; found, 405.0928.

EA $C_{18}H_{22}O_2N_4Br$: calcd., C 53.34, H 5.22, N 13.82; found, C 53.40, H 5.39, N 14.03.

2-(2-Bromophenyl)-*N*-(*tert.*-butyl)imidazo[1,2-*a*]pyrazine-3-amine (128g)
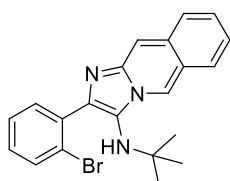
Isoquinoline-3-amine (500 mg, 3.47 mmol, 1.00 equiv), 2-bromobenzaldehyde (642 mg, 0.40 mL, 3.47 mmol, 1.00 equiv), *tert.*-butyl isocyanide (288 mg, 0.39 mL, 3.47 mmol, 1.00 equiv) and a 1 M solution of perchloric acid in methanol (34.8 mg, 0.35 mL, 0.35 mmol, 0.10 equiv) were reacted in 10 mL methanol (10 mL) for 5 d. The solvent was

removed under reduced pressure and the residue was purified *via* flash chromatography (SiO$_2$, CH/EtOAc/NEt$_3$ 6:1:0.01 to 2:1:0.04). **128g** was obtained as a white solid (603 mg, 1.53 mmol, 44%).

R$_f$ (SiO$_2$, CH/EtOAc 1:2) = 0.25.

^{1}H-NMR (500 MHz, CDCl$_3$) δ [ppm] = 9.93 (dd, *J* = 8.7, 1.1 Hz, 1H), 7.73 (ddd, *J* = 9.9, 7.7, 1.7 Hz, 2H), 7.66 (dd, *J* = 8.1, 1.2 Hz, 1H), 7.57 (ddd, *J* = 8.7, 7.1, 1.6 Hz, 1H), 7.48 (q, *J* = 9.4 Hz, 2H), 7.43 (tt, *J* = 7.5, 1.4 Hz, 2H), 7.24 (dd, *J* = 6.0, 1.7 Hz, 1H), 3.39 (s, 1H, N*H*), 0.93 (s, 9H, C*H$_3$*).

^{13}C-NMR (126 MHz, CDCl$_3$) δ [ppm] = 141.10 (C$_q$), 139.12 (C$_q$), 136.85 (C$_q$), 135.44 (C$_q$), 133.32 (CH$_{Ar}$), 132.83 (CH$_{Ar}$), 130.11 (C$_q$), 129.53 (CH$_{Ar}$), 128.70 (CH$_{Ar}$), 127.74 (CH$_{Ar}$), 127.26 (CH$_{Ar}$), 126.67 (CH$_{Ar}$), 124.79 (C$_q$), 124.62 (CH$_{Ar}$), 122.86 (C$_q$), 118.36 (CH$_{Ar}$), 117.55 (CH$_{Ar}$), 56.57 (C$_q$), 29.71 (3C, CH$_3$).

IR (ATR) $\tilde{v}$ [cm^{-1}] = 3207, 3119, 3074, 3054, 3034, 2962, 2925, 2900, 2871, 2860, 1608, 1557, 1548, 1533, 1466, 1442, 1432, 1385, 1360, 1349, 1324, 1256, 1221, 1210, 1167, 1157, 1135, 1115, 1021, 1009, 980, 958, 945, 897, 803, 781, 768, 745, 715, 680, 662, 640, 615, 599, 557, 537, 523, 514, 490, 472, 459, 441, 419, 399, 385, 377.

FAB-MS *m/z* (%):397 (24), 396 [M(^{81}Br) + H]$^+$ (97), 395 [M(^{81}Br)]$^+$ (51), 394 [M(^{79}Br) + H]$^+$ (100), 393 [M(^{79}Br)]$^+$ (30), 340 (15), 339 (34), 338 (44), 337 (34), 336 (30), 313 (12), 311 (20), 309 (8), 129 (14), 128 (35).

HRMS-FAB (*m/z*): [M + H]$^+$ calcd. for C$_{21}$H$_{21}$N$_3$^{79}Br, 394.0919; found, 394.0921.

EA: C$_{21}$H$_{20}$N$_3$Br: calcd. C 63.97, H 5.11, N 10.66; found. C 64.05, H 5.07, N 10.55.

N-(Cyclohexyl)pyrido[2',1':2,3]imidazo[4,5-*c*]isoquinolin-5-amine (129aa)
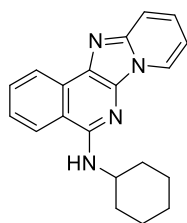
GBB product **128a** (200 mg, 0.58 mmol, 1.00 equiv), *tert*-butyl isonitrile (95.1 mg, 0.11 mL, 0.87 mmol, 1.50 equiv), potassium acetate (171 mg, 1.74 mmol, 3.00 equiv), Pd-Peppsi-iPr (19.8 mg, 0.03 mmol, 0.05 equiv) and XPhos (27.7 mg, 0.06 mmol, 0.10 equiv) were reacted in anhydrous DMF (3 mL) for 18 h at 120 °C. The solvent was removed under reduced pressure and the residue was purified *via* flash chromatography (SiO$_2$, CH/EtOAc/NEt$_3$ 20:1:0.05 to 2:1:0.05). **129aa** was obtained as a yellow solid (172 mg, 0.54 mmol, 94%).

R$_f$ (SiO$_2$, CH/EtOAc 2:1) = 0.11.

^{1}H NMR (500 MHz, CDCl$_3$) δ [ppm] = 8.64 (dd, *J* = 8.1, 1.2 Hz, 1H, C*H^1*), 8.59 (dt, *J* = 6.9, 1.3 Hz, 1H, C*H^7*), 7.89 (d, *J* = 8.3 Hz, 1H, C*H^4*), 7.75 (ddd, *J* = 8.1, 7.0, 1.0 Hz, 1H, C*H^2*), 7.73-7.70 (m, 1H, C*H^{10}*), 7.52 (ddd, *J* = 8.4, 7.0, 1.3 Hz, 1H, C*H^3*), 7.32-7.22 (m, 1H, C*H^9*), 6.87 (td, *J* = 6.7, 1.1 Hz, 1H, C*H^8*), 5.37 (d, *J* = 7.2 1H, N*H*), 4.29 (dt, *J* = 7.0, 3.8 Hz, 1H, C*H^{12}*), 2.27-2.21 (m, 2H, C*H$_2$*), 1.84 (dt, *J* = 13.5, 3.9 Hz, 2H, C*H$_2$*), 1.72 (dt, *J* = 12.8, 3.9 Hz, 2H, C*H$_2$*), 1.58-1.47 (m, 2H, C*H$_2$*), 1.38-1.34 (m, 2H, C*H$_2$*).

^{13}C NMR (101 MHz, CDCl$_3$) δ [ppm] = 151.5 (C$_q$, *C^5*), 143.4 (C$_q$, *C^{10a}*), 134.6 (C$_q$, *C^{11a}*), 130.9 (C$_q$, *C^{11b}*), 130.4 (CH$_{Ar}$, *CH^2*), 126.3 (CH$_{Ar}$, *CH^9*), 125.8 (CH$_{Ar}$, *CH^3*), 124.5 (C$_q$, *C^{6a}*), 123.3 (CH$_{Ar}$, *CH^1*), 123.2 (CH$_{Ar}$, *CH^7*), 122.7 (CH$_{Ar}$, *CH^4*), 119.0 (C$_q$, *C^{4a}*), 117.3 (CH$_{Ar}$, *CH^{10}*), 111.2 (CH$_{Ar}$, *CH^8*), 50.3 (CH), 33.3 (2C, CH$_2$), 26.1 (CH$_2$), 25.3 (2C, CH$_2$).

IR (ATR) ṽ [cm^{-1}] = 3273 (vw), 2923 (w), 2850 (w), 1623 (w), 1583 (w), 1540 (w), 1506 (m), 1449 (w), 1420 (w), 1378 (w), 1348 (w), 1316 (w), 1255 (w), 1144 (w), 1109 (w), 1026 (w), 922 (w), 743 (w), 729 (m), 669 (w), 642 (w), 520 (w), 443 (vw), 420 (vw).

FAB-MS m/z (%): 317 [M + H]$^+$ (100), 316 [M]$^+$ (83), 234 [M − C$_6$H$_{11}$ + H]$^+$ (13), 233 [M − C$_6$H$_{11}$]$^+$ (4).

HRMS-FAB (m/z): [M + H]$^+$ calcd. for C$_{20}$H$_{21}$N$_4$, 317.1766; found, 317.1767.

N-(*tert.*-Butyl)pyrido[2',1':2,3]imidazo[4,5-*c*]isoquinolin-5-amine (129ab)
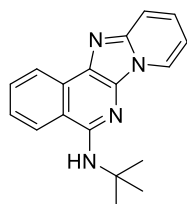
GBB product **128a** (200 mg, 0.58 mmol, 1.00 equiv), *tert.*-butyl isonitrile (72.5 mg, 0.10 mL, 0.87 mmol, 1.50 equiv), potassium acetate (171 mg, 1.74 mmol, 3.00 equiv), Pd-Peppsi-iPr (19.8 mg, 0.03 mmol, 0.05 equiv) and XPhos (27.7 mg, 0.06 mmol, 0.10 equiv) were reacted in anhydrous DMF (3 mL) for 18 h at 120 °C. The solvent was removed under reduced pressure and the residue was purified *via* flash chromatography (SiO$_2$, CH/EtOAc/NEt$_3$ 20:1:0.05 to 2:1:0.05). **129ab** was obtained as a yellow solid (40.8 mg, 0.14 mmol, 24%).

R_f (SiO$_2$, CH/EtOAc 2:1) = 0.12.

^{1}H NMR (500 MHz, CDCl$_3$) δ [ppm] = 8.65 (dt, J = 8.1, 1.1 Hz, 1H, CH^1), 8.60 (dt, J = 6.8, 1.3 Hz, 1H, CH^7), 7.84 (dt, J = 8.4, 0.9 Hz, 1H, CH^4), 7.78 (ddd, J = 8.1, 7.0, 1.1 Hz, 1H, CH^2), 7.70 (dt, J = 9.2, 1.1 Hz, 1H, CH^{10}), 7.54 (ddd, J = 8.4, 7.0, 1.3 Hz, 1H, CH^3), 7.27 (ddd, J = 9.2, 6.6, 1.3 Hz, 1H, CH^9), 6.87 (td, J = 6.7, 1.1 Hz, 1H, CH^8), 5.33 (s, 1H, NH), 1.69 (s, 9H, 3 x CH$_3$).

^{13}C NMR (101 MHz, CDCl$_3$) δ [ppm] = 151.3 (C$_q$, C^5), 143.8 (C$_q$, C^{10a}), 134.4 (C$_q$, C^{11a}), 131.4 (C$_q$, C^{11b}), 130.2 (CH$_{Ar}$, CH^2), 126.0 (CH$_{Ar}$, CH^9), 125.7 (CH$_{Ar}$, CH^3), 125.0 (C$_q$, C^{6a}), 123.3 (CH$_{Ar}$, CH^1), 123.2 (CH$_{Ar}$, CH^7), 122.8 (CH$_{Ar}$, CH^4), 119.5 (C$_q$, C^{4a}), 117.7 (CH$_{Ar}$, CH^{10}), 111.0 (CH$_{Ar}$, CH^8), 52.3 (C$_q$), 29.2 (3C, CH$_3$).

IR (ATR) ṽ [cm^{-1}] = 3312 (w), 3047 (w), 2962 (m), 2924 (m), 2870 (w), 2856 (w), 1664 (w), 1632 (w), 1621 (m), 1582 (m), 1560 (m), 1536 (m), 1504 (vs), 1483 (m), 1449 (s), 1421 (vs), 1378 (s), 1346 (vs), 1302 (vs), 1271 (s), 1258 (vs), 1225 (vs), 1221 (vs), 1205 (vs), 1154 (m), 1147 (s), 1123 (m), 1082 (m), 1071 (s), 1028 (s), 1004 (m), 938 (m), 929 (m), 860 (w), 823 (m), 802 (m), 788 (m), 765 (vs), 741 (vs), 732 (vs), 707 (s), 694 (m), 669 (vs), 650 (s), 635 (s), 611 (m), 591 (m), 565 (m), 521 (vs), 486 (m), 439 (vs), 422 (s), 404 (s), 381 (vs).

FAB-MS m/z (%): 292 (22), 291 [M + H]$^+$ (100), 290 (83), 289 (6), 275 (7), 236 (6), 235 (26), 234 (32), 133 (16).

HRMS-FAB (m/z): [M + H]$^+$ calcd. for C$_{18}$H$_{19}$N$_4$, 291.1604; found, 291.1602.

N-(Isopropyl)pyrido[2',1':2,3]imidazo[4,5-c]isoquinolin-5-amine (129ac)
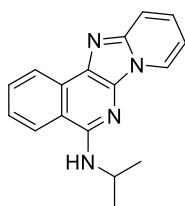
GBB product **128a** (200 mg, 0.58 mmol, 1.00 equiv), isopropyl isonitrile (60.22 mg, 0.08 mL, 0.87 mmol, 1.5 equiv), potassium acetate (171 mg, 1.74 mmol, 3.00 equiv), Pd-Peppsi-iPr (19.8 mg, 0.03 mmol, 0.05 equiv) and XPhos (27.7 mg, 0.06 mmol, 0.10 equiv) were reacted in anhydrous DMF (3 mL) for 18 h at 120 °C. The solvent was removed under reduced pressure and the residue was purified *via* flash chromatography (SiO$_2$, CH/EtOAc/NEt$_3$ 20:1:0.05 to 2:1:0.05). **129ac** was obtained as a yellow solid (43 mg, 0.16 mmol, 27%).

***R**$_f$* (SiO$_2$, CH/EtOAc 2:1) = 0.14.

¹H NMR (500 MHz, CDCl$_3$) δ [ppm] = 8.63 (dd, *J* = 8.4, 0.9 Hz, 1H, C*H^1*), 8.59 (dt, *J* = 6.8, 1.2 Hz, 1H, C*H^7*), 7.89 (dt, *J* = 8.4, 0.9 Hz, 1H, C*H^4*), 7.76 (ddd, *J* = 8.1, 7.0, 1.1 Hz, 1H, C*H^2*), 7.67 (dt, *J* = 9.2, 1.1z Hz, 1H, C*H^{10})*, 7.50 (ddd, *J* = 8.4, 7.0, 1.4 Hz, 1H, C*H^3*), 7.23 (ddd, *J* = 9.2, 6.6, 1.4 Hz, 1H, C*H^9*), 6.82 (td, *J* = 6.7, 1.1 Hz, 1H, C*H^8*), 5.27 (d, *J* = 7.0, 1H, N*H*), 4.60 (h, *J* = 6.5 Hz 1H, C*H^{12})*, 1.40 (d, *J* = 6.5 Hz, 6H, 2xC*H$_3$*). –

¹³C NMR (101 MHz, CDCl$_3$) δ [ppm] = 151.3 (C$_q$, *C^5*), 143.9 (C$_q$, *C^{10a}*), 134.7 (C$_q$, *C^{11a}*), 131.4 (C$_q$, *C^{11b}*), 130.3 (CH$_{Ar}$, *CH^2*), 125.7 (CH$_{Ar}$, *CH^9*), 125.5 (CH$_{Ar}$, *CH^3*), 125.5 (C$_q$, *C^{6a}*), 123.2 (CH$_{Ar}$, *CH^1*), 123.0 (CH$_{Ar}$, *CH^7*), 122.7 (CH$_{Ar}$, *CH^4*), 118.9 (C$_q$, *C^{4a}*), 117.6 (CH$_{Ar}$, *CH^{10}*), 110.7 (CH$_{Ar}$, *CH^8*), 43.2 (CH), 23.0 (2C, CH$_3$).

IR (ATR) $\tilde{v}$ [cm^{-1}] = 3276 (w), 3054 (w), 2972 (w), 2953 (w), 2925 (w), 2868 (w), 1632 (w), 1622 (m), 1581 (m), 1562 (m), 1541 (s), 1504 (vs), 1451 (m), 1438 (m), 1418 (s), 1380 (s), 1353 (s), 1316 (m), 1293 (s), 1279 (m), 1254 (vs), 1220 (m), 1180 (m), 1167 (m), 1160 (m), 1143 (m), 1133 (m), 1120 (m), 1082 (m), 1068 (m), 1027 (m), 1000 (w), 963 (w), 943 (w), 926 (w), 888 (w), 877 (w), 853 (w), 844 (w), 823 (w), 772 (vs), 754 (w), 739 (vs), 730 (vs), 713 (s), 693 (m), 671 (s), 643 (s), 613 (m), 589 (m), 565 (m), 521 (vs), 506 (m), 475 (m), 453 (m), 446 (m), 433 (m), 418 (s), 399 (s), 377 (s).

FAB-MS *m/z* (%): 278 (19), 277 [M + H]$^+$ (100), 276 (78), 275 (9), 261 (15), 235 (13), 234 (14), 233 (5), 219 (5), 154 (14), 138 (5), 137 (7), 136 (21), 133 (12), 107 (8), 105 (5), 91 (12), 90 (9), 89 (9).

HRMS-FAB (*m/z*): [M + H]$^+$ calcd. for C$_{17}$H$_{17}$N$_4$, 277.1448; found, 277.1448.

N-((1s,3s)-Adamantan-1-yl)pyrido[2'1':2,3]imidazo[4,5-c]isoquinolin-5-amine (129ad)[192]
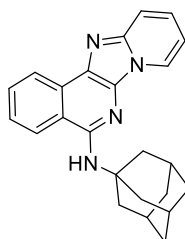
GBB product **128a** (200 mg, 0.58 mmol, 1.00 equiv), 1-isocyanoadamantane (141 mg, 0.87 mmol, 1.5 equiv), potassium acetate (171 mg, 1.74 mmol, 3.00 equiv), Pd-Peppsi-iPr (19.8 mg, 0.03 mmol, 0.05 equiv) and XPhos (27.7 mg, 0.06 mmol, 0.10 equiv) were reacted in anhydrous DMF (3 mL) for 18 h at 120 °C. The solvent was removed under reduced pressure and the residue was purified *via* flash chromatography (SiO$_2$, CH/EtOAc/NEt$_3$ 20:1:0.05 to 2:1:0.05). **129ad** was obtained as a yellow solid (144 mg, 0.16 mmol, 67%).

***R**$_f$* (SiO$_2$, CH/EtOAc 2:1) = 0.28.

¹H NMR (500 MHz, CDCl$_3$) δ [ppm] = 8.63 (dd, *J* = 8.1, 1.3 Hz, 1H, C*H^1*), 8.53 (dt, *J* = 7.0, 1.3 Hz, 1H, C*H^7*), 7.84 (d, *J* = 8.3 Hz, 1H, C*H^4*), 7.77 (ddd, *J* = 8.1, 6.9, 1.0 Hz 1H, C*H^2*), 7.68 (dt, *J* = 9.2, 1.3 Hz, 1H, C*H^{10}*), 7.53 (ddd,

J = 8.4, 7.0 1.3 Hz, 1H, CH^3), 7.25 (ddd, J = 9.8, 6.6, 1.4 Hz, 1H, CH^9), 6.86 (td, J = 6.6, 1.1 Hz, 1H, CH^8), 5.18 (s, 1H, NH), 2.4 (d, J = 2.9 Hz, 6H, CH_2), 2.21 (s, 3H, CH), 1.86-1.78 (m, 6H, CH_2).

13C NMR (101 MHz, CDCl$_3$) δ [ppm] = 151.0 (C$_q$, C^5), 143.9 (C$_q$, C^{10a}), 134.3 (C$_q$, C^{11a}), 131.5 (C$_q$, C^{11b}), 130.1 (CH$_{Ar}$, CH^2), 125.7 (CH$_{Ar}$, CH^9), 125.5 (CH$_{Ar}$, CH^3), 125.2 (C$_q$, C^{6a}), 123.2 (CH$_{Ar}$, CH^1), 123.1 (CH$_{Ar}$, CH^7), 122.8 (CH$_{Ar}$, CH^4), 119.4 (C$_q$, C^{4a}), 117.8 (CH$_{Ar}$, CH^{10}), 110.9 (CH$_{Ar}$, CH^8), 52.9 (C$_q$), 42.0 (3C, CH$_2$), 37.0 (3C, CH$_2$), 29.9 (3C, CH).

IR (ATR) $\tilde{\upsilon}$ [cm^{-1}] = 3384 (w), 3274 (w), 3080 (w), 2902 (vs), 2861 (m), 2846 (s), 1632 (w), 1623 (w), 1584 (s), 1561 (s), 1536 (m), 1509 (vs), 1451 (m), 1421 (s), 1381 (m), 1347 (vs), 1302 (vs), 1272 (s), 1258 (m), 1241 (s), 1133 (m), 1095 (m), 943 (w), 936 (w), 764 (s), 744 (vs), 734 (vs), 705 (m), 669 (s), 637 (m), 516 (s), 388 (m).

FAB-MS *m/z* (%): 370 (23), 369 (91), 368 [M + H]$^+$ (100), 367 (15), 234 (7), 154 (6), 135 (17), 93 (5).

N-(2-Morpholinoethyl)pyrido[2',1':2,3]imidazo[4,5-*c*]isoquinolin-5-amine (129ae)[192]
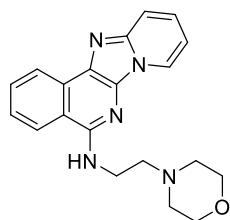
GBB product **128a** (185 mg, 0.54 mmol, 1.00 equiv), 4-(2-isocyanoehtyl)morpholine (113.0 mg, 0.11 mL, 0.81 mmol, 1.50 equiv), potassium acetate (158.2 mg, 1.61 mmol, 3.00 equiv), Pd-Peppsi-iPr (18.3 mg, 0.03 mmol, 0.05 equiv) and XPhos (25.6 mg, 0.05 mmol, 0.10 equiv) were reacted in anhydrous DMF (3 mL) for 18 h at 120 °C. The solvent was removed under reduced pressure and the residue was purified *via* flash chromatography (SiO$_2$, CH/EtOAc/NEt$_3$ 20:1:0.05 to 1:10:0.05). **129ae** was obtained as a yellow solid (57.0 mg, 0.16 mmol, 31%).

R$_f$ (SiO$_2$, EtOAc) = 0.09.

1H NMR (500 MHz, CDCl$_3$) δ [ppm] = 8.65 (d, J = 8.1 Hz, 1H, CH^1), 8.59 (d, J = 6.8 Hz, 1H, CH^7), 7.95 (d, J = 8.3 Hz, 1H, CH^4), 7.80 (t, J = 7.5 Hz, 1H, CH^2), 7.69 (dt, J = 9.2 Hz, 1H, CH^{10}), 7.58 (ddd, J = 8.0, 7.0, 1.4 Hz, 1H, CH^3), 7.28-7.25 (m, 1H, CH^9), 6.86 (t, J = 6.7 Hz, 1H, CH^8), 6.24 (t, J = 4.7, 1H, NH), 3.79 (dt, J = 9.1, 5.0 Hz, 6H, CH_2^{12+15}), 2.81 (t, J = 6.0 Hz, 2H, CH_2^{13}), 2.59 (t, J = 4.4Hz, 4H, CH_2^{14}).

13C NMR (101 MHz, CDCl$_3$) δ [ppm] = 152.2 (C$_q$, C^5), 144.0 (C$_q$, C^{10a}), 134.7 (C$_q$, C^{11a}), 131.4 (C$_q$, C^{11b}), 130.5 (CH$_{Ar}$), 125.8 (CH$_{Ar}$), 125.8 (CH$_{Ar}$), 123.2 (CH$_{Ar}$), 123.2 (C$_q$, C^{6a}), 123.0 (CH$_{Ar}$), 123.0 (CH$_{Ar}$), 119.1 (C$_q$), 117.9 (CH$_{Ar}$), 111.9 (CH$_{Ar}$), 67.2 (2C, CH$_2$), 57.0 (CH$_2$), 53.5 (CH$_2$), 38,1 (2C, CH$_2$).

IR (ATR) $\tilde{\upsilon}$ [cm^{-1}] = 3271 (m), 3075 (w), 2952 (m), 2942 (w), 2932 (w), 2890 (w), 2868 (w), 2851 (m), 2812 (m), 2765 (w), 1655 (m), 1632 (s), 1625 (s), 1582 (vs), 1548 (vs), 1524 (vs), 1507 (vs), 1445 (s), 1421 (vs), 1377 (vs), 1350 (vs), 1306 (vs), 1258 (vs), 1217 (s), 1170 (m), 1145 (s), 1116 (vs), 1068 (s), 1034 (s), 1007 (s), 950 (m), 929 (s), 914 (s), 887 (s), 866 (s), 824 (m), 805 (m), 773 (vs), 744 (vs), 732 (vs), 711 (s), 670 (s), 636 (vs), 628 (vs), 613 (s), 591 (s), 568 (s), 547 (s), 521 (vs), 473 (s), 438 (s), 421 (s), 402 (m), 390 (s), 382 (s).

FAB-MS *m/z* (%): 349 (27), 348 [M + H]$^+$ (100), 347 (59), 346 (18), 261 (38), 259 (14), 248 (10), 247 (31), 235 (15), 234 (42), 233 (10), 219 (11), 149 (10), 114 (16), 100 (66), 91 (11).

HRMS-FAB (*m/z*): [M + H]$^+$ calcd. for C$_{20}$H$_{22}$N$_5$O$_1$: 348.1817; found, 348.1819.

(*S*)-*N*-(1-Phenylethyl)pyrido[2',1':2,3]imidazo[4,5-c]isoquinoline-5-amine (129af)[193]
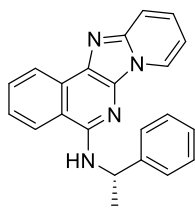
GBB-product **128a** (100 mg, 0.29 mmol, 1.00 equiv), (*S*)-methyl benzyl isonitrile (41 mg, 0.06 mL, 0.73 mmol, 1.5 equiv), potassium acetate (86 mg, 0.87 mmol, 3.00 equiv), Pd(dba)$_2$ (8.4 mg, 0.015 mmol, 0.05 equiv) and XPhos (14 mg, 0.029 mmol, 0.10 equiv) were reacted in anhydrous DMF (2 mL) for 18 h at 120 °C. The solvent was removed under reduced pressure and the residue was purified *via* preparative TLC (SiO$_2$, CH/EtOAc/NEt$_3$ 6:1:0.04 to 1:1:0.04). **129af** was obtained as a yellow solid (53 mg, 0.14 mmol, 57%).

***R**$_f$* (SiO$_2$, CH/EtOAc 1:2) = 0.25.

^{1}H-NMR (400 MHz, CDCl$_3$) δ [ppm] = 8.65 (dd, *J* = 8.2, 1.2 Hz, 1H, C*H*$_{Ar}$), 8.53 (d, *J* = 6.8 Hz, 1H, C*H*$_{Ar}$), 8.03 (d, *J* = 8.4 Hz, 1H, C*H*$_{Ar}$), 7.82 – 7.77 (m, 1H, C*H*$_{Ar}$), 7.71 (dddd, *J* = 8.2, 7.1, 6.0, 1.0 Hz, 1H, C*H*$_{Ar}$), 7.58 – 7.53 (m, 2H, C*H*$_{Ar}$), 7.38 – 7.29 (m, 4H, C*H*$_{Ar}$), 7.25 (d, *J* = 7.0 Hz, 1H, C*H*$_{Ar}$), 6.96 (td, *J* = 6.8, 1.1 Hz, 1H, C*H*$_{Ar}$), 5.99 (d, *J* = 6.5 Hz, 1H, N*H*), 5.55 (td, *J* = 6.7, 1.9 Hz, 1H, C*H*$_{Ar}$), 1.76 (d, *J* = 6.9 Hz, 3H, C*H*$_3$).

^{13}C-NMR (101 MHz, CDCl$_3$) δ [ppm] = 169.2 (C$_q$), 151.6 (C$_q$), 145.0 (C$_q$), 143.3 (C$_q$), 142.3 (C$_q$), 134.0 (C$_q$), 130.8 (CH$_{Ar}$), 128.8 (CH$_{Ar}$), 128.7 (CH$_{Ar}$), 127.8 (CH$_{Ar}$), 127.5 (CH$_{Ar}$), 127.2 (CH$_{Ar}$), 126.5 (CH$_{Ar}$), 126.3 (CH$_{Ar}$), 123.5 (CH$_{Ar}$), 123.4 (CH$_{Ar}$), 123.0 (CH$_{Ar}$), 119.0 (C$_q$), 116.5 (CH$_{Ar}$), 112.3 (CH$_{Ar}$), 51.5 (C$_q$), 22.8 (CH$_3$).

IR (ATR) $\tilde{\upsilon}$ [cm^{-1}] = 3246 (w), 2970 (w), 1648 (m), 1606 (m), 1507 (m), 1447 (m), 1421 (m), 1376 (m), 1279 (m), 1252 (m), 1209 (m), 1135 (m), 1027 (w), 908 (w), 747 (m), 730 (m), 698 (s), 674 (m), 645 (w), 540 (w), 514 (m), 417 (w).

FAB-MS *m/z* (%): 339 [M + H]$^+$ (100), 338 [M]$^+$ (47).

HRMS-FAB (*m/z*): [M + H]$^+$ calcd. for C$_{22}$H$_{19}$N$_4$, 339.1610; found, 339.1608.

N-(2,6-Dimethylphenyl)pyrido[2'1':2,3]imidazo[4,5-*c*]isoquinolin-5-amine (129ag)[192]
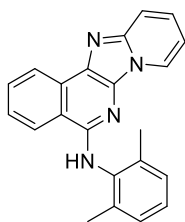
GBB product **128a** (200 mg, 0.58 mmol, 1.00 equiv), 2-isocyano-1,3-dimethylbenzene (114 mg, 0.87 mmol, 1.5 equiv), potassium acetate (171 mg, 1.74 mmol, 3.00 equiv), Pd-Peppsi-iPr (19.8 mg, 0.03 mmol, 0.05 equiv) and XPhos (27.7 mg, 0.06 mmol, 0.10 equiv) were reacted in anhydrous DMF (3 mL) for 18 h at 120 °C. The solvent was removed under reduced pressure and the residue was purified *via* flash chromatography (SiO$_2$, CH/EtOAc/NEt$_3$ 20:1:0.05 to 2:1:0.05). **129ag** was obtained as a yellow solid (21 mg, 0.06 mmol, 11%).

***R**$_f$* (SiO$_2$, CH/EtOAc 2:1) = 0.25.

^{1}H NMR (500 MHz, CDCl$_3$) δ [ppm] = 8.73 (dd, *J* = 8.3, 1.3 Hz, 1H, C*H*^{1}), 8.31 (dt, *J* = 6.9, 1.3 Hz, 1H, C*H*^{7}), 8.20 (d, *J* = 8.3 Hz, 1H, C*H*^{4}), 7.87 (ddd, *J* = 8.1, 7.0, 1.0 Hz, 1H, C*H*^{2}), 7.69-7.63 (m, 2H, C*H*$^{3+10}$), 7.26-7.23 (m, 1H, C*H*^{9}), 7.21-7.17 (m, 3H, C*H*$_{Ar}$), 6.84-6.83 (m, 1H, N*H*), 6.75 (td, *J* = 6.7, 1.1 Hz, 1H, C*H*^{8}), 2.29 (s, 6H, C*H*$_3$).

^{13}C NMR (101 MHz, CDCl$_3$) δ [ppm] = 149.8 (C$_q$, *C*^{5}), 144.4 (C$_q$, *C*^{10a}), 137.2 (C$_q$, *C*^{12}), 135.7 (2C, C$_q$), 134.4 (C$_q$, *C*^{11a}) 131.6 (C$_q$, *C*^{11b}), 130.6 (CH$_{Ar}$, *C*H^2), 128.3 (*C*H$_{Ar}$), 128.1 (C$_q$, *C*^{6a}), 126.4 (CH$_{Ar}$, *C*H^3), 126.2 (CH$_{Ar}$, *C*H^9), 126.1 (2C,

CH$_{Ar}$), 123.7 (CH$_{Ar}$, CH^7), 123.3 (CH$_{Ar}$, CH^1), 123.2 (CH$_{Ar}$, CH^4), 118.9 (C$_q$, C^{4a}), 117.6 (CH$_{Ar}$, CH^{10}), 110.8 (C$_q$, C^8), 19.0 (2C, CH_3).

IR (ATR) $\tilde{v}$ [cm^{-1}] = 3262 (w), 2962 (w), 2919 (w), 2847 (w), 1650 (w), 1625 (m), 1578 (m), 1562 (m), 1537 (m), 1503 (vs), 1470 (vs), 1451 (s), 1417 (vs), 1377 (vs), 1347 (vs), 1300 (vs), 1281 (s), 1252 (s), 1218 (s), 1156 (m), 1142 (m), 1095 (s), 1075 (s), 1027 (s), 986 (m), 928 (m), 899 (w), 871 (w), 840 (w), 832 (w), 813 (w), 805 (w), 765 (vs), 748 (vs), 734 (vs), 707 (s), 681 (m), 667 (vs), 645 (vs), 611 (vs), 591 (vs), 571 (s), 548 (s), 520 (vs), 469 (s), 458 (s), 445 (s), 421 (s), 415 (s), 399 (s), 391 (s), 380 (s).

FAB-MS *m/z* (%): 339 (85), 338 [M + H]$^+$ (82), 233 (68), 217 (57), 192 (83), 154 (95), 138 (38), 137 (57), 136 (100), 107 (47), 105 (34), 95 (43), 91 (69), 90 (43), 89 (47).

HRMS-FAB (*m/z*): [M]$^+$ calcd. for C$_{22}$H$_{18}$N$_4$, 338.1526; found, 338.1528.

N-(Cyclohexylpyrazino[2',1':2,3]imidazo[4,5-*c*]isoquinolin-5-amine (129ba)
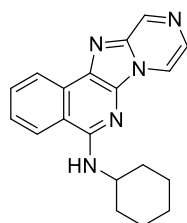
GBB product **128b** (200 mg, 0.58 mmol, 1.00 equiv), cyclohexyl isonitrile (95.2 mg, 0.11 mL, 0.87 mmol, 1.50 equiv), potassium acetate (171 mg, 1.74 mmol, 3.00 equiv), Pd-Peppsi-iPr(19.8 mg, 0.03 mmol, 0.05 equiv) and XPhos (27.7 mg, 0.06 mmol, 0.10 equiv) were reacted in anhydrous DMF (3 mL) for 18 h at 120 °C. The solvent was removed under reduced pressure and the residue was purified *via* flash chromatography (SiO$_2$, CH/EtOAc/NEt$_3$ 20:1:0.05 to 2:1:0.05). **129ba** was obtained as a yellow solid (124 mg, 0.39 mmol, 67%).

R$_f$ (SiO$_2$, CH/EtOAc 2:1) = 0.22.

^{1}H NMR (500 MHz, CDCl$_3$) δ [ppm] = 9.16 (s, 1H, CH^{10}), 8.64 (d, *J* = 8.0, 1H, CH^1), 8.43 (d, *J* = 4.5 Hz, 1H, CH^7), 7.91-7.88 (m, 2H,z CH^{8+4}), 7.82 (t, *J* = 7.56 Hz, 1H, CH^2), 7.60 (t, *J* = 7.7 Hz, 1H, CH^3), 5.50 (d, *J* = 7.3 Hz, 1H, NH), 4.35-4.28 (m, 1H, CH^{12}), 2.25 (dd, *J* = 12.4, 4.4 Hz, 2H, CH_2), 1.85 (dt, *J* = 13.5, 4.0 Hz, 2H, CH_2), 1.58-1.50 (m, 2H, CH_2), 1.40-1.23 (m, 4H, CH_2).

^{13}C NMR (101 MHz, CDCl$_3$) δ [ppm] = 152.6 (C$_q$, C^5), 144.4 (C$_q$, C^{10}), 138.3 (C$_q$, C^{6a}), 134.6 (C$_q$, C^{10a}), 131.5 (C$_q$, C^{11b}), 130.9 (CH$_{Ar}$, CH^2), 127.8 (C$_q$, C^{11a}), 127.4 (CH$_{Ar}$, CH^8), 126.8 (CH$_{Ar}$, CH^3), 123.3 (CH$_{Ar}$, CH^1), 122.8 (CH$_{Ar}$, CH^4), 120.0 (C$_q$, C^{4a}), 115.9 (CH$_{Ar}$, CH^7), 50.3 (CH), 33.2 (CH$_2$), 26.0 (CH$_2$), 25.3 (CH$_2$).

IR (ATR) $\tilde{v}$ [cm^{-1}] = 3233 (w), 2920 (w), 2851 (w), 1655 (w), 1573 (m), 1543 (m), 1493 (m), 1449 (w), 1373 (w), 1327 (w), 1293 (w), 1253 (m), 1150 (w), 1067 (w), 1030 (w), 1005 (w), 938 (w), 890 (w), 763 (w), 711 (w), 664 (w), 646 (w), 597 (w), 567 (w), 522 (w), 417 (w).

FAB-MS *m/z* (%): 318 [M + H]$^+$ (100), 317 [M]$^+$ (56), 235 [M − C$_6$H$_{11}$ + H]$^+$ (24).

HRMS-FAB (*m/z*): [M + H]$^+$ calcd. for C$_{19}$H$_{20}$N$_5$, 318.1719; found, 318.1717.

N-(tert-Butyl)pyrazino[2',1':2,3]imidazo[4,5-c]isoquinolin-5-amine (129bb)
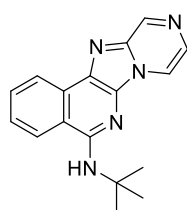
GBB product **128b** (120 mg, 0.35 mmol, 1.00 equiv), tert-butyl isonitrile (43.3 mg, 0.06 mL, 0.52 mmol, 1.50 equiv), potassium acetate (102 mg, 1.04 mmol, 3.00 equiv), Pd-Peppsi-iPr(11.8 mg, 0.02 mmol, 0.05 equiv) and XPhos (16.6 mg, 0.03 mmol, 0.10 equiv) were reacted in anhydrous DMF (3 mL) for 18 h at 120 °C. The crude product was purified *via* flash chromatography (SiO$_2$, CH/EtOAc/NEt$_3$ 20:1:0.05 to 2:1:0.05). **129bb** was obtained as a yellow solid (20 mg, 0.07 mmol, 20%).

R$_f$ (SiO$_2$, CH/EtOAc 2:1) = 0.18.

^{1}H NMR (400 MHz, CDCl$_3$) δ [ppm] = 9.18 (d, *J* = 1.5 Hz, 1H, C*H^{10}*), 8.67 (d, *J* = 7.9 Hz, 1H, C*H^1*), 8.43 (dd, *J* = 4.6, 1.6 Hz, 1H, C*H^7*), 7.92 (d, *J* = 4.6 Hz 1H, C*H^8*), 7.86-7.81 (m, 2H, C*H^{2+4}*), 7.63-7.55 (m, 1H, C*H^3*), 5.51 (s, 1H, N*H*), 1,7 (s, 9H, C*H$_3$*).

^{13}C NMR (101 MHz, CDCl$_3$) δ [ppm] = 152.5 (C$_q$, *C^5*), 144.5 (C$_q$, *C^{10}*), 138.4 (C$_q$, *C^{6a}*), 134.2 (C$_q$, C^{10a}), 131.7 (C$_q$, *C^{11b}*), 130.8 (CH$_{Ar}$, *CH^2*), 127.9 (C$_q$, *C^{11a}*), 127.2 (CH$_{Ar}$, *CH^8*), 126.9 (CH$_{Ar}$, *CH^3*), 123.4 (CH$_{Ar}$, *CH^1*), 122.9 (CH$_{Ar}$, *CH^4*), 120.5 (C$_q$, *C^{4a}*), 115.9 (C$_q$, *C^7*), 52.6 (C$_q$), 29.1 (3C, *C*H$_3$).

IR (ATR) $\tilde{\upsilon}$ [cm^{-1}] = 3418 (w), 2965 (m), 2918 (w), 2868 (w), 1728 (w), 1613 (w), 1608 (vw), 1572 (vs), 1538 (vs), 1524 (s), 1496 (s), 1487 (s), 1476 (vs), 1451 (s), 1435 (m), 1421 (m), 1383 (m), 1370 (s), 1356 (m), 1346 (m), 1322 (m), 1299 (s), 1286 (m), 1269 (s), 1256 (vs), 1213 (vs), 1179 (m), 1171 (m), 1152 (s), 1128 (m), 1102 (m), 1094 (m), 1079 (m), 1030 (m), 1009 (m), 929 (m), 892 (w), 867 (w), 798 (m), 765 (vs), 738 (m), 711 (s), 698 (m), 670 (vs), 656 (s), 633 (vs), 595 (vs), 561 (m), 523 (vs), 480 (m), 442 (s), 419 (m), 412 (m), 390 (s).

FAB-MS *m/z* (%): 293 (26), 292 [M + H]$^+$ (100), 291 (56), 259 (15), 237 (17), 236 (52), 235 (43), 207 (12), 189 (11), 177 (12), 147 (29), 145 (11), 138 (11), 137 (20), 136 (48), 135 (11), 133 (12), 131 (14), 129 (12), 128 (11), 123 (13), 121 (15), 120 (12), 119 (13), 117 (14), 115 (14), 109 (19), 107 (28), 106 (14), 105 (25), 97 (16), 95 (29), 93 (16), 91 (46), 90 (26), 89 (21).

HRMS-FAB (*m/z*): [M + H]$^+$ calcd. for C$_{18}$H$_{19}$N$_4$, 292.1557; found, 292.1559.

N-Cyclohexylpyrido[1',2':1,2]imidazo[4,5-f][1,7]naphthyridin-5-amine (129ca)[193]
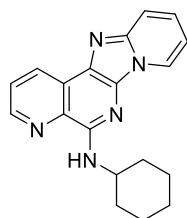
GBB-product **128c** (75 mg, 0.22 mmol, 1.00 equiv), cyclohexyl isonitrile (36 mg, 0.05 mL, 0.33 mmol, 1.50 equiv), potassium acetate (64 mg, 0.65 mmol, 3.00 equiv), Pd(dba)$_2$ (6.2 mg, 0.011 mmol, 0.05 equiv) and XPhos (10 mg, 0.022 mmol, 0.10 equiv) were reacted in 2 mL DMF for 18 h at 120 °C. After purification *via* preparative TLC (SiO$_2$, CH/EtOAc/NEt$_3$ 6:1:0.04, then 1:1:0.04) product **129ca** was obtained as a yellow solid (18 mg, 0.06 mmol, 39%).

R$_f$ (SiO$_2$, CH/EtOAc 1:2) = 0.18.

^{1}H-NMR (400 MHz, CDCl$_3$) δ [ppm] = 8.84 (dd, *J* = 8.2, 1.9 Hz, 1H, C*H$_{Ar}$*), 8.76 (dd, *J* = 4.4, 1.7 Hz, 1H, C*H$_{Ar}$*), 8.60 (d, *J* = 6.9 Hz, 1H, C*H$_{Ar}$*), 7.68 – 7.62 (m, 1H, C*H$_{Ar}$*), 7.31 – 7.20 (m, 1H, C*H$_{Ar}$*), 7.06 (d, *J* = 8.1 Hz, 1H, C*H$_{Ar}$*), 6.85 (t, *J* = 6.7 Hz, 1H, C*H$_{Ar}$*), 5.49 (d, *J* = 60.5 Hz, 1H, N*H*), 4.24 (dtt, *J* = 10.0, 7.7, 4.0 Hz, 1H, C*H*), 2.38 – 2.13 (m, 2H, C*H$_2$*),

1.85 (dt, *J* = 12.4, 3.8 Hz, 2H, C*H₂*), 1.70 (ddq, *J* = 13.5, 8.4, 4.0 Hz, 2H, C*H₂*), 1.59 – 1.50 (m, 2H, C*H₂*), 1.50 – 1.41 (m, 2H, C*H₂*).

¹³C-NMR (101 MHz, CDCl₃) *δ* [ppm] = 152.1 (C_q), 147.0 (*CH*_Ar), 144.1 (C_q), 135.28 (C_q), 135.2 (C_q), 130.7 (*CH*_Ar), 126.4 (C_q), 125.8 (*CH*_Ar), 125.3 (*CH*_Ar), 123.4 (*CH*_Ar), 123.4 (C_q), 117.7 (*CH*_Ar), 111.0 (*CH*_Ar), 49.6 (*CH*), 33.1 (2C, *CH₂*), 26.1 (2C, *CH₂*), 25.3 (*CH₂*).

IR (ATR) *ṽ* [cm⁻¹] = 3391 (w), 2923 (m), 2851 (m), 1655 (m), 1585 (m), 1520 (s), 1447 (m), 1398 (m), 1375 (m), 1347 (m), 1303 (w), 1252 (m), 1228 (m), 1151 (w), 1112 (w), 1075 (w), 918 (w), 890 (w), 815 (w), 797 (w), 734 (m), 668 (m), 644 (m), 424 (m), 409 (w).

FAB-MS *m/z* (%): 318 [M + H]⁺ (100), 317 [M]⁺ (98), 235 [M − C₆H₁₁ + H]⁺ (18), 234 [M − C₆H₁₁]⁺ (3).

HRMS-FAB (*m/z*): [M + H]⁺ calcd. for C₁₉H₂₀N₅, 318.1719; found, 318.1720.

N-Cyclohexyl-2,3-dimethoxypyrido[2′,1′:2,3]imidazo[4,5-*c*]isoquinolin-5-amine (129ea)
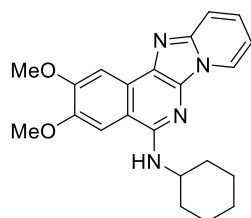
GBB-product **128e** (200 mg, 495 µmol, 1.00 equiv), cyclohexyl isonitrile (81 mg, 92 µL, 741 µmol, 1.50 equiv), potassium acetate (146 mg, 1.48 mmol, 3.00 equiv), Pd-Peppsi-iPr (16.9 mg, 24.7 µmol, 0.05 equiv) and XPhos (23.6 mg, 49.5 µmol, 0.10 equiv) were reacted in anhydrous 2 mL DMF (2 ml) for 16 h at 120 °C. The solvent was removed under reduced pressure and the residue was purified *via* flash chromatography (SiO₂, CH/EtOAc/NEt₃ 6:1:0.01 to 1:2:0.04). **129ea** was obtained as a yellow solid (113 mg, 300 µmol, 61%).

R_f (SiO₂, CH/EtOAc 1:2) = 0.08.

¹H-NMR (500 MHz, CDCl₃) *δ* [ppm] = 8.60 (d, *J* = 6.8 Hz, 1H, CH⁷), 7.99 (s, 1H, CH¹), 7.69 (d, *J* = 9.1 Hz, 1H, CH¹⁰), 7.27 (t, *J* = 7.2 Hz, 1H, CH⁹), 7.19 (s, 1H, CH⁴), 6.87 (td, *J* = 6.8, 1.1 Hz, 1H, CH⁸), 5.14 (d, *J* = 6.3 Hz, 1H, N*H*), 4.38 – 4.25 (m, 1H, C*H*), 4.08 (s, 3H, OC*H₃*), 4.01 (s, 3H, OC*H₃*), 2.28 (dd, *J* = 12.5, 3.9 Hz, 2H, C*H₂*), 1.84 (dt, *J* = 13.6, 3.8 Hz, 2H, C*H₂*), 1.73 (dt, *J* = 12.9, 3.7 Hz, 1H, C*H₂*), 1.59 – 1.45 (m, 2H, C*H₂*), 1.43 – 1.26 (m, 3H, C*H₂*).

¹³C-NMR (126 MHz, CDCl₃) *δ* [ppm] = 152.6 (C_q, *C²*), 150.6 (C_q, *C⁵*), 148.7 (C_q, *C³*), 143.3 (C_q, *C¹⁰ᵃ*), 134.1 (C_q, *C⁶ᵃ*), 126.8 (C_q, *C¹¹ᵇ*), 126.2 (*CH*_Ar, *CH⁹*), 124.8 (C_q, *C¹¹ᵃ*), 123.4 (*CH*_Ar, *CH⁷*), 117.1 (*CH*_Ar, *CH¹⁰*), 113.2 (C_q, *C⁴ᵃ*), 111.0 (*CH*_Ar, *CH⁸*), 103.5 (*CH*_Ar, *CH⁴*), 103.0 (*CH*_Ar, *CH¹*), 56.5 (*CH₃*), 56.4 (*CH₃*), 50.5 (*CH*), 33.5 (2C, *CH₂*), 26.2 (*CH₂*), 25.5 (2C, *CH₂*).

IR (ATR) *ṽ* [cm⁻¹] = 3223 (w), 2999 (w), 2925 (m), 2850 (w), 1731 (w), 1621 (w), 1589 (m), 1568 (m), 1547 (s), 1520 (m), 1503 (s), 1487 (vs), 1459 (m), 1432 (vs), 1385 (s), 1370 (m), 1351 (s), 1322 (m), 1290 (m), 1252 (vs), 1215 (vs), 1203 (vs), 1179 (vs), 1146 (s), 1112 (m), 1067 (s), 1047 (m), 1033 (m), 1004 (m), 993 (m), 938 (w), 929 (w), 888 (w), 864 (m), 849 (m), 824 (s), 803 (w), 779 (m), 748 (vs), 735 (s), 652 (m), 626 (s), 589 (m), 572 (m), 557 (m), 534 (w), 513 (w), 466 (w), 452 (w), 414 (m), 388 (w), 378 (w).

FAB-MS *m/z* (%): 378 (19), 377 (81), 376 [M + H]⁺ (100), 375 (13), 154 (14), 136 (11).

HRMS-FAB (*m/z*): [M + H]+ calcd. for C₂₂H₂₄O₂N₄, 376.1894; found, 376.1893.

N-(tert.-Butyl)-2,3-dimethoxypyrido[2',1':2,3]imidazo[4,5-c]isoquinoline-5-amine (129eb)
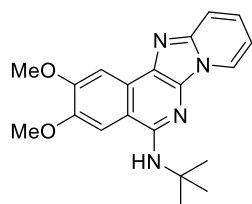
GBB-product **128e** (100 mg, 0.25 mmol, 1.00 equiv), *tert*-butyl isonitrile (31 mg, 0.04 mL, 0.37 mmol, 1.50 equiv), potassium acetate (73 mg, 0.74 mmol, 3.00 equiv), $Pd(dba)_2$ (7.1 mg, 0.012 mmol, 0.05 equiv) and XPhos (12 mg, 0.025 mmol, 0.10 equiv) were reacted in anhydrous DMF (2 mL) for 18 h at 120 °C. The solvent was removed under reduced pressure and the residue was purified *via* preparative TLC (SiO_2, CH/EtOAc/NEt₃ 6:1:0.04 to 1:1:0.04). **129eb** was obtained as a yellow solid (47 mg, 0.13 mmol, 54%).

R_f (SiO_2, CH/EtOAc 1:1) = 0.45.

¹H-NMR (400 MHz, CDCl₃) δ [ppm] = 8.56 (d, J = 6.8 Hz, 1H, C*H*), 7.97 (d, J = 6.7 Hz, 1H, C*H*), 7.65 (dd, J = 9.1, 1.1 Hz, 1H, C*H*), 7.28 − 7.20 (m, 1H, C*H*), 7.11 (s, 1H, C*H*), 6.83 (td, J = 6.7, 1.1 Hz, 1H, C*H*), 5.04 (s, 1H, N*H*), 4.07 (s, 3H, OC*H₃*), 4.01 (s, 3H, OC*H₃*), 1.67 (s, 9H, C*H₃*).

¹³C-NMR (101 MHz, CDCl₃) δ [ppm] = 152.4 (C_q), 150.3 (C_q), 148.6 (C_q), 143.6 (C_q), 133.8 (C_q), 127.0 (C_q), 125.9 (CH_Ar), 125.0 (C_q), 123.2 (CH_Ar), 117.3 (CH_Ar), 113.6 (C_q), 110.7 (CH_Ar), 103.6 (CH_Ar), 102.9 (CH_Ar), 56.5 (CH₃), 56.3 (CH₃), 52.3 (C_q), 29.3 (3C, CH₃).

IR (ATR) $\tilde{v}$ [cm⁻¹] = 2961 (vw), 2255 (w), 2172 (w), 1624 (w), 1590 (w), 1574 (w), 1538 (w), 1479 (w), 1430 (w), 1390 (w), 1346 (w), 1310 (w), 1290 (w), 1251 (w), 1201 (m), 1180 (w), 1090 (w), 1071 (w), 1035 (w), 1005 (w), 993 (w), 938 (w), 913 (w), 854 (w), 824 (w), 787 (w), 745 (w), 723 (m), 662 (w).

FAB-MS *m/z* (%): 351 [M + H]⁺ (84), 350 [M]⁺ (100), 294 [M − tBu + H]⁺ (15), 293 [M − tBu]⁺ (3).

HRMS-FAB (*m/z*): [M]⁺ calcd. for $C_{22}H_{22}O_2N_4$, 350.1743; found, 350.1742.

N-Isopropyl-2,3-dimethoxypyrido[2',1':2,3]imidazo[4,5-c]isoquinoline-5-amine (129ec)[193]
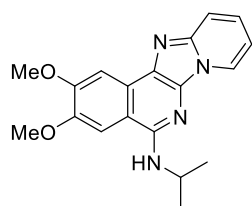
GBB-product **128e** (100 mg, 0.25 mmol, 1.00 equiv), isopropyl isonitrile (26 mg, 0.04 mL, 0.37 mmol, 1.50 equiv), potassium acetate (73 mg, 0.74 mmol, 3.00 equiv), $Pd(dba)_2$ (7.1 mg, 0.012 mmol, 0.05 equiv) and XPhos (12 mg, 0.025 mmol, 0.10 equiv) were reacted in anhydrous DMF (2 mL) for 18 h at 120 °C. The solvent was removed under reduced pressure and the residue was purified *via* preparative TLC (SiO_2, CH/EtOAc/NEt₃ 6:1:0.04 to 1:1:0.04). **129ec** was obtained as a yellow solid (32 mg, 0.10 mmol, 39%).

R_f (SiO_2, CH/EtOAc 1:1) = 0.45.

¹H-NMR (400 MHz, CDCl₃) δ [ppm] = 8.63 − 8.56 (m, 1H, C*H*), 8.02 − 7.94 (m, 1H, C*H*), 7.75 − 7.59 (m, 1H, C*H*), 7.23 (d, J = 23.5 Hz, 2H, C*H*), 6.88 − 6.82 (m, 1H, C*H*), 5.10 (s, 1H, N*H*), 4.60 (d, J = 6.8 Hz, 1H, C*H*), 4.09 − 4.05 (m, 3H, OC*H₃*), 4.03 − 3.99 (m, 3H, OC*H₃*), 1.48 − 1.34 (m, 6H, C*H₃*).

¹³C-NMR (101 MHz, CDCl₃) δ [ppm] = 152.6 (C_q), 150.6 (C_q), 148.7 (C_q), 143.6 (C_q), 134.2 (C_q), 126.9 (C_q), 125.8 (CH_Ar), 125.2 (C_q), 123.3 (CH_Ar), 117.3 (CH_Ar), 113.2 (C_q), 110.8 (CH_Ar), 103.5 (CH_Ar), 103.0 (CH_Ar), 56.5 (CH₃), 56.4 (CH₃), 43.4 (CH), 23.1 (2C, CH₃).

IR (ATR) $\tilde{\upsilon}$ [cm^{-1}] = 3419 (w), 3235 (vw), 2965 (w), 2255 (vw), 1626 (w), 1588 (w), 1573 (w), 1546 (w), 1487 (m), 1433 (m), 1387 (w), 1349 (w), 1321 (w), 1293 (w), 1250 (m), 1204 (m), 1181 (m), 1087 (w), 1070 (w), 1034 (w), 1005 (w), 915 (w), 850 (w), 824 (w), 783 (w), 728 (m), 656 (w), 628 (m), 571 (w).

FAB-MS *m/z* (%): 337 [M + H]$^+$ (84), 336 [M]$^+$ (100).

HRMS-FAB (*m/z*): [M]$^+$ calcd. for $C_{19}H_{20}O_2N_4$, 336.1586; found, 336.1585.

N- Cyclohexyl -2,3-dimethoxypyrazino[2',1':2,3]imidazo[4,5-c]isoquinolin-5-amine (129fa)
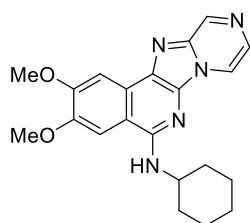
GBB-product **128f** (200 mg, 0.58 mmol, 1.00 equiv), *tert*-butyl isocyanide (61.5 mg, 0.08 mL, 0.74 mmol, 1.5 equiv), potassium acetate (145 mg, 1.48 mmol, 3.00 equiv), Pd-Peppsi-iPr (16.8 mg, 0.02 mmol, 0.05 equiv) and XPhos (23.5 mg, 0.05 mmol, 0.10 equiv) were reacted in 3 mL DMF for 18 h at 120 °C. After purification *via* flash chromatography (SiO$_2$, CH/EtOAc/NEt$_3$ 20:1:0.05 to 1:2:0.05) insertion product **129fa** was obtained as a yellow solid (77 mg, 0.20 mmol, 41%).

R_f (SiO$_2$, CH/EtOAc 1:2) = 0.21.

^{1}H NMR (400 MHz, CDCl$_3$) δ [ppm] = 9.11 (d, *J* = 1.6 Hz, 1H, C*H*$_{Ar}$), 8.41 (dd, *J* = 4.6, 1.6 Hz, 1H, C*H*$_{Ar}$), 7.93 (s, 1H, C*H*$_{Ar}$), 7.87 (d, *J* = 4.6 Hz, 1H, C*H*$_{Ar}$), 7.20 (s, 1H, C*H*$_{Ar}$), 5.41 (d, *J* = 7.2 Hz, 1H, N*H*), 4.29 (dtd, *J* = 10.7, 6.9, 3.6 Hz), 4.05 (s, 3H, OC*H*$_3$), 3.98 (s, 3H, OC*H*$_3$), 2.24 (dd, *J* = 12.4, 3.9 Hz, 2H, C*H*$_2$), 1.86 – 1.80 (m, 2H, C*H*$_2$), 1.71 (dt, *J* = 13.2, 3.7 Hz, 1H, C*H*$_2$), 1.60 – 1.43 (m, 2H, C*H*$_2$), 1.42 – 1.25 (m, 3H, C*H*$_2$).

^{13}C NMR (101 MHz, CDCl$_3$) δ [ppm] = 152.7 (C$_q$), 151.9 (C$_q$), 149.4 (C$_q$), 143.9 (C$_q$), 138.1 (C$_q$), 134.0 (C$_q$), 127.6 (CH$_{Ar}$), 127.4 (CH$_{Ar}$), 127.0 (CH$_{Ar}$), 115.9 (CH$_{Ar}$), 114.1 (CH$_{Ar}$), 103.8 (C$_q$), 103.1 (C$_q$), 56.5 (CH$_3$), 56.3 (CH$_3$), 50.5 (CH), 33.3 (2C, CH$_2$), 26.0 (CH$_2$), 25.4 (2C, CH$_2$).

IR (ATR) $\tilde{\upsilon}$ [cm^{-1}] = 3408 (w), 3312 (w), 2924 (m), 2850 (m), 1615 (w), 1574 (s), 1540 (s), 1486 (vs), 1432 (vs), 1381 (s), 1346 (s), 1282 (s), 1248 (vs), 1205 (vs), 1180 (vs), 1069 (s), 1027 (m), 1006 (s), 999 (s), 856 (s), 826 (m), 786 (vs), 626 (vs), 599 (s), 412 (s), 377 (s).

FAB-MS *m/z* (%): 379 [M + 2H]$^+$ (29), 378 [M + H]$^+$ (100), 377 [M]$^+$ (56), 376 [M − H]$^+$ (11), 362 (7), 296 (15), 295 (20), 280 (12), 133 (11).

HRMS-FAB (*m/z*): [M + H]$^+$ calcd. for $C_{21}H_{24}O_2N_5$, 378.1925; found, 378.1923.

N-(*tert*-Butyl)-2,3-dimethoxypyrazino[2',1':2,3]imidazo[4,5-*c*]isoquinolin-5-amine (129fb)
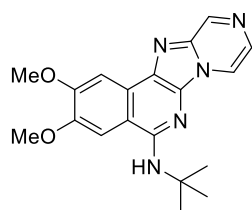
GBB product **129f** (200 mg, 0.58 mmol, 1.00 equiv), *tert*-butyl isonitrile (61.5 mg, 0.08 mL, 0.74 mmol, 1.50 equiv), potassium acetate (145 mg, 1.48 mmol, 3.00 equiv), Pd-Peppsi-iPr (16.8 mg, 0.02 mmol, 0.05 equiv) and XPhos (23.5 mg, 0.05 mmol, 0.10 equiv) were reacted in anhydrous DMF (3 mL) for 18 h at 120 °C. The solvent was removed under reduced pressure and the residue was purified *via* flash chromatography (SiO$_2$, CH/EtOAc/NEt$_3$ 20:1:0.05 to 1:2:0.05). **129fb** was obtained as a yellow solid (16 mg, 0.05 mmol, 9%).

***R*$_f$** (SiO$_2$, CH/EtOAc 1:2) = 0.20.

^{1}H NMR (400 MHz, CDCl$_3$) δ [ppm] = 9.18 (d, J = 1.5 Hz, 1H, CH^{10}), 8.44 (dd, J = 4.6,1.6 Hz, 1H, CH^8), 8.00 (s, 1H, CH^1), 7.93 (d, J = 4.6 Hz, 1H, CH^7), 7.08 (d, J = 3.7 Hz, 1H, CH^4), 5.15 (s, 1H, NH), 4.13 (s, 3H, OCH_3), 4.07 (s, 3H, OCH_3), 1,70 (s, 9H, CH$_3$).

^{13}C NMR (101 MHz, CDCl$_3$) δ [ppm] = 152.8 (C$_q$, C^2), 151.8 (C$_q$, C^5), 149.5 (C$_q$, C^3), 144.0 (C$_q$,C^{10}), 138.1 (C$_q$, C^{10a}), 133.7 (C$_q$, C^{6a}), 127.8 (CH$_{Ar}$, CH^7), 127.2 (C$_q$, C^{11b}), 127.0 (C$_q$, C^{11a}), 115.9 (CH$_{Ar}$, CH^8), 114.6 (C$_q$, C^4), 103.8 (CH$_{Ar}$, CH^4), 103.4 (CH$_{Ar}$, CH^1), 56.5 (CH$_3$), 56.4 (CH$_3$), 52.7 (C$_q$), 29.3 (3C, CH$_3$).

IR (ATR) $\tilde{v}$ [cm^{-1}] = 3336 (w), 2958 (m), 2922 (m), 2859 (w), 1662 (w), 1615 (m), 1577 (m), 1540 (s), 1490 (vs), 1463 (s), 1455 (s), 1435 (vs), 1380 (s), 1363 (s), 1349 (s), 1324 (m), 1288 (s), 1276 (s), 1252 (vs), 1217 (vs), 1203 (vs), 1179 (vs), 1137 (vs), 1096 (vs), 1077 (vs), 1028 (vs), 1009 (vs), 999 (vs), 946 (s), 931 (s), 858 (s), 826 (s), 792 (vs), 737 (m), 718 (s), 676 (s), 666 (m), 647 (m), 630 (vs), 599 (vs), 578 (s), 555 (s), 545 (s), 528 (s), 510 (s), 453 (vs), 441 (vs), 426 (vs), 416 (vs), 402 (vs), 388 (vs), 381 (vs).

FAB-MS *m/z* (%): 353 (24), 352 [M + H]$^+$ (100), 351 (71), 296 (18), 295 (21), 187 (11), 171 (12), 155 (11), 154 (22), 149 (24), 138 (10), 137 (17), 136 (23), 133 (44), 118 (30), 107 (12), 95 (11), 91 (17), 89 (12).

HRMS-FAB (*m/z*): [M + H]$^+$ calcd. for C$_{19}$H$_{22}$O$_2$N$_4$, 352.1768; found, 352.1766.

11-(tert-Butylamino)-6-(isopropylimino)-1*H*,6*H*-pyrido[2',1':2,3]imidazo[5,1-*a*]isoindol-1-one (130)
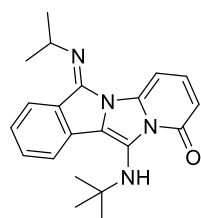
GBB-product **128d** (200 mg, 495 µmol, 1.00 equiv), cyclohexyl isonitrile (81 mg, 92 µL, 741 µmol, 1.50 equiv), potassium acetate (146 mg, 1.48 mmol, 3.00 equiv), Pd-Peppsi-iPr (16.9 mg, 24.7 µmol, 0.05 equiv) and XPhos (23.6 mg, 49.5 µmol, 0.10 equiv) were reacted in 2 mL DMF for 16 h at 120 °C. The residue was purified *via* flash chromatography (SiO$_2$, CH/EtOAc/NEt$_3$ 6:1:0.01 to 1:2:0.04). **130** was obtained as a yellow solid (113 mg, 300 µmol, 61%).

***R*$_f$** (SiO$_2$, CH/EtOAc 1:2) = 0.30.

^{1}H-NMR (400 MHz, CDCl$_3$) δ [ppm] = 7.96 (d, J = 7.9 Hz, 1H), 7.91 (d, J = 7.7 Hz, 1H), 7.50 (td, J = 7.7, 1.1 Hz, 1H), 7.43 – 7.31 (m, 2H), 6.98 (s, 1H), 6.54 (s, 1H, NH), 6.01 (dd, J = 8.7, 1.1 Hz, 1H), 4.63 (h, J = 6.2 Hz, 1H), 1.40 (d, J = 6.2Hz, 6H, CH_3), 1.33 (s, 9H, CH_3).

¹³C-NMR (100 MHz, CDCl₃) δ [ppm] = 162.6 (C$_q$), 145.9 (C$_q$), 145.2 (C$_q$), 139.6 (CH$_{Ar}$), 136.6 (C$_q$), 132.2 (C$_q$), 131.3 (CH$_{Ar}$), 130.6 (C$_q$), 130.0 (C$_q$), 128.0 (CH$_{Ar}$), 127.4 (CH$_{Ar}$), 123.1 (CH$_{Ar}$), 107.3 (CH$_{Ar}$), 89.3 (CH$_{Ar}$), 58.2 (C$_q$), 49.5 (CH), 30.0 (3C, CH₃), 24.2 (2C, CH₃).

IR (ATR) $\tilde{v}$ [cm⁻¹] = 3303 (w), 2963 (m), 2928 (m), 2861 (w), 1681 (s), 1657 (vs), 1608 (m), 1564 (vs), 1520 (vs), 1497 (s), 1459 (vs), 1441 (vs), 1431 (vs), 1405 (s), 1361 (vs), 1349 (vs), 1306 (s), 1295 (s), 1261 (s), 1247 (s), 1214 (vs), 1196 (s), 1180 (s), 1169 (vs), 1156 (vs), 1137 (vs), 1118 (vs), 1071 (s), 1030 (s), 1014 (m), 967 (m), 942 (m), 911 (m), 866 (m), 851 (m), 796 (s), 766 (vs), 755 (vs), 728 (vs), 697 (s), 669 (s), 643 (s), 602 (s), 565 (s), 543 (s), 521 (s), 490 (s), 475 (s), 438 (m), 416 (m).

FAB-MS *m/z* (%): 349 (90), 348 (100), 293 (60), 292 (78), 291 (63), 278 (75), 214 (60), 136 (93), 107 (64), 91 (64).

HRMS-FAB (*m/z*): [M + H]+ calcd. for C₂₁H₂₄O₁N₄, 348.1945; found, 348.1946.

5.4.5 Miniaturized Synthesis of Fluorophore Arrays *via* nano3D Printing

Phenanthrene-9,10-diamine (150)
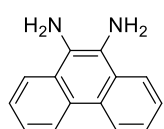
According to a procedure by COLAK *et al.*,[158, 194] phenanthen-9,10-dione (2.00 g, 9.61 mmol, 1.00 equiv), hydroxylamine hydrochloride (1.47 g, 879 µL, 21.1 mmol, 2.20 equiv), and pyridine (1.90 g, 1.94 mL, 24.0 mmol, 2.50 equiv) were stirred at 130°C for 3h. After cooling to r.t., the product was filtered off. **149** was obtained as a brown solid (1.69 g, 7.1 mmol, 74%) and used without further purification.

149 (1.69 g, 7.11 mmol, 1.00 equiv), 10 wt% Pd/C (847 mg, 7.96 mmol, 1.12 equiv) and hydrazine hydrate (17 mL) were stirred in ethanol (85 mL) at 80°C for 24 h. The solvent was removed under reduced pressure, the product was poured into water (300 mL) and filtered off. **150** was obtained as green solid (949 mg, 4.56 mmol, 64%).

^{1}H-NMR (400 MHz, DMSO-d_6): δ [ppm] = 8.38 (dd, J = 3.1, 1.3 Hz, 2H, 2 CH_{Ar}), 8.33 (dd, J = 3.2, 1.4 Hz, 2H, 2 CH_{Ar}), 8.15 (dd, J = 7.8, 1.5 Hz, 2H, 2 CH_{Ar}), 8.03 (dd, J = 8.3, 1.3 Hz, 2H, 2 CH_{Ar}), 4.96 (s, 4H, 2 NH_2).

^{13}C-NMR (101 MHz, DMSO-d_6): δ [ppm] = 137.3 (2C, C_q), 136.7 (2C, C_q), 133.3 (2C, CH_{Ar}), 129.9 (2C, CH_{Ar}), 125.0 (2C, CH_{Ar}), 124.8 (2C, CH_{Ar}), 123.2 (2C, C_q).

IR (ATR) $\tilde{v}$ [cm^{-1}] = 3200 (w), 1674 (w), 1589 (m), 1575 (m), 1451 (m), 1422 (w), 1374 (w), 1295 (w), 1281 (m), 1251 (m), 1224 (w), 1188 (m), 1159 (w), 1122 (w), 1096 (w), 1011 (m), 943 (w), 924 (w), 898 (w), 868 (w), 758 (vs), 722 (s), 714 (vs), 696 (m), 681 (m), 657 (w), 633 (w), 618 (w), 585 (w), 555 (w), 534 (vs), 479 (w), 463 (w), 448 (m), 432 (s), 422 (m), 408 (m), 388 (w), 377 (m).

FAB-MS *m/z* (%): 208 [M + H]$^+$ (18), 207 (82), 181 (9), 180 (82), 179 (100), 178 (35), 177 (16), 153 (11), 152 (34), 151 (27), 150 (14), 76 (10).

HRMS-FAB (*m/z*): [M + H]$^+$ calcd. for $C_{14}H_{12}N_2$, 207.0917; found 207.0917.

_N_-(4-Methylphenyl)-2-nitroaniline (152a)[194]
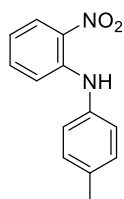
1-Fluoro-2-nitrobenzene (500 mg, 375 µL, 3.54 mmol, 1.00 equiv), 4-methylaniline (418 mg, 398 µL, 3.90 mmol, 1.10 equiv) und Cs_2CO_3 (2.31 g, 7.09 mmol, 2.00 equiv) were stirred in DMF (20 mL) at r.t. for 16 h. The solvent was removed under reduced pressure and the residue was purified *via* flash chromatography (SiO$_2$, CH/EE 20:1). **152a** was obtained as a red solid (339 mg, 1.49 mmol, 42%).

R_f (SiO$_2$, CH/EtOAc 4:1): 0.67.

^{1}H-NMR (400 MHz, CDCl$_3$): δ [ppm] = 9.48 (s, 1H, NH), 8.21 (dd, J = 8.6, 1.6 Hz, 1H, CH_{Ar}), 7.36 (ddd, J = 8.7, 6.8, 1.7 Hz, 1H, CH_{Ar}), 7.25 (d, J = 8.2 Hz, 2H, 2 CH_{Ar}), 7.18 (m, 3H, 3 CH_{Ar}), 6.76 (ddd, J = 8.4, 6.9, 1.3 Hz, 1H, CH_{Ar}), 2.41 (s, 3H, CH_3).

^{13}C-NMR (101 MHz, CDCl$_3$): δ [ppm] = 143.7 (C_q), 135.9 (C_q), 135.7 (C_q), 135.7 (CH_{Ar}), 132.8 (C_q), 130.4 (2C, CH_{Ar}), 126.6 (CH_{Ar}), 124.8 (2C, CH_{Ar}), 117.1 (CH_{Ar}), 116.0 (CH_{Ar}), 20.9 (CH_3).

IR (ATR) $\tilde{v}$ [cm⁻¹] = 3332 (m), 3080 (w), 3063 (w), 3041 (w), 2911 (w), 2851 (w), 1618 (m), 1608 (s), 1587 (w), 1568 (s), 1503 (vs), 1441 (m), 1421 (s), 1350 (vs), 1323 (s), 1300 (w), 1249 (vs), 1220 (vs), 1176 (s), 1163 (s), 1145 (vs), 1125 (s), 1109 (s), 1075 (s), 1040 (s), 1016 (s), 965 (m), 950 (m), 938 (m), 894 (m), 849 (s), 822 (m), 802 (vs), 775 (m), 766 (m), 734 (vs), 691 (m), 673 (m), 646 (m), 618 (s), 554 (s), 513 (vs), 489 (vs), 445 (m), 394 (m).

FAB-MS *m/z* (%): 228 [M]⁺ (100), 181 [M − NO₂]⁺ (67), 69 (81).

HRMS-FAB (*m/z*): [M + H]⁺ calcd. for $C_{13}H_{12}N_2O_2$, 228.0893; found, 228.0892.

(2-Aminophenyl)-(*p*-tolyl)amine (146a)[194]
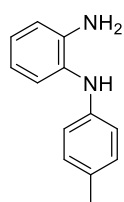
152a (300 mg, 1.31 mmol, 1.00 equiv) and 10% Pd/C (30.0 mg, 282 µmol, 0.214 equiv) was stirred in methanol (20 mL) at r.t. for 16 h under H₂ atmosphere. The mixture was filtered through a pad of Celite®, and the solvent was removed under reduced pressure. **146a** was obtained as a red solid (222 mg, 1.12 mmol, 85%).

R_f (SiO₂, CH/EtOAc 4:1): 0.34.

¹H-NMR (400 MHz, DMSO-d_6): δ [ppm] = 6.95 (dd, *J* = 8.1, 6.6 Hz, 3H, C*H*$_{Ar}$), 6.79 (td, *J* = 7.5, 1.5 Hz, 1H, C*H*$_{Ar}$), 6.72 (dd, *J* = 7.9, 1.6 Hz, 1H, C*H*$_{Ar}$), 6.67 (m, 2H, C*H*$_{Ar}$), 6.52 (td, *J* = 7.5, 1.6 Hz, 1H, C*H*$_{Ar}$), 4.70 (s, 2H, N*H*$_2$), 2.19 (s, 3H, C*H*$_3$).

¹³C-NMR (101 MHz, DMSO-d_6): δ [ppm] = 143.8 (C_q), 142.3 (C_q), 129.8 (2C, CH$_{Ar}$), 128.8 (C_q), 126.9 (C_q), 124.0 (CH$_{Ar}$), 122.6 (CH$_{Ar}$), 117.0 (CH$_{Ar}$), 115.6 (CH$_{Ar}$), 115.6 (2C, CH$_{Ar}$), 20.7 (CH₃).

IR (ATR) $\tilde{v}$ [cm⁻¹] = 3427 (w), 3336 (m), 3041 (w), 3014 (w), 2914 (w), 2857 (w), 2728 (w), 1609 (vs), 1591 (m), 1510 (vs), 1499 (vs), 1458 (m), 1439 (s), 1397 (m), 1377 (w), 1296 (vs), 1254 (s), 1218 (m), 1179 (m), 1156 (m), 1137 (m), 1122 (m), 1047 (m), 1027 (m), 1007 (m), 926 (w), 887 (w), 866 (w), 841 (w), 807 (vs), 742 (vs), 704 (m), 653 (s), 633 (vs), 581 (vs), 547 (vs), 496 (vs), 459 (vs), 439 (vs), 416 (vs), 384 (s).

FAB-MS *m/z* (%): 198 [M]⁺ (100), 197 [M − H]⁺ (24), 183.2 [M − NH]⁺ (28).

HRMS-FAB (*m/z*): [M + H]⁺ calcd. for $C_{13}H_{14}N_2$, 198.1152; found, 198.1152.

N-(2-Nitrophenyl)[1,1′-biphenyl]-3-amine (152b)
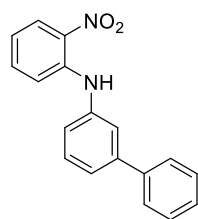
1-Fluoro-2-nitrobenzene (500 mg, 375 µL, 3.54 mmol, 1.00 equiv), 3-Phenylaniline (472 mg, 2.79 mmol, 0.79 equiv) and Cs₂CO₃ (2.31 g, 7.09 mmol, 2.00 equiv) was stirred in DMF (20 mL) at r.t. for 16 h. The solvent was removed under reduced pressure and the residue was purified *via* flash chromatography (SiO₂, CH/EE 20:1). **152b** was obtained as an orange solid (191 mg, 658 µmol, 19%).

R_f (SiO₂, CH/EtOAc 4:1) = 0.59.

¹H-NMR (400 MHz, DMSO-d_6): δ [ppm] = 9.46 (s, 1H, N*H*), 8.13 (dd, *J* = 8.5, 1.6 Hz, 1H, C*H*$_{Ar}$), 7.68 (m, 2H, 2 C*H*$_{Ar}$), 7.62 (m, 1H, C*H*$_{Ar}$), 7.49 (m, 6H, C*H*$_{Ar}$), 7.38 (m, 1H, C*H*$_{Ar}$), 7.32 (m, 2H, 2 C*H*$_{Ar}$).

¹³C-NMR (101 MHz, DMSO-d_6): δ [ppm] = 142.2 (C$_q$), 142.1 (C$_q$), 140.4 (C$_q$), 140.1 (C$_q$), 136.5 (CH$_{Ar}$), 134.3 (C$_q$), 130.5 (CH$_{Ar}$), 129.4 (2C, CH$_{Ar}$), 128.3 (CH$_{Ar}$), 127.2 (2C, CH$_{Ar}$), 126.7 (CH$_{Ar}$), 123.5 (CH$_{Ar}$), 122.8 (CH$_{Ar}$), 122.2 (CH$_{Ar}$), 118.7 (CH$_{Ar}$), 117.5 (CH$_{Ar}$).

IR (ATR) $\tilde{v}$ [cm^{-1}] = 3347 (w), 3058 (w), 3031 (w), 1615 (s), 1595 (s), 1571 (vs), 1494 (vs), 1434 (s), 1409 (m), 1346 (vs), 1324 (s), 1256 (vs), 1222 (s), 1160 (m), 1146 (vs), 1094 (w), 1077 (m), 1057 (m), 1038 (s), 1009 (m), 914 (w), 890 (w), 854 (m), 819 (w), 796 (w), 779 (w), 759 (s), 739 (vs), 697 (vs), 653 (w), 616 (w), 585 (w), 537 (w), 514 (m), 463 (w), 432 (w), 405 (vw).

FAB-MS *m/z* (%): 291 [M + H]$^+$ (82), 290.2 [M]$^+$ (100), 154 [M – C$_6$H$_6$N$_2$O$_2$]$^+$ (94), 136.1 [M – C$_{12}$H$_{10}$]$^+$ (66).

HRMS-FAB (*m/z*): [M + H]$^+$ calcd. for C$_{18}$H$_{14}$N$_2$O$_2$, 290.1050; found, 290.1049.

*N*¹-([1,1'-Biphenyl]-3-yl)benzene-1,2-diamine (146b)
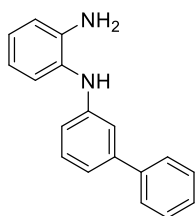
152b (170 mg, 586 µmol, 1.00 equiv) and 10 wt% Pd/C (30.0 mg, 282 µmol, 0.21 equiv) was stirred in methanol (20 mL) at r.t. for 16 h under H$_2$ atmosphere. The mixture was filtered through a pad of Celite®, and the solvent was removed under reduced pressure. **146b** was obtained as a red solid (109 mg, 429 µmol, 72%).

¹H-NMR (400 MHz, DMSO-d_6): δ [ppm] = 7.53 (m, 2H, C*H*$_{Ar}$), 7.44 (dd, *J* = 8.4, 7.0 Hz, 2H, C*H*$_{Ar}$), 7.34 (m, 1H, C*H*$_{Ar}$), 7.27 (s, 1H, N*H*), 7.21 (t, *J* = 7.8 Hz, 1H, C*H*$_{Ar}$), 7.05 (dd, *J* = 7.8, 1.5 Hz, 1H, C*H*$_{Ar}$), 6.94 (m, 2H, C*H*$_{Ar}$), 6.87 (td, *J* = 7.5, 1.5 Hz, 1H, C*H*$_{Ar}$), 6.76 (dd, *J* = 7.9, 1.5 Hz, 1H, C*H*$_{Ar}$), 6.71 (ddd, *J* = 8.1, 2.3, 1.0 Hz, 1H, C*H*$_{Ar}$), 6.57 (td, *J* = 7.5, 1.5 Hz, 1H, C*H*$_{Ar}$), 4.78 (s, 2H, N*H*$_2$).

¹³C-NMR (101 MHz, DMSO-d_6): δ [ppm] = 147.1 (C$_q$) 143.2 (C$_q$), 141.5 (C$_q$), 141.4 (C$_q$), 129.9 (CH$_{Ar}$), 129.3 (2C, CH$_{Ar}$), 127.7 (C$_q$), 127.7 (CH$_{Ar}$), 127.0 (2C, CH$_{Ar}$), 125.0 (CH$_{Ar}$), 124.3 (CH$_{Ar}$), 117.0 (CH$_{Ar}$), 116.6 (CH$_{Ar}$), 115.7 (CH$_{Ar}$), 113.9 (CH$_{Ar}$), 113.1 (CH$_{Ar}$).

IR (ATR) $\tilde{v}$ [cm^{-1}] = 3408 (w), 3371 (w), 3363 (w), 3327 (m), 3203 (w), 3054 (w), 3024 (w), 2980 (w), 2969 (w), 2928 (w), 2919 (w), 2897 (w), 2861 (w), 1604 (s), 1584 (s), 1570 (s), 1489 (vs), 1475 (vs), 1452 (s), 1435 (s), 1414 (m), 1381 (m), 1334 (w), 1310 (s), 1286 (s), 1232 (s), 1200 (m), 1166 (m), 1153 (m), 1133 (m), 1088 (w), 1072 (m), 1050 (m), 1023 (s), 1006 (m), 993 (m), 970 (w), 931 (w), 916 (w), 907 (w), 866 (s), 846 (w), 820 (w), 788 (m), 756 (vs), 745 (vs), 697 (vs), 650 (vs), 613 (vs), 586 (s), 562 (s), 535 (vs), 523 (vs), 504 (vs), 466 (vs), 458 (vs), 439 (vs).

FAB-MS *m/z* (%): 261 [M + H]$^+$ (70), 260 [M]$^+$ (100), 259 [M – H]$^+$ (24).

HRMS-FAB (*m/z*): [M + H]$^+$ calcd. for C$_{18}$H$_{16}$N$_2$, 260.1308; found, 260.1309.

1-Adamantyl-2(nitrophenyl)amine (152c)[194]
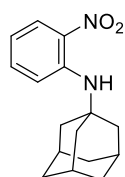
1-Fluoro-2-nitrobenzene (500 mg, 375 µL, 3.54 mmol, 1.00 equiv), 1-adamantylamine (590 mg, 3.90 mmol, 1.10 equiv) und Cs_2CO_3 (2.31 g, 7.09 mmol, 2.00 equiv) were stirred in DMF (20 mL) at r.t. for 16 h. The solvent was removed under reduced pressure and the residue was purified *via* flash chromatography (SiO_2, CH/EE 20:1). **152c** was obtained as an orange solid (757 mg, 2.78 mmol, 78%).

R_f (SiO_2, CH/EtOAc 4:1): 0.76.

1H-NMR (400 MHz, $CDCl_3$): δ [ppm] = 8.09 (dd, *J* = 8.7, 1.7 Hz, 1H, C*H*$_{Ar}$), 7.26 (ddd, *J* = 8.6, 6.8, 1.8 Hz, 1H, C*H*$_{Ar}$), 7.12 (dd, *J* = 8.8, 1.2 Hz, 1H, C*H*$_{Ar}$), 6.50 (ddd, *J* = 8.3, 6.8, 1.2 Hz, 1H, C*H*$_{Ar}$), 2.11 (m, 3H, 3 C*H*), 2.04 (d, *J* = 2.9 Hz, 6H, 6 C*H*$_2$), 1.68 (q, *J* = 2.4 Hz, 6H, 6 C*H*$_2$), 1.48 (s, 1H, N*H*).

13C-NMR (101 MHz, $CDCl_3$): δ [ppm] = 145.0 (C_q), 135.1 (CH_{Ar}), 132.5 (C_q), 127.6 (CH_{Ar}), 116.9 (CH_{Ar}), 114.8 (CH_{Ar}), 52.9 (C_q), 42.5 (3C, CH_2), 36.4 (3C, CH_2), 29.7 (3C, CH).

IR (ATR) $\tilde{v}$ [cm^{-1}] = 3339 (w), 2945 (w), 2907 (vs), 2846 (s), 2670 (w), 2656 (w), 2574 (w), 2548 (w), 1615 (s), 1574 (s), 1507 (vs), 1475 (s), 1453 (s), 1435 (m), 1422 (s), 1367 (m), 1354 (s), 1341 (s), 1327 (s), 1306 (s), 1292 (m), 1275 (s), 1238 (vs), 1222 (vs), 1184 (s), 1154 (vs), 1122 (vs), 1103 (s), 1094 (s), 1061 (s), 1041 (vs), 1033 (vs), 987 (s), 979 (s), 955 (s), 948 (s), 935 (s), 878 (m), 858 (s), 851 (s), 839 (m), 832 (m), 815 (m), 776 (m), 735 (vs), 696 (s), 670 (s), 654 (s), 585 (m), 562 (vs), 521 (vs), 463 (s), 453 (s), 432 (m), 408 (s), 399 (m), 394 (s), 378 (m).

FAB-MS *m/z* (%): 273 [M + H]$^+$ (56), 272 [M]$^+$ (56), 154 (99), 135 (100).

HRMS-FAB (*m/z*): [M]$^+$ calcd. for $C_{16}H_{20}N_2O_2$, 272.1519; found 272.1520.

2-*N*-(1-Adamantyl)benzene-1,2-diamine (146c)[194]
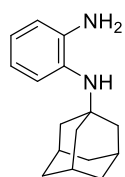
152c (700 mg, 2.57 mmol, 1.00 equiv) und 10 wt% Pd/C (30.0 mg, 282 µmol, 0.214 equiv) were stirred in methanol (20.0 mL) at r.t. for 16 h under a H_2 atmosphere. The mixture was filtered through a pad of Celite®, and the solvent was removed under reduced pressure. **146c** was obtained as a red liquid (578 mg, 2.38 mmol, 93%).

R_f (SiO_2, CH/EtOAc 4:1): 0.36.

1H-NMR (400 MHz, DMSO-d_6): δ [ppm] = 6.79 (dd, *J* = 7.9, 1.4 Hz, 1H, C*H*$_{Ar}$), 6.63 (m, 2H, 2 C*H*$_{Ar}$), 6.46 (td, *J* = 7.4, 1.9 Hz, 1H, C*H*$_{Ar}$), 4.75 (s, 2H, N*H*$_2$), 2.17 (s, 1H, N*H*), 2.04 (m, 3H, 3 C*H*), 1.79 (d, *J* = 2.9 Hz, 6H, 6 C*H*$_2$), 1.59 (dt, *J* = 11.5, 3.0 Hz, 6H, 6 C*H*$_2$).

13C-NMR (101 MHz, DMSO-d_6): δ [ppm] = 141.8 (C_q), 123.4 (CH_{Ar}), 123.4 (CH_{Ar}), 121.5 (C_q), 117.0 (CH_{Ar}), 115.7 (CH_{Ar}), 43.2 (C_q), 39.5 (3C, CH_2), 36.6 (3C, CH_2), 29.6 (3C, CH).

IR (ATR) $\tilde{v}$ [cm^{-1}] = 3393 (w), 3329 (w), 2901 (vs), 2846 (s), 2755 (w), 2679 (w), 2635 (w), 1616 (w), 1592 (m), 1503 (vs), 1472 (m), 1448 (s), 1357 (m), 1341 (m), 1309 (m), 1286 (w), 1264 (vs), 1213 (m), 1186 (w), 1156 (w), 1133

(m), 1112 (w), 1095 (m), 1069 (w), 1037 (w), 979 (w), 938 (w), 905 (w), 849 (w), 815 (w), 798 (w), 779 (w), 732 (vs), 674 (m), 642 (m), 595 (m), 550 (m), 503 (m), 492 (m), 479 (m), 449 (vs), 415 (m), 397 (m), 384 (m).

FAB-MS *m/z* (%): 243 [M + H]⁺ (53), 242 [M]⁺ (100), 241 [M − H]⁺ (28), 93 (10).

HRMS-FAB (*m/z*): [M + H]⁺ calcd. for $C_{16}H_{22}N_2$, 242.1778; found 242.1778.

3,5-Dimethyl-N-(2-nitrophenyl)aniline (152d)[194]
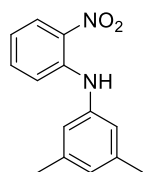
1-Fluoro-2-nitrobenzene (500 mg, 375 µL, 3.54 mmol, 1.00 equiv), 3,5-dimethylaniline (472 mg, 486 µL, 3.90 mmol, 1.10 equiv) and Cs_2CO_3 (2.31 g, 7.09 mmol, 2.00 equiv) were stirred in DMF (20 mL) at r.t. for 16 h. The solvent was removed under reduced pressure and the residue was purified *via* flash chromatography (SiO₂, CH/EE 20:1). **152d** was obtained as an orange solid (285 mg, 1.18 mmol, 33%).

*R*ₓ (SiO₂, CH/EtOAc 4:1) = 0.62.

¹H-NMR (400 MHz, DMSO-*d₆*): δ [ppm] = 9.29 (s, 1H, N*H*), 8.11 (dd, *J* = 8.6, 1.6 Hz, 1H, C*H*ₐᵣ), 7.51 (ddd, *J* = 8.7, 6.9, 1.7 Hz, 1H, C*H*ₐᵣ), 7.20 (dd, *J* = 8.6, 1.2 Hz, 1H, C*H*ₐᵣ), 6.94 (d, *J* = 1.5 Hz, 2H, C*H*ₐᵣ), 6.86 (m, 2H, 2 C*H*ₐᵣ), 2.28 (s, 6H, C*H₃*).

¹³C-NMR (101 MHz, DMSO-*d₆*): δ [ppm] = 142.7 (Cq), 139.4 (Cq), 139.2 (2C, Cq), 136.5 (CHₐᵣ), 133.70 (Cq), 127.0 (CHₐᵣ), 126.8 (CHₐᵣ), 121.8 (2C, CHₐᵣ), 118.3 (CHₐᵣ), 116.7 (CHₐᵣ), 21.2 (2C, CH₃).

IR (ATR) ũ [cm⁻¹] = 3342 (m), 3315 (m), 3095 (w), 3031 (m), 2951 (m), 2915 (m), 2853 (m), 1609 (s), 1592 (s), 1571 (vs), 1497 (vs), 1486 (vs), 1468 (s), 1460 (s), 1432 (s), 1405 (s), 1373 (m), 1350 (vs), 1324 (s), 1298 (m), 1265 (vs), 1245 (vs), 1215 (vs), 1160 (vs), 1137 (vs), 1116 (vs), 1079 (s), 1050 (s), 1031 (vs), 996 (s), 950 (s), 888 (s), 860 (s), 846 (vs), 819 (s), 778 (s), 741 (vs), 721 (s), 691 (s), 670 (vs), 608 (s), 585 (s), 547 (s), 523 (vs), 503 (vs), 465 (s), 431 (m), 401 (m), 375 (m).

FAB-MS *m/z* (%): 243 (81), 242 [M + H]⁺ (100), 209 (23), 195.1 [M − NO₂]⁺ (10).

HRMS-FAB (*m/z*): [M + H]⁺ calcd. for $C_{14}H_{14}N_2O_2$, 242.1050; found, 242.1048.

2-*N*-(3,5-Dimethylphenyl)benzene-1,2-diamine (146d)[194]
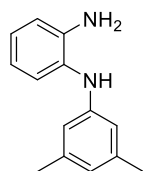
152d (227 mg, 937 µmol, 1.00 equiv) and 10 wt% Pd/C (23 mg, 216 µmol, 0.231 equiv) was stirred in methanol (20 mL) at r.t. for 16 h under H₂ atmosphere. The mixture was filtered through a pad of Celite®, and the solvent was removed under reduced pressure. **146d** was obtained as a red solid (172 mg, 0.81 mmol, 86%).

¹H-NMR (400 MHz, DMSO-*d₆*): δ [ppm] = 6.97 (dd, *J* = 7.8, 1.5 Hz, 1H, C*H*ₐᵣ), 6.94 (s, 1H, N*H*), 6.83 (td, *J* = 7.5, 1.5 Hz, 1H, C*H*ₐᵣ), 6.72 (dd, *J* = 7.9, 1.5 Hz, 1H, C*H*ₐᵣ), 6.54 (td, *J* = 7.5, 1.6 Hz, 1H, C*H*ₐᵣ), 6.32 (d, *J* = 8.8 Hz, 3H, 3 C*H*ₐᵣ), 4.70 (s, 2H, N*H₂*), 2.14 (s, 6H, C*H₃*).

¹³C-NMR (101 MHz, DMSO-d_6): δ [ppm] = 146.5 (C_q), 143.0 (C_q), 138.1 (2C, C_q), 128.1 (C_q), 124.6 (CH_{Ar}), 124.1 (CH_{Ar}), 120.0 (CH_{Ar}), 116.9 (CH_{Ar}), 115.6 (CH_{Ar}), 112.8 (2C, CH_{Ar}), 21.6 (2C, CH_3).

IR (ATR) $\tilde{\upsilon}$ [cm⁻¹] = 3370 (m), 3298 (w), 3269 (m), 3135 (w), 3116 (w), 3029 (w), 3006 (w), 2963 (w), 2914 (w), 2857 (w), 2758 (w), 2730 (w), 2663 (w), 2619 (w), 2584 (vw), 2560 (vw), 2469 (vw), 1608 (s), 1588 (vs), 1524 (s), 1486 (vs), 1456 (vs), 1412 (m), 1375 (w), 1343 (vs), 1316 (s), 1269 (vs), 1259 (s), 1213 (s), 1167 (m), 1136 (s), 1075 (w), 1035 (m), 1027 (m), 1007 (w), 953 (w), 919 (w), 875 (w), 860 (m), 832 (vs), 805 (s), 775 (vs), 738 (vs), 697 (vs), 670 (s), 605 (s), 591 (s), 555 (vs), 537 (vs), 527 (vs), 455 (vs), 443 (s), 421 (m), 407 (m), 390 (m), 387 (m), 375 (m).

FAB-MS *m/z* (%): 213 [M + H]⁺ (13), 212 [M]⁺ (81), 211 [M – H]⁺ (11), 197 [M – NH]⁺ (54), 196 [M – NH₂]⁺ (15) 121 [M – C₆H₅N]⁺ (25), 66 (100).

HRMS-FAB (*m/z*): [M + H]⁺ calcd. for $C_{14}H_{16}N_2$, 212.1308; found, 212.1308.

Benzo[*g*]pteridine-2,4(1H,3H)-dione (142a)
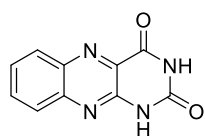
o-Phenylenediamine (381 mg, 3.52 mmol, 1.00 equiv), alloxan (500 mg, 3.52 mmol, 1.00 equiv), boronic acid (218 mg, 3.52 mmol, 1.00 equiv) were dissolved in water (20 mL). The mixture was stirred at r.t. for 2 h. The precipitate was filtered off and washed with acetic acid (30 mL), water (10 mL) and diethyl ether (30 mL). **142a** was obtained as a yellow solid (597 mg, 2.79 mmol, 79%).

¹H-NMR (400 MHz, DMSO-d_6): δ [ppm] = 11.96 (s, 1H, N*H*), 11.76 (s, 1H, N*H*), 8.17 (dt, *J* = 8.5, 1.1 Hz, 1H, C*H*$_{Ar}$), 7.93 (m, 2H, 2 C*H*$_{Ar}$), 7.79 (ddd, *J* = 8.3, 5.3, 3.0 Hz, 1H, C*H*$_{Ar}$).

¹³C-NMR (101 MHz, DMSO-d_6): δ [ppm] = 150.6 (C_q, CO), 147.3 (C_q, CO), 143.1 (C_q), 139.7 (C_q), 133.8 (CH_{Ar}), 132.2 (C_q), 130.7 (CH_{Ar}), 128.9 (CH_{Ar}), 127.4 (CH_{Ar}).

IR (ATR) $\tilde{\upsilon}$ [cm⁻¹] = 3197 (m), 3172 (m), 3138 (m), 3102 (m), 3084 (m), 3044 (m), 2992 (m), 2969 (m), 2929 (w), 2868 (w), 2840 (w), 2820 (w), 2769 (w), 2727 (w), 1734 (s), 1690 (vs), 1618 (m), 1582 (vs), 1574 (s), 1504 (s), 1486 (m), 1446 (s), 1391 (s), 1363 (vs), 1334 (vs), 1316 (s), 1307 (s), 1272 (vs), 1248 (s), 1222 (s), 1213 (s), 1176 (m), 1153 (m), 1145 (s), 1111 (m), 1088 (w), 1061 (w), 1034 (m), 1013 (m), 989 (w), 915 (w), 894 (w), 867 (m), 810 (m), 768 (vs), 722 (s), 704 (vs), 677 (s), 640 (m), 584 (vs), 540 (vs), 511 (vs), 428 (vs), 377 (s).

EI-MS *m/z* (%): 215 (10), 214 [M + H]⁺ (100), 171 (13), 143 (94), 116 (23), 69 (14).

HRMS-FAB (*m/z*): [M + H]⁺ calcd. for $C_{10}H_6N_4O_2$, 214.0485; found, 214.0484.

EA: calcd. for $C_{10}H_6N_4O_2$, N 26.16 C 56.08 H 2.82; found, N 25.40 C 55.67 H 2.78.

1H-Naphtho[2,3-*g*]pteridine-2,4-quinone (142b)
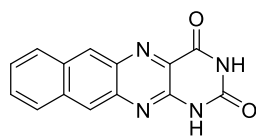
Naphthaleine-1,2-diamine (500 mg, 3.16 mmol, 1.00 equiv), alloxan (449 mg, 3.16 mmol, 1.00 equiv), boronic acid (195 mg, 3.16 mmol, 1.00 equiv) were dissolved in water (20 mL). The mixture was stirred at r.t. for 2 h. The precipitate was filtered off and washed with acetic acid (30 mL), water (10 mL) and 30 diethyl ether (30 mL). **142b** was obtained as an orange solid (491 mg, 1.86 mmol, 59%).

¹H-NMR (400 MHz, DMSO-d_6): δ [ppm] = 11.96 (s, 1H, N*H*), 11.76 (s, 1H, N*H*), 8.91 (s, 1H, C*H*$_{Ar}$), 8.52 (s, 1H, C*H*$_{Ar}$), 8.27 (d, *J* = 8.4 Hz, 1H, C*H*$_{Ar}$), 8.20 (d, *J* = 8.5 Hz, 1H, C*H*$_{Ar}$), 7.68 (ddd, *J* = 8.3, 6.5, 1.3 Hz, 1H, C*H*$_{Ar}$), 7.62 (ddd, *J* = 8.0, 6.6, 1.2 Hz, 1H, C*H*$_{Ar}$).

¹³C-NMR (101 MHz, DMSO-d_6): δ [ppm] = 150.6 (C_q, CO), 146.6 (C_q, CO), 138.9 (C_q), 137.0 (2 C_{Ar}), 135.8 (C_q), 134.5 (C_q), 132.6 (C_q), 129.9 (CH$_{Ar}$), 129.3 (CH$_{Ar}$), 128.7 (CH$_{Ar}$), 128.3 (CH$_{Ar}$), 126.7 (CH$_{Ar}$), 124.5 (CH$_{Ar}$).

IR (ATR) ṽ [cm⁻¹] = 3176 (w), 3105 (w), 3058 (w), 2837 (w), 1738 (vs), 1725 (vs), 1673 (vs), 1605 (m), 1574 (vs), 1537 (m), 1421 (s), 1401 (s), 1388 (m), 1371 (vs), 1346 (s), 1323 (s), 1282 (vs), 1269 (vs), 914 (m), 891 (m), 881 (m), 824 (s), 806 (m), 783 (m), 755 (vs), 747 (s), 674 (m), 649 (m), 632 (m), 510 (s), 492 (m), 473 (vs), 421 (vs), 407 (vs), 375 (m).

FAB-MS *m/z* (%): 265 [M + H]⁺ (14), 155 (31), 154 (100), 139 (15), 138 (37), 137 (68), 136 (64), 124 (10), 120 (12), 107 (21), 91 (15), 90 (10), 89 (16).

HRMS-FAB (*m/z*): [M + H]⁺ calcd. for $C_{14}H_8N_4O_2$, 265.0720; found 265.0721.

9H-Phenanthro[9,10-*g*]pteridine-11,13-quinone (142c)[194]
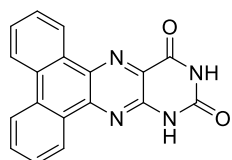
150 (200 mg, 0.96 mmol, 1.00 equiv), alloxan (136 mg, 0.96 mmol, 1.00 equiv), boric acid (59.4 mg, 0.96 mmol, 1.00 equiv) were dissolved in water (20 mL). The mixture was stirred at r.t. for 2 h. The precipitate was filtered off and washed with acetic acid (30 mL), water (10 mL) and diethyl ether (30 mL). **142c** was isolated as a deep red solid (62 mg, 197 µmol, 21%).

¹H-NMR (400 MHz, DMSO-d_6): δ [ppm] = 12.19 (s, 1H, N*H*), 11.82 (s, 1H, N*H*), 9.06 (m, 2H, 2 C*H*$_{Ar}$), 8.87 (m, 2H, 2 C*H*$_{Ar}$), 7.95 (ddd, *J* = 8.4, 7.1, 1.5 Hz, 1H, C*H*$_{Ar}$), 7.86 (tdd, *J* = 6.6, 3.7, 2.2 Hz, 3H, 3 C*H*$_{Ar}$).

¹³C-NMR (101 MHz, DMSO-d_6): δ [ppm] = 161.3 (2 C_{Ar}), 150.6 (C_q, CO), 148.3 (C_q, CO), 142.9 (C_q), 137.1 (C_q), 132.9 (C_q), 131.8 (CH$_{Ar}$), 130.4 (C_q), 130.0 (C_q), 129.6 (C_q), 128.9 (CH$_{Ar}$), 128.8 (CH$_{Ar}$), 128.6 (CH$_{Ar}$), 126.4 (CH$_{Ar}$), 124.9 (CH$_{Ar}$), 124.2 (CH$_{Ar}$), 124.1 (CH$_{Ar}$).

IR (ATR) ṽ [cm⁻¹] = 3152 (w), 3063 (w), 2941 (w), 2849 (w), 2788 (w), 1717 (m), 1698 (s), 1618 (m), 1604 (m), 1589 (m), 1568 (s), 1540 (m), 1503 (w), 1490 (w), 1452 (m), 1405 (s), 1374 (vs), 1341 (m), 1312 (w), 1286 (m), 1222 (w), 1154 (w), 1129 (w), 1115 (w), 1079 (w), 1065 (w), 1037 (w), 1024 (w), 989 (w), 960 (w), 860 (m), 819 (w), 803 (w), 755 (vs), 720 (vs), 693 (m), 647 (w), 616 (w), 611 (w), 579 (w), 551 (w), 540 (vs), 526 (s), 504 (m), 489 (m), 472 (w), 439 (s), 424 (s), 407 (m).

FAB-MS *m/z* (%): 308 [M + H]⁺, 307 [M]⁺.

HRMS-FAB (*m/z*): [M + H]⁺ calcd. for $C_{18}H_{10}N_4O_2$, 315.0877; found 315.0875.

7,8-Dimethyl-10H-benzo[*g*]pteridine-2,4-dione (142d)
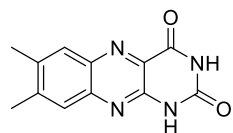
4,5-Dimethylbenzene-1,2-diamine (479 mg, 3.52 mmol, 1.00 equiv), alloxan (500 mg, 3.52 mmol, 1.00 equiv), boronic acid (218 mg, 3.52 mmol, 1.00 equiv) were dissolved in water (20 mL). The mixture was stirred at r.t. for 2 h. The precipitate was filtered off and washed with acetic acid (30 mL), water (10 mL) and 30 diethyl ether (30 mL). **142d** was obtained as a red solid (670 mg, 2.77 mmol, 79%).

¹H-NMR (400 MHz, DMSO-d_6): δ [ppm] = 11.85 (s, 1H, N*H*), 11.68 (s, 1H, N*H*), 7.92 (d, *J* = 1.4 Hz, 1H, C*H*$_{Ar}$), 7.72 (d, *J* = 1.2 Hz, 1H, C*H*$_{Ar}$), 3.33 (s, 6H, C*H*$_3$).

¹³C-NMR (101 MHz, DMSO-d_6): δ [ppm] = 161.1 (C$_q$, CO), 150.6 (C$_q$, CO), 146.9 (C$_q$), 145.1 (C$_q$), 142.1 (C$_q$), 139.4 (C$_q$), 138.8 (C$_q$), 131.2 (C$_q$), 129.2 (CH$_{Ar}$), 126.3 (CH$_{Ar}$), 20.7 (CH$_3$), 20.1 (CH$_3$).

IR (ATR) $\tilde{v}$ [cm⁻¹] = 3167 (m), 3091 (s), 3058 (m), 2987 (m), 2928 (w), 2912 (w), 2868 (w), 2834 (w), 1724 (s), 1697 (vs), 1625 (m), 1575 (s), 1558 (s), 1483 (s), 1460 (s), 1443 (s), 1421 (vs), 1385 (s), 1356 (vs), 1337 (vs), 1279 (vs), 1259 (s), 1252 (s), 1213 (vs), 1186 (s), 1142 (m), 1050 (w), 1024 (m), 1004 (m), 897 (w), 881 (s), 817 (vs), 793 (vs), 769 (vs), 748 (vs), 732 (vs), 683 (s), 671 (m), 652 (s), 603 (m), 574 (vs), 548 (m), 524 (vs), 497 (m), 476 (vs), 449 (vs), 439 (s), 414 (vs), 387 (vs).

FAB-MS *m/z* (%): 243 [M + H]⁺ (11), 89 (100), 87 (42).

HRMS-FAB (*m/z*): [M + H]⁺ calcd. for $C_{12}H_{10}N_4O_2$, 243.0877; found, 243.0877.

7,8-Difluoro-10H-benzo[*g*]pteridine-2,4-dione (142e)[194]
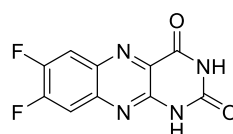
4,5-Difluorobenzene-1,2-diamine (507 mg, 3.52 mmol, 1.00 equiv), alloxan (500 mg, 3.52 mmol, 1.00 equiv), boronic acid (218 mg, 3.52 mmol, 1.00 equiv) were dissolved in water (20 mL). The mixture was stirred at r.t. for 2 h. The precipitate was filtered off and washed with acetic acid (30 mL), water (10 mL) and diethyl ether (30 mL). **142e** was obtained as a purple solid (603 mg, 2.41 mmol, 68%).

¹H-NMR (500 MHz, DMSO-d_6): δ [ppm] = 12.02 (s, 1H, N*H*), 11.82 (s, 1H, N*H*), 8.30 (dd, *J* = 10.9, 8.5 Hz, 1H, C*H*$_{Ar}$), 8.00 (dd, *J* = 11.3, 8.2 Hz, 1H, C*H*$_{Ar}$).

¹³C-NMR (126 MHz, DMSO-d_6): δ [ppm] = 155.0 (d, *J* = 16.7 Hz, C$_q$), 153.0 (d, *J* = 16.3 Hz, C$_q$), 151.6 (d, *J* = 16.3 Hz, C$_q$), 149.7 (d, *J* = 16.6 Hz, C$_q$), 147.7 (d, *J* = 3.2 Hz, C$_q$), 141.1 (d, *J* = 11.0 Hz, CH$_{Ar}$), 136.7 (d, *J* = 11.0 Hz, CH$_{Ar}$). , 132.5 (d, *J* = 3.2 Hz, C$_q$), 116.5 (d, *J* = 17.8 Hz, C$_q$), 113.5 (d, *J* = 17.9 Hz, C$_q$).

IR (ATR) $\tilde{v}$ [cm⁻¹] = 3581 (vw), 3480 (vw), 3187 (w), 3053 (m), 3030 (m), 2952 (w), 2934 (w), 2890 (w), 2860 (w), 1732 (vs), 1694 (vs), 1636 (w), 1589 (s), 1578 (m), 1509 (s), 1492 (vs), 1476 (s), 1442 (m), 1401 (m), 1346 (vs),

1286 (vs), 1244 (vs), 1230 (vs), 1207 (s), 1184 (m), 1159 (m), 1031 (w), 1023 (w), 916 (m), 890 (vs), 877 (vs), 844 (m), 822 (m), 812 (s), 802 (s), 769 (s), 749 (vs), 688 (m), 657 (s), 637 (m), 589 (m), 524 (vs), 494 (vs), 456 (s), 443 (vs), 418 (vs), 384 (s).

FAB-MS *m/z* (%): 252 (25), 251 [M + H]$^+$ (100), 138 (20), 137 (45), 136 (42), 107 (14), 89 (12).

HRMS-FAB (*m/z*): [M + H]$^+$ calcd. for $C_{10}H_4F_2N_4O_2$, 251.0375; found, 251.0377.

7,8-Dichloro-10H-benzo[g]pteridin-2,4-dione (142f)[194]
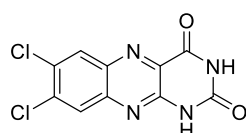
4,5-Dichlorobenzene-1,2-diamine (623 mg, 3.52 mmol, 1.00 equiv), alloxan (500 mg, 3.52 mmol, 1.00 equiv), boric acid (218 mg, 3.52 mmol, 1.00 equiv) were dissolved in water (20 mL). The mixture was stirred at r.t. for 2 h. The precipitate was filtered off and washed with acetic acid (30 mL), water (10 mL) and diethyl ether (30 mL). **142f** was obtained as an orange solid (728 mg, 2.57 mmol, 68%).

^{1}H-NMR (400 MHz, DMSO-d_6): δ [ppm] = 12.12 (d, *J* = 2.0 Hz, 1H, N*H*), 11.85 (d, *J* = 1.9 Hz, 1H, N*H*), 8.52 (s, 1H, C*H*$_{Ar}$), 8.22 (s, 1H, C*H*$_{Ar}$).

^{13}C-NMR (101 MHz, DMSO-d_6): δ [ppm] = 160.5 (C_q), 150.5 (C_q, CO), 148.2 (C_q, CO), 142.1 (CH$_{Ar}$), 138.4 (CH$_{Ar}$), 136.4 (C_q), 133.7 (C_q),131.1 (C_q), 131.1 (C_q), 128.3 (C_q).

IR (ATR, ṽ) = 3193 (m), 3139 (m), 3094 (m), 3043 (m), 2961 (w), 2894 (w), 2820 (w), 1747 (s), 1737 (vs), 1698 (vs), 1606 (w), 1578 (s), 1536 (w), 1485 (w), 1448 (vs), 1417 (m), 1380 (s), 1354 (s), 1347 (s), 1334 (vs), 1288 (s), 1272 (vs), 1222 (w), 1190 (s), 1140 (m), 1128 (m), 1106 (m), 1033 (w), 982 (w), 909 (m), 895 (w), 881 (s), 873 (s), 812 (vs), 761 (s), 754 (s), 698 (m), 667 (w), 652 (w), 635 (s), 579 (m), 561 (s), 499 (vs), 445 (vs), 416 (vs), 388 (s), 377 (m).

FAB-MS *m/z* (%): 283 [M]$^+$ (8), 155 (35), 154 (100), 153 (8), 152 (10), 139 (18), 138 (41), 137 (67), 136 (68), 135 (8), 124 (11), 123 (8), 121 (9), 120 (13), 119 (8), 107 (23), 106 (8), 105 (10), 97 (12), 95 (15), 91 (18), 90 (12), 89 (18).

HRMS-FAB (*m/z*): [M + H]$^+$ ber. für $C_{10}H_4Cl_2N_4O_2$, 282.9784; found 282.9783.

EA: calcd. for $C_{10}H_4Cl_2N_4O_2$ N 19.79 C 42.43 H 1.42; found N 19.23 C 42.29 H 1.63.

7,8-Dibromo-10H-benzo[g]pteridine-2,4-dione (142g)[194]
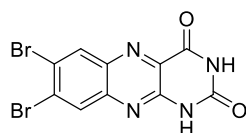
4,5-Dibromobenzene-1,2-diamine (936 mg, 3.52 mmol, 1.00 equiv), alloxan (500 mg, 3.52 mmol, 1.00 equiv), boronic acid (218 mg, 3.52 mmol, 1.00 equiv) were dissolved in water (20 mL). The mixture was stirred at r.t. for 2 h. The precipitate was filtered off and washed with acetic acid (30 mL), water (10 mL) and diethyl ether (30 mL). **142g** was obtained as an orange solid (1.19 g, 3.21 mmol, 91%).

^{1}H-NMR (400 MHz, DMSO-d_6): δ [ppm] = 12.11 (s, 1H, N*H*), 11.84 (s, 1H, N*H*), 8.62 (s, 1H, C*H*$_{Ar}$), 8.34 (s, 1H, C*H*$_{Ar}$).

¹³C-NMR (101 MHz, DMSO-d_6): δ [ppm] = 160.5 (C_q), 150.5 (C_q, CO), 148.2 (C_q, CO), 142.4 (C_q), 138.9 (C_q), 134.3 (CH_{Ar}), 133.7 (C_q), 131.4 (CH_{Ar}), 129.5 (C_q), 123.7 (C_q).

IR (ATR, ṽ) = 3172 (w), 3065 (m), 3048 (m), 2982 (w), 2935 (w), 2878 (w), 2856 (m), 2764 (w), 1737 (vs), 1704 (vs), 1606 (m), 1572 (s), 1558 (s), 1439 (vs), 1409 (s), 1373 (m), 1354 (vs), 1340 (vs), 1279 (vs), 1187 (s), 1162 (w), 1136 (m), 1099 (m), 1048 (w), 1028 (w), 1016 (w), 948 (w), 914 (s), 880 (s), 834 (vs), 807 (s), 776 (m), 747 (s), 687 (w), 670 (w), 635 (m), 625 (s), 562 (s), 538 (vs), 467 (vs), 445 (vs), 433 (vs), 404 (vs), 375 (s).

FAB-MS m/z (%):371 [M]⁺ (11), 177 (22), 175 (13), 133 (100), 131 (20), 91 (27), 90 (19), 89 (26).

HRMS-FAB (m/z): [M + H]* ber. für $C_{10}H_4Br_2N_4O_2$, 370.8774; gef. 370.8775.

10-(*p*-Tolyl)-10,10a-dihydrobenzo[*g*]pteridine-2,4(1H,3H)-dione (142h)[194]
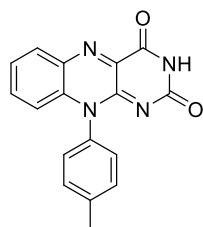
(2-Aminophenyl)-(*p*-tolyl)amine (50 mg, 252 µmol, 1.00 equiv), alloxan (35.8 mg, 252 µmol, 1.00 equiv), boric acid (59.4 mg, 252 µmol, 1.00 equiv) were dissolved in water (20 mL). The mixture was stirred at r.t. for 2 h. The precipitate was filtered off and washed with acetic acid (30 mL), water (10 mL) and diethyl ether (30 mL). **142h** was obtained as a yellow solid (25 mg, 81.6 µmol, 16%).

¹H-NMR (400 MHz, DMSO-d_6): δ [ppm] = 11.96 (s, 1H, NH), 11.41 (s, 1H, NH), 8.19 (dd, J = 8.1, 1.5 Hz, 1H, CH_{Ar}), 7.75 (ddd, J = 8.7, 7.1, 1.6 Hz, 1H, CH_{Ar}), 7.62 (ddd, J = 8.3, 7.1, 1.2 Hz, 1H, CH_{Ar}), 7.52 (d, J = 8.1 Hz, 2H, 2 CH_{Ar}), 7.31 (m, 2H, 2 CH_{Ar}), 6.81 (dd, J = 8.6, 1.2 Hz, 1H, CH_{Ar}), 1.92 (s, 3H, CH_3).

¹³C-NMR (101 MHz, DMSO-d_6): δ [ppm] = 160.6 (C_q, CO), 156.0 (C_q, CO), 139.7 (C_q), 139.7 (C_q), 135.5 (C_q), 135.4 (CH_{Ar}), 134.6 (C_q), 134.0 (C_q), 132.1 (C_q), 131.5 (CH_{Ar}), 130.8 (2C, CH_{Ar}), 128.0 (2C, CH_{Ar}), 126.5 (CH_{Ar}), 117.3 (CH_{Ar}), 21.3 (CH_3).

IR (ATR, ṽ) = 3173 (w), 3098 (w), 3060 (m), 2978 (w), 2953 (w), 2934 (w), 2904 (w), 2888 (w), 2833 (w), 1724 (s), 1674 (vs), 1612 (m), 1582 (m), 1531 (vs), 1507 (vs), 1486 (vs), 1459 (vs), 1419 (vs), 1397 (s), 1361 (m), 1307 (m), 1268 (vs), 1211 (s), 1188 (vs), 1169 (m), 1129 (m), 1109 (vs), 1052 (m), 1030 (m), 1001 (m), 962 (w), 941 (m), 912 (w), 897 (w), 882 (m), 847 (m), 830 (s), 813 (m), 806 (m), 773 (vs), 766 (s), 751 (vs), 737 (m), 720 (s), 691 (vs), 671 (m), 662 (s), 640 (m), 622 (s), 615 (s), 602 (s), 550 (m), 533 (vs), 493 (m), 462 (s), 435 (vs), 408 (s), 394 (s), 381 (m).

FAB-MS m/z (%): 307 [M + H]⁺ (17), 306 [M]⁺ (51), 305 (100), 154 (33), 136 (23).

HRMS-FAB (m/z): [M + H]⁺ calcd. for $C_{17}H_{14}N_4O_2$, 306.1111; found, 306.1114.

10-([1,1'-Biphenyl]-3-yl)-2,3,10,10a-tetrahydrobenzo[*g*]pteridin-4(1H)-one (142i)[194]
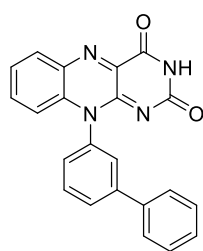
N[1]-([1,1'-Biphenyl]-3-yl)benzene-1,2-diamine (95 mg, 365 µmol, 1.00 equiv), alloxan (51.8 mg, 365 µmol, 1.00 equiv), boric acid (22.6 mg, 365 µmol, 1.00 equiv) were dissolved in water (20 mL). The mixture was stirred at r.t. for 2 h. The precipitate was filtered off and washed with acetic acid (30 mL), water (10 mL) and 30 diethyl ether (30 mL). **142i** was isolated as a red solid (11 mg, 29.9 µmol, 8%).

^{1}H-NMR (400 MHz, DMSO-d_6): δ [ppm] = 11.46 (s, 2H, N*H*), 8.22 (dd, *J* = 8.1, 1.5 Hz, 2H, C*H*$_{Ar}$), 8.00 (ddd, *J* = 7.9, 1.9, 1.0 Hz, 2H, C*H*$_{Ar}$), 7.64 (ddd, *J* = 8.2, 7.1, 1.2 Hz, 2H, C*H*$_{Ar}$), 7.51 (dd, *J* = 8.4, 7.0 Hz, 4H, C*H*$_{Ar}$), 7.45 (m, 3H, C*H*$_{Ar}$).

^{13}C-NMR (101 MHz, DMSO-d_6): δ [ppm] = 160.0 (C$_q$), 156.1 (C$_q$, CO), 152.3 (C$_q$, CO), 142.7 (C$_q$), 139.9 (C$_q$), 139.1 (C$_q$), 137.3 (C$_q$), 135.4 (CH$_{Ar}$), 135.3 (C$_q$), 134.5 (C$_q$), 131.5 (CH$_{Ar}$), 131.2 (CH$_{Ar}$), 129.9 (2C, CH$_{Ar}$), 128.3 (CH$_{Ar}$), 128.6 (CH$_{Ar}$), 127.2 (CH$_{Ar}$), 127.2 (2C, CH$_{Ar}$), 126.4 (CH$_{Ar}$), 126.4 (CH$_{Ar}$), 117.3 (CH$_{Ar}$).

IR (ATR, ṽ) = 3173 (w), 3098 (w), 3060 (m), 2978 (w), 2953 (w), 2934 (w), 2904 (w), 2888 (w), 2833 (w), 1724 (s), 1674 (vs), 1612 (m), 1582 (m), 1531 (vs), 1507 (vs), 1486 (vs), 1459 (vs), 1419 (vs), 1397 (s), 1361 (m), 1307 (m), 1268 (vs), 1211 (s), 1188 (vs), 1169 (m), 1129 (m), 1109 (vs), 1052 (m), 1030 (m), 1001 (m), 962 (w), 941 (m), 912 (w), 897 (w), 882 (m), 847 (m), 830 (s), 813 (m), 806 (m), 773 (vs), 766 (s), 751 (vs), 737 (m), 720 (s), 691 (vs), 671 (m), 662 (s), 640 (m), 622 (s), 615 (s), 602 (s), 550 (m), 533 (vs), 493 (m), 462 (s), 435 (vs), 408 (s), 394 (s), 381 (m).

FAB-MS *m/z* (%): 368 [M + H]$^+$ (7), 367 (14), 307 (26), 289 (12), 155 (33), 154 (100), 139 (16), 138 (39), 137 (62), 136 (64), 105 (11), 97 (16), 95 (18), 91 (20), 90 (13), 89 (18).

HRMS-FAB (*m/z*): [M + H]$^+$ calcd. for C$_{22}$H$_{16}$N$_4$O$_2$, 368.1268; found 368.1269.

N-((1s,3s)-adamantan-1-yl)-2-((E)-4-(dimethylamino)styryl)imidazo[1,2-a]pyrazin-3-amine (154)
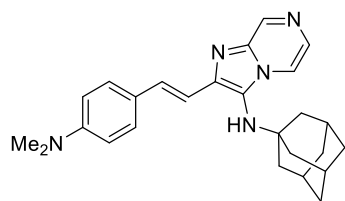
2-Aminopyrazine (200 mg, 2.10 mmol, 1.00 equiv), *N,N*-dimethylamino cinnamic aldehyde (369 mg, 2.10 mmol, 1.00 equiv), 1-adamantyl isonitrile (339 mg, 2.10 mmol, 1.00 equiv) and 2,2,2-trichloro acetic acid (17 mg, 105 µmol, 0.05 equiv) were dissolved in a mixture of in methanol (10 mL). The mixture was stirred at r.t. for 72 h. The solvent was removed under reduced pressure and the residue was purified *via* flash chromatography (SiO$_2$, CH/EtOAc/NEt$_3$ 4:1:0.01 to 1:1:0.01). **154** was isolated as a yellow solid (710 mg, 1.72 mol, 82%).

R_f (SiO$_2$, CH/EtOAc 1:1) = 0.44.

^{1}H NMR (400 MHz, CDCl$_3$) δ [ppm] = 8.91 (d, *J* = 1.4 Hz, 1H, C*H*$_{Ar}$), 8.10 (dd, *J* = 4.5, 1.5 Hz, 1H, C*H*$_{Ar}$), 7.78 (d, *J* = 4.6 Hz, 1H, C*H*$_{Ar}$), 7.63 (d, *J* = 15.9 Hz, 1H, C*H*$_{DB}$), 7.53 – 7.45 (m, 2H, C*H*$_{Ar}$), 6.98 (d, J = 15.9 Hz, 1H, C*H*$_{DB}$), 6.77 – 6.70 (m, 2H, C*H*$_{Ar}$), 3.00 (s, 6H, C*H*$_3$), 2.09 (d, *J* = 4.4 Hz, 4H), 1.77 (d, *J* = 2.9 Hz, 7H), 1.69 – 1.54 (m, 8H).

¹³C NMR (101 MHz, CDCl₃) δ [ppm] = 150.6 (C$_q$), 142.5 (CH$_{Ar}$), 141.7 (C$_q$), 138.0 (C$_q$), 132.1 (CH$_{Ar}$), 128.7 (CH), 128.1 (2C, CH$_{Ar}$), 125.6 (C$_q$), 124.5 (C$_q$), 116.2 (CH$_{Ar}$), 113.7 (CH), 112.5 (2C, CH$_{Ar}$), 56.5 (C$_q$), 44.2(CH$_2$), 40.6 (CH), 36.3 (CH$_2$), 29.8 (CH).

IR (ATR) $\tilde{v}$ [cm⁻¹] = 3197 (m), 2901 (s), 2843 (s), 2820 (m), 1599 (vs), 1555 (w), 1524 (vs), 1516 (vs), 1446 (m), 1431 (m), 1417 (m), 1357 (vs), 1344 (vs), 1306 (m), 1282 (vs), 1256 (w), 1224 (s), 1207 (s), 1180 (vs), 1164 (vs), 1147 (vs), 1119 (s), 1089 (s), 1064 (m), 1041 (m), 1017 (m), 990 (m), 970 (vs), 946 (s), 929 (m), 916 (m), 897 (m), 819 (vs), 802 (vs), 773 (s), 747 (m), 730 (m), 705 (s), 694 (s), 650 (w), 633 (m), 616 (s), 601 (s), 578 (m), 561 (m), 524 (s), 511 (s), 486 (m), 465 (m), 458 (w), 441 (m), 422 (w), 399 (m), 390 (m), 380 (w).

FAB-MS *m/z* (%): 414 [M + H]⁺ (93), 413 [M]⁺ (100).

HRMS-FAB (*m/z*): [M + H]⁺ calcd. for C₂₆H₃₁N₅, 413.2574; found, 413.2572.

2-Bromo-4-(piperidin-1-yl)phenol (166)
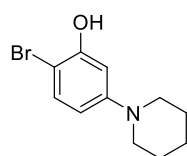
According to a modified procedure by FUKINO *et al.*,[164a] a mixture of 4-amino-2-bromophenol (2.00 g, 10.6 mmol, 1.00 equiv), 1,5-dibromopentane (2.69 g, 1.59 mL, 11.7 mmol, 1.10 equiv), *N*-ethyl-*N*-propan-2-ylpropan-2-amine (3.16 g, 4.16 mL, 24.5 mmol, 2.30 equiv) in toluene (25 mL) was heated to 110 °C for 24 h. After cooling to r.t., the solution was neutralized with 1M NaOH. The resulting solution was extracted with ethyl acetate, and combined organic phases were separated, dried over Na₂SO₄ and evaporated to give the crude product. The solvent was removed under reduced pressure and the residue was purified by column chromatography (SiO₂, CH/EE 4:1 to 2:1). **166** was obtained as a colorless solid (2.10 g, 8.19 mmol, 77%).

R$_f$ (SiO₂, CH/EtOAc, 2:1) = 0.60.

¹H NMR (500 MHz, CDCl₃) δ [ppm] = 7.15–7.10 (m, 1H, C*H*$_{Ar}$), 6.97–6.90 (m, 2H, C*H*$_{Ar}$), 5.63 (br, 1H, O*H*), 3.05 (t, *J* = 5.5 Hz, 4H, C*H*$_2$), 1.77 (p, *J* = 5.5 Hz, 4H, C*H*$_2$), 1.60–1.53 (m, 2H, C*H*$_2$).

¹³C NMR (126 MHz, CDCl₃) δ [ppm] = 147.1 (C$_q$), 146.2 (C$_q$), 121.2 (CH$_{Ar}$), 119.5 (CH$_{Ar}$), 116.4 (CH$_{Ar}$), 110.4 (CH$_{Ar}$), 52.8 (2C, CH$_2$), 25.7 (2C, CH$_2$), 23.9 (CH$_2$).

IR (ATR) $\tilde{v}$ [cm⁻¹] = 3218 (w), 2990 (w), 2936 (m), 2918 (w), 2851 (w), 2816 (w), 1564 (w), 1494 (vs), 1463 (m), 1448 (s), 1411 (w), 1384 (w), 1357 (w), 1326 (w), 1293 (m), 1279 (w), 1254 (w), 1227 (vs), 1211 (vs), 1167 (vs), 1145 (s), 1120 (vs), 1109 (vs), 1069 (m), 1048 (m), 1026 (vs), 963 (w), 924 (vs), 857 (s), 832 (vs), 806 (s), 721 (vs), 671 (m), 602 (m), 567 (m), 520 (s), 480 (m), 446 (m), 419 (s), 398 (s).

FAB-MS *m/z* (%): 258 (33), 257 (98), 256 (80), 255 [M + H]⁺ (100), 254 (52), 154 (13).

HRMS (FAB) *m/z*: [M + H]⁺ calcd. for C₁₁H₁₄O₁N₁⁷⁹Br₁, 255.0253; found, 255.0255.

5-(Piperidin-1-yl)-2-(trimethylsilyl)phenyl trifluoromethanesulfonate (167)
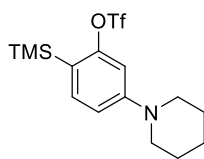
According to a modified procedure by HALLANI *et al. et al.*,[164b] **166** (500 mg, 1.95 mmol, 1.00 equiv) was dissolved in dry THF (5 mL). To this solution, hexamethyldisilazane (630 mg, 808 µL, 3.90 mmol, 2.00 equiv) was added dropwise, and the resulting reaction mixture was heated to 65 °C for 30 min. The solvent was removed under reduced pressure and the crude material was used in the next step without any purification. The residue was dissolved in dry THF (10 mL). The solution was cooled to −78 °C and a 1.6 M solution of *t*BuLi in hexane (313 mg, 3.05 mL, 4.88 mmol, 2.50 equiv) was added dropwise and the reaction was stirred for 1 h. The reaction was quenched by the addition of water (1 mL). The solvent was removed under reduced pressure. The crude product was employed in the next step without any further purification. The residue was dissolved in dry CH_2Cl_2 (10 mL). The mixture was cooled to 0 °C, triflic anhydride (661 mg, 393 µL, 2.34 mmol, 1.20 equiv) and triethylamine (415 mg, 568 µL, 4.09 mmol, 2.10 equiv) were added and the reaction was stirred for 2 h at. The solvent was removed under reduced pressure and the residue was purified by flash column chromatography (SiO_2, CH/EE 8:1 to 2:1). **167** was obtained as a colorless oil (975 mg, 2.56 mmol, 33%).

R_f (SiO_2, CH/EtOAc, 4:1) = 0.76.

^{1}H NMR (500 MHz, $CDCl_3$) δ [ppm] = 7.17 (d, J = 9.1 Hz, 1H, CH^6), 7.00 (d, J = 3.0 Hz, 1H, CH^3), 6.89 (dd, J = 9.2, 3.1 Hz, 1H, CH^5), 3.18–3.12 (m, 4H, CH_2), 1.71 (h, J = 5.7 Hz, 4H, CH_2), 1.63–1.53 (m, 2H, CH_2), 0.35 (s, 9H, CH_3).

^{13}C NMR (126 MHz, $CDCl_3$) δ [ppm] = 151.12 (C_q, C^4), 147.60 (C_q, C^1), 132.99 (C_q, C^2), 123.29 (CH), 120.40 (CH), 118.7 (C_q, J = 320.1 Hz, CF$_3$), 118.13 (CH), 50.68 (2C, CH$_2$), 25.90 (2C, CH$_2$), 24.22 (CH$_2$), 0.60 (3C, CH$_3$).

^{19}F NMR (471 MHz, $CDCl_3$) δ [ppm] = − 74.01.

IR (ATR) $\tilde{v}$ [cm^{-1}] = 2936 (w), 2856 (w), 2809 (w), 2798 (w), 1571 (m), 1477 (m), 1452 (w), 1415 (vs), 1397 (s), 1343 (w), 1290 (w), 1248 (s), 1237 (s), 1205 (vs), 1167 (m), 1140 (vs), 1130 (vs), 1054 (m), 1037 (s), 941 (w), 885 (vs), 839 (vs), 813 (s), 793 (s), 758 (s), 693 (m), 679 (m), 646 (m), 623 (s), 602 (vs), 524 (m), 494 (m), 466 (m), 446 (m), 425 (m), 415 (m), 397 (w).

FAB-MS *m/z* = (%): 382 (30), 381 [M + H]$^+$ (65), 380 (38), 250 (12), 249 (47), 248 (100), 246 (13), 233 (26), 232 (38), 177 (11), 133 (33), 89 (92), 87 (44).

HRMS (FAB) *m/z*: [M + H]$^+$ calcd. for $C_{15}H_{22}O_3N_1F_3{}^{32}S_1{}^{28}Si_1$, 381.1036; found, 381.1038.

5.4.6 Development of a Novel Route towards Bemotrizinol

2,4-Dichloro-6-(4-methoxyphenyl)-1,3,5-triazine (170)
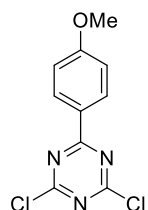
Grignard Route

Magnesium turnings (729 mg, 30.0 mmol, 1.00 equiv) was suspended in anhydrous THF (60 mL). 4-Bromoanisole (5.61 g, 3.75 mL, 30.0 mmol, 1.00 equiv) dissolved in anhydrous THF (100 mL) was added dropwise to the mixture while heating to 60 °C. The solution was stirred for 1.5 h. Subsequently, the mixture was added dropwise to a solution of cyanuric chloride (5.53 g, 30.0 mmol, 1.00 equiv) in anhydrous THF (100 mL) at 0 °C over 30 min. The solvent was removed under reduced pressure and the residue was washed with isopropanol and recrystallized from a mixture of toluene and hexane (1:1). **170** was obtained as an off-white solid (4.40 g, 17.2 mmol, 57%).

Friedel Crafts Acylation Route

Cyanuric chloride (100 mg, 542 µmol, 1.00 equiv) was dissolved in dichloromethane or chlorobenzene (10 ml). Nafion beads (40 mg) and anisole (59 µL, 58.6 mg, 542 µmol, 1.00 equiv) were added and the solution was stirred at r.t. for 18 h.

R_f (SiO$_2$, CH/EtOAc, 4:1) = 0.66.

^{1}H NMR (400 MHz, CDCl$_3$) δ [ppm] = 8.40 (dd, J = 8.9, 3.0 Hz, 2H), 6.96 (dd, J = 9.1, 2.2 Hz, 2H), 3.89 (s, 3H).

^{13}C NMR (100 MHz, CDCl$_3$) δ [ppm] = 174.2 (C$_q$, C^p), 171.7 (2C, C$_q$), 165.3 (C$_q$, COMe), 132.3 (2C, CH$_{Ar}$), 125.1 (C$_q$, CN), 114.5(2C, CH$_{Ar}$), 55.7 (CH$_3$).

IR (ATR) $\tilde{v}$ [cm^{-1}] = 2975 (w), 2936 (w), 2901 (w), 2844 (w), 1604 (w), 1577 (w), 1514 (s), 1476 (vs), 1455 (s), 1442 (s), 1418 (m), 1388 (s), 1332 (w), 1317 (m), 1302 (m), 1256 (vs), 1244 (vs), 1180 (s), 1167 (s), 1152 (s), 1108 (s), 1016 (s), 975 (m), 902 (m), 844 (vs), 813 (s), 795 (vs), 776 (vs), 670 (s), 635 (m), 589 (vs), 547 (s), 510 (vs), 482 (s), 469 (s), 395 (m).

FAB-MS m/z (%): 259 (10), 258 (8), 257 (70), 256 (12), 255 [M + H]$^+$ (100), 159 (43), 133 (21), 118 (7), 103 (8), 90 (26), 89 (5), 87 (18), 69 (5), 63 (5).

HRMS-FAB (*m/z*): [M + H]$^+$ calcd. for C$_{10}$H$_7$O$_1$N$_3$^{35}Cl$_2$, 254.9961; found, 254.9962.

1-Bromo-3-((2-ethylhexyl)oxy)benzene (176)
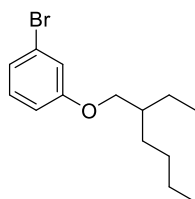
To a solution of 3-bromophenol (4.00 g, 23.1 mmol, 1.00 equiv) and isooctyl bromide (5.36 g, 27.7 mmol, 1.20 equiv) in DMF (100 mL) was added potassium carbonate (4.79 g, 34.7 mmol, 1.50 equiv) and the mixture was stirred at 110 °C for 12 h. After cooling to r.t., water (40 mL) was added, and the mixture was extracted with ethyl acetate (50 mL). The combined organic layers were dried over Na_2SO_4. The solvent was removed under reduced pressure. and the residue was purified *via* flash chromatography (SiO_2, CH/EE 40:1). **176** was obtained as a pale-yellow oil (5.32 g, 18.7 mmol, 81%).

R_f (SiO_2, CH/EtOAc, 4:1) = 0.81.

^{1}H NMR (400 MHz, $CDCl_3$) δ [ppm] = 7.13 (t, J = 8.3 Hz, 1H), 7.08 – 7.03 (m, 2H), 6.83 (ddd, J = 8.2, 2.4, 1.2 Hz, 1H), 3.87 – 3.76 (m, 2H, CH_2), 1.71 (hept, J = 6.1 Hz, 1H, CH), 1.55 – 1.36 (m, 4H), 1.35 – 1.26 (m, 5H), 0.97 – 0.84 (m, 6H, CH_3).

^{13}C NMR (100 MHz, $CDCl_3$) δ [ppm] = 160.4 (C_q, C^1), 130.6 (CH_{Ar}), 123.6 (CH_{Ar}), 122.9 (C_q, C^3), 117.9 (CH_{Ar}), 113.7 (CH_{Ar}), 70.9 (CH_2), 39.5 (CH), 30.6 (CH_2), 29.2 (CH_2), 24.0 (CH_2), 23.2 (CH_2), 14.2 (CH_3), 11.2 (CH_3).

IR (ATR) $\tilde{v}$ [cm^{-1}] = 2958 (s), 2925 (s), 2871 (m), 2859 (m), 1588 (vs), 1572 (vs), 1465 (vs), 1434 (m), 1424 (m), 1381 (m), 1323 (m), 1302 (m), 1283 (vs), 1242 (vs), 1227 (vs), 1166 (w), 1156 (m), 1119 (w), 1089 (m), 1064 (s), 1031 (vs), 1016 (vs), 992 (vs), 973 (m), 929 (m), 860 (vs), 837 (s), 764 (vs), 728 (m), 680 (vs), 603 (w), 601 (w), 441 (m).

FAB-MS m/z (%): 287 (61), 286 (65), 285 (100) [M + 2 H]$^+$, 284 (56), 283 (49), 187 (19), 185 (19), 175 (54), 174 (26), 173 (54), 172 (22), 154 (29), 89 (78), 87 (33).

HRMS-FAB (*m/z*): [M + H]$^+$ calcd. for $C_{14}H_{21}O_1{}^{79}Br_1$, 284.0770; found, 284.0772.

3-((2-Ethylhexyl)oxy)phenol (177)
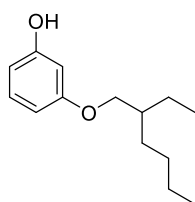
176 (700 mg, 2.45 mmol, 1.00 equiv), Pd_2dba_3 (45 mg, 49.1 µmol, 0.02 equiv), XPhos (94 mg, 196 µmol, 0.08 equiv) and JOJ (303 mg, 5.40 mmol, 2.20 equiv) were dissolved in a 4:1 mixture of 1,4-dioxane and water (5 mL) under an argon atmosphere. The mixture was heated to 100 °C for 20 h. After cooling to room temperature, the solution was neutralized with 1 M HCl. The mixture was extracted with EtOAc, and the combined organic layers were dried over Na_2SO_4. The solvent was removed under reduced pressure and the residue was purified *via* flash chromatography (SiO_2, $CHCl_3$). **177** was obtained as a red oil (408 mg, 1.84 mmol, 75%).

R_f (SiO_2, CH/EtOAc, 4:1) = 0.52.

^{1}H NMR (400 MHz, $CDCl_3$) δ [ppm] = 7.16 – 7.07 (m, 1H, CH_{Ar}), 6.53 – 6.45 (m, 1H, CH_{Ar}), 6.44 – 6.35 (m, 2H, CH_{Ar}), 4.66 (s, 1H), 3.81 (dd, J = 5.7, 1.3 Hz, 2H), 1.71 (hept, J = 6.2 Hz, 1H), 1.50 – 1.35 (m, 2H), 1.35 – 1.29 (m, 4H), 0.99 – 0.85 (m, 6H).

^{13}C NMR (100 MHz, $CDCl_3$) δ [ppm] = 161.0 (C_q), 156.7 (C_q), 130.2 (CH_{Ar}), 107.5 (CH_{Ar}), 107.3 (CH_{Ar}), 102.2 (CH_{Ar}), 70.6 (CH_2), 39.5 (CH), 30.7 (CH_2), 29.2 (CH_2), 24.0 (CH_2), 23.2 (CH_2), 14.2 (CH_3), 11.2 (CH_3).

IR (ATR) $\tilde{v}$ [cm^{-1}] = 3376 (w), 2958 (m), 2927 (s), 2871 (m), 2860 (m), 1591 (vs), 1530 (m), 1494 (vs), 1458 (vs), 1371 (m), 1353 (s), 1327 (m), 1306 (m), 1282 (s), 1251 (s), 1232 (s), 1171 (vs), 1145 (vs), 1101 (s), 1028 (s), 1021 (s), 994 (m), 977 (m), 960 (m), 832 (vs), 796 (s), 765 (s), 728 (m), 684 (s), 642 (m), 629 (m), 622 (m), 596 (s), 528 (m), 511 (m), 460 (m).

FAB-MS m/z (%): 222 (27), 111 (18), 110 (100).

HRMS-FAB (*m/z*): [M + H]$^+$ calcd. for $C_{14}H_{22}O_2$, 222.1614; found, 222.1616.

3-((2-Ethylhexyl)oxy)cyclohex-2-en-1-one (180)
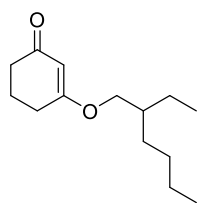
To a stirred solution of cyclohexane-1,3-dione (5.00 g, 44.6 mmol, 1.00 equiv) and 2-ethyl-1-hexanol (10.5 mL, 8.71 g, 66.9 mmol, 1.00 equiv) in toluene (50 mL) was added methane sulfonic acid (87 µL, 129 mg, 1.34 mmol, 0.03 equiv). The mixture was heated to 110 °C for 20 h. After cooling to room temperature, the solution was neutralized with aqueous Na$_2$CO$_3$ solution. The organic layer was separated, washed with water and brine dried over Na$_2$SO$_4$. The solvent was removed under reduced pressure. The crude product was purified *via* vacuum distillation: removal of residual isooctanol at 450 mbar and 80 °C, then distillation of product at 10 mbar and 200 °C. **180** was obtained as a pale-yellow oil (6.90 g, 30.8 mmol, 69%).

R$_f$ (SiO$_2$, CH/EtOAc, 4:1) = 0.76.

^{1}H NMR (500 MHz, CDCl$_3$) δ [ppm] = 5.35 (s, 1H), 3.75 – 3.66 (m, 2H), 2.40 (t, *J* = 6.3 Hz, 2H), 2.34 (dd, J = 7.3, 6.0 Hz, 2H), 1.97 (p, *J* = 6.5 Hz, 2H), 1.70 – 1.61 (m, 2H), 1.40 (tdd, *J* = 7.5, 6.1, 3.8 Hz, 2H), 1.36 – 1.21 (m, 5H), 0.89 (td, *J* = 7.1, 3.0 Hz, 6H).

^{13}C NMR (126 MHz, CDCl$_3$) δ [ppm] = 200.0 (C$_q$, *C*O), 178.4 (C$_q$), 102.8 (CH), 71.2 (CH$_2$), 38.9 (CH), 36.9 (CH$_2$), 30.5 (CH$_2$), 29.2 (CH$_2$), 29.1 (CH$_2$), 23.9 (CH$_2$), 23.1 (CH$_2$), 21.4 (CH$_2$), 14.2 (CH$_3$), 11.1 (CH$_3$).

IR (ATR) $\tilde{v}$ [cm^{-1}] = 2955 (m), 2928 (m), 2871 (w), 2860 (w), 1727 (vw), 1652 (vs), 1602 (vs), 1458 (m), 1428 (w), 1400 (w), 1368 (s), 1349 (m), 1326 (m), 1310 (w), 1237 (m), 1217 (vs), 1181 (vs), 1133 (s), 1058 (w), 1003 (m), 958 (m), 931 (w), 905 (w), 863 (m), 823 (m), 772 (w), 759 (w), 728 (w), 662 (w), 606 (w), 535 (w), 460 (w), 446 (w), 425 (w), 384 (w).

FAB-MS m/z (%): 224 [M+H]$^+$ (39), 181 (66), 131 (71), 113 (86), 112 (30), 100 (18), 84 (26), 71 (42), 70 (30), 69 (100), 57 (43).

HRMS-FAB (*m/z*): [M + H]$^+$ calcd. for $C_{14}H_{24}O_2$, 224.1771; found, 224.1770.

2-(4,6-Diphenyl-1,3,5-triazin-2-yl)-1-(4-methoxyphenyl)ethan-1-one (185a)
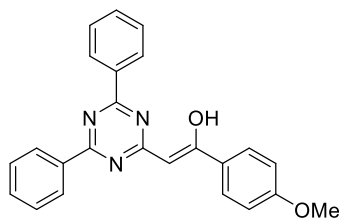
To a solution of 4-methoxyacetophenone (309 mg, 2.05 mmol, 1.10 equiv) in anhydrous THF (15 mL) under argon was added a 2 M solution of LDA in THF (240 mg, 1.12 mL, 2.24 mmol, 1.20 equiv) at –78°C. The solution was stirred for 30 min. Subsequently, the cooling was removed and 2-chloro-4,6-diphenyl-1,3,5-triazine (500 mg, 1.87 mmol, 1.00 equiv) dissolved in anhydrous THF (5 mL) was added dropwise to the reaction mixture and the resulting yellow solution was stirred for 15 h at 65°C. The solvent was removed under reduced pressure, and the residue was purified *via* flash chromatography (SiO$_2$, CH/EE 10:1). **185b** was isolated as an orange solid (334 mg, 874 µmol, 47%).

R$_f$ (SiO$_2$, CH/EtOAc, 4:1) = 0.51.

^{1}H-NMR (400 MHz, CDCl$_3$) δ [ppm] = 15.03 (s, 1H, O*H*), 8.77 – 8.30 (m, 4H, C*H*$_{Ar}$), 7.98 – 7.88 (m, 2H, C*H*$_{Ar}$), 7.67 – 7.45 (m, 6H, C*H*$_{Ar}$), 7.04 – 6.94 (m, 2H, C*H*$_{Ar}$), 6.35 (s, 1H, C*H*), 3.88 (s, 3H, OC*H*$_3$).

^{13}C-NMR (100 MHz, CDCl$_3$) δ [ppm] = 172.6 (C$_q$, *C*O), 171.7 (2C, *C*$_q$), 162.2 (C$_q$, *C*OMe), 136.3 (C$_q$), 135.0 (C$_q$), 132.9 (CH$_{Ar}$), 132.7 (CH$_{Ar}$), 129.2 (2C, CH$_{Ar}$), 129.0 (2C, CH$_{Ar}$), 128.8 (2C, CH$_{Ar}$), 128.2 (2C, CH$_{Ar}$), 127.4 (2C, CH$_{Ar}$), 114.1 (2C, CH$_{Ar}$), 93.9 (CH), 55.6 (CH$_3$).

IR (ATR) ṽ [cm^{-1}] = 3067 (w), 2936 (w), 2834 (w), 1628 (w), 1605 (w), 1591 (w), 1531 (vs), 1504 (vs), 1494 (vs), 1456 (s), 1434 (s), 1411 (s), 1380 (s), 1327 (s), 1305 (m), 1292 (m), 1258 (s), 1239 (vs), 1171 (vs), 1152 (m), 1116 (m), 1061 (m), 1037 (m), 1028 (s), 1001 (w), 990 (m), 943 (w), 871 (w), 851 (w), 830 (vs), 792 (vs), 754 (m), 732 (w), 693 (vs), 683 (vs), 662 (s), 646 (s), 635 (m), 618 (w), 579 (m), 562 (m), 511 (w), 501 (w), 470 (m), 452 (w), 419 (w), 375 (w).

FAB-MS *m/z* (%): 382 [M + H]$^+$ (62), 381 (32), 155 (34), 154 (100), 138 (39), 137 (62), 136 (94), 135 (80), 121 (29), 109 (49), 107 (50), 105 (44), 104 (67), 97 (49), 95 (85), 93 (44), 91 (61), 89 (30).

6-(4,6-Diphenyl-1,3,5-triazin-2-yl)-3-ethoxycyclohex-2-en-1-one (185b)
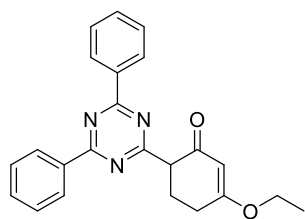
To a solution of 3-ethoxycyclohexenone (262 mg, 272 µL, 1.87 mmol, 1.00 equiv) in anhydrous THF (15 mL) under argon was added a 2 M solution of LDA in THF (400 mg, 1.87 mL, 3.73 mmol, 2.00 equiv) at –78 °C. The solution was stirred for 30 min. Subsequently, the cooling was removed and 2-chloro-4,6-diphenyl-1,3,5-triazine (500 mg, 1.87 mmol, 1.00 equiv) dissolved in anhydrous THF (5 mL) was added dropwise to the reaction mixture and the resulting yellow solution was stirred for 15 h at 65°C. The solvent was removed under reduced pressure, and the residue was purified *via* flash chromatography (CH/EE 10:1). **185b** was isolated as an orange solid (375 mg, 1.01 mmol, 54%).

R$_f$ (SiO$_2$, CH/EtOAc, 4:1) = 0.26.

¹H-NMR (500 MHz, CDCl₃) δ [ppm] = 8.68 – 8.58 (m, 4H, CH_{Ar}), 7.61 – 7.54 (m, 2H, CH_{Ar}), 7.54 – 7.49 (m, 4H, CH_{Ar}), 5.54 (s, 1H, CH^2), 4.06 – 3.91 (m, 3H, CH_2 + CH^6), 2.84 – 2.73 (m, 1H), 2.68 – 2.55 (m, 2H), 2.39 (dq, J = 13.2, 5.2 Hz, 1H), 1.47 – 1.35 (m, 3H, CH_3).

¹³C-NMR (126 MHz, CDCl₃) δ [ppm] = 196.7 (C$_q$, C^1), 177.8 (2C, C$_q$), 177.7 (C$_q$, C^3), 171.6 (C$_q$), 136.0 (2C, C$_q$), 132.6 (2C, CH_{Ar}), 129.2 (4C, CH_{Ar}), 128.7 (4C, CH_{Ar}), 102.9 (CH_{Ar}), 64.6 (CH_2), 55.4 (CH), 28.0 (CH_2), 26.4 (CH_2), 14.3 (CH_3).

IR (ATR) ṽ [cm⁻¹] = 3067 (w), 2979 (w), 2939 (w), 1653 (w), 1601 (s), 1587 (m), 1510 (vs), 1438 (s), 1424 (s), 1377 (vs), 1370 (vs), 1332 (vs), 1313 (s), 1276 (s), 1249 (s), 1187 (vs), 1159 (s), 1112 (m), 1023 (vs), 999 (m), 980 (m), 935 (w), 909 (m), 894 (m), 846 (m), 837 (m), 822 (m), 796 (s), 762 (s), 748 (s), 718 (s), 683 (vs), 662 (s), 643 (s), 619 (m), 609 (m), 598 (s), 574 (m), 550 (w), 517 (w), 472 (m), 453 (m).

FAB-MS m/z (%): 373 (28), 372 [M + 2 H]⁺ (100), 371 (22), 370 (10), 343 (11), 307 (35), 289 (22), 155 (26), 154 (92), 152 (11), 139 (14), 138 (28), 137 (50), 136 (58), 120 (10), 107 (19), 105 (11), 104 (19), 91 (15), 90 (12), 89 (21).

HRMS-FAB (m/z): [M + H]⁺ calcd. for C₂₃H₂₂O₂N₃, 371.1707; found, 372.1707.

EA: C₂₃H₂₁N₃O₂: calcd. C 74.37, H 5.70, N 11.31; found. C 74.59, H 5.63, N 11.13.

6,6'-(6-(4-Methoxyphenyl)-1,3,5-triazine-2,4-diyl)bis(3-((2-ethylhexyl)oxy)cyclohex-2-en-1-one) (186)
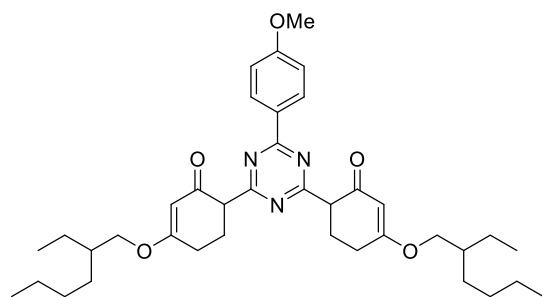
To a solution of **180** (876 mg, 3.90 mmol, 2.00 equiv) in anhydrous THF was added a 2 M solution of LDA in THF (2.44 mL, 523 mg, 4.88 mmol, 2.50 equiv) at −78 °C under argon atmosphere. The solution was stirred for 30 min. Subsequently, the cooling was removed and **170** (500 mg, 1.95 mmol, 1.00 equiv) dissolved in anhydrous THF (10 mL) was added dropwise to the reaction mixture and the resulting yellow solution was stirred for 16 h at 60 °C. The solvent was removed under reduced pressure, and the residue was purified *via* flash chromatography (SiO₂, CH/EtOAc 20:1). **186** was isolated as a yellow resin (350 mg, 554 µmol, 28%).

R_f (SiO₂, CH/EtOAc, 4:1) = 0.46.

¹H-NMR (500 MHz, CDCl₃) δ [ppm] = 8.45 (d, J = 9.0 Hz, 2H), 6.96 (d, J = 9.0 Hz, 2H), 5.50 (s, 2H), 3.91–3.86 (m, 1H), 3.89 (s, 3H), 3.86–3.70 (m, 4H), 2.83 (t, J = 8.4 Hz, 1H), 2.73– 2.62 (m, 1H), 2.61–2.53 (m, 2H), 2.45 (td, J = 8.4, 3.0 Hz, 1H), 2.40 (t, J = 6.3 Hz, 1H), 2.37–2.27 (m, 2H), 1.98 (p, J = 6.5 Hz, 1H), 1.75–1.60 (m, 2H), 1.48–1.21 (m, 16H), 0.97–0.77 (m, 12H). Minor signals at 15.28 (s), 13.59 (s).

¹³C-NMR (126 MHz, CDCl₃) δ [ppm] = 195.5 (2C, C$_q$, CO), 179.4 (2C, C$_q$, CN), 178.1 (2C, C$_q$, COR), 172.9 (C$_q$), 164.4 (C$_q$), 131.8 (2C, CH_{Ar}), 126.6, 114.3 (2C, CH_{Ar}), 102.7 (2C, CH_{DB}), 71.6 (2C, CH_2), 55.7 (CH_3), 55.3 (2C, CH), 38.9 (2C, CH), 30.5 (2C, CH_2), 29.1 (2C, CH_2), 28.1 (2C, CH_2), 26.2 (2C, CH_2), 23.9 (2C, CH_2), 23.1 (2C, CH_2), 14.2 (2C, CH_3), 11.1 (2C, CH_3).

IR (ATR) $\tilde{v}$ [cm^{-1}] = 2956 (w), 2928 (w), 2871 (w), 2859 (w), 1728 (vw), 1655 (w), 1636 (w), 1604 (s), 1579 (m), 1503 (vs), 1462 (vs), 1402 (vs), 1375 (vs), 1327 (vs), 1312 (vs), 1281 (s), 1255 (vs), 1222 (vs), 1184 (vs), 1166 (vs), 1123 (s), 1113 (s), 1064 (s), 1028 (s), 1006 (s), 975 (m), 965 (m), 935 (m), 909 (m), 851 (s), 820 (s), 813 (s), 792 (m), 732 (s), 680 (m), 666 (m), 636 (m), 591 (s), 511 (m), 456 (w).

FAB-MS *m/z* (%):

HRMS-FAB (*m/z*): [M + H]$^+$ calcd. for C$_{38}$H$_{50}$O$_5$N$_3$, 628.3745; found, 628.3747.

6,6'-(6-(4-Methoxyphenyl)-1,3,5-triazine-2,4-diyl)bis(3-((2-ethylhexyl)oxy)phenol) – Bemotrizinol (1)
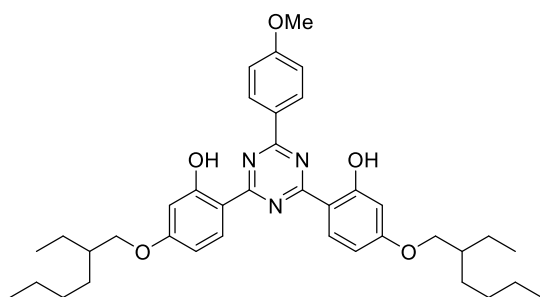
In a 10 mL ElectraSyn vial, THBMT (20.0 mg, 31.7 µmol, 1.00 equiv), Bu$_4$NBF$_4$ (208 mg, 633 µmol, 20.0 equiv), were dissolved in anhydrous CH$_2$Cl$_2$ (7 mL). The solution was electrolyzed under a constant voltage of 2.0 V for 4.2 F/mol using a platinum anode and a graphite cathode. After completion of the electrolysis, the solvent was removed under reduced pressure, and the residue was purified *via* flash chromatography (SiO$_2$, CH/EtOAc 20:1). **1** was isolated as a yellow resin (2.00 mg, 3.19 µmol, 10%).

R_f (SiO$_2$, CH/EtOAc, 4:1) = 0.70.

^{1}H-NMR (500 MHz, CDCl$_3$) δ [ppm] = 13.40 (s, 2H), 8.53 – 7.86 (m, 4H), 6.93 (d, J = 8.9 Hz, 2H), 6.49 (dd, J = 8.9, 2.5 Hz, 2H), 6.42 (d, J = 2.5 Hz, 2H), 3.88 (dd, J = 5.9, 2.1 Hz, 4H), 3.85 (s, 3H), 1.76 (h, J = 6.2 Hz, 2H), 1.60 – 1.39 (m, 6H), 1.39 – 1.31 (m, 2H), 1.00 – 0.90 (m, 12H).

^{13}C-NMR (126 MHz, CDCl$_3$) δ [ppm] = 170.0 (2C, C$_q$, *C*N), 167.4 (C$_q$, *C*N), 165.5 (2C, C$_q$), 164.7 (2C, C$_q$), 163.9 (C$_q$), 131.2 (2C, C$_q$), 130.6 (2C, CH$_{Ar}$), 126.6 (C$_q$), 114.3 (2C, CH$_{Ar}$), 110.1, 108.5 (2C, CH$_{Ar}$), 101.8 (2C, CH$_{Ar}$), 70.9 (2C, CH$_2$), 55.5 (CH$_3$), 39.3 (2C, CH), 30.6 (2C, CH$_2$), 29.2 (2C, CH$_2$), 23.9 (2C, CH$_2$), 23.2 (2C, CH$_2$), 14.2 (2C, CH$_3$), 11.2 (2C, CH$_3$).

IR (ATR) $\tilde{v}$ [cm^{-1}] = 2956 (w), 2924 (m), 2868 (w), 2859 (w), 1628 (m), 1585 (vs), 1530 (vs), 1502 (vs), 1451 (s), 1439 (s), 1422 (s), 1414 (s), 1390 (m), 1370 (vs), 1353 (vs), 1319 (m), 1306 (m), 1249 (vs), 1232 (vs), 1186 (vs), 1170 (vs), 1159 (vs), 1119 (s), 1099 (vs), 1050 (m), 1020 (vs), 973 (m), 851 (w), 832 (vs), 796 (vs), 747 (m), 718 (m), 642 (m), 629 (m), 622 (s), 596 (vs), 510 (m), 462 (m), 411 (w).

FAB-MS *m/z* (%): 630 (14), 629 (27), 628 (51), 627 (14), 446 (33), 445 (48), 444 (100), 443 (70), 373 (18), 334 (11), 333 (14), 332 (44), 331 (29), 330 (37), 261 (10), 220 (29), 136 (13), 134 (33).

HRMS-FAB (*m/z*): [M + H]$^+$ calcd. for C$_{38}$H$_{50}$O$_5$N$_3$, 628.3745; found, 628.3747.

5.5 Crystallographic Data

Crystal structures in this section were measured and solved by Dr. MARTIN NIEGER at the University of Helsinki.

Table 1. Overview over the numbering and sample code of crystals.

Entry	Compound		Internal ID
1	2-(1,4(1,4)-Dibenzenacyclohexaphane-1^2-yl)-*N*-(*tert*-butyl)imidazo[1,2-*a*]pyridin-3-amine	**92b**	**SB1178_HY**
2	(*E*)-*N*-(2-(1,4(1,4)-Dibenzenacyclohexaphane-1^2-yl)imidazo[1,2-*a*]pyrazin-3-yl)-1-phenyl methanimine	**93a'**	**SB1143_HY**
3	2,2'-(1,4(1,4)-Dibenzenacyclohexaphane-1^2,4^3-diyl)bis(*N*-pentylimidazo[1,2-*a*]pyridin-3-amine)	**96**	**SB1447_HY**
4	2-(3,5-bis¬(3-(*tert*-butylamino)imidazo[1,2-*a*]pyridin-2-yl)phenyl)anthracene-9,10-dione	**109**	**SB1468_HY**
5	17-((*E*)-5-Ethyl-6-methylhept-3-en-2-yl)-10,13-dimethyl-3-(tosylmethyl)-2,3,4,7,8,9,10,11,12,13,14,15,16,17-tetradecahydro-1H-cyclopenta-[*a*]phenanthrene	**118d**	**SB1398_HY**
6	*N*-(Adamantan-1-yl)pyrido[2',1':2,3]imidazo[4,5-*c*]isoquinolin-5-amine	**129ad**	**SB1335_HY**
7	*N*-Cyclohexylpyrazino[2',1':2,3]imidazo[4,5-*c*]isoquinolin-5-amine	**129ba**	**SB1132_HY**
8	(*E*)-11-(*tert*-Butyl-amino)-6-(isopropylimino)-1*H*,6*H*-pyrido[2',1':2,3]imidazo[5,1-*a*]isoindol-1-one	**130**	**SB1161_HY**
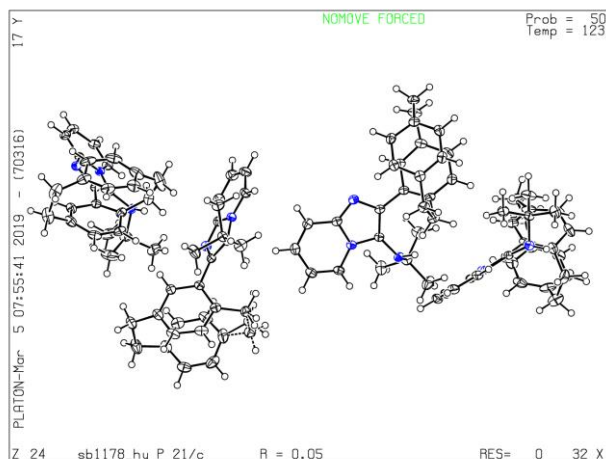
SB1178_HY

4 crystallographic independent molecules

one CH2 group in a C2H4 bridge disordered

2-(1,4(1,4)-Dibenzenacyclohexaphane-1²-yl)-*N*-(*tert*-butyl)imidazo[1,2-*a*]pyridin-3-amine (92b)

Crystal data

$C_{27}H_{29}N_3$	$F(000) = 3392$
$M_r = 395.53$	$D_x = 1.240$ Mg m^{-3}
Monoclinic, $P2_1/c$ *(no.14)*	Cu $K\alpha$ radiation, $\lambda = 1.54178$ Å
$a = 25.0296$ (7) Å	Cell parameters from 9635 reflections
$b = 30.8444$ (9) Å	$\theta = 3.3–72.0°$
$c = 11.0646$ (3) Å	$\mu = 0.56$ mm^{-1}
$\beta = 97.162$ (1)°	$T = 123$ K
$V = 8475.5$ (4) Å^3	Plates, yellow
$Z = 16$	$0.20 \times 0.16 \times 0.10$ mm

Data collection

Bruker D8 VENTURE diffractometer with PhotonII CPAD detector	14959 reflections with $I > 2\sigma(I)$
Radiation source: INCOATEC microfocus sealed tube	$R_{int} = 0.039$
rotation in ϕ and ω, 1°, shutterless scans	$\theta_{max} = 72.3°$, $\theta_{min} = 2.3°$
Absorption correction: multi-scan *SADABS* (Sheldrick, 2014)	$h = -29 \rightarrow 30$
$T_{min} = 0.861$, $T_{max} = 0.929$	$k = -38 \rightarrow 38$
153306 measured reflections	$l = -13 \rightarrow 11$
16694 independent reflections	

Refinement

Refinement on F^2	Primary atom site location: dual
Least-squares matrix: full	Secondary atom site location: difference Fourier map
$R[F^2 > 2\sigma(F^2)] = 0.045$	Hydrogen site location: mixed
$wR(F^2) = 0.122$	H atoms treated by a mixture of independent and constrained refinement
$S = 1.02$	$w = 1/[\sigma^2(F_o^2) + (0.0597P)^2 + 4.3609P]$ where $P = (F_o^2 + 2F_c^2)/3$
16694 reflections	$(\Delta/\sigma)_{max} = 0.001$
1092 parameters	$\Delta\rangle_{max} = 1.09$ e Å^{-3}
1175 restraints	$\Delta\rangle_{min} = -0.43$ e Å^{-3}
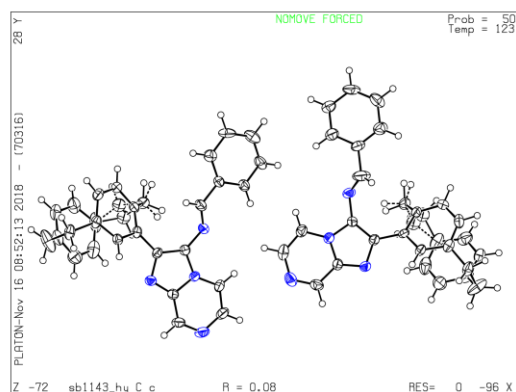
SB1143_HY

imine instead of amine
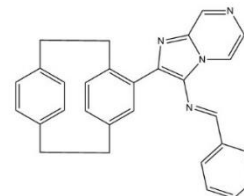
(E)-N-(2-(1,4(1,4)-dibenzenacyclohexaphane-1²-yl)imidazo[1,2-*a*]pyrazin-3-yl)-1-
phenylmethanimine

(*E*)-*N*-(2-(1,4(1,4)-Dibenzenacyclohexaphane-1²-yl)imidazo[1,2-*a*]pyrazin-3-yl)-1-phenyl methanimine (93a')

Crystal data

$C_{29}H_{24}N_4$	$F(000) = 1808$
$M_r = 428.52$	$D_x = 1.315$ Mg m^{-3}
Monoclinic, *Cc* (*no.9*	Cu $K\alpha$ radiation, $\lambda = 1.54178$ Å
$a = 7.8586$ (4) Å	Cell parameters from 4960 reflections
$b = 12.3823$ (7) Å	$\theta = 3.9–72.2°$
$c = 44.509$ (2) Å	$\mu = 0.61$ mm^{-1}
$\beta = 91.100$ (3)°	$T = 123$ K
$V = 4330.2$ (4) Å³	Blocks, colourless
$Z = 8$	$0.06 \times 0.04 \times 0.02$ mm

Data collection

Bruker D8 VENTURE diffractometer with PhotonII CPAD detector	6765 reflections with $I > 2\sigma(I)$
Radiation source: INCOATEC microfocus sealed tube	$R_{int} = 0.058$
rotation in ϕ and ω, 1°, shutterless scans	$\theta_{max} = 72.5°$, $\theta_{min} = 4.0°$
Absorption correction: multi-scan *SADABS* (Sheldrick, 2014)	$h = -9 \rightarrow 9$
$T_{min} = 0.782$, $T_{max} = 0.971$	$k = -15 \rightarrow 13$
15284 measured reflections	$l = -52 \rightarrow 54$
7922 independent reflections	

Refinement

Refinement on F^2	Secondary atom site location: difference Fourier map
Least-squares matrix: full	Hydrogen site location: inferred from neighbouring sites
$R[F^2 > 2\sigma(F^2)] = 0.079$	H-atom parameters constrained
$wR(F^2) = 0.208$	$w = 1/[\sigma^2(F_o^2) + (0.090P)^2 + 10.P]$ where $P = (F_o^2 + 2F_c^2)/3$
$S = 1.05$	$(\Delta/\sigma)_{max} < 0.001$
7922 reflections	$\Delta\rangle_{max} = 0.38$ e Å^{-3}
593 parameters	$\Delta\rangle_{min} = -0.26$ e Å^{-3}
62 restraints	Absolute structure: Flack x determined using 2333 quotients [(I+)-(I-)]/[(I+)+(I-)] (Parsons, Flack and Wagner, Acta Cryst. B69 (2013) 249-259).
Primary atom site location: dual	Absolute structure parameter: -0.3 (7)
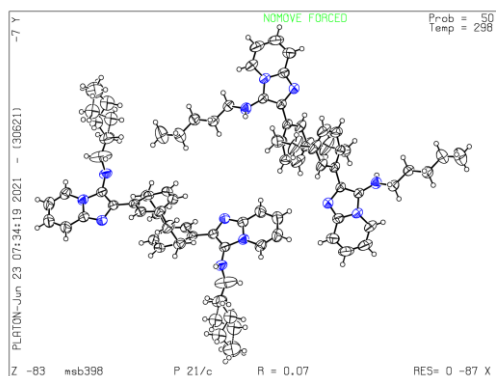
SB1447_HY

poor crystal, incomplete data, one n-pentyl moiety disordered

Ci symmetry, 2 x 0.5 molecules per asymmetric unit

Only proof of the structure and the conformation

2,2'-(1,4(1,4)-Dibenzenacyclohexaphane-1^2,4^3-diyl)bis(*N*-pentylimidazo[1,2-*a*]pyridin-3-amine) (96)

Crystal data

C$_{40}$H$_{46}$N$_6$	*Z* = 4
M$_r$ = 610.83	*F*(000) = 1312
Monoclinic, *P*2$_1$/*c* (*no.14*)	*D$_x$* = 1.207 Mg m^{-3}
a = 20.873 (4) Å	Cu *K*α radiation, λ = 1.54178 Å
b = 8.583 (2) Å	μ = 0.56 mm^{-1}
c = 20.676 (4) Å	*T* = 298 K
β = 114.84 (1)°	0.18 × 0.12 × 0.03 mm
V = 3361.5 (12) Å^3	

SB1468_HY
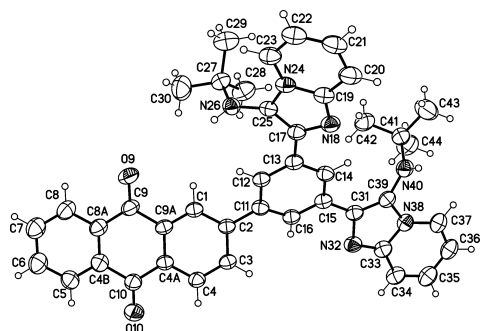
poor crystal quality, high displacement parameters, 0.5 MeOH and one water solvent found per formula moiety

constitution and conformation determined

in two voids one diffuse water per void found, squeezed out

2-(3,5-Bis-(3-(tert-butylamino)imidazo[1,2-a] pyridin-2-yl)phenyl)anthracene-9,10-dione (109)

Crystal data

$C_{42}H_{38}N_6O_2 \cdot 1.5(H_2O) \cdot 0.5(CH_4O)$	$F(000) = 1488$
$M_r = 701.83$	$D_x = 1.233$ Mg m^{-3}
Monoclinic, $P2_1$ (no.4)	Cu $K\alpha$ radiation, $\lambda = 1.54178$ Å
$a = 10.1391$ (8) Å	Cell parameters from 9944 reflections
$b = 18.3961$ (15) Å	$\theta = 2.1–71.0°$
$c = 20.2654$ (16) Å	$\mu = 0.65$ mm^{-1}
$\beta = 91.066$ (5)°	$T = 298$ K
$V = 3779.2$ (5) Å^3	Blocks, orange
$Z = 4$	$0.24 \times 0.06 \times 0.03$ mm

Data collection

Bruker D8 VENTURE diffractometer with PhotonII CPAD detector	10186 reflections with $I > 2\sigma(I)$
Radiation source: INCOATEC microfocus sealed tube	$R_{int} = 0.078$
rotation in ϕ and ω, 1°, shutterless scans	$\theta_{max} = 85.9°$, $\theta_{min} = 2.2°$
Absorption correction: multi-scan *SADABS* (Sheldrick, 2014)	$h = -12 \rightarrow 10$
$T_{min} = 0.705$, $T_{max} = 0.971$	$k = -23 \rightarrow 20$
45175 measured reflections	$l = -24 \rightarrow 24$
14106 independent reflections	

Refinement

Refinement on F^2	Hydrogen site location: mixed
Least-squares matrix: full	H-atom parameters constrained
$R[F^2 > 2\sigma(F^2)] = 0.093$	$w = 1/[\sigma^2(F_o^2) + (0.155P)^2 + 0.9P]$ where $P = (F_o^2 + 2F_c^2)/3$
$wR(F^2) = 0.269$	$(\Delta/\sigma)_{max} = 0.009$
$S = 1.06$	$\Delta\rangle_{max} = 0.38$ e Å^{-3}
14106 reflections	$\Delta\rangle_{min} = -0.29$ e Å^{-3}
940 parameters	Extinction correction: *SHELXL2014*/7 (Sheldrick 2014), Fc*=kFc[1+0.001xFc$^2\lambda^3$/sin(2θ)]$^{-1/4}$
2677 restraints	Extinction coefficient: 0.0035 (5)
Primary atom site location: dual	Absolute structure: Flack x determined using 3355 quotients [(I+)-(I-)]/[(I+)+(I-)] (Parsons, Flack and Wagner, Acta Cryst. B69 (2013) 249-259).
Secondary atom site location: difference Fourier map	Absolute structure parameter: -0.1 (3)
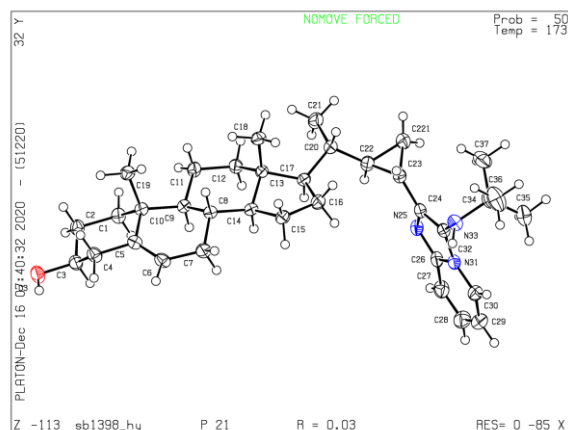
SB1398_HY

absolute configuration determined crystallographically and from an unchanged chiral center

17-((*E*)-5-Ethyl-6-methylhept-3-en-2-yl)-10,13-dimethyl-3-(tosylmethyl)-2,3,4,7,8,9,10,11,12,13,14,15,16,17-tetradecahydro-1H-cyclopenta-[*a*]phenanthrene (118d)[120]

Crystal data

$C_{35}H_{51}N_3O$	$F(000) = 580$
$M_r = 529.78$	$D_x = 1.145$ Mg m^{-3}
Monoclinic, $P2_1$ (no.4)	Cu $K\alpha$ radiation, $\lambda = 1.54178$ Å
$a = 9.6804$ (3) Å	Cell parameters from 9933 reflections
$b = 7.6297$ (2) Å	$\theta = 4.2$–72.1°
$c = 21.3249$ (6) Å	$\mu = 0.52$ mm^{-1}
$\beta = 102.664$ (1)°	$T = 173$ K
$V = 1536.71$ (8) Å^3	Plates, colourless
$Z = 2$	$0.16 \times 0.12 \times 0.04$ mm

Data collection

Bruker D8 VENTURE diffractometer with PhotonII CPAD detector	5619 reflections with $I > 2\sigma(I)$
Radiation source: INCOATEC microfocus sealed tube	$R_{int} = 0.027$
rotation in ϕ and ω, 1°, shutterless scans	$\theta_{max} = 72.2°$, $\theta_{min} = 2.1°$
Absorption correction: multi-scan *SADABS* (Sheldrick, 2014)	$h = -11 \rightarrow 11$
$T_{min} = 0.891$, $T_{max} = 0.971$	$k = -8 \rightarrow 9$
22228 measured reflections	$l = -25 \rightarrow 26$
5825 independent reflections	

Refinement

Refinement on F^2	Secondary atom site location: difference Fourier map
Least-squares matrix: full	Hydrogen site location: difference Fourier map
$R[F^2 > 2\sigma(F^2)] = 0.031$	H atoms treated by a mixture of independent and constrained refinement
$wR(F^2) = 0.080$	$w = 1/[\sigma^2(F_o^2) + (0.0406P)^2 + 0.2819P]$ where $P = (F_o^2 + 2F_c^2)/3$
$S = 1.03$	$(\Delta/\sigma)_{max} < 0.001$
5825 reflections	$\Delta\rangle_{max} = 0.18$ e Å^{-3}
358 parameters	$\Delta\rangle_{min} = -0.15$ e Å^{-3}
3 restraints	Absolute structure: Flack x determined using 2391 quotients [(I+)-(I-)]/[(I+)+(I-)] (Parsons, Flack and Wagner, Acta Cryst. B69 (2013) 249-259).
Primary atom site location: dual	Absolute structure parameter: -0.15 (10)
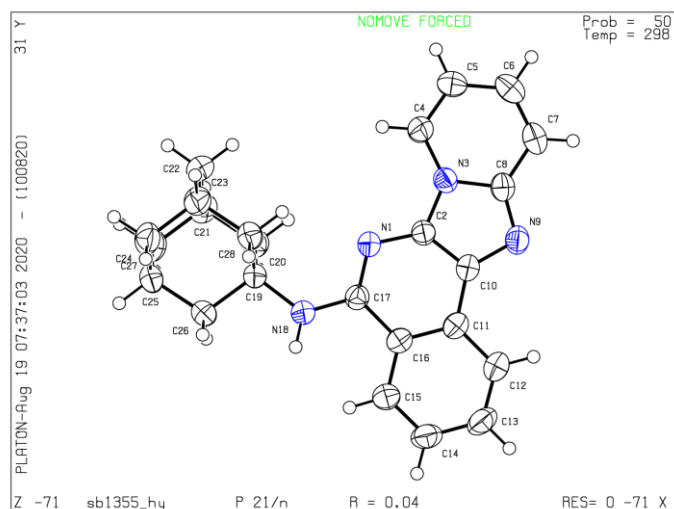
SB1355_HY

N-(Adamantan-1-yl)pyrido[2',1':2,3]imidazo[4,5-*c*]isoquinolin-5-amine (129ad)

Crystal data

C$_{24}$H$_{24}$N$_4$	$F(000) = 784$
$M_r = 368.47$	$D_x = 1.278$ Mg m^{-3}
Monoclinic, $P2_1/n$ (*no.14*)	Cu $K\alpha$ radiation, $\lambda = 1.54178$ Å
$a = 6.5540$ (6) Å	Cell parameters from 9929 reflections
$b = 12.6859$ (12) Å	$\theta = 3.8–72.1°$
$c = 23.2169$ (21) Å	$\mu = 0.60$ mm^{-1}
$\beta = 97.357$ (4)°	$T = 298$ K
$V = 1914.4$ (3) Å^3	Plates, yellow
$Z = 4$	$0.24 \times 0.12 \times 0.03$ mm

Data collection

Bruker D8 VENTURE diffractometer with PhotonII CPAD detector	3445 reflections with $I > 2\sigma(I)$
Radiation source: INCOATEC microfocus sealed tube	$R_{int} = 0.029$
rotation in ϕ and ω, 1°, shutterless scans	$\theta_{max} = 72.1°$, $\theta_{min} = 3.8°$
Absorption correction: multi-scan *SADABS* (Sheldrick, 2014)	$h = -7 \rightarrow 8$
$T_{min} = 0.831$, $T_{max} = 0.971$	$k = -15 \rightarrow 15$
26584 measured reflections	$l = -28 \rightarrow 28$
3764 independent reflections	

Refinement

Refinement on F^2	Primary atom site location: dual
Least-squares matrix: full	Secondary atom site location: difference Fourier map
$R[F^2 > 2\sigma(F^2)] = 0.039$	Hydrogen site location: difference Fourier map
$wR(F^2) = 0.097$	H atoms treated by a mixture of independent and constrained refinement
$S = 1.03$	$w = 1/[\sigma^2(F_o^2) + (0.0382P)^2 + 0.5418P]$ where $P = (F_o^2 + 2F_c^2)/3$
3764 reflections	$(\Delta/\sigma)_{max} = 0.001$
256 parameters	$\Delta\rangle_{max} = 0.18$ e Å^{-3}
0 restraints	$\Delta\rangle_{min} = -0.18$ e Å^{-3}
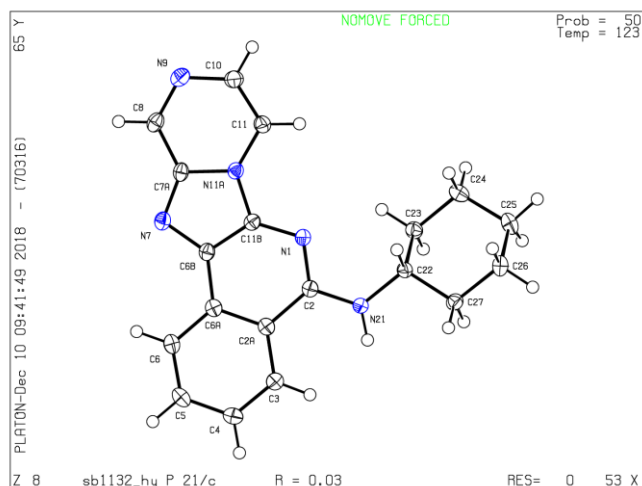
SB1132_HY

N-Cyclohexylpyrazino[2',1':2,3]imidazo[4,5-*c*]isoquinolin-5-amine (129ba)

Crystal data

$C_{19}H_{19}N_5$	$F(000) = 672$
$M_r = 317.39$	$D_x = 1.363$ Mg m^{-3}
Monoclinic, $P2_1/c$ (*no.14*)	Cu $K\alpha$ radiation, $\lambda = 1.54178$ Å
$a = 7.7193$ (2) Å	Cell parameters from 9962 reflections
$b = 19.0741$ (6) Å	$\theta = 4.8–72.2°$
$c = 10.7854$ (3) Å	$\mu = 0.67$ mm^{-1}
$\beta = 103.055$ (1)°	$T = 123$ K
$V = 1546.98$ (8) Å^3	Plates, yellow
$Z = 4$	$0.30 \times 0.18 \times 0.12$ mm

Data collection

Bruker D8 VENTURE diffractometer with PhotonII CPAD detector	2978 reflections with $I > 2\sigma(I)$
Radiation source: INCOATEC microfocus sealed tube	$R_{int} = 0.026$
rotation in ϕ and ω, 1°, shutterless scans	$\theta_{max} = 72.3°$, $\theta_{min} = 4.8°$
Absorption correction: multi-scan *SADABS* (Sheldrick, 2014)	$h = -9 \rightarrow 9$
$T_{min} = 0.815$, $T_{max} = 0.815$	$k = -23 \rightarrow 23$
27211 measured reflections	$l = -13 \rightarrow 13$
3049 independent reflections	

Refinement

Refinement on F^2	Primary atom site location: dual
Least-squares matrix: full	Secondary atom site location: difference Fourier map
$R[F^2 > 2\sigma(F^2)] = 0.034$	Hydrogen site location: difference Fourier map
$wR(F^2) = 0.085$	H atoms treated by a mixture of independent and constrained refinement
$S = 1.03$	$w = 1/[\sigma^2(F_o^2) + (0.0391P)^2 + 0.6426P]$ where $P = (F_o^2 + 2F_c^2)/3$
3049 reflections	$(\Delta/\sigma)_{max} < 0.001$
220 parameters	$\Delta\rangle_{max} = 0.27$ e Å^{-3}
1 restraint	$\Delta\rangle_{min} = -0.21$ e Å^{-3}
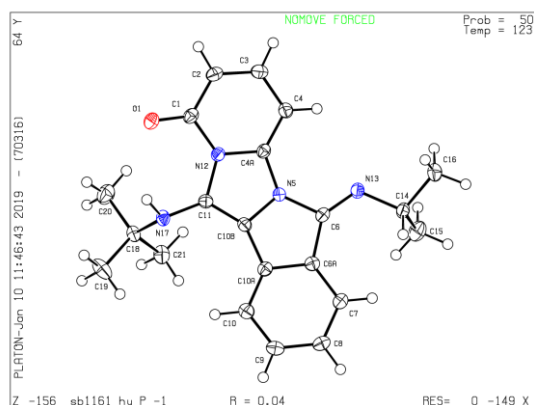
(*E*)-11-(*tert*-Butyl-amino)-6-(isopropylimino)-1H,6H-pyrido[2',1':2,3]imidazo[5,1-*a*]isoindol-1-one (130)

Crystal data

$C_{21}H_{24}N_4O$	$Z = 2$
$M_r = 348.44$	$F(000) = 372$
Triclinic, *P*-1 (no.2)	$D_x = 1.303$ Mg m^{-3}
$a = 9.3835$ (3) Å	Cu $K\alpha$ radiation, $\lambda = 1.54178$ Å
$b = 10.5528$ (3) Å	Cell parameters from 9882 reflections
$c = 11.1436$ (3) Å	$\theta = 4.9$–72.1°
$\alpha = 113.802$ (1)°	$\mu = 0.65$ mm^{-1}
$\beta = 114.890$ (1)°	$T = 123$ K
$\gamma = 91.828$ (1)°	Blocks, yellow
$V = 888.36$ (5) Å^3	$0.18 \times 0.14 \times 0.06$ mm

Data collection

Bruker D8 VENTURE diffractometer with PhotonII CPAD detector	3337 reflections with $I > 2\sigma(I)$
Radiation source: INCOATEC microfocus sealed tube	$R_{int} = 0.020$
rotation in ϕ and ω, 1°, shutterless scans	$\theta_{max} = 72.2°$, $\theta_{min} = 4.9°$
Absorption correction: multi-scan *SADABS* (Sheldrick, 2014)	$h = -11 \rightarrow 11$
$T_{min} = 0.901$, $T_{max} = 0.958$	$k = -12 \rightarrow 13$
13276 measured reflections	$l = -13 \rightarrow 13$
3476 independent reflections	

Refinement

Refinement on F^2	Primary atom site location: dual
Least-squares matrix: full	Secondary atom site location: difference Fourier map
$R[F^2 > 2\sigma(F^2)] = 0.035$	Hydrogen site location: difference Fourier map
$wR(F^2) = 0.094$	H atoms treated by a mixture of independent and constrained refinement
$S = 1.04$	$w = 1/[\sigma^2(F_o^2) + (0.0459P)^2 + 0.3211P]$ where $P = (F_o^2 + 2F_c^2)/3$
3476 reflections	$(\Delta/\sigma)_{max} < 0.001$
238 parameters	$\Delta\rangle_{max} = 0.28$ e Å^{-3}
1 restraint	$\Delta\rangle_{min} = -0.20$ e Å^{-3}

6   Abbreviations and Units

6.1   List of Abbreviations

δ	Chemical Shift (NMR)
ΔE_{ST}	Singlet-Triplet Energy Gap
ṽ	Wavenumber (IR)
aq.	aqueous
Ar	Aromatic
Aq	Anthraquinone
ATR	Attenuated Total Reflection
BMT/BEMT	Bemotrizinol
bp	Base Pairs
bpy	Bis-pyridyl
Bz	Benzoyl
Calcd.	Calculated
cf.	*confer* lat.: compare
CH	Cyclohexane
cLIFT	Combinatorial Laser-induced Forward Transfer
COF	Covalent Organic Framework
COSY	Correlation Spectroscopy
CV	Cyclovoltammetry
DBPS	Dulbecco's phosphate-buffered saline
ddH$_2$O	Deionized Distilled Water
DDQ	2,3-Dichloro-5,6-dicyano-1,4-benzoquinone
DFT	Density Functional Theory
Diopat	di-*ortho*-Hydroxyphenyl Asymmetric Triazine
DIY	Do it yourself
DMEM	Dulbecco's Modified Eagle Medium
DMF	*N,N*-Dimethylformamide
DMSO	Dimethylsulfoxide
DNA	Desoxyribonucleic Acid
dppf	1,1′-Bi(diphenylphosphino)ferrocene
DPV	Differential Pulse Voltammetry
ds-DNA	Double-stranded Desoxyribonucleic Acid
E. coli	*Escherichia coli*
EDD	Electrochemically Driven Desaturation
e.g.	*exempli gratia* lat.: for example
EMSA	Electrophoresis Mobility Shift Assay
equiv	Equivalents

ESI-MS	electrospray Ionization Mass Spectrometry
ESIPT	excited State Intramolecular Proton Transfer
et al.	*et alii/aliae/alia* lat.: and others
etc.	*et cetera* lat.: and so forth
FAB-MS	Fast Atom Bombardment Mass Spectrometry
FAD	Flavin-Adenine Dinucleotide
FBS	Fetal bovine serum
FCA	FRIEDEL-CRAFTS Acylation
FDA	Food and Drug Administration
FID	Fluorescent Intercalator Displacement
FMN	Flavin mononucleotide
FRET	FÖRSTER Resonance Energy Transfer
FOMO	Frontier Molecular Orbital
GABA	Gamma-Butyric Acid
GBB	GROEBKE-BLACKBURN-BIENAYMÉ 3-Component Reaction
GC/MS	Gas Chromatography
HeLa	Human cervical cancer cell line originating from patient Henrietta Lacks
HIV	Human Immunodeficiency Virus
HMBC	Heteronuclear Multiple Bond Correlation
HMDS	Hexamethyldisilazane
HOMO	Highest Occupied Molecular Orbital
HSQC	Heteronuclear Single Quantum Coherence
IBX	Iodobenzoic acid
i.e.	*id est* lat.: that is to say
ImPy	Imidazo[1,2-*a*]pyridine
IOC	Institute of Organic Chemistry
IR	Infrared Spectroscopy
ISC	Intersystem Crossing
J	Coupling constant (NMR)
KIT	Karlsruhe Institute of Technology
LDA	Lithium diisopropyl amide
LIFT	Laser-induced Forward Transfer
lig	Ligand
LiHMDS	Lithium hexamethyldisilazane
LUMO	Lowest Unoccupied Molecular Orbital
M	molar
m/z	Mass-to Charge ratio
MALDI	Matrix-Assisted Laser Desorption Ionization
MCR	Multicomponent Reaction
m.p.	Melting Point

MS	Mass Spectrometry
MTT	3-(4,5-Dimethylthiazol-2-yl)-2,5-diphenyltetrazolium bromide
MW	Microwave
3-NBA	3-Nitrobenzyl Alcohol
NMR	Nuclear Magnetic Resonance Spectroscopy
NPI	*N*-substituted benzo[de]isoquinoline-1,3-dione
oc-DNA	Open Circular DNA
OLED	Organic Light Emitting Diode
PBS	Phosphate-buffered Saline
PCP	[2.2]Paracyclophane
Pd/C	Palladium on activated Charcoal
Pd-Peppsi iPr	Pyridine-Enhanced Pre-Catalyst Preparation Stabilization and Initiation
$PE_{40/60}$	Petrol ether
PEGMA	Poly(ethylene glycol) methacrylate
PM2	*Pseudoaltermonas Virus 2*
ppm	parts per million
pUC19	Plasmid
quant.	quantitative
R	Residue
RISC	Reverse Intersystem Crossing
R_f	Retardation factor
rpm	Revolutions per minute
r.t.	Room Temperature
S_0	Ground State
S_1	1st Excited Singlet State
sat.	saturated
sc-DNA	Supercoiled DNA
SCE	Standard Calomel Electrode
S_NAr	Nucleophilic aromatic substitution
T_1	1st Excited Triplet State
TADF	Thermally Activated Delayed Fluorescence
Tc-MIBI	Technetium Methyl iso-Butyl Isonitrile
THBMT	Tetrahydro Bemotrizinol
THF	Tetrahydrofuran
TMS	Trimethylsilyl
TLC	Thin Layer Chromatography
Trz	Diphenyl-1,3,5-triazine
UV	Ultraviolet Light
Vis	Visible

6.2 List of Units

A	Ampere
°C	Degrees Celsius
cm	Centimeter
d	Days
eV	Electron Volt
F	Farraday
g	Gram
h	Hours
Hz	Hertz
K	Kelvin
L	Liters
mbar	Millibar
mg	Milligram
µg	Microgram
MHz	Megahertz
min	Minutes
mL	Milliliter
µL	Microliter
mmol	Millimole
µmol	Micromole
mol	Mole
mV	Millivolt
nm	Nanometer
ns	Nanoseconds
s	Seconds
V	Volt
W	Watt

7 Bibliography

[1]   R. M. Christie, *Colour Chemistry*, 2nd ed., The Royal Society of Chemistry, Camebridge, **2015**.

[2]   K. Hübner, *Chemie in unserer Zeit* **2006**, *40*, 274-275.

[3]   J. Griffiths, *Chemie in unserer Zeit* **1993**, *27*, 21-31.

[4]   M. Klessinger, *Chemie in unserer Zeit* **1978**, *12*, 1-11.

[5]   P. W. Atkins, J. de Paula, J. J. Keeler, C. Hartmann, *Physikalische Chemie*, Wiley, **2021**.

[6]   S. E. Braslavsky, *Pure Appl. Chem.* **2007**, *79*, 293-465.

[7]   R. C. Hilborn, *Am. J. Phys.* **1982**, *50*, 982-986.

[8]   a) J. B. Birks, D. J. Dyson, B. H. Flowers, *Proc. R. Soc. Lond. A* **1963**, *275*, 135-148; b) S. J. Strickler, R. A. Berg, *J. Chem. Phys.* **1962**, *37*, 814-822.

[9]   B. Valeur, M. N. Berberan-Santos, *Molecular Fluorescence: Principles and Applications*, Wiley-VCH, Weinheim, **2013**.

[10]   A. Marini, A. Muñoz-Losa, A. Biancardi, B. Mennucci, *J. Phys. Chem. B* **2010**, *114*, 17128-17135.

[11]   J. Zhao, S. Ji, Y. Chen, H. Guo, P. Yang, *Phys. Chem. Chem. Phys.* **2012**, *14*, 8803-8817.

[12]   H. C. Joshi, L. Antonov, *Molecules* **2021**, *26*, 1475.

[13]   a) L. Chen, P.-Y. Fu, H.-P. Wang, M. Pan, *Adv. Opt. Mater.* **2021**, *9*, 2001952; b) Y. Li, D. Dahal, C. S. Abeywickrama, Y. Pang, *ACS Omega* **2021**, *6*, 6547-6553.

[14]   C. K. Madsen, J. H. Zhao, *Optical Filter Design and Analysis: A Signal Processing Approach*, Wiley, **1999**.

[15]   G. Hong, X. Gan, C. Leonhardt, Z. Zhang, J. Seibert, J. M. Busch, S. Bräse, *Adv. Mater.* **2021**, *33*, e2005630.

[16]   C. A. Parker, C. G. Hatchard, *Trans. Faraday Soc.* **1961**, *57*, 1894-1904.

[17]   a) P. F. Jones, A. R. Calloway, *Chem. Phys. Lett.* **1971**, *10*, 438-443; b) M. Sikorski, I. V. Khmelinskii, W. Augustyniak, F. Wilkinson, *J. Chem. Soc. Faraday Trans.* **1996**, *92*, 3487-3490; c) B. S. Yamanashi, D. M. Hercules, *Appl. Spectrosc.* **1971**, *25*, 457-460; d) F. A. Salazar, A. Fedorov, M. N. Berberan-Santos, *Chem. Phys. Lett.* **1997**, *271*, 361-366.

[18]   a) H. Uoyama, K. Goushi, K. Shizu, H. Nomura, C. Adachi, *Nature* **2012**, *492*, 234-238; b) A. Endo, M. Ogasawara, A. Takahashi, D. Yokoyama, Y. Kato, C. Adachi, *Adv. Mater.* **2009**, *21*, 4802-4806; c) A. Endo, K. Sato, K. Yoshimura, T. Kai, A. Kawada, H. Miyazaki, C. Adachi, *Appl. Phys. Lett.* **2011**, *98*, 083302.

[19]   a) Z. Yang, Z. Mao, Z. Xie, Y. Zhang, S. Liu, J. Zhao, J. Xu, Z. Chi, M. P. Aldred, *Chem. Soc. Rev.* **2017**, *46*, 915-1016; b) M. Y. Wong, E. Zysman-Colman, *Adv. Mater.* **2017**, *29*, 1605444; c) X. Liang, Z.-L. Tu, Y.-X. Zheng, *Chem. Eur. J.* **2019**, *25*, 5623-5642.

[20]   Y. Tao, K. Yuan, T. Chen, P. Xu, H. Li, R. Chen, C. Zheng, L. Zhang, W. Huang, *Adv. Mater.* **2014**, *26*, 7931-7958.

[21]   a) F. P. Gasparro, M. Mitchnick, J. F. Nash, *Photochem. Photobiol.* **1998**, *68*, 243-256; b) H. Sahoo, *J. Photochem. Photobiol. C: Photochem. Rev.* **2011**, *12*, 20-30; c) H. Schneckenburger, *Methods Appl. Fluoresc.* **2019**, *8*, 013001.

[22]   L. Wu, C. Huang, B. P. Emery, A. C. Sedgwick, S. D. Bull, X.-P. He, H. Tian, J. Yoon, J. L. Sessler, T. D. James, *Chem. Soc. Rev.* **2020**, *49*, 5110-5139.

[23]   a) E. Betzig, G. H. Patterson, R. Sougrat, O. W. Lindwasser, S. Olenych, J. S. Bonifacino, M. W. Davidson, J. Lippincott-Schwartz, H. F. Hess, *Science* **2006**, *313*, 1642-1645; b) R. M. Dickson, A. B. Cubitt, R. Y. Tsien, W. E. Moerner, *Nature* **1997**, *388*, 355-357; c) S. W. Hell, J. Wichmann, *Org. Lett.* **1994**, *19*, 780-782.

[24]   a) C. W. Tang, S. A. VanSlyke, *Appl. Phys. Lett.* **1987**, *51*, 913-915; b) B. Geffroy, P. le Roy, C. Prat, *Polym. Int.* **2006**, *55*, 572-582; c) A. Salehi, X. Fu, D.-H. Shin, F. So, *Adv. Funct. Mater.* **2019**, *29*, 1808803.

[25]   A. J. C. Kuehne, M. C. Gather, *Chem. Rev.* **2016**, *116*, 12823-12864.

[26]   a) M. K. Nazeeruddin, E. Baranoff, M. Grätzel, *Solar Energy* **2011**, *85*, 1172-1178; b) B. O'Regan, M. Grätzel, *Nature* **1991**, *353*, 737-740.

[27]   A. A. Nagarkar, S. E. Root, M. J. Fink, A. S. Ten, B. J. Cafferty, D. S. Richardson, M. Mrksich, G. M. Whitesides, *ACS Cent. Sci.* **2021**, *7*, 1728-1735.

[28]   E. Guerra, M. Llompart, C. Garcia-Jares, *Cosmetics* **2018**, *5*, 47.

[29]   M. V. Orna, *J. Chem. Edu.* **2001**, *78*, 1305.

[30]   S. Zhang, H. Tappe, W. Helmling, P. Mischke, K. Rebsamen, U. Reiher, W. Russ, L. Schläfer, P. Vermehren, in *Ullmann's Encyclopedia of Industrial Chemistry*, pp. 1-20.

[31]   M. S. T. Gonçalves, *Chem. Rev.* **2009**, *109*, 190-212.

[32]   a) Y. Chen, Y. Gao, Y. He, G. Zhang, H. Wen, Y. Wang, Q.-P. Wu, H. Cui, *J. Med. Chem.* **2021**, *64*, 1001-1017; b) P. Vaidyanathan, E. Appleton, D. Tran, A. Vahid, G. Church, D. Densmore, *Communications Biology* **2021**, *4*, 118.

[33]   R. Alford, H. M. Simpson, J. Duberman, G. C. Hill, M. Ogawa, C. Regino, H. Kobayashi, P. L. Choyke, *Mol. Imaging* **2009**, *8*, 7290.2009.00031.

[34]   A. M. Smith, M. C. Mancini, S. Nie, *Nat. Nanotechnol.* **2009**, *4*, 710-711.

[35]   a) C. W. Cunningham, A. Mukhopadhyay, G. H. Lushington, B. S. J. Blagg, T. E. Prisinzano, J. P. Krise, *Mol. Pharm.* **2010**, *7*, 1301-1310; b) A. Borrelli, A. L. Tornesello, M. L. Tornesello, F. M. Buonaguro, *Molecules* **2018**, *23*, 295; c) S.-K. Chung, K. K. Maiti, W. S. Lee, *Int. J. Pharm.* **2008**, *354*, 16-22.

[36]   T. Veuthey, G. Herrera, V. I. Dodero, *Front. Biosc.* **2014**, *19*, 91-112.

[37]   a) M. Cavaco, C. Pérez-Peinado, J. Valle, R. D. M. Silva, J. D. G. Correia, D. Andreu, M. A. R. B. Castanho, V. Neves, *Front. Bioeng. Biotech.* **2020**, *8*; b) H. Sahoo, *RSC Adv.* **2012**, *2*, 7017-7029.

[38]   a) N. Chiu, T. K. Christopoulos, *Advances in Immunoassay Technology*, IntechOpen, **2012**; b) J. M. Berg, J. L. Tymoczko, G. J. Gatto, L. Stryer, A. Held, G. Maxam, L. Seidler, B. Häcker, B. Jarosch, *Stryer Biochemie*, Springer Berlin Heidelberg, **2017**; c) W. Müller-Esterl, *Biochemie: Eine Einführung für Mediziner und Naturwissenschaftler - Unter Mitarbeit von Ulrich Brandt, Oliver Anderka, Stefan Kerscher, Stefan Kieß und Katrin Ridinger*, Springer Berlin Heidelberg, **2017**.

[39]   a) H. J. Round, *Electr. World* **1907**, *19*, 309; b) A. Bernanose, *Br. J. Appl. Phys.* **1955**, *6*, S54-S55; c) M. Pope, H. P. Kallmann, P. Magnante, *J. Chem. Phys.* **1963**, *38*, 2042-2043; d) M. Sano, M. Pope, H. Kallmann, *J. Chem. Phys.* **1965**, *43*, 2920-2921; e) U. Mitschke, P. Bäuerle, *J. Mater. Chem.* **2000**, *10*, 1471-1507.

[40]   a) A. Buckley, *Organic Light-Emitting Diodes (OLEDs): Materials, Devices and Applications*, Elsevier Science, **2013**; b) D. J. Gaspar, E. Polikarpov, *OLED Fundamentals: Materials, Devices, and Processing of Organic Light-Emitting Diodes*, CRC Press, **2015**.

[41]   a) Q. Wei, N. Fei, A. Islam, T. Lei, L. Hong, R. Peng, X. Fan, L. Chen, P. Gao, Z. Ge, *Adv. Opt. Mater.* **2018**, *6*, 1800512; b) Z. Xu, B. Z. Tang, Y. Wang, D. Ma, *J. Mater. Chem. C* **2020**, *8*, 2614-2642.

[42]   C.-Y. Chan, M. Tanaka, Y.-T. Lee, Y.-W. Wong, H. Nakanotani, T. Hatakeyama, C. Adachi, *Nat. Photonics* **2021**, *15*, 203-207.

[43]   S. Madronich, in *Environmenntal UV Photobiololy* (Eds.: A. R. Young, J. Moan, L. O. Björn, W. Nultsch), Springer US, Boston, MA, **1993**, pp. 1-39.

[44]   a) E. A. Dutra, E. R. M. Kedor-Hackmann, M. I. R. M. Santoro, *Revista Brasileira de Ciências Farmacêuticas* **2004**, *40*, 381-385; b) S. Schalka, V. M. S. d. Reis, *Anais Brasileiros de Dermatologia* **2011**, *86*, 507-515; c) C. Stenberg, O. Larkö, *Arch. Dermatol.* **1985**, *121*, 1400-1402.

[45]   I. Fajzulin, X. Zhu, M. Möller, *J. Coat. Technol. Res.* **2015**, *12*, 617-632.

[46]   S. Mongiat, B. Herzog, C. Deshayes, P. König, U. Osterwalder, *Cosmet. Toiletries* **2003**, *118*, 47-54.

[47]   a) M. Silvia Díaz-Cruz, M. Llorca, D. Barceló, *Trends Analyt. Chem.* **2008**, *27*, 873-887; b) S. Kim, K. Choi, *Environment International* **2014**, *70*, 143-157.

[48]   a) C. L. Hexsel, S. D. Bangert, A. A. Hebert, H. W. Lim, *J. Am. Acad. Dermatol.* **2008**, *59*, 316-323; b) S. Narla, H. W. Lim, *Photochem. Photobiol. Sci.* **2020**, *19*, 66-70.

[49]   A. Dömling, I. Ugi, *Angew. Chem. Int. Ed.* **2000**, *39*, 3168-3210.

[50]   H. Bienaymé, C. Hulme, G. Oddon, P. Schmitt, *Chem. Eur. J.* **2000**, *6*, 3321-3329.

[51]   R. C. Cioc, E. Ruijter, R. V. A. Orru, *Green Chem.* **2014**, *16*, 2958-2975.

[52]   a) M. Smietana, E. Benedetti, C. Bressy, S. Arseniyadis, in *Efficiency in Natural Product Total Synthesis*, **2018**, pp. 319-344; b) R. Afshari, A. Shaabani, *ACS Comb. Sci.* **2018**, *20*, 499-528; c) C. Lamberth, *Bioorg. Med. Chem.* **2020**, *28*, 115471.

[53]   Z. Wang, A. Domling, in *Multicomponent Reactions towards Heterocycles*, **2022**, pp. 91-137.

[54]   B. Yang, Y. Zhao, Y. Wei, C. Fu, L. Tao, *Polym. Chem.* **2015**, *6*, 8233-8239.

[55]   a) A. C. Boukis, *Dissertation: Moleküle als potentielle Datenspeichersysteme: Multikomponentenreaktionen sind der Schlüssel*, Karlsruhe Institute of Technology, **2018**; b) M. Stahlberger, *Master Thesis: Development of Novel Sequential Synthesis Strategies involving Isocyanide-based Multi-Component Reactions*, Karlsruhe Institute of Technology, **2017**.

[56]   a) A. Strecker, *Ann. Chem. Pharm.* **1850**, *75*, 27-45; b) A. Strecker, *Ann. Chem. Pharm.* **1854**, *91*, 349-351.

[57]   C. Mannich, W. Krösche, *Arch. Pharm.* **1912**, *250*, 647-667.

[58]   A. Hantzsch, *Ber. Dtsch. Chem. Ges.* **1881**, *14*, 1637-1638.

[59]   a) P. Biginelli, *Ber. Dtsch. Chem. Ges.* **1891**, *24*, 2962-2967; b) P. Biginelli, *Ber. Dtsch. Chem. Ges.* **1891**, *24*, 1317-1319.

[60]   K. Gewald, E. Schinke, H. Böttcher, *Chem. Ber.* **1966**, *99*, 94-100.

[61]   a) N. A. Petasis, I. Akritopoulou, *Tetrahedron Lett.* **1993**, *34*, 583-586; b) N. A. Petasis, I. A. Zavialov, *J. Am. Chem. Soc.* **1997**, *119*, 445-446; c) N. A. Petasis, I. A. Zavialov, *J. Am. Chem. Soc.* **1998**, *120*, 11798-11799.

[62]   a) I. Ugi, S. Heck, *Comb. Chem. High Throughput Screen.* **2001**, *4*, 1-34; b) J. M. Knapp, M. J. Kurth, J. T. Shaw, A. Younai, in *Diversity‐Oriented Synthesis*, **2013**, pp. 27-57.

[63]   a) A. Boltjes, A. Dömling, *Eur. J. Org. Chem.* **2019**, *2019*, 7007-7049; b) E. Ruijter, R. V. Orru, *Drug. Discov. Today Technol.* **2013**, *10*, e15-20.

[64]   I. Ugi, B. Werner, A. Dömling, *Molecules* **2003**, *8*, 53-66.

[65]   A. S. Mikherdov, A. S. Novikov, V. P. Boyarskiy, V. Y. Kukushkin, *Nat. Commun.* **2020**, *11*, 2921.

[66]   J. A. Green, P. T. Hoffmann, in *Isonitrile Chemistry* (Ed.: I. Ugi), Academic Press, New York, **1971**, p. 2.

[67]   a) P. S. Baran, J. M. Richter, *J. Am. Chem. Soc.* **2005**, *127*, 15394-15396; b) M. J. Garson, J. S. Simpson, *Nat. Prod. Rep.* **2004**, *21*, 164-179; c) A. Massarotti, F. Brunelli, S. Aprile, M. Giustiniano, G. C. Tron, *Chem. Rev.* **2021**, *121*, 10742-10788; d) K. Stratmann, R. E. Moore, R. Bonjouklian, J. B. Deeter, G. M. L. Patterson, S. Shaffer, C. D. Smith, T. A. Smitka, *J. Am. Chem. Soc.* **1994**, *116*, 9935-9942; e) T. Yamaguchi, Y. Miyake, A. Miyamura, N. Ishiwata, K. Tatsuta, *J. Antibiot.* **2006**, *59*, 729-734; f) X. Zhang, L. Evanno, E. Poupon, *Eur. J. Org. Chem.* **2020**, *13*, 1919-1929.

[68]   U. Galli, G. C. Tron, B. Purghè, G. Grosa, S. Aprile, *Chem. Res. Toxicol.* **2020**, *33*, 955-966.

[69]   S. Wu, J. Huang, S. Gazzarrini, S. He, L. Chen, J. Li, L. Xing, C. Li, L. Chen, C. G. Neochoritis, G. P. Liao, H. Zhou, A. Dömling, A. Moroni, W. Wang, *ChemMedChem* **2015**, *10*, 1837-1845.

[70]   R. Ramozzi, N. Chéron, B. Braïda, P. C. Hiberty, P. Fleurat-Lessard, *New J. Chem.* **2012**, *36*.

[71]   M. Giustiniano, A. Basso, V. Mercalli, A. Massarotti, E. Novellino, G. C. Tron, J. Zhu, *Chem. Soc. Rev.* **2017**, *46*, 1295-1357.

[72]   M. Knorn, E. Lutsker, O. Reiser, *Chem. Soc. Rev.* **2020**, *49*, 7730-7752.

[73]   a) V. P. Boyarskiy, N. A. Bokach, K. V. Luzyanin, V. Y. Kukushkin, *Chem. Rev.* **2015**, *115*, 2698-2779; b) S. Chakrabarty, S. Choudhary, A. Doshi, F. Q. Liu, R. Mohan, M. P. Ravindra, D. Shah, X. Yang, F. F. Fleming, *Adv. Synth. Catal.* **2014**, *356*, 2135-2196; c) J. W. Collet, T. R. Roose, E. Ruijter, B. U. W. Maes, R. V. A.

Orru, *Angew. Chem. Int. Ed.* **2020**, *59*, 540-558; d) J. W. Collet, T. R. Roose, B. Weijers, B. U. W. Maes, E. Ruijter, R. V. A. Orru, *Molecules* **2020**, *25*; e) S. Lang, *Chem. Soc. Rev.* **2013**, *42*, 4867-4880; f) G. Qiu, Q. Ding, J. Wu, *Chem. Soc. Rev.* **2013**, *42*, 5257-5269; g) T. Vlaar, E. Ruijter, B. U. Maes, R. V. Orru, *Angew. Chem. Int. Ed.* **2013**, *52*, 7084-7097.

[74]   W. Lieke, *Liebigs Ann. Chem.* **1859**, *112*, 316-321.

[75]   A. W. Hofmann, *Liebigs Ann. Chem.* **1868**, *144*, 107-119.

[76]   Y. X. Si, P. F. Zhu, S. L. Zhang, *Org. Lett.* **2020**, *22*, 9086-9090.

[77]   I. Ugi, R. Meyer, *Angew. Chem.* **1958**, *70*, 702-703.

[78]   a) R. Appel, R. Kleinstück, K.-D. Ziehn, *Angew. Chem.* **1971**, *4*, 143; b) J. E. Baldwin, I. A. O'Neil, *Synlett* **1990**, *1990*, 603-604; c) S. M. Creedon, H. K. Crowley, D. G. McCarthy, *J. Chem. Soc., Perkin Trans.* **1998**, *1*, 1015-1017; d) Q.-L. Luo, X. Wang, Q.-G. Wang, *Synthesis* **2014**, *47*, 49-54; e) P. Patil, M. Ahmadian-Moghaddam, A. Dömling, *Green Chem.* **2020**, *22*, 6902-6911; f) I. Ugi, U. Fetzer, U. Holzer, H. Knupper, K. Offermann, *Angew. Chem. Int. Ed.* **1965**, *4*, 472-484; g) K. A. Waibel, R. Nickisch, N. Möhl, R. Seim, M. A. R. Meier, *Green Chem.* **2020**, *22*, 933-941.

[79]   a) P. L. Gassmann, T. L. Guggenheim, *J. Am. Chem. Soc.* **1982**, *104*, 5846-5850; b) Y. Kitano, K. Chiba, M. Tada, *Tetrahedron Lett.* **1998**, *39*, 1911-1912.

[80]   a) J. E. Baldwin, Y. Yamaguchi, *Tetrahedron Lett.* **1989**, *30*, 3335-3338; b) Y.-S. Liu, M. Z. Bei, Z. H. Zhou, K. Takaki, Y. Fujiwara, *Chem. Lett.* **1992**, 1143-1144; c) Z. J. Witczak, *Tetrahedron Lett.* **1986**, *27*, 155-158.

[81]   M. C. Leech, A. Petti, N. Tanbouza, A. Mastrodonato, I. C. A. Goodall, T. Ollevier, A. P. Dobbs, K. Lam, *Org. Lett.* **2021**.

[82]   a) L. Banfi, A. Basso, C. Lambruschini, L. Moni, R. Riva, *Chem. Sci.* **2021**, *12*, 15445-15472; b) M. Passerini, G. Ragni, *Gazz. Chim. Ital.* **1921**, *61*, 964-969; c) M. Passerini, L. Simone, *Gazz. Chim. Ital.* **1921**, *51*, 126-129.

[83]   a) I. Ugi, *Angew. Chem. Int. Ed.* **1962**, *1*, 8-21; b) I. Ugi, K. Offermann, H. Herlinger, D. Marquarding, *Liebigs Ann. Chem.* **1967**, *709*, 1-10; c) I. Ugi, C. Steinbrückner, *Angew. Chem.* **1960**, *72*, 267-268.

[84]   a) L. El Kaïm, M. Gizolme, L. Grimaud, *Org. Lett.* **2006**, *8*, 5021-5023; b) L. El Kaïm, L. Grimaud, *Eur. J. Org. Chem.* **2014**, *2014*, 7749-7762.

[85]   C. G. Neochoritis, S. Stotani, B. Mishra, A. Dömling, *Org. Lett.* **2015**, *17*, 2002-2005.

[86]   a) Y. Méndez, A. V. Vasco, A. R. Humpierre, B. Westermann, *ACS Omega* **2020**, *5*, 25505-25510; b) H. Stockmann, A. A. Neves, S. Stairs, K. M. Brindle, F. J. Leeper, *Org. Biomol. Chem.* **2011**, *9*, 7303-7305; c) L. Zhang, M. Isselstein, J. Kohler, N. Eleftheriadis, N. M. Huisjes, M. Guirao-Ortiz, A. Narducci, J. H. Smit, J. Stoffels, H. Harz, H. Leonhardt, A. Herrmann, T. Cordes, *Angew. Chem. Int. Ed.* **2022**, e202112959; d) Y. Zhu, J. Y. Liao, L. Qian, *Front. Chem.* **2021**, *9*, 670751.

[87]   a) F. de Moliner, N. Kielland, R. Lavilla, M. Vendrell, *Angew. Chem. Int. Ed.* **2017**, *56*, 3758-3769; b) N. S. Finney, *Curr. Opin. Chem. Biol.* **2006**, *10*, 238-245; c) L. Levi, T. J. Muller, *Chem. Soc. Rev.* **2016**, *45*, 2825-2846; d) R. O. Rocha, M. O. Rodrigues, B. A. D. Neto, *ACS Omega* **2020**, *5*, 972-979; e) M. Vendrell, D. Zhai, J. C. Er, Y. T. Chang, *Chem. Rev.* **2012**, *112*, 4391-4420.

[88]   a) H. Bienaymé, K. Bouzid, *Angew. Chem. Int. Ed.* **1998**, *110*, 2349-2352; b) C. Blackburn, B. Guan, P. Fleming, K. Shiosaki, S. Tsai, *Tetrahedron Lett.* **1998**, *39*, 3635-3638; c) K. Groebke, L. Weber, F. Mehlin, *Synlett* **1998**, 661-663.

[89]   G. S. Mandair, M. Light, A. Russell, M. Hursthouse, M. Bradley, *Tetrahedron Lett.* **2002**, *43*, 4267-4269.

[90]   S. Khatun, A. Singh, G. N. Bader, F. A. Sofi, *J. Biomol. Struct.* **2021**, 1-24.

[91]   B. E. Evans, K. E. Rittle, M. G. Bock, R. M. DiPardo, R. M. Freidinger, W. L. Whitter, G. F. Lundell, D. F. Veber, P. S. Anderson, R. S. L. Chang, V. L. Lotti, D. J. Cerino, T. B. Chen, P. J. Kling, K. A. Kunkel, J. P. Springer, J. Hirshfield, *J. Med. Chem.* **1988**, *31*, 2235-2246.

[92]   R. N. Rao, K. Chanda, *Chem. Commun.* **2022**, *58*, 343-382.

[93]   a) M. Baumann, I. R. Baxendale, S. V. Ley, N. Nikbin, *Beilstein J. Org. Chem.* **2011**, *7*, 442-495; b) D. Vanda, P. Zajdel, M. Soural, *Eur. J. Med. Chem.* **2019**, *181*, 111569.

[94]   A. Nagle, T. Wu, K. Kuhen, K. Gagaring, R. Borboa, C. Francek, Z. Chen, D. Plouffe, X. Lin, C. Caldwell, J. Ek, S. Skolnik, F. Liu, J. Wang, J. Chang, C. Li, B. Liu, T. Hollenbeck, T. Tuntland, J. Isbell, T. Chuan, P. B. Alper, C. Fischli, R. Brun, S. B. Lakshminarayana, M. Rottmann, T. T. Diagana, E. A. Winzeler, R. Glynne, D. C. Tully, A. K. Chatterjee, *J. Med. Chem.* **2012**, *55*, 4244-4273.

[95]   a) P. Kocienski, *Synfacts* **2020**, *16*, 1014; b) H. Lei, Z. Li, T. Li, H. Wu, J. Yang, X. Yang, Y. Yang, N. Jiang, X. Zhai, *Bioorganic Chemistry* **2022**, *120*, 105590.

[96]   M. Pedrola, M. Jorba, E. Jardas, F. Jardi, O. Ghashghaei, M. Viñas, R. Lavilla, *Front. Chem.* **2019**, *7*, 475.

[97]   M. L. Bode, D. Gravestock, S. S. Moleele, C. W. van der Westhuyzen, S. C. Pelly, P. A. Steenkamp, H. C. Hoppe, T. Khan, L. A. Nkabinde, *Bioorg. Med. Chem.* **2011**, *19*, 4227-4237.

[98]   R. Butera, M. Wazynska, K. Magiera-Mularz, J. Plewka, B. Musielak, E. Surmiak, D. Sala, R. Kitel, M. de Bruyn, H. W. Nijman, P. H. Elsinga, T. A. Holak, A. Dömling, *ACS Med. Chem. Lett.* **2021**, *12*, 768-773.

[99]   a) S. Shaaban, B. F. Abdel-Wahab, *Mol. Divers.* **2016**, *20*, 233-254; b) N. Bedard, A. Fistrovich, K. Schofield, A. Shaw, C. Hulme, in *Multicomponent Reactions towards Heterocycles*, **2022**, pp. 339-409.

[100]   O. N. Burchak, L. Mugherli, M. Ostuni, J. J. Lacapere, M. Y. Balakirev, *J. Am. Chem. Soc.* **2011**, *133*, 10058-10061.

[101]   A. Shahrisa, S. Esmati, *Synlett* **2013**, *24*, 595-602.

[102]   U. Balijapalli, S. K. Iyer, *Dyes and Pigments* **2015**, *121*, 88-98.

[103]   a) A. Sehlinger, M. A. R. Meier, in *Multi-Component and Sequential Reactions in Polymer Synthesis* (Ed.: P. Theato), Springer International Publishing, Cham, **2015**, pp. 61-86; b) S. C. Solleder, M. A. R. Meier, *Angew. Chem. Int. Ed.* **2014**, *53*, 711-714.

[104]   J. Liu, T. Yang, Z. P. Wang, P. L. Wang, J. Feng, S. Y. Ding, W. Wang, *J. Am. Chem. Soc.* **2020**, *142*, 20956-20961.

[105]   Z. Hassan, E. Spuling, D. M. Knoll, J. Lahann, S. Bräse, *Chem. Soc. Rev.* **2018**, *47*, 6947-6963.

[106]   a) *Modern Cyclophane Chemistry*, Wiley-VCH, Weinheim, **2004**; b) H. Hopf, *Isr. J. Chem.* **2012**, *52*, 18-19.

[107]   a) J. Paradies, *Synthesis* **2011**, *23*, 3749-3766; b) S. Bräse, in *Asymmetric Synthesis: The Essentials* (Eds.: M. Christmann, S. Bräse), Wiley-VCH, Weinheim, **2006**; c) S. E. Gibson, J. D. Knight, *Org. Biomol. Chem.* **2003**, *1*, 1256-1269.

[108]   Z. Hassan, E. Spuling, D. M. Knoll, S. Bräse, *Angew. Chem. Int. Ed.* **2020**, *59*, 2156-2170.

[109]   a) E. Spuling, N. Sharma, I. D. W. Samuel, E. Zysman-Colman, S. Bräse, *Chem. Commun.* **2018**, *54*, 9278-9281; b) N. Sharma, E. Spuling, C. M. Mattern, W. Li, O. Fuhr, Y. Tsuchiya, C. Adachi, S. Bräse, I. D. W. Samuel, E. Zysman-Colman, *Chem. Sci.* **2019**, *10*, 6689-6696; c) A. Marrocchi, I. Tomasi , L. Vaccaro, *Isr. J. Chem.* **2012**, *52*, 41-52.

[110]   D. M. Knoll, C. Zippel, Z. Hassan, M. Nieger, P. Weis, M. M. Kappes, S. Bräse, *Dalton Trans.* **2019**, *48*, 17704-17708.

[111]   a) C. Braun, E. Spuling, N. B. Heine, M. Cakici, M. Nieger, S. Bräse, *Adv. Synth. Catal.* **2016**, *358*, 1664-1670; b) D. M. Knoll, S. Bräse, *ACS Omega* **2018**, *3*, 12158-12162.

[112]   K. I. Sugiura, *Front. Chem.* **2020**, *8*, 700.

[113]   S. Clément, L. Guyard, M. Knorr, S. Dilsky, C. Strohmann, M. Arroyo, *J. Organomet. Chem.* **2007**, *692*, 839-850.

[114]   A. V. Lygin, A. de Meijere, *Org. Lett.* **2009**, *11*, 389-392.

[115]   V. Göker, S. R. Kohl, F. Rominger, G. Meyer-Eppler, L. Volbach, G. Schnakenburg, A. Lützen, A. S. K. Hashmi, *J. Organomet. Chem.* **2015**, *795*, 45-52.

[116]   C. Zippel, T. Bartholomeyzik, C. Friedmann, Z. Hassan, M. Nieger, S. Bräse, *Eur. J. Org. Chem.* **2021**, 5090-5093.

[117]   a) C. Bolm, K. Wenz, G. Raabe, *J. Organomet. Chem.* **2002**, *662*, 23-33; b) M. Catellani, E. Motti, N. Della Ca', *Acc. Chem. Res.* **2008**, *41*, 1512-1522; c) J. E. Glover, P. G. Plieger, G. J. Rowlands, *Aust. J. Chem.* **2014**, *67*, 374-380.

[118]   S. Kothavale, K. H. Lee, J. Y. Lee, *Chem. Eur. J.* **2020**, *26*, 845-852.

[119]   S. Liu, H. Zhang, Y. Li, J. Liu, L. Du, M. Chen, R. T. K. Kwok, J. W. Y. Lam, D. L. Phillips, B. Z. Tang, *Angew. Chem. Int. Ed.* **2018**, *57*, 15189-15193.

[120]   N. Rosenbaum, *Dissertation: Development of Novel Routes and Methods for the Semisynthesis of the Marine Steroid Demethylgorgosterol and Unnatural Analogs*, Karlsruhe Institute of Technology, Karlsruhe, **2021**.

[121]   W. Bergmann, M. J. McLean, D. Lester, *J. Org. Chem.* **1943**, *8*, 271-282.

[122]   N. Rosenbaum, L. Schmidt, F. Mohr, O. Fuhr, M. Nieger, S. Bräse, *Eur. J. Org. Chem.* **2021**, *2021*, 1568-1574.

[123]   a) Y. Zhang, L. Wang, Q. Rao, Y. Bu, T. Xu, X. Zhu, J. Zhang, Y. Tian, H. Zhou, *Sens. Actuators B Chem.* **2020**, *321*, 128460; b) K. Scheller, C. E. Sekeris, G. Krohne, R. Hock, I. A. Hansen, U. Scheer, *Eur. J. Cell Biol.* **2000**, *79*, 299-307; c) J. M. McManus, K. Bohn, M. Alyamani, Y.-M. Chung, E. A. Klein, N. Sharifi, *PLOS ONE* **2019**, *14*, e0224081; d) I. Kokkinopoulou, P. Moutsatsou, *Int. J. Mol. Sci.* **2021**, *22*; e) P. Sommer, H. M. Cowley, *Cell Biol. Int.* **2001**, *25*, 103-111.

[124]   T. Zarganes-Tzitzikas, A. L. Chandgude, A. Dömling, *Chem. Rec.* **2015**, *15*, 981-996.

[125]   a) V. Gracias, J. D. Moore, S. W. Djuric, *Tetrahedron Lett.* **2004**, *45*, 417-420; b) C. Kalinski, M. Umkehrer, J. Schmidt, G. Ross, J. Kolb, C. Burdack, W. Hiller, S. D. Hoffmann, *Tetrahedron Lett.* **2006**, *47*, 4683-4686; c) R. Krelaus, B. Westermann, *Tetrahedron Lett.* **2004**, *45*, 5987-5990; d) A. Kumar, D. D. Vachhani, S. G. Modha, S. K. Sharma, V. S. Parmar, E. V. Van der Eycken, *Beilstein J. Org. Chem.* **2013**, *9*, 2097-2102; e) S. G. Modha, A. Kumar, D. D. Vachhani, J. Jacobs, S. K. Sharma, V. S. Parmar, L. Van Meervelt, E. V. Van der Eycken, *Angew. Chem. Int. Ed.* **2012**, *51*, 9572-9575; f) S. Pandey, S. Khan, A. Singh, H. M. Gauniyal, B. Kumar, P. M. Chauhan, *J. Org. Chem.* **2012**, *77*, 10211-10227; g) K. Pérez-Labrada, I. Brouard, I. Méndez, C. S. Pérez, J. A. Gavín, D. G. Rivera, *Eur. J. Org. Chem.* **2014**, *2014*, 3671-3683; h) A. A. Peshkov, V. A. Peshkov, O. P. Pereshivko, E. V. Van der Eycken, *Tetrahedron* **2015**, *71*, 3863-3871; i) A. D. Santos, L. El Kaim, L. Grimaud, C. Ronsseray, *Beilstein J. Org. Chem.* **2011**, *7*, 1310-1314; j) U. K. Sharma, N. Sharma, D. D. Vachhani, E. V. Van der Eycken, *Chem. Soc. Rev.* **2015**, *44*, 1836-1860; k) J. Shi, J. Wu, C. Cui, W. M. Dai, *J. Org. Chem.* **2016**, *81*, 10392-10403; l) Z. Xu, F. De Moliner, A. P. Cappelli, C. Hulme, *Angew. Chem. Int. Ed.* **2012**, *51*, 8037-8040.

[126]   a) B. Liu, Y. Li, H. Jiang, M. Yin, H. Huang, *Adv. Synth. Catal.* **2012**, *354*, 2288-2300; b) S. Sharma, A. Jain, *Tetrahedron Lett.* **2014**, *55*, 6051-6054; c) T. Tang, X. D. Fei, Z. Y. Ge, Z. Chen, Y. M. Zhu, S. J. Ji, *J. Org. Chem.* **2013**, *78*, 3170-3175.

[127]   V. Tyagi, S. Khan, A. Giri, H. M. Gauniyal, B. Sridhar, P. M. S. Chauhan, *Org. Lett.* **2012**, *14*, 3126-3129.

[128]   a) A. El Akkaoui, M.-A. Hiebel, A. Mouaddib, S. Berteina-Raboin, G. Guillaumet, *Tetrahedron* **2012**, *68*, 9131-9138; b) V. Tyagi, S. Khan, V. Bajpai, H. M. Gauniyal, B. Kumar, P. M. S. Chauhan, *J. Org. Chem.* **2012**, *77*, 1414-1421.

[129]   Z. Tber, M. A. Hiebel, H. Allouchi, A. El Hakmaoui, M. Akssira, G. Guillaumet, S. Berteina-Raboin, *RSC Adv.* **2015**, *5*, 35201-35210.

[130]   Y. Li, J. H. Huang, J. L. Wang, G. T. Song, D. Y. Tang, F. Yao, H. K. Lin, W. Yan, H. Y. Li, Z. G. Xu, Z. Z. Chen, *J. Org. Chem.* **2019**, *84*, 12632-12638.

[131]   a) O. Chavignon, M. Raihane, P. Deplat, J. L. Chabard, A. Gueiffier, Y. Blanche, G. Dauphin, J. Teulad, *Heterocycles* **1995**, *41*, 2019-2027; b) N. Devi, D. Singh, R. K. Sunkaria, C. C. Malakar, S. Mehra, R. K. Rawal, V. Singh, *ChemistrySelect* **2016**, *1*, 4696-4703.

[132]   A. Favier, M. Blackledge, J.-P. Simorre, S. Crouzy, V. Dabouis, A. Gueiffier, D. Marion, J.-C. Debouzy, *Biochemistry* **2001**, *40*, 8717-8726.

[133]   a) L. F. Tietze, *Chem. Rev.* **1996**, *96*, 115-136; b) L. F. Tietze, U. Beifuss, *Angew. Chem. Int. Ed.* **1993**, *32*, 131-312.

[134] G. Van Baelen, S. Kuijer, L. Rycek, S. Sergeyev, E. Janssen, F. J. de Kanter, B. U. Maes, E. Ruijter, R. V. Orru, *Chem. Eur. J.* **2011**, *17*, 15039-15044.

[135] L. A. Perego, P. Fleurat-Lessard, L. El Kaïm, I. Ciofini, L. Grimaud, *Chem. Eur. J.* **2016**, *22*, 15491-15500.

[136] M. Suginome, Y. Ito, in *Polymer Synthesis*, Springer Berlin Heidelberg, Berlin, Heidelberg, **2004**, pp. 77-136.

[137] a) D. Jacquemin, M. Khelladi, A. De Nicola, G. Ulrich, *Dyes and Pigments* **2019**, *163*, 475-482; b) C. Azarias, Š. Budzák, A. D. Laurent, G. Ulrich, D. Jacquemin, *Chem. Sci.* **2016**, *7*, 3763-3774.

[138] a) J. Mann, *Life Saving Drugs, The Elusive Magic Bullet*, Royal Society of Chemistry, Cambridge, **2007**; b) W. B. Pratt, *The Anticancer Drugs*, Oxford University Press, Oxford, **1994**.

[139] M. Wink, *Diversity* **2020**, *12*.

[140] a) G. Mazzini, M. Danova, in *Histochemistry of Single Molecules: Methods and Protocols* (Eds.: C. Pellicciari, M. Biggiogera), Springer New York, New York, NY, **2017**, pp. 239-259; b) R. M. Martin, H. Leonhardt, M. C. Cardoso, *Cytometry Part A* **2005**, *67A*, 45-52; c) H. A. Crissman, G. T. Hirons, in *Methods Cell Biol., Vol. 41* (Eds.: Z. Darzynkiewicz, J. Paul Robinson, H. A. Crissman), Academic Press, **1994**, pp. 195-209; d) C. Schneeberger, P. Speiser, F. Kury, R. Zeillinger, *PCR Methods Appl.* **1995**, *4*, 234-238.

[141] O. Steinlein, *Etablierung und Anwendung des pUCAssays als in vitro-Testsystem*, Karlsruhe Institute of Technology, **2020**.

[142] M. J. Waring, *J. Mol. Biol.* **1965**, *13*, 269-282.

[143] N. J. Wheate, S. Walker, G. E. Craig, R. Oun, *Dalton Trans.* **2010**, *39*, 8113-8127.

[144] C.-S. Lee, Y. Hashimoto, K. Shudo, M. Nagao, *Heterocycles* **1984**, *22*, 2249-2253.

[145] A. Kellett, Z. Molphy, C. Slator, V. McKee, N. P. Farrell, *Chem. Soc. Rev.* **2019**, *48*, 971-988.

[146] T. R. Strick, J.-F. Allemand, D. Bensimon, V. Croquette, *Biophys. J.* **1998**, *74*, 2016-2028.

[147] a) M. Asmuss, L. H. F. Mullenders, A. Eker, A. Hartwig, *Carcinogenesis* **2000**, *21*, 2097-2104; b) R. H. Männistö, H. M. Kivelä, L. Paulin, D. H. Bamford, J. K. H. Bamford, *Virology* **1999**, *262*, 355-363.

[148] a) M. Cetraz, V. Sen, S. Schoch, K. Streule, V. Golubev, A. Hartwig, B. Köberle, *Arch. Toxicol.* **2017**, *91*, 785-797; b) S. Kawanishi, S. Inoue, K. Yamamoto, *Carcinogenesis* **1989**, *10*, 2231-2235; c) G. Pratviel, J. Bernadou, B. Meunier, *Angew. Chem. Int. Ed.* **1995**, *34*, 746-769.

[149] a) D. S. Mattes, N. Jung, L. K. Weber, S. Bräse, F. Breitling, *Adv. Mater.* **2019**, *31*, 1806656; b) W. Feng, E. Ueda, P. A. Levkin, *Adv. Mater.* **2018**, *30*, 1706111.

[150] F. F. Loeffler, T. C. Foertsch, R. Popov, D. S. Mattes, M. Schlageter, M. Sedlmayr, B. Ridder, F. X. Dang, C. von Bojnicic-Kninski, L. K. Weber, A. Fischer, J. Greifenstein, V. Bykovskaya, I. Buliev, F. R. Bischoff, L. Hahn, M. A. Meier, S. Bräse, A. K. Powell, T. S. Balaban, F. Breitling, A. Nesterov-Mueller, *Nat. Commun.* **2016**, *7*, 11844.

[151] a) D. S. Mattes, B. Streit, D. R. Bhandari, J. Greifenstein, T. C. Foertsch, S. W. Münch, B. Ridder, V. B.-K. C, A. Nesterov-Mueller, B. Spengler, U. Schepers, S. Bräse, F. F. Loeffler, F. Breitling, *Macromol. Rapid. Commun.* **2019**, *40*, e1800533; b) B. Ridder, D. S. Mattes, A. Nesterov-Mueller, F. Breitling, M. A. R. Meier, *Chem. Commun.* **2017**, *53*, 5553-5556; c) C. von Bojnicic-Kninski, V. Bykovskaya, F. Maerkle, R. Popov, A. Palermo, D. S. Mattes, L. K. Weber, B. Ridder, T. C. Foertsch, A. Welle, F. F. Loeffler, F. Breitling, A. Nesterov-Mueller, *Adv. Funct. Mater.* **2016**, *26*, 7067-7073.

[152] A. Klinkusch, *Dissertation: Miniaturisierte Synthese von kombinatorischen Arrays fluoreszierender Moleküle via nano3D-Laserprinting*, Karlsruhe Institute of Technology, **2021**.

[153] P. Serra, A. Piqué, *Adv. Mater. Technol.* **2019**, *4*.

[154] G. Paris, A. Klinkusch, J. Heidepriem, A. Tsouka, J. Zhang, M. Mende, D. S. Mattes, D. Mager, H. Riegler, S. Eickelmann, F. F. Loeffler, *Appl. Surf. Sci.* **2020**, *508*.

[155] a) P. Chaiyen, N. S. Scrutton, *The FEBS Journal* **2015**, *282*, 3001-3002; b) S. O. Mansoorabadi, C. J. Thibodeaux, H.-w. Liu, *J. Org. Chem.* **2007**, *72*, 6329-6342.

[156]   a) S. Chen, M. S. Hossain, F. W. Foss, *ACS Sustainable Chem. Eng.* **2013**, *1*, 1045-1051; b) H. Grajek, *Curr. Topics Biophys.* **2012**, *34*, 53-65; c) V. Piano, B. A. Palfey, A. Mattevi, *Trends Biochem. Sci.* **2017**, *42*, 457-469; d) V. Srivastava, P. K. Singh, A. Srivastava, P. P. Singh, *RSC Adv.* **2021**, *11*, 14251-14259.

[157]   a) R. Kuhn, F. Weygand, *Ber. Dtsch. Chem. Ges.* **1934**, *67*, 1409-1413; b) H. Bredereck, W. Pfleiderer, *Chem. Ber.* **1954**, *87*, 1119-1123; c) J. Butenandt, R. Epple, E.-U. Wallenborn, A. P. M. Eker, V. Gramlich, T. Carell, *Chem. Eur. J.* **2000**, *6*, 62-72.

[158]   B. Colak, A. Büyükkoyuncu, F. Baycan Koyuncu, S. Koyuncu, *Polymer* **2017**, *123*, 366-375.

[159]   A. Hagemeyer, P. Strasser, A. F. Volpe, *High-Throughput Screening in Chemical Catalysis: Technologies, Strategies and Applications*, Wiley-VCH, Weinheim, **2006**.

[160]   a) T. J. Crowley, R. A. Berner, *Science* **2001**, *292*, 870-872; b) C. Hepburn, E. Adlen, J. Beddington, E. A. Carter, S. Fuss, N. Mac Dowell, J. C. Minx, P. Smith, C. K. Williams, *Nature* **2019**, *575*, 87-97.

[161]   a) Y. Quan, J. Zhu, G. Zheng, *Small Science* **2021**, *1*, 2100043; b) V. Kumaravel, J. Bartlett, S. C. Pillai, *ACS Energy Letters* **2020**, *5*, 486-519; c) L. D. Ramírez-Valencia, E. Bailón-García, F. Carrasco-Marín, A. F. Pérez-Cadenas, *Catalysts* **2021**, *11*, 351; d) S. Dabral, T. Schaub, *Adv. Synth. Catal.* **2019**, *361*, 223-246; e) G. Yuan, C. Qi, W. Wu, H. Jiang, *Curr. Opin. Green Sust. Chem.* **2017**, *3*, 22-27; f) S. Pradhan, S. Roy, B. Sahoo, I. Chatterjee, *Chem. Eur. J.* **2021**, *27*, 2254-2269.

[162]   T. Kaicharla, M. Thangaraj, A. T. Biju, *Org. Lett.* **2014**, *16*, 1728-1731.

[163]   R. Orita, M. Franckevicius, A. Vyšniauskas, V. Gulbinas, H. Sugiyama, H. Uekusa, K. Kanosue, R. Ishige, S. Ando, *Phys. Chem. Chem. Phys.* **2018**, *20*, 16033-16044.

[164]   a) N. Fukino, S. Kamino, M. Takahashi, D. Sawada, *J. Org. Chem.* **2017**, *82*, 13626-13631; b) R. K. Hallani, M. Moser, H. Bristow, M. V. C. Jenart, H. Faber, M. Neophytou, E. Yarali, A. F. Paterson, T. D. Anthopoulos, I. McCulloch, *J. Org. Chem.* **2020**, *85*, 277-283.

[165]   J. Ashby, H. Tinwell, J. Plautz, K. Twomey, P. A. Lefevre, *Regul. Toxicol. Pharmacol.* **2001**, *34*, 287-291.

[166]   D. Hüglin, E. Borsos, H. Luther, B. Herzog, F. Bachmann, *Vol. EP0775698A1*, Germany, **1997**.

[167]   M. J. Paterson, M. A. Robb, L. Blancafort, A. D. DeBellis, *J. Phys. Chem. A* **2005**, *109*, 7527-7535.

[168]   W.-F. Jiang, H.-L. Wang, Z.-Q. Li, *J. Chem. Res.* **2008**, *2008*, 664-665.

[169]   M. Bandini, *J. Am. Chem. Soc.* **2010**, *132*, 7821-7822.

[170]   a) A. Kawada, S. Mitamuraa, S. Kobayashi, *J. Chem. Soc., Chem. Commun.* **1993**, 1157-1158; b) I. Komoto, J.-i. Matsuo, S. Kobayashi, *Top. Catal.* **2002**, *19*, 43-47.

[171]   a) Z. Bohström, H. Härelind, K. Holmberg, *J. Mol. Catal. A* **2013**, *366*, 171-178; b) B. Chiche, A. Finiels, C. Gauthier, P. Geneste, J. Graille, D. Pioch, *J. Org. Chem.* **1986**, *51*, 2128-2130; c) G. Satori, R. Maggi, *Chem. Rev.* **2006**, *106*, 1077-1104; d) C. Venkatesan, T. Jaimol, P. Moreau, A. Finiels, A. Ramaswamy, A. Singh, *Catal. Lett.* **2001**, *75*, 119-123.

[172]   G. Gelbard, *Ind. Eng. Chem. Res.* **2005**, *44*, 8468-8498.

[173]   C. Hoarau, T. R. R. Pettus, *Synlett* **2003**, *1*, 127-137.

[174]   a) A. Díaz-Ortiz, A. de la Hoz, A. Moreno, A. Sánchez-Migallón, G. Valiente, *Green Chem.* **2002**, *4*, 339-343; b) R. Martínez-Alvarez, A. Herrera, P. Ramiro, M. Chioua, R. Chioua, *Synthesis* **2004**, 503-505; c) T. Muller, S. Bräse, *RSC Adv.* **2014**, *4*; d) P. Puthiaraj, Y.-R. Lee, S. Zhang, W.-S. Ahn, *J. Mater. Chem. A* **2016**, *4*, 16288-16311.

[175]   A. Herrera, A. Riaño, R. Moreno, B. Caso, Z. D. Pardo, I. Fernández, E. Sáez, D. Molero, A. Sánchez-Vázquez, R. Martínez-Alvarez, *J. Org. Chem.* **2014**, *79*, 7012-7024.

[176]   a) G. Blotny, *Tetrahedron* **2006**, *62*, 9507-9522; b) S. Samaritani, P. Peluso, C. Malanga, R. Menicagli, *Eur. J. Org. Chem.* **2002**, *2002*, 1551-1555; c) R. Menicagli, C. Malanga, P. Peluso, *Synth. Commun.* **1994**, *24*, 2153-2158.

[177]   a) E. Troschke, S. Gratz, T. Lubken, L. Borchardt, *Angew. Chem. Int. Ed.* **2017**, *56*, 6859-6863; b) C. Wang, J. Zhang, J. Tang, G. Zou, *Adv. Synth. Catal.* **2017**, *359*, 2514-2519; c) T.-M. Geng, X.-C. Fang, F.-Q. Wang, F. Zhu, *Macromol. Mater. Eng.* **2021**, *306*, 2100461; d) R. Menicagli, S. Samaritani, V. Zucchelli, *Tetrahedron* **2000**, *56*, 9705-9711; e) L. Hintermann, L. Xiao, A. Labonne, *Angew. Chem. Int. Ed.* **2008**,

47, 8246-8250; f) J. W. Lee, J. T. Bork, H.-H. Ha, A. Samanta, Y.-T. Chang, *Aust. J. Chem.* **2009**, *62*, 1000-1006.

[178]   H. J. Schulz, J. Liebscher, P. Luger, M. Quian, J. Mulzer, *J. Heterocyclic Chem.* **1992**, *29*, 1125-1132.

[179]   a) M. T. Barros, S. S. Dey, C. D. Maycock, P. Rodrigues, *Chem. Commun.* **2012**, *48*, 10901-10903; b) A. S. Kotnis, *Tetrahedron Lett.* **1991**, *32*, 3441-3444; c) Y.-F. Liang, S. Song, L. Ai, X. Li, N. Jiao, *Green Chem.* **2016**, *18*, 6462-6467; d) M. J. Mphahlele, *Molecules* **2009**, *14*, 5308-5322.

[180]   F. Zhou, M. O. Simon, C. J. Li, *Chem. Eur. J.* **2013**, *19*, 7151-7155.

[181]   K. C. Nicolaou, T. Montagnon, P. S. Baran, Y.-L. Zhong, *J. Am. Chem. Soc.* **2002**, *124*, 2245-2258.

[182]   a) A. V. Iosub, S. S. Stahl, *ACS Catal.* **2016**, *6*, 8201-8213; b) Y. Izawa, C. Zheng, S. S. Stahl, *Angew. Chem. Int. Ed.* **2013**, *52*, 3672-3675; c) T. Diao, D. Pun, S. S. Stahl, *J. Am. Chem. Soc.* **2013**, *135*, 8205-8212; d) W. P. Hong, A. V. Iosub, S. S. Stahl, *J. Am. Chem. Soc.* **2013**, *135*, 13664-13667; e) D. Pun, T. Diao, S. S. Stahl, *J. Am. Chem. Soc.* **2013**, *135*, 8213-8221; f) S. J. Tereniak, S. S. Stahl, *J. Am. Chem. Soc.* **2017**, *139*, 14533-14541; g) T. Diao, S. S. Stahl, *J. Am. Chem. Soc.* **2011**, *133*, 14566-14569; h) Y. Izawa, D. Pun, S. S. Stahl, *Science* **2011**, *333*, 209-213.

[183]   K. Kikushima, Y. Nishina, *RSC Adv.* **2013**, *3*.

[184]   J. Zhang, Q. Jiang, D. Yang, X. Zhao, Y. Dong, R. Liu, *Chem. Sci.* **2015**, *6*, 4674-4680.

[185]   a) D. S. P. Cardoso, B. Šljukić, D. M. F. Santos, C. A. C. Sequeira, *Org. Process Res. Dev.* **2017**, *21*, 1213-1226; b) O. Hammerich, B. Speißer, *Organic Electrochemistry*, 5 th ed., CRC Press Taylor & Francis Group, Boca Raton, **2016**; c) D. Pollok, S. R. Waldvogel, *Chem. Sci.* **2020**, *11*, 12386-12400.

[186]   S. Gnaim, Y. Takahira, H. R. Wilke, Z. Yao, J. Li, D. Delbrayelle, P. G. Echeverria, J. C. Vantourout, P. S. Baran, *Nat. Chem.* **2021**, *13*, 367-372.

[187]   a) S. H. K. Reddy, K. Chiba, Y. Sun, K. D. Moeller, *Tetrahedron* **2001**, *57*, 5183-5197; b) T. Shono, Y. Matsumura, Y. Nakagawa, *J. Am. Chem. Soc.* **1974**, *96*, 3532-3536.

[188]   C. Kingston, M. D. Palkowitz, Y. Takahira, J. C. Vantourout, B. K. Peters, Y. Kawamata, P. S. Baran, *Acc. Chem. Res.* **2020**, *53*, 72-83.

[189]   a) F. Hundemer, *Dissertation: Modular Design Strategies for TADF Emitters: Towards Highly Efficient Materials for OLED Application*, Karlsruhe Institute of Technology, **2020**; b) C. Zippel, *Dissertation: Synthesis and Application of [2.2]Paracyclophane Derivatives in Catalysis and Material Science*, Karlsruhe Institute of Technology, **2021**.

[190]   N. Schwarz, *Vertieferbericht: Synthese neuartiger [2.2]Paracylophan-basierter Fluorophore mittels Multikomponentenreaktionen*, Karlsruhe Institute of Technology, **2019**.

[191]   M. Mergel, *Bachelor Thesis: Modulare Synthese von Imidazo[1,2-a]pyridinbasierten TADF-Emittern*, Karlsruhe Institute of Technology, **2021**.

[192]   C. R. Adam, *Vertieferbericht: Combinatorial Synthesis of Fluorophores via Multi Component Reactions*, Karlsruhe Institute of Technology, **2020**.

[193]   M. Rotter, *Bachelor Thesis: Synthese N-verbrückter polyzyklischer Verbindungen mittels Multikomponentenreaktionen und Isocyanid-Insertionen*, Karlsruhe Institute of Technology, **2018**.

[194]   A. Vranić, *Vertieferbericht: Kombinatorische Synthese von flavin-basierten Fluorophoren*, Karlsruhe Institute of Technology, **2021**.

8 Appendix

8.1 Curriculum Vitae

MAREEN STAHLBERGER

◎ 20.03.1994 in Rastatt

✉ mareen.stahlberger@googlemail.com

🎓 EDUCATION

12/2017 – 04/2021	**Doctorate** at the Institute of Organic Chemistry, Faculty of Chemistry and Biosciences, Karlsruhe Institute of Technology, under the supervision of Prof. Dr. Stefan Bräse
	Title: Modular Concepts for the Synthesis of Functional Chromophores
10/2016 – 11/2017	**Master of Science** in Chemistry, Karlsruhe Institute of Technology
	Grade: 1.0 ("**sehr gut**")
	Master Thesis under the supervision of Prof. Dr. Stefan Bräse
	Title: Development of Novel Sequential Synthesis Strategies involving Isonitrile-based Multi-Component Reactions
10/2012 – 09/2016	**Bachelor of Science** in Chemistry, Karlsruhe Institute of Technology
	Grade: 1.1 ("**sehr gut**")
	Bachelor Thesis under the supervision of Prof. Dr. Stefan Bräse
	Title: Development of a Synthesis Method for 2,2-Difluorochromenes
09/2004 – 06/2012	**Abitur**, Goethe-Gymnasium Gaggenau
	Grade: 1.0 ("**sehr gut**")

🏅 AWARDS AND SCHOLARSHIPS

01/2020	**Soroptimist Club Murgtal**:
	Stipendium für Frauen in MINT Fächern

8.2 List of Publications

Revied Articles and Patents

[1]   Z. Hassan, **M. Stahlberger**, N. Rosenbaum, S. Bräse, *Angew. Chem. Int. Ed*. **2021**, 60, 15138–15152.

Criegee Intermediates Beyond Ozonolysis: Synthetic and Mechanistic Insights.

[2]   **M. Stahlberger**, N. Schwarz, C. Zippel, J. Hohmann, M. Nieger, Z. Hassan, S. Bräse, *Chem. Eur. J.* **2022**, 28, e202103511.

Diversity-oriented Synthesis of [2.2]Paracyclophane-derived Fused Imidazo[1,2-*a*]heterocycles by Groebke–Blackburn–Bienaymé Reaction: Accessing Cyclophanyl Imidazole Ligands Library

[3]   **M. Stahlberger**, O. Steinlein, C. R. Adam, M. Rotter, J. Hohmann, M. Nieger, B. Köberle and S. Bräse, *Org. Biomol. Chem.* **2022**, 20, 3598.

Fluorescent Annulated Imidazo[4,5-c]isoquinolines *via* a GBB-3CR/Imidoylation Sequence – DNA-Interactions in pUC-19 Gel Electrophoresis Mobility Shift Assay

[4]   **M. Stahlberger**, S. Bräse, N. Bugdahn, *patent pending*.

Method for producing 2,4,6-substituted triazines.

[5]   P. Gartner, D. Gottwald, I. Perner-Nochta, **M. Stahlberger**, S. Bräse, J. Hubbuch, G. Lanza, *patent pending.*

Der Bio-tag, eine enzymatische Kennzeichungstechnologie

[6]   **M. Stahlberger**, N. Rosenbaum, D. Feser, S. Gornik, M. Nieger, U. Schepers, A. Guse, S. Bräse, *in preparation*.

Synthesis of Imidazo[1,2-*a*]pyridine-substituted Gorgosterol Derivatives and their Application as Fluorescent Probes for the Investigation of Coral Symbiosis

Conference Posters and Presentations

[1]   ORCHEM Berlin, **2018**, poster presentation.

Sequential Syntheses of *N*-rich Heterocycles involving Multicomponent Reactions

[2]   TOCUS Stuttgart, **2021**, conference talk.

Modular Synthesis Methods towards Fluorescent Molecules

9   Acknowledgements

Claudine – du hattest immer ein offenes Ohr für mich und warst in einer schwierigen Zeit immer da um mir zuzuhören und besonnene Ratschläge zu geben. Danke, dass du bei allem so verständnisvoll bist und nicht verurteilst, dass ich nicht so stark bin wie du.

Bantle, Robin – ihr beiden habt es immer geschafft, mich egal in welcher Situation zum Lachen zu bringen, und dafür möchte ich euch ganz besonders danken. Eure manchmal vielleicht etwas fragwürdigen Arten von Humor haben es so oft geschafft erste Situationen nicht mehr ganz so ernst aussehen zu lassen und das war viel wert.

Nicolai – obwohl mich deine Playlist im Labor ständig zur Weißglut gebracht hat, habe ich die Zeit mit dir im Labor immer genossen. Deine akribische Arbeitsweise hat sich immer gut mit meinem kreativen Chaos ergänzt und du hast mir bei so manchem synthetischen Problem ein Füllhorn an guten Tipps geben können. Doch auch darüber hinaus hast du mich die ganze Zeit immer unterstützt und dein Wände durchdringendes Lachen werde ich wohl nie vergessen. Danke für die fast 5 Jahre geteilten Frusts in Labor 306.

Jannik – Füße auf dem Tisch und Laptop auf dem Schoß, deine überaus motivierte Arbeitsweise hat sich perfekt in unser Labor eingefügt und du bist mir mit deinem breiten Grinsen und deiner humorvollen Art mit Dingen umzugehen richtig ans Herz gewachsen. Und dass wir am IMT weiter zusammenarbeiten können.

Jens – auch wenn es Tage gab, an denen dir meine Säulen und meine Fluorophore bis zum Hals standen, finde ich, wir waren ein gutes Team. Du warst nicht nur meine Hände am Abzug, du warst auch eine große Hilfe außerhalb des Labors und – auch wenn du das vielleicht anders definiert – ein guter Freund. Danke, dass du dich entschieden hast, nochmal die Schulbank zu drücken.

Zipp – ich weiß, dass der Laboralltag in 306 oft chaotisch und meine Bench für dich ein Alptraum war. Aber ich bin so froh, dass du trotzdem immer mit deiner ruhigen und besonnenen Art für mich da warst, ganz besonders wenn ich mich beschweren wollte. Du hast es immer geschafft, mich zu motivieren und warst bei jedem Unsinn dabei. Und vor allem als ich dich am meisten gebraucht hab. Danke für 4 perfekte Jahre als Laborpartner und Sonnenschein.

Felix, Katha, Kris – Es ist unfassbar, dass seit unserer Schulzeit schon fast 10 Jahre vergangen sind und dass wir uns teilweise ja schon seit beinahe 28 Jahren kennen. Zu sehen wie wir uns alle seitdem entsiegelt haben ist unglaublich und dabei fühlt es sich mit euch trotzdem immer noch so an als wären wir 18 und hätten alles vor uns. Ihr seid mein Anker ins Murgtal und ich hoffe, dass wir in X Jahren immer noch zusammensitzen und uns Stuss erzählen können.

Anna – du bist meine beste Freundin und ohne deine Unterstützung wäre das hier nie so geworden, wie es ist. Du und deine wundervolle Familie habt mich aufgenommen und ich bin so dankbar dafür, so viel mit euch teilen zu können, seien es Spielenachmittage mit den Kids, Filmabende oder die nächtlichen Privatkonzerte unter eurem Pavillon. Seit der Schule bist du an meiner Seite und wir haben so viel durchgestanden. Dir muss ich nichts erklären und egal ob deeptalk oder Unsinn, wir verstehen uns immer.

Meiner ganzen Familie möchte ich natürlich auch danken: meinen Tanten, Onkels und meinen Cousinen und Cousin.

Vor allem gilt dabei mein Dank meinen Eltern und Großeltern und meiner Schwester Monja.

Mama, Papa – ihr habt mich zu der Person gemacht, die ich heute bin, auch wenn das nicht immer einfach war. Aber egal was war, ihr wusstet immer, dass ich das hier schaffe, auf meine eigene Weise. Danke, dass ihr mir immer geholfen habt und Verständnis habt, für alle Höhen und Tiefen. Ihr wart immer stolz auf uns und habt uns ermöglicht, unser Potential auszuleben. Danke für alles, ihr habt das schon recht gemacht! Hoffentlich können wir euch eines Tages dafür das Cottage am Meer schenken. Oma und Omi, ihr wart von Anfang an auch maßgeblich an unserem Werdegang beteiligt und habt uns unterstützt, wo es nur ging, sei es das Mittagessen nach der Schule oder die verständnisvollen Gespräche. Aber darüber hinaus wart ihr – genau wie Mama – immer die besten Vorbilder für uns: starke, selbstbewusste Frauen, die schon zu Zeiten ihren eigenen Weg gegangen sind als das alles andere als selbstverständlich war. Wir konnten immer zu euch aufschauen aber auch ganz auf Augenhöhe mit euch reden. Dafür bin ich sehr dankbar. Opa, dir gilt an dieser Stelle besonderer Dank. Du warst immer mein größtes Vorbild und hast mir den Weg gezeigt, der mich letztendlich zu einer Wissenschaftlerin gemacht hat. Von Schollenverschiebung bis hin zum Abendstern, du hast mir von klein auf die Welt erklärt und auch wenn sich das in manchen Themen gewandelt hat, du bist und bleibst mein Held.

Moni – auch wenn du hier am Ende stehst, ohne dich wäre das alles nie möglich gewesen. Und das nicht nur, dass du mit deinem poshen Britsch diese Arbeit aufgehübscht. Du warst immer für mich da, egal wie es mir ging und auch egal wie viele Kilometer uns trennten. Denn auch per FaceTime warst du immer zu erreichen, wenn ich dich gebraucht habe. Oder wenn es einfach nur juicy Gossip gab. Aber nicht nur das, du hast für mich gekämpft, wenn es sein musste, und hast im Zweifelsfall alles stehen und liegen lassen. Ich weiß, du bist selbst so stark, dass ich dir das nie zurückgeben kann, aber wir haben ja noch ein ganzes Leben vor uns.